Optical degradation mechanisms and accelerated reliability evaluation for LEDs

Huang, Jianlin

DOI
10.4233/uuid:299c48c9-5bc7-4c5a-aab8-1b82696fbb5b

Publication date
2016

Document Version
Final published version

Citation (APA)
Huang, J. (2016). *Optical degradation mechanisms and accelerated reliability evaluation for LEDs*. [Dissertation (TU Delft), Delft University of Technology]. https://doi.org/10.4233/uuid:299c48c9-5bc7-4c5a-aab8-1b82696fbb5b

OPTICAL DEGRADATION MECHANISMS AND ACCELERATED RELIABILITY EVALUATION FOR LEDS

OPTICAL DEGRADATION MECHANISMS AND ACCELERATED RELIABILITY EVALUATION FOR LEDS

Proefschrift

ter verkrijging van de graad van doctor
aan de Technische Universiteit Delft,
op gezag van de Rector Magnificus prof. ir. K.C.A.M. Luyben,
voorzitter van het College voor Promoties,
in het openbaar te verdedigen op maandag 19 september 2016 om 12:30 uur

door

Jianlin HUANG

Master of Science in Mechanical Engineering, Guilin University of Electronic Technology, China
geboren te Guangxi, China.

This dissertation has been approved by the

promotor: Prof. dr. G.Q. Zhang
copromotor: Dr. W.D. van Driel

Composition of the doctoral committee:

Rector Magnificus	chairman
Prof. dr. G.Q. Zhang	EWI
Dr. W.D. van Driel	UD-EWI
Independent members:	
Prof. dr. J.M.J. den Toonder	TU Eindhoven
Prof. dr. X. Fan	Lamar U., USA
Prof. dr. P.M. Sarro	EWI
Prof. dr. C.I.M. Beenakker	EWI
Other members:	
Dr. D. Golubović	Lumileds

Keywords: light-emitting diode, mid-power LED, optical degradation, lifetime, Wiener process, Brownian motion

Printed by: IPSKAMP Printing

ISBN 000-00-0000-000-0

An electronic version of this dissertation is available at
http://repository.tudelft.nl/.

CONTENTS

1

INTRODUCTION

1

1.1. RESEARCH MOTIVATION

A rapid growth of the light-emitting diodes (LED)-based lighting applications has revolutionized the lighting industry over the past 10 years. In some particular applications, such as automobile taillights, flash lights, high-power white LED has gained a remarkable success. In the other markets, like that of indoor/outdoor general illumination, there is still an expecting revolution [1]. In the indoor/outdoor market segment, mid-power white LEDs have been considered as the potential candidate [2, 3]. They have been widely utilized in many indoor lighting products, such as TLED, bulb and PAR. For outdoor illumination applications, manufacturers are making efforts to develop robust, cost competitive mid-power LEDs which meet the demanding reliability requirements in this environment. The strong growth of the LED lighting market is mainly due to the continuous improvements on the lumen per Watt (lm/W) and lumen per dollar (lm/$). Over the past decade, most of the improvements in materials and device design have enabled the evolution of efficiency of quantum well (EQE) from 25% in the early 2000s, to over 70% today [4]. As the excellent candidate for next generation light source, 303 lm/W for white-light LEDs has been obtained in labs, and 200 lm/W already commercially available at present [5, 6].

According to a report made by the U.S. Department of Energy (DOE) [7], LED lighting is projected to gain significant market penetration. It is expected to represent 48% of lumen-hour sales of the general-illumination market by 2020, and 84% by 2030. Though these energy savings are impressive, there is a huge opportunity for even further savings by accelerating investment in cost and efficacy improvements. However, many problems have to be resolved when using LEDs. There are seven challenges that lighting designers face when using LEDs, that is: (i) LED glare and shadowing, (ii) LED dimming not as smooth as claimed, (iii) lack of color and (iv) measurement standardization, (v) thermal management, (vi) interchangeability, and (vii) need for lower costs [8]. Among these challenges, (ii) to (v), and (vii), are related to reliability. For example, bad thermal management will seriously decrease the lumen output of an LED package [9, 10].

A significant amount of studies have been performed on the reliability of high-power white-light LEDs [11–19], while fewer studies were found on the reliability of mid-power white-light LEDs [20–22]. This is probably because mid-power white-light LED is a relatively new type of LED packages [23–29]. Mid-power white-light LEDs are basically good for low- to medium-cost general lighting applications because mid-power white-light LEDs match the output, in terms of both luminosity and light quality of this target market. However, as the strong demands increase continuously for mid-power white-light LED products which have lower cost while higher luminosity, the reliability is becoming

a critical issue.

1.2. PROBLEM DESCRIPTION

In applications, LED products may suffer from serious lumen degradation [30], color shift [31], electrical deterioration [32], and so forth, depending on their usage conditions [33–35]. It has been indicated that the reliability of a white-light LED package can be attributed to a combination of chip-related and package-related mechanisms [36–39]. A comprehensive review has also summarized the possible degradation modes and degradation mechanisms which may be triggered during operating life [40]. Specifically, for a mid-power white-light LED package, the lumen degradation can be attributed to an increase of non-raditaive and Ohmic contact resistance [39–43], the degradation of the LED package housing materials [44–46], the yellowing of the encapsulant [47, 48], or contamination of silver-coating lead frames [49]. In order to clearly understand the degradation mechanisms, some researchers have made great efforts to separate the major degradation mechanisms into contributions of the individual package components [50]. However, until now, it is still unclear that which one is the major degradation for mid-power white-light LED packages during operating conditions.

On the other hand, although many degradation mechanisms are triggered during operation conditions, the optical degradation of the white-light LEDs is very slow, and the lifetime is very high. The typical lifetime is as high as 50,000 hours at room temperature [51]. Thus, the temperature operating degradation test (e.g., IES LM-80-08 test) is very time-consuming, which needs at least 6,000 hours to perform the lifetime prediction. This is unacceptable with respect to the rapid growth of the LED market. As a result, it is imperative to develop an efficient accelerated degradation test method. And corresponding to LM-80-08 test, the IES standard TM-21-11 provides a methodology by using the average normalized lumen maintenance data and performs non-linear regression for lifetime modeling. This method, however, cannot capture dynamic and random variation of the degradation process of LED devices. In addition, this method cannot capture the failure distribution, although it is much more relevant in reliability analysis. This may not be effective for maintenance decision making by either LED manufacturers or designers. To overcome these drawbacks, a more accurate lifetime model should be developed for the white-light LED packages.

1

1.3. RESEARCH OBJECTIVE

According to the problem description above, the purpose of this thesis is to understand the degradation mechanisms of the mid-power white-light LEDs under various stress conditions. By comparing the degradation mechanisms, a lifetime testing method will be developed to replace the test standard, – LM-80-08, which is widely used in the LED industry while it needs 6,000 hours to perform the lifetime prediction. Furthermore, based on the new testing method, a new model for the lifetime is also proposed. Compared to the widely used standard TM-21-11, this model provides more accurate lifetime prediction for the LEDs. Spefically, we propose the research objective as follows:

(1) To study effects of material degradation – The degradation of package materials including lead frames, blue chips, package housing, silicone encapsulant, and phosphors are considered to affect the lumen output of the LED package. An optical simulation model can be used to understand the degradation kinetics of an LED package, which is induced by the material degradation. The simulation model also can be used to separate the total lumen degradation into contributions of the individual package materials.

(2) To study optical degradation mechanisms – To perform a series of experiments to explore the optical degradation mechanisms of the LED packages. The degradation mechanisms may involve all kinds of materials in the package, and may vary when different stresses are involved. The objective is to identify the major degradation mechanisms of the LED packages. On the one hand, by comparing the degradation mechanisms among all these test conditions, an alternative is expected to replace the LM-80-08 test, which is very time-consuming for lifetime prediction for the LED packages.

(3) To develop a more accurate lifetime model for the LED packages – A lifetime model is developed by using the theories of stochastic processes. Compared to method provided by the standard TM-21-11, the lifetime model can be used to capture the dynamic and random variations of the degradation process of the LED devices. This model also can be used to describe the failure distribution, which is important for reliability evaluation.

1.4. RESEARCH STRUCTURE

The research structure is schematically depicted in Fig. 1.1.

As indicated in Fig. 1.1, the research can be divided into 3 parts:

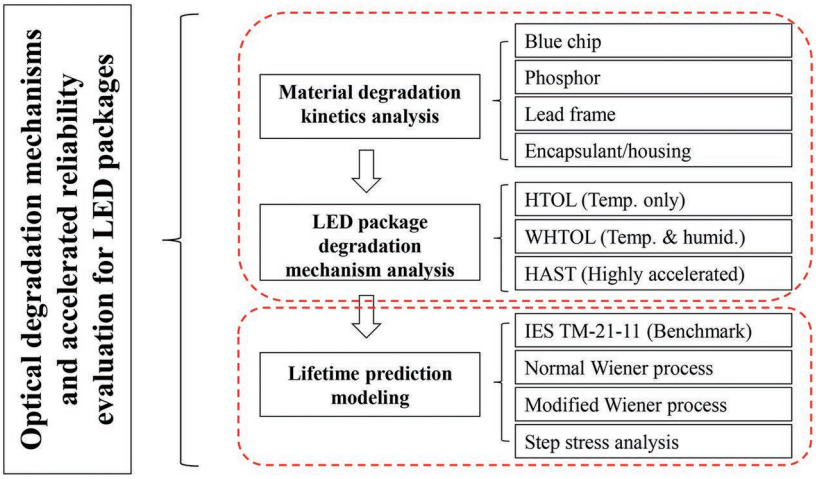

Figure 1.1: Research structure

(1) Material degradation kinetics analysis. A detailed simulation model will be established by using *Lighttools* [52], a commercial light tracing software. The efficiency decrease of the blue chips and phosphors, the reflectivity degradation of the lead frame and package housing, the transmissivity of the silicone encapsulant, is obtained respectively by a series of experiments which are performed on the material samples. These samples are specially prepared to obtain input parameters for simulation modeling. Then these experiment data are included in the simulation model. The spectra of the LED package are extracted to analyze the lumen degradation kinetics due to material degradation.

(2) LED package degradation mechanism analysis. The optical degradation mechanisms will be investigated by performing high temperature operating life tests (HTOL), wet-high temperature operating life tests (WHTOL), and highly accelerated temperature humidity stress test (HAST). After the accelerated degradation experiments on the LED packages, the optical and electrical characteristics are carefully analyzed. Detailed failure analysis is also performed by using C-mode scanning acoustic microscope (CSAM), scanning electronic microscopy SEM/EDX, and so forth.

(3) Lifetime prediction modeling. Based on the theories of the Wiener process, lifetime models will be developed for both the constant stress accelerated degradation test (CSADT) and step stress accelerated degradation test (SSADT). In order to obtain more accurate lifetime prediction, an estimator is proposed by including more in-

formation of the degradation data. Experiments are then performed to validate the feasibility of our models.

REFERENCES

[1] Joeyho, *Ledinside estimates automotive led market value to reach us $2.29b by 2020,* http://www.ledinside.com/node/24379 (2015), [online].

[2] A. Tao, *Mid- to low-power leds comprised 70 percent of led revenue in 2014,* https://technology.ihs.com/531481/mid-to-low-power-leds-comprised-70-percent-of-led-revenue-in-2014 (2015), [online].

[3] LeahRae, *Lighting-use led market scale hits us $4.88b, says trendforce,* http://www.ledinside.com/intelligence/2014/7/lighting_use_led_market_scale_hits_us_488b_says_trendforce (2014), [online].

[4] S. P. DenBaars, D. Feezell, K. Kelchner, S. Pimputkar, C.-C. Pan, C.-C. Yen, S. Tanaka, Y. Zhao, N. Pfaff, and R. Farrell, *Development of gallium-nitride-based light-emitting diodes (leds) and laser diodes for energy-efficient lighting and displays,* Acta Materialia **61**, 945 (2013).

[5] Cree Inc., *Cree first to break 300 lumens-per-watt barrier,* http://www.cree.com/News-and-Events/Cree-News/Press-Releases/2014/March/300LPW-LED-barrier (2014), [online].

[6] Cree Inc., *Cree introduces the next generation of xlamp xpg platform,* http://www.cree.com/News-and-Events/Cree-News/Press-Releases/2016/April/Cree-Introduces-the-Next-Generation-of-XLamp-XPG-Platfor (2016), [online].

[7] U.S. Department of Energy, *Led lighting forecast,* http://www.energy.gov/eere/ssl/led-lighting-forecast (2013), [online].

[8] Judy.lin, *Seven challenges lighting designers face when using leds,* http://www.ledinside.com/showreport/2014/3/seven_challenges_lighting_designers_face_when_using_leds (2014), [online].

[9] B. Yan, J. P. You, N. T. Tran, Y. He, and F. G. Shi, *Influence of die attach layer on thermal performance of high power light emitting diodes,* IEEE Transactions on Components and Packaging Technologies **33**, 722 (2010).

[10] N. M. Rada and G. E. Triplett, *Thermal and spectral analysis of self-heating effects in high-power leds,* Solid-State Electronics **54**, 378 (2010).

[11] R. Mueller-Mach, G. O. Mueller, M. R. Krames, and T. Trottier, *High-power phosphor-converted light-emitting diodes based on iii-nitrides,* IEEE Journal of Selected Topics in Quantum Electronics **8**, 339 (2002).

[12] L. Trevisanello, M. Meneghini, G. Mura, M. Vanzi, M. Pavesi, G. Meneghesso, and E. Zanoni, *Accelerated life test of high brightness light emitting diodes,* IEEE Transactions on Device and Materials Reliability **8**, 304 (2008).

[13] S. Buso, G. Spiazzi, M. Meneghini, and G. Meneghesso, *Performance degradation of high-brightness light emitting diodes under dc and pulsed bias,* IEEE Transactions on Device and Materials Reliability **8**, 312 (2008).

[14] C.-C. Tsai, J. Wang, M.-H. Chen, Y.-C. Hsu, Y.-J. Lin, C.-W. Lee, S.-B. Huang, H.-L. Hu, and W.-H. Cheng, *Investigation of ce: Yag doping effect on thermal aging for high-power phosphor-converted white-light-emitting diodes,* IEEE Transactions on Device and Materials Reliability **9**, 367 (2009).

[15] S.-C. Yang, P. Lin, C.-P. Wang, S. B. Huang, C.-L. Chen, P.-F. Chiang, A.-T. Lee, and M.-T. Chu, *Failure and degradation mechanisms of high-power white light emitting diodes,* Microelectronics Reliability **50**, 959 (2010).

[16] B. Saulys, J. Matukas, V. Palenskis, S. Pralgauskaite, and G. Kulikauskas, *Light-emitting diode degradation and low-frequency noise characteristics,* Acta Physica Polonica A **199**, 514 (2011).

[17] B.-H. Liou, C.-M. Chen, R.-H. Horng, Y.-C. Chiang, and D.-S. Wuu, *Improvement of thermal management of high-power gan-based light-emitting diodes,* Microelectronics Reliability **52**, 861 (2012).

[18] D. Liu, H. Yang, and P. Yang, *Experimental and numerical approach on junction temperature of high-power led,* Microelectronics Reliability **54**, 926 (2014).

[19] M.-Y. Tsai, C.-Y. Tang, C. Wang, Y. Tsai, and C.-H. Chen, *Investigation on some parameters affecting optical degradation of led packages during high-temperature aging,* IEEE Transactions on Device and Materials Reliability **15**, 335 (2015).

[20] J. W. Jang, S. Y. Choi, and J. K. Son, *Degradation model of led based on accelerated life test,* in *2011 18th IEEE International Symposium on the Physical and Failure Analysis of Integrated Circuits (IPFA)* (IEEE) pp. 1–4.

[21] L. Zhang, Y. Zhu, W. Wang, X. Bi, H. Chen, K.-S. Leung, Y. Wu, and J. Wu, *Study on ag-plated cu lead frame and its effect to led performance under thermal aging,* IEEE Transactions on Device and Materials Reliability **14**, 1022 (2014).

[22] M. Buffolo, C. De Santi, M. Meneghini, D. Rigon, G. Meneghesso, and E. Zanoni, *Long-term degradation mechanisms of mid-power leds for lighting applications,* Microelectronics Reliability **55**, 1754 (2015).

[23] H. Fan, X. Li, J. Shen, and M. Chen, *An effective prediction method for led lumen maintenance,* in *2012 13th International Conference on Electronic Packaging Technology and High Density Packaging (ICEPT-HDP)* (IEEE) pp. 1560–1563.

[24] Philips Lumileds, *Philips lumileds brings new standards to mid-power leds for illumination,* http://www.lumileds.com/uploads/news/id190/PR178.pdf (2012), [online].

[25] Seoul Semiconductor, *Seoul semiconductor achieves 180 lm/w and cuts cost 50% with new mid-power leds,* http://www.seoulsemicon.com/en/html/company/press_view.asp?Idx=245 (2013), [online].

[26] LeahRae, *Seoul semiconductor launches 3030 to compete with nichia 757 series,* http://www.ledinside.com/news/2013/10/seoul_semiconductor_launches_3030_to_compete_with_nichia_757_series (2013), [online].

[27] Judy.lin, *Philips lumileds targets mid-power led market as lighting market competition intensifies,* http://www.ledinside.com/news/2013/8/philips_lumileds_targets_mid_power_led_market_as_lighting_market_competition_intensifies (2013), [online].

[28] Judy.lin, *Trend of led package manufacturers entering emc lead frame technology to target mid/high power led,* http://www.ledinside.com/intelligence/2013/7/asia_manufacturers_emc_lead_frame_strategy (2015), [online].

[29] B. Bureau, *Mid-power leds will drive market in coming years,* http://bizled.co.in/mid-power-leds-will-drive-market/ (2015), [online].

[30] Z. Liu, T. Wei, E. Guo, X. Yi, L. Wang, J. Wang, G. Wang, Y. Shi, I. Ferguson, and J. Li, *Efficiency droop in ingan/gan multiple-quantum-well blue light-emitting diodes grown on free-standing gan substrate,* Applied Physics Letters **99**, 091104 (2011).

[31] H.-K. Fu, C.-W. Lin, T.-T. Chen, C.-L. Chen, P.-T. Chou, and C.-J. Sun, *Investigation of dynamic color deviation mechanisms of high power light-emitting diode,* Microelectronics Reliability **52**, 866 (2012).

[32] Y. Chiou, T. Chiang, D. Kuo, S. Chang, T. Ko, and S. Hon, *The reliability analysis of gan-based light-emitting diodes with different current-blocking layers,* Semiconductor Science and Technology **26**, 085005 (2011).

[33] S. Chhajed, J. Cho, E. F. Schubert, J. K. Kim, D. D. Koleske, and M. H. Crawford, *Temperature-dependent light-output characteristics of gainn light-emitting diodes with different dislocation densities,* physica status solidi (a) **208**, 947 (2011).

[34] C. M. Tan and P. Singh, *Time evolution degradation physics in high power white leds under high temperature-humidity conditions,* IEEE Transactions on Device and Materials Reliability **14**, 742 (2014).

[35] E. Jung, J. H. Ryu, C. H. Hong, and H. Kim, *Optical degradation of phosphor-converted white gan-based light-emitting diodes under electro-thermal stress,* Journal of The Electrochemical Society **158**, H132 (2011).

[36] Y. P. Zhang, Z.-H. Zhang, W. Liu, S. T. Tan, Z. G. Ju, X. L. Zhang, Y. Ji, L. C. Wang, Z. Kyaw, and N. Hasanov, *Nonradiative recombination—critical in choosing quantum well number for ingan/gan light-emitting diodes,* Optics express **23**, A34 (2015).

[37] Z. Li, K. Li, and H. Choi, *Mechanism of optical degradation in microstructured ingan,* Journal of Applied Physics **108**, 114511 (2010).

[38] X. Chen, S. Wang, M. Chen, and S. Liu, *Phosphor settling induced mechanical degradation of silicone/phosphor composite in light emitting diode packages,* Journal of Applied Polymer Science **132** (2015).

[39] E. Jung and H. Kim, *Rapid optical degradation of gan-based light-emitting diodes by a current-crowding-induced self-accelerating thermal process,* IEEE Transactions on Electron Devices **61**, 825 (2014).

[40] M.-H. Chang, D. Das, P. Varde, and M. Pecht, *Light emitting diodes reliability review,* Microelectronics Reliability **52**, 762 (2012).

[41] M. Meneghini, L.-R. Trevisanello, G. Meneghesso, and E. Zanoni, *A review on the reliability of gan-based leds,* IEEE Transactions on Device and Materials Reliability **8**, 323 (2008).

[42] T. Yanagisawa and T. Kojima, *Degradation of ingan blue light-emitting diodes under continuous and low-speed pulse operations,* Microelectronics Reliability **43**, 977 (2003).

[43] K. Kohler, T. Stephan, A. Perona, J. Wiegert, M. Maier, M. Kunzer, and J. Wagner, *Control of the mg doping profile in iii-n light-emitting diodes and its effect on the electroluminescence efficiency,* Journal of applied physics **97**, 104914 (2005).

[44] A. Torikai and H. Hasegawa, *Accelerated photodegradation of poly (vinyl chloride),* Polymer Degradation and Stability **63**, 441 (1999).

[45] N. Narendran, Y. Gu, J. Freyssinier, H. Yu, and L. Deng, *Solid-state lighting: failure analysis of white leds,* Journal of Crystal Growth **268**, 449 (2004).

[46] J. W. Jang, S. Y. Choi, and J. K. Son, *Degradation model of led based on accelerated life test,* in *2011 18th IEEE International Symposium on the Physical and Failure Analysis of Integrated Circuits (IPFA)* (IEEE, 2011) pp. 1–4.

[47] J.-S. Liou, C.-C. Tsai, W.-C. Cheng, S.-Y. Huang, G.-H. Cheng, J.-K. Chang, J. Wang, and W.-H. Cheng, *Mttf evaluations of encapsulation materials for led package in accelerated thermal tests,* in *16th Opto-Electronics and Communications Conference*.

[48] M. Bahadur, A. W. Norris, A. Zarisfi, J. S. Alger, and C. C. Windiate, *Silicone materials for led packaging,* in *SPIE Optics+ Photonics* (International Society for Optics and Photonics) pp. 63370F–63370F–7.

[49] G. Mura, G. Cassanelli, F. Fantini, and M. Vanzi, *Sulfur-contamination of high power white led,* Microelectronics Reliability **48**, 1208 (2008).

[50] B.-M. Song and B. Han, *Analytical/experimental hybrid approach based on spectral power distribution for quantitative degradation analysis of phosphor converted led,* IEEE Transactions on Device and Materials Reliability **14**, 365 (2014).

[51] N. Narendran and Y. Gu, *Life of led-based white light sources,* Journal of Display Technology **1**, 167 (2005).

[52] M. Zollers, *Phosphor modeling in lighttools,* https://optics.synopsys.com/lighttools/pdfs/ModelingPhosphorsInLightTools.pdf (2011), [online].

2

LITERATURE REVIEW

2.1. THE DEVELOPMENT OF WHITE-LIGHT LED PACKAGES

2.1.1. TYPES OF WHITE-LIGHT LED PACKAGES

ACCORDING to the theory of three primary colors, the white light can be produced by mixing the blue, green, and red lights together. Based on this method, the white-light LEDs can be manufactured by two different technologies. The first one is the so-called RGB LEDs, in which the red, green and blue lights are emitted by different dies [1, 2], as shown in Fig. 2.1(a). These lights are mixed together to produce white lights. The other one is the phosphor-converted LEDs (pc-LEDs) [3, 4], as shown in Fig. 2.1(b). The blue lights pumped from LED chip are down-converted to yellow lights by the phosphor powders. These down-converted lights mixed with the rest blue lights to produce white lights. These phosphor-converted white LEDs (PC-LEDs) can be also achieved by using UV LED plus the combination of red, green, and blue phosphors [5], or using blue LED and the combination of green and red phosphors [6]. The pc-LED is the most popular method in realizing a white-light LED packages, due to its advantages of color tuning, and electrical control.

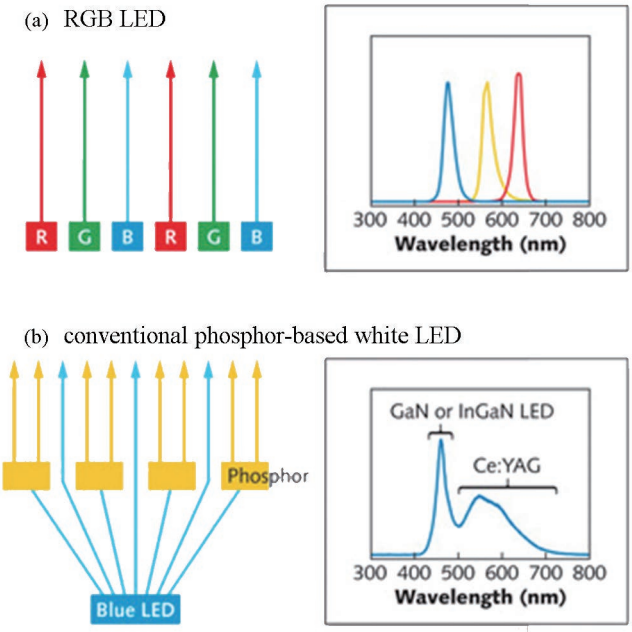

Figure 2.1: Two types of white-light LED packages [7]

On the other hand, according to the input electrical power, the LED packages can

be also categorized as 3 groups, i.e., lower-power, mid-power, and high-power LEDs, as shown in Table 2.1.

Table 2.1: Definition of power LED packages

LED Type	Power
Low-power LEDs	P < 0.2 W
Mid-power LEDs	0.2 W < P < 1 W
High-power LEDs	P > 1 W

However, the definition of the power LEDs always changes time to time, due to the rapid development of the LED illumination industry. A special case is that, for instance, an LED product packaged with 2 mid-power LED chips which are connected in series. The power of this LED product will exceed 1 W if the driving current were higher than 160 mA. In this situation, it is difficult to say it is a mid-power LED or a high-power LED according to the definitions in Table 2.1. In general, it is still considered as a mid-power LED.

2.1.2. STRUCTURE OF WHITE-LIGHT LED PACKAGES

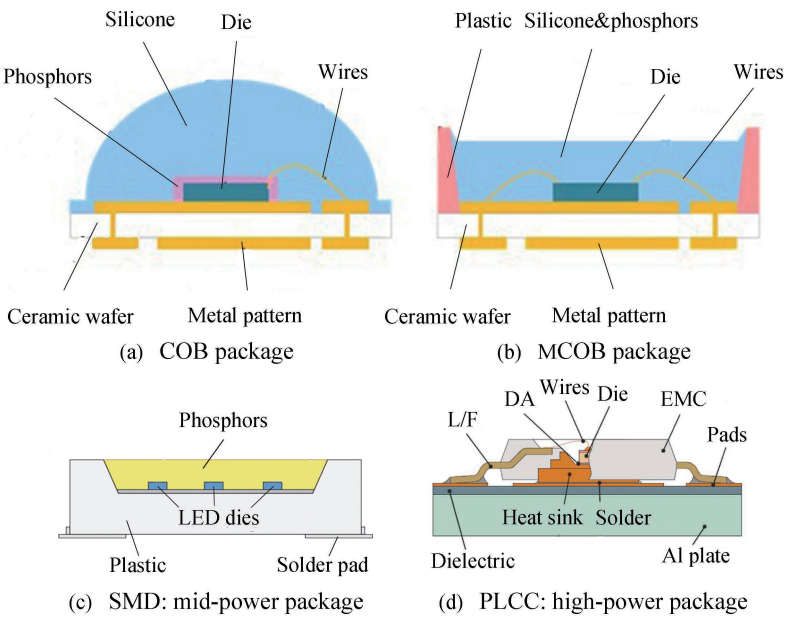

Figure 2.2: Structures of the LED packages

The structures of the LED packages can be different, depending on the types of packages. Fig. 2.2 shows several types of LED packages. In general, the LED package is composed of five components, i.e., blue dies, lead-frames, silicone, phosphor powders, and package housing [8]. The LED dies are connected either by metal wires [9, 10], or in forms of flip chip [11, 12]. Besides, vertical-structured GaN-based blue LEDs are developing, which is considered as a promising technology for realizing high-efficiency and high power LEDs [13, 14]. As a result, the pumped blue lights propagating through the silicone encapsulant, are down-converted to yellow/red lights by the phosphors. These down-converted lights, mixed together with the rest blue light, emitting white-lights out of the LED packages. Table 2.2 lists the components and corresponding materials of the white-light LED packages.

Table 2.2: Package materials of a white-light LED package

Component	Material	Function
LED die	GaN, InGaN, etc.	Blue lights
Phosphors	YAG, nitride-based, etc.	Yellow/red lights
Package housing	PPA, EMC, SMC, etc.	Mechanical protection, light reflection
Lead frames	SiC, AlN, Copper, etc.	Heat dissipation, electrical connection, mechanical protection
Encapsulant	epoxy, silicone, etc.	Light extraction, mechanical protection
Wires	Gold, aluminum, copper, etc.	Electrical connection

2.1.3. WORKING PRINCIPLES OF WHITE-LIGHT LED PACKAGES

The LED is a diode that restricts the direction of movement of charge carriers. The current can flow from the p-type side (the anode) to the n-type side (the cathode), but not in the opposite direction. In a diode a n-type semiconductor is brought into contact with a p-type semiconductor creating a p-n junction [15].

When a p-n junction is first created, mobile electrons from the n-doped region diffuse into the p-doped region where there is a large population of holes (places for electrons in which no electron is present) with which the electrons “recombine”. As recombination proceeds and more ions are created, an increasing electric field develops through the depletion zone which acts to slow and then finally stop recombination. At this point, there is a “built-in” potential across the depletion zone. If an external voltage is placed across the diode with the polarity opposing the bult-in potential, recombination can once again proceed resulting in substantial electric current through the p-n

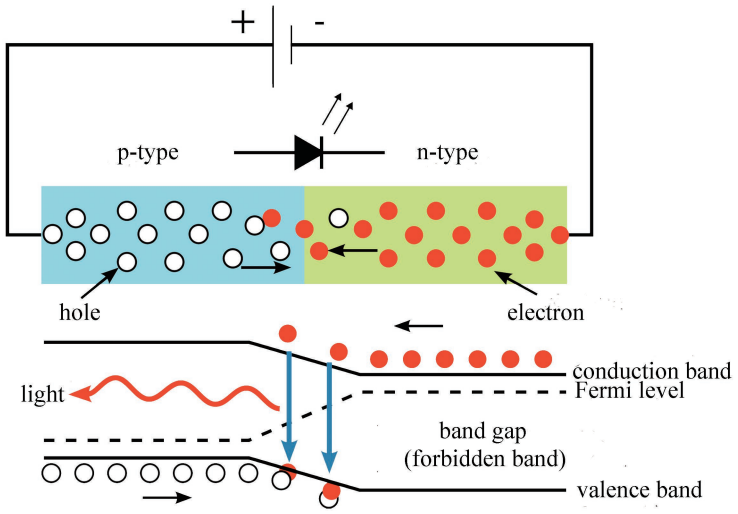

Figure 2.3: Working principles of the LED chip [16]

junction. As a result of the recombination, photons are released and lights are emitted from the LED dies, as indicated in Fig. 2.3. In order to produce blue lights, the LED die is carefully doped with specific dopants, so that it can emits short-wavelength lights with a peak wavelength in the range between 450 and 470 nm. Then, a phosphor layer (usually yttrium aluminum garnets doped with rare earths) is used to convert the short-wavelength radiation emitted by the LEDs into a broad yellow-green spectrum [15]. The sum of the blue peak emitted by the devices and of the luminescence of the phosphors is perceived as white light. The chromatic properties (color rendering index and correlated color temperature) of the white-light source can be tuned by varying the composition of the phosphors. For instance, phosphors based on aluminates can be used to achieve green emission, whereas phosphors based on nitrides generate a luminescence signal in the red spectral region. In an LED based light source, phosphors can be placed some centimeters away from the blue LEDs (remote phosphors) [17, 18], dispersed into the package cup (uniform phosphors/in-cup phosphors) [19], or directly deposited on the LED chip (conformal phosphors/direct phosphors) [20], as indicated in Fig. 2.4. The first approach significantly increases the dimensions of the light source but has the important advantage of minimizing the self-heating of the phosphors, while the last approach generates the most heat dissipation due to self-heating of the phosphors.

Basically, a white-light LED can be characterized by color temperature, color rendering, and luminous flux.

(1) Color temperature. The light source color temperature is determined by compar-

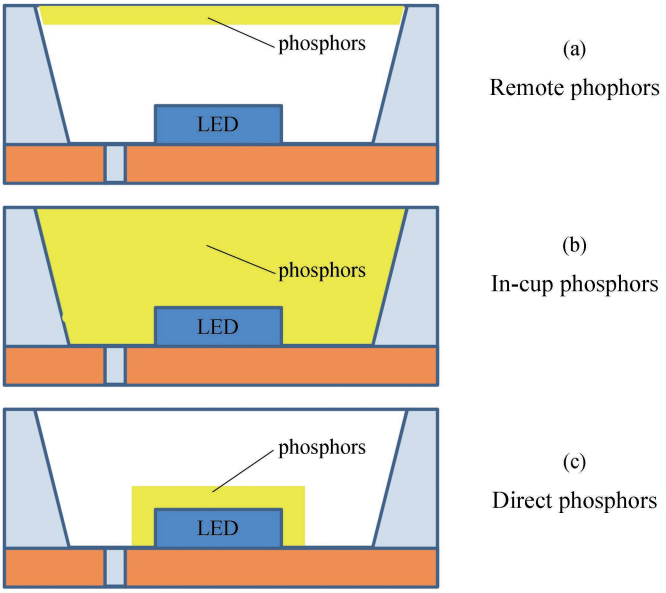

Figure 2.4: Three types of phosphor-converted LED packages

ing its spectra with that of a black body heated between 2000 K and 10000 K, as indicated in Fig. 2.5. For multi-chromatic fluorescent or electroluminescent (LED) sources, which have an irregular spectrum and thus resemble less than the spectrum of a black body, a Correlated Color Temperature (CCT) is calculated. White LEDs have appeared with the development of phosphors that convert blue into a large spectrum or by adding a yellow phosphor and a red phosphor to the blue LED that reduces the color temperature between 2500 K and 5000 K.

(2) Color rendering. The color rendering index gives the capacity of a source to restore the colors of an illuminated object with regards to an ideal source. The color rendering depends on the spectra of lights emitted. The more this spectrum is conditions and thereby closes to that of sun light, the better shall be its rendering. A light source may be used for general lighting as soon as its color rendering exceeds 80%.

A white LED produced from a blue LED covered with yellow phosphor generally had bad color rendering (< 80), as the emitted light lacked red and did not restore this color correctly. Today, with the improvement of phosphors, LED manufacturers have successfully developed white LEDs with a color rendering index greater than 80.

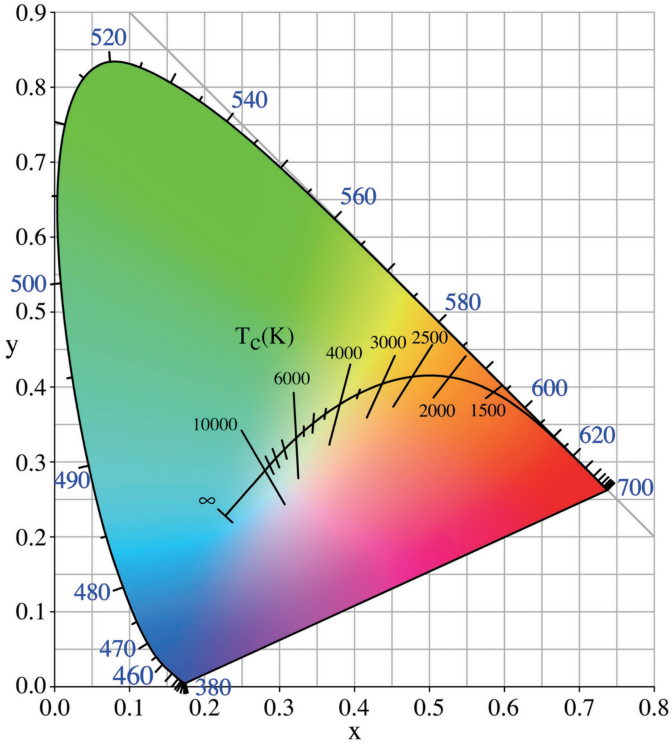

Figure 2.5: The CIE 1931 x,y chromaticity space, also showing the chromaticities of black-body light sources of various temperatures (Planckian locus), and lines of constant correlated color temperature.

(3) Luminous efficiency. The efficiency of a light source is determined by the luminous flux (lm) emitted per unit of power consumed by the light source (W): lumen/Watt (lm/W). The luminous efficiency also takes into account the perception of light by the human eye. This perception varies with the wavelength.

2.2. DEGRADATION OF WHITE-LIGHT LED PACKAGE

2.2.1. EPI-LAYER DEFECT AND DISLOCATION

It is widely reported that crystal defect formations and motions, which exist in the epitaxial layer structure, induce light output degradation during operation [21–25]. Crystal defects such as dislocations reduce the internal quantum efficiency of an LED as they can act as non-radiative recombination centers, thus reduce the light output from active layer [26, 27].

Several models have been developed to describe the degradation of LEDs [28]. Yet

the most popular model for compound semiconductors is based on the multi-phonon emission model [29, 30]. It assumes that during non-radiative recombination the recombination site is adiabatically decoupled from the rest of the lattice and the energy liberated during recombination has no chance to dissipate uniformly via phonon coupling to the whole lattice. Instead, large lattice relaxation occurs. As a consequence of the lattice relaxation, defect reactions such as defect dissociation, creation or migration could take place. Each of these reactions can be thermally activated but the usual thermal activation energy is high – of the order of electron volts – i.e., their probability is extremely low at normal operational temperatures. However, the energy liberated during recombination lowers the thermal barrier to such an extent that the above described defect reactions become viable at operational temperatures. This is why these mechanisms are called recombination enhanced defect reactions. The energy liberated in a recombination process depends on the depth of the recombination site. The energy liberated usually increases with increased band gap.

Defects introduced during crystal growth are classified into two types: interface defects and bulk defects [31]. Defects belonging to the former type are stacking faults, V-shaped dislocations, dislocation clusters, micro-wins, inclusions, and misfit dislocations, and the latter group includes precipitates and dislocation loops. Moreover, extended defects such as threading dislocations and micro-pipes gathering point defects were reported [32]. Defects in the substrate can also be propagated into the epi-layer.

The degradation rate related to dislocation motion seems to be high. Such degradation is attributed to defect motion enhancement by non-radiative recombination at the defects [33]. During the LED operation process in which an amount of heat assembled in the active region, the dislocation generated defects can rapidly propagate through the crystal via climbing or gliding processes and become a network of non-radiative regions [34]. The dislocation climb motion is caused by point defect multiplication, which is led by the recombination enhancement effect. It is known that dislocation glide motion in semiconductors is dominated by the Peierls mechanism and that the dislocation velocity (V_d) of semiconductors depends on applied shear stress as the driving force of dislocation glide motion (τ) and dislocation mobility (μ), as shown in the following equations [33, 35]:

$$V_d = \tau \mu \tag{2.1}$$

$$\mu = V_0/\tau_0 \exp(-E_d/kT) \tag{2.2}$$

In the above, V_d is the activation energy of dislocation motion, T is the temperature, V_0 is a constant, and τ_0 is a constant (1 MPa). The dislocation mobility is defined as the

dislocation velocity under an applied shear stress of 1 MN/m^2. The applied shear stress (τ) is caused by internal misfit strain, thermal strain, and external mechanical strain.

Degradation modes of defect generation in LED dies are divided into 2 types: rapid degradation and gradual degradation [36]. Rapid degradation was found to be related to the generation or growth of dark spot/line defects. Two primary causes for the dark spot defects were identified as precipitation of host atoms and the migration of electrode metal into the semiconductor, respectively. The generation of dark spot defects occurs associated with an increase in leakage current. The gradual degradation, as reported by Cao *et al.* [37], is attributed to defect generation in the active layer or the cladding layers. These defects act as non-radiative recombination centers and carrier tunneling channels. Slow generation or reaction of defects in the space-charge region, especially point defects such as vacancies and interstitials, which result in more carrier tunneling into the QW region [38]. Defect complexes associated with the deep levels could be the original source of the point defect reaction [31]. Gradual degradation then proceed as follows: (1) non-radiative recombination occurs at some defects, which causes a point defect reaction and fresh point defect generation; (2) the new defects can also act as non-radiative recombination centers, thus we have positive feedback for these two processes; (3) the generated point defects migrate and condense at some nucleation centers; (4) defect clusters and/or micro-loops are formed as byproducts [31]. Typical characteristics of gradual degradation are slow decrease of output power, uniform darkening of the active region or formation of dark-spot defects (DSDs), and an increase in deep levels. The increase of defect density due to aging is observed most clearly in the low bias $I-V$ characteristic of LED. The overall light emission intensity decreased due to aging, can be explained with use of the continuity equation for the injected electron density n [39], which is shown as follows.

At steady-state conditions $dn/dt = 0$, the light emission intensity L at low forward current where non-radiative recombination of carriers is dominating. This implies that Eq. (2.3) holds if $AN_0(t)n(t) \gg Bn^2(t)$.

$$L = Bn^2(t) \approx (B/A^2)(J/ed) \tag{2.3}$$

where $n \approx (1/A)(J/ed)$, derived from continuity equation at steady-state condition by considering $AN_d(t) \gg Bn^2(t)$. L is quadratic with current density J, representing the low current region. As the current density increases the radiative recombination of carriers start to dominate, i.e., $AN_0(t)n(t) < Bn^2(t)$, and the light intensity L increases linearly with current density. The non-radiative recombination coefficient A can be ex-

pressed by the Shockley Hall Read recombination rate [40]:

$$A = N_d(t)\nu_{th}\sigma$$

where $N_d(t)$ is the defect density of traps, ν_{th} the carrier thermal velocity and σ the electron capture cross section. An increased defect density $N_d(t)$, will reduce the total light intensity L for a certain value of the forward current.

Based on the continuity equation, it can be concluded that the generation of defects in the active region during the aging process reduce the light output from the LED in the low current region of the $L-I$ characteristic. At higher current values these non-radiative recombination channels are saturated, so their effects have disappeared. That is, the positive stress effect becomes evident in the luminescence spectrum [38]. With the increasing of injected current into an LED, the luminescence efficiency can reach a higher value and maintain the same efficiency at higher current densities until current induced thermal effects play a significant role in the luminescence efficiency. However, David S. Meyaard *et al.* [41] reported that the drop in light output being attributed to two different mechanisms: the increase in Shockley-Read-Hall recombination and the increase in the electron leakage from the active region. Either of these effects alone cannot explain the downward shifting trends of external quantum efficiency (EQE) at both high and low current levels. Under normal operating current densities, a combination of increased SRH recombination and the increase in the electron leakage are shown to contribute to reduced light output from the device at high temperatures. Therefore, in order to improve the high temperature performance of LEDs, two issues must be considered: reducing dislocation density to minimize Shockley-Read-Hall recombination and eliminating the cause of the electron leakage.

The light output degradation of LEDs is highly dependent on drive current and temperature [30, 42, 43]. The degradation was a result of an increased non-radiative recombination in the active region during ageing test. The mechanism is related with the generation of defects in the active region and cladding regions due to the high current flow through quantum well structure and the increase of light emitting diode chip temperature [40].

2.2.2. DOPANT DIFFUSION FROM P-LAYER TO EXPI-LAYER

Sufficient control of p-type conductivity is one of the most important subjects to improve the performance of LED devices using III–V nitrides. In order to improve the p-type conductivity, Mg has been commonly used as the acceptor dopant for III–V ni-

trides [44]. However, Mg diffuses to the quantum wells (QWs) during the growth of p-GaN layer, may result in a decrease of the emission efficiency of multiple quantum-well (MQW) because the Mg can act as the non-radiative recombination center [45]. In addition, the non-radiative transition of carriers from the conduction band of multi-quantum wells (MQWs) to an acceptor level of the deep donor acceptor pair (DDAP) is possible since the acceptor level of the DDAP bands in the p-GaN layer is located above the valance band of the MQW in UV LED [46]. This parasitic carrier transition process can compete with the main radiative emission process in the MQWs, leading to a further decrease in the quantum efficiency of the LED.

Preliminary report has demonstrated that the efficiency of GaInN QW LEDs is very sensitive to the Mg concentration in the AlGaN/Mg barrier [47]. Too high Mg concentrations in close vicinity to the GaInN QWs tend to increase nonradiative recombination rates, whereas a too low Mg concentration results in an insufficient hole injection into the active region. K. Köhler *et al.* [45] claimed that the actual Mg profile close to the active region was found to be influenced by segregation as well as by diffusion during growth. Starting from low growth temperatures an increase in Mg concentration close to the active region results in an improved hole injection and thus increased electroluminescence (EL) efficiency. However, for a too high growth temperature, an excessive spread of the Mg atoms into the active region leads to non-radiative recombination in the QW active region and thus a reduction in EL output. Min-Ki Kwon *et al.* [48] investigated the effect of Mg concentration in the p-layer by comparing LEDs with different doping profile- gradually doped p-GaN:Mg layer (GD p-GaN) and uniformly doped p-GaN:Mg layer (UD p-GaN) and concluded that the improved performance of former one could be attributed to the decrease in diffusion of Mg into MQWs and the suppression of electron transport from the conduction band of the MQW to the acceptor level of the deep donor acceptor pair bands in the p-GaN layer by a gradient doping of Mg in p-GaN layer. Improper annealing condition may cause the degradation of the p-GaN layer. Thermal treatment was usually conducted on Mg doped post-grown GaN to activate Mg dopant. It has been reported that by increasing the annealing duration under certain temperature, the monotonic decrease was found in the trap center concentration, activation energy and capture cross section, indicating Mg activation during the annealing process [49]. In the case of thermal annealing, it is supposed that Mg activation occurs through thermal dissociation of Mg–H complexes and the removal of hydrogen. Thermal release is impeded by the high stability of the passivated state, and this can cause retention of the H to temperatures where degradation of the semiconductor may occur [50]. Furthermore, a significant dependence of the semiconductor resistivity on the du-

ration of annealing in O_2 was also observed [51]. The resistivity increased slightly after longer activation times. The reason for the increase in resistance of the GaN with prolonged activation is not known, but penetration of oxygen into the p-GaN is a possible cause.

It was considerd that the metastable dopant behavior could be triggered at high temperature or high injected current [52]. M Pavesi *et al.* found thermal quenching of InGaN/AlGaN/GaN LED over 200 K from the spectral and spatial homogeneity of the device emission verified by acquiring CL spectra. It suggests a donor-to-acceptor pair nature for the optical transition, related to native donor levels and to shallow acceptor levels resulting from the formation of Mg related metastable complexes (possibly Mg–H_2) due to a combined electrical and thermal effect [32]. G. Meneghesso *et al.* [53] reported the apparent carrier density increases and reduction of the junction depletion width in GaN LEDs under long term DC aging test. The authors attributed this to the decomposition of Magnesium (Mg) complexes, Mg reactivation and to the non-radiative recombination centers.

2.2.3. ELECTRICAL CONTACT METALLURGICAL INTER-DIFFUSION

The increase in contact resistance is thought to be caused by thermally activated metal–metal and metal–semiconductor inter-diffusion [54, 55]. M. Meneghini *et al.* [56] identified that emission crowding and series resistance increase, was attributed to the thermally-activated indiffusion of hydrogen from the passivation to the p-layer, and subsequent p-doping compensation. A reduction of the active acceptor concentration, due to the interaction between hydrogen and magnesium, can worsen the properties of the anode contact, changing its transport characteristics, and vary the resistivity and injection properties of the p-layer, thus leading to the measured $I-V$ modifications. The degradation process is thought to take place mainly out of the pad region. Therefore, after stress, current should have a preferential path under the pad, and emission should be mostly concentrated in this region. This may be the mechanism concentrating the emission near the contact, and reducing the overall output power.

High injected current into the LED or high ambient temperature is considered as the causes which result in the increase of contact resistance. Matteo Meneghini *et al.* [57] studied thermally activated failure mechanisms of unpackaged InGaN/GaN LEDs. The authors found decrease of the optical power (OP) after thermal treatment. The OP degradation was found to be more prominent for high measuring current levels. The OP degradation is attributed to the significant crowding of the light emission around the central pad of the devices, resulting in a significant reduction of the effective con-

duction and emission area. G. Meneghesso *et al.* [53] studied the reliability of blue LEDs submitted to DC aging test and found that the increase of the parasitic series resistance, is attributed to degradation of the semi-transparent ohmic contact on top of the p-layer, and induces increasingly severe current crowding effects at increasing the current during tests.

2.2.4. DIE CRACKING

A few researchers reported light output degradation induced by die cracking during life test [58]. The crack propagated through the p-contact and the active layer thus isolating part of the LED from the electrical stimulus and reducing its light output accordingly.

One of the possible causes is that, during die manufacturing, silicon wafer is subjected to several stressful steps, i.e. backside grinding and wafer cutting (dicing), before dies can be used for packaging [59]. At the grinding stage, radial grinding marks are generated on the wafer backside face as a result of wafer thinning via coarse and fine grinding wheels. Furthermore, micro-cracks are induced along the edges of dies after stringent cutting processes. Possible residual stresses are also built up along with the addressed geometrical defects. In general, these die defects will degrade the strength of a silicon die and serve as the origins of cracks initiation and propagation during subsequent assembly steps such as die attach, epoxy curing, molding, and post mold cure. Micro-cracks from improper cutting process serving as crack initiator and further reduces the die strength.

Die damage is also caused during wire bonding process. If the bonding pressure is bigger than the limit pressure that the die can endure, the die will be damaged [34]. Fracture of silicon dies occurs not only in the package assembly phase, but also at various stages of reliability tests necessary for package qualification.

With these micro-cracks resulting from manufacturing, extreme thermal shocks can break the dies of LEDs. Due to the mismatch of thermal expansion coefficients of the package materials, high thermal stresses arise at operating temperatures and micro-cracks propagate, finally lead to failure of the device [60]. On the other hand, LED packages can be subjected to mechanical stress when a high drive current is applied (which causes Joule heating at a fast rate) or when high ambient temperature conditions are suddenly applied [61].

2.2.5. ENCAPSULANT CARBONIZATION

Some researchers reported that the carbonization of encapsulant was mainly due to a combination of Joule heating and the elevated ambient temperatures [62], which was

often found in high-power white-light LED packages during high temperature bias test. The most apparent evidence is the blackening of encapsulant, near the top surface of the blue chip, or near the lead frame [63]. A significant Joule heating due to the high resistances of the Ohmic contacts [64], the n-type and p-type cladding layers [65, 66], and the degradation of heat conduction materials [67, 68] were reported during operation applications [69, 70]. Self-heating induces serious carbonization if the junction temperature is higher than the critical temperature of encapsulant carbonization. Under the applied current, the short wavelength emission could make the plastic packaging material close to the chip surface degraded. The working chip will give rise to the ambient temperatures and the high temperatures may accelerate the degradation process. At the same time, because of the oxygen existing on the surface of the plastic, some chemical reactions occurred on the interface between the chip and the plastic on the high temperatures. The plastic encapsulation material on the diode surface could be carbonized. Then the carbonized plastic deposited on the chip surface equably and formed the black stains at last [71]. In turn, carbonization decreases the encapsulant's insulation resistance, significantly inhibiting its ability to provide electrical insulation between adjacent bond wires and leads. This phenomenon can initiate a runaway process in which current through the plastic increases as its insulation resistance decreases, leading to joule heating of the plastic. This Joule heating further decreases the insulation resistance and can eventually cause combustion of the encapsulant [72, 73].

Another potential carbonization mechanism is the phosphor self-heating [74, 75]. For white-light LEDs, green/red phosphors are applied to down-convert the blue light spectra to a longer wavelength, i.e., green/red lights. Unfortunately, not all absorbed blue lights are transferred to green/red lights. Due to non-radiative transfer and Stokes shift, part of the absorbed blue lights is released in terms of heat [76]. Due to low quantum efficiency, during the light conversion, localized heating of small particles of phosphor occurs [77]. The heat accumulation increases rapidly at higher operating ambient temperature [78], because of the thermal quenching characteristic of phosphors [79, 80]. This results from the enhancement of cascade multi-phonon relaxation, a temperature dependent energy transfer or crossover process [81]. Based on this analysis, some researchers reported a much higher temperature inside silicone than the junction temperature of blue chip. Results showed that as small as 3-mW heat generation on a 20-μm diameter spherical phosphor particle might lead to excessive temperatures which can be a major source of light output degradation and reliability concern for high brightness LEDs. The temperature inside the silicone volume varied from 195 °C to 316 °C [74, 82–84], depending on the LED products.

In addition to the effects of Joule heating and phosphor self-heating, shorter wavelength irradiation damage is considered as another possible root cause of encapsulant carbonization. For a practical LED package under the blue light radiation, high temperature and a small amount of oxygen, epoxy resin will be gradually discolored. This is due to the opening of C-O and C=O bonds, and the dissociative C and O atoms occurring on the die surface. Finally a large amount of carbon or carbon oxide could accumulate on the interface between die and encapsulant, resulting in a black zone and darkening of the die surface [85].

The carbonization acts as a barrier that stops any light reflection from the plastic ring that covers the outer edge of the copper cup that hosts the chip [86]. Either high drive current or excessive ambient temperature can induce encapsulant carbonization. Daniel L. Barton *et al.* [62] conducted tests with various driving currents, in corresponding to different junction temperatures. The author stated that the rapid degradation observed at higher currents was correlated to carbonization of the plastic encapsulation material on the diode surface, which leads to the formation of a conductive path across the LED and subsequently to the destruction of the diode itself. Their test result showed that the temperature where the degradation begins to affect the encapsulant in a time frame important to LED is thought to be between 135 °C and 145 °C. Zhou *et al.* [85] studied the reliability of a high power LED packaging and found that the thermal overstress on the epoxy along the interface owing to the high junction temperature is the main factor to degrade the epoxy gradually. EDAX results illuminates that the percentage of C and O elements in failed samples is higher than that in the normal one. The presence of oxygen observed on the surface of degraded LED die is associated with the darkening. As a result, a darkening area made up of carbon as well its oxide occurs on the LED die surface and depresses the luminous efficiency.

2.2.6. POLYMER MATERIALS YELLOWING

Except for carbonization which is observed at extreme conditions, yellowing of the polymer materials was reported during long-term operating [87–89]. The yellowing can be frequently observed at the packaging materials, including polycarbonate [90], epoxy [91], and silicone [92]. Yellowing increases light output degradation because it reduces the package transparency/reflectivity, and finally decreases light extraction from the package [58, 62]. Either thermal ageing or UV/blue lights exposure induces packaging materials yellowing [90].

Mehr *et al.* [93] found that formation of oxidation products is identified as the main mechanism of yellowing for the polycarbonate which was aged by thermal stress. Ther-

mal ageing of polycarbonate lens could significantly deteriorate the optical properties of LEDs. It was postulated that side chain and ring oxidations are likely to take place during thermal degradation [90, 94]. Rearrangement and oxidation in polycarbonate could result in discoloration and yellowing of polycarbonate encapsulant materials [95–97]. Discoloration due to the formation of oxidation products and rearrangement (Fries) products or a combination of them could result in a decrease in the transmission of polycarbonate plates. Depending on the temperature the degradation mechanism could be altered. It is believed that the higher the temperature, the more important the influence of rearrangement products on yellowing is [96]. Factor *et al.* [98] showed that the main reason for discoloration and yellowing of thermally-aged polycarbonate is the formation and subsequent oxidation of phenolic end groups.

The degradation of the polycarbonate under UV/blue lights exposure, has been attributed to two different mechanisms: photo-Fries rearrangement and photo-oxidation [99–102]. Rivaton *et al.* [99] reported that the photo-Fries rearrangement reaction is more likely to occur at wavelengths shorter than 300 nm, whereas photo-oxidation reactions are more important when light of longer wavelengths (> 340 nm) is used. On the other hand, Diepens *et al.* [103] argued that the photo-Fries rearrangement products are also formed, when wavelength longer than 300 nm are used. Mehr *et al.* [104] indicated that there are two stages in the yellowing of polycarbonate plates when aged under blue lights exposure. The first stage induces very slow rate of yellowing, and then the second yellowing stage, where the yellowing is accelerated and the rate of yellowing is comparatively faster. Both photo-Fries and photo-oxidation products are identified as the mechanisms of photo-degradation. However, photo-Fries reactions could have more important influences on the yellowing, compared to the oxidation reactions.

Severe yellowing have been found in high-power LED packages with epoxy encapsulants [105]. The yellowing issue of optical grade epoxy occurs during the exposure of the epoxy encapsulant to blue or UV light. Yellowing of epoxy encapsulant also occurs when the encapsulant material is subjected to large amounts of heat. In high-power LED packages, there are large amounts of heat generated and accumulated inside the package, especially around LED chips, resulting in yellowing of epoxy encapsulant surrounding LED chips. The yellowing of the epoxy results in a significant loss of light output over time. Typically, this phenomenon is due to the aromatic group or free radical in the epoxy encapsulant [106]. Hsu *et al.* [107] found that the epoxy can have dissociated easily to form free radicals at high temperatures. As a result, epoxies form many different types of chromophoric structure, including the yellow quinone structure [108]. The presence of free radicals enhances the formation of these types of chromophoric

group. Furthermore, a very small amount of chromophoric group can cause a dramatic yellowing of the polymer.

Because of the heat generated during LED operation, siloxane-based encapsulants have recently been preferred as an alternative to epoxy-based encapsulants [109, 110]. In particular, a siloxane containing methyl groups shows high thermal stability and low refractive index, a phenyl-siloxane has an improved refractive index due to the high polarizability of the phenyl groups [111]. However, at high temperatures, the transparency of the phenyl-siloxane encapsulant can be reduced by yellowing, since the phenyl groups are susceptible to thermal oxidation and cleavage from the siloxane backbone [112]. Bae *et al.* [113] observed the yellowing of the siloxane-based encapsulants at an elevated temperature (180 °C) due to its high catalyst content (200 ppm) and the presence of unreacted groups, probably due to the thermal oxidation and cleavage from the siloxane backbone of the un-crosslinked vinyl groups or phenyl groups. The linear siloxane bonds are cut during thermal pyrolysis, forming ring structures. During the pyrolysis process, the phenyl radical is cleaved from the siloxane chain and causes the discoloration to yellow [114]. Moreover, the authors also indicated that high non-polymerized methacrylate groups, can lower the optical transmittance and thermal stability. This behavior is interpreted by thermal degradation of methacylate groups in the silicone hybrimers. That is, non-polymerized methacrylate groups can be the source of yellowing in thermal degradation [115].

2.2.7. LEAD-FRAME DETERIORATION

As a non-hermetic LED package which uses silicone for encapsulants, it cannot prevent toxic chemical elements (S, Cl, etc.) and moistures from the package. As a consequent, the lead frames are easily contaminated during use operations [116]. As a typical failure in the mid-power LED packages, silver–sulfur compounds have been detected at the internal lead frame of several commercial plastic packaged white LEDs [117]. The sulfur contamination resulted all electrically open or degraded at the switching-on after mounting on the final boards. The authors attributed the failure to the in-diffusion of S-rich moisture from the surrounding atmosphere, possibly in a highly contaminated environment. Moreover, Zhang *et al.* [118] concluded that the failure process underwent delamination between lead frame and reflector polymer composites followed by chemical penetration, composite corrosion, silver migration, and finally caused blackening failure. Delamination and corrosive de-flash agent were considered as the key factors for the failure mode. The possible chemical reactions can be listed as follows

[119]:

$$4Ag + 2H_2 + O_2 \rightarrow 2Ag_2S + 2H_2O \tag{2.4}$$

$$2Ag + SO_2 + O_2 \rightarrow Ag_2SO_4 \tag{2.5}$$

The other degradation mechanism of the lead frame is copper diffusion during thermal ageing test [120]. During thermal storage, Ag plating layer recrystallization first takes place, and Cu diffusion through Ag layer initializes at the same time. The time that Cu appears on lead frame top-surface depends on the thickness of the plating layer. Meanwhile, the contamination ions (mainly chlorine) in the air can react with the lead frame surface. Thermodynamically, the diffused Cu can nucleate as particles after reach certain supersaturation degree. The particles pile up when more nuclei generate. Under thermal aging condition, the particles are very active, which can react with the oxygen in atmosphere. Finally, these particles can form as bands so as to decrease the surface energy. The optical reflectance decrease is consistent with the formation and growth of the Cu particles, as well as the transformation of the surface morphology.

2.2.8. PHOSPHOR THERMAL QUENCHING AND DEGRADATION

In white LEDs, light is generated through the combined use of a blue semiconductor chip, and a phosphor layer, which emits radiation in the yellow-green spectral region. The choice of the material system used for the realization of the phosphors allows one to tailor the emitted spectrum [121].

Thermal quenching is one of the important technological parameters for phosphors used in white LEDs [122–124]. Phosphor thermal quenching induces light output degradations, include a decrease in light output, color shift, and the broadening of full width at half maximum (FWHM). With increasing temperature, the non-radiative transition probability by thermal activation and release of the luminescent center through the crossing point between the excited state and the ground state increases and then quenches the luminescence. The electron phonon interaction is enhanced at high temperature as a result of increased population density of phonon, which broadens FWHM. The integral emission intensity, proportional to the quantum efficiency, decreases slightly less than the peak intensity. To better understand the temperature dependence of photoluminescence and to determine the activation energy for thermal quenching, the Arrhenius equation was fitted to the thermal quenching data [59]:

$$I(T) = \frac{I_0}{1 + c \times \exp\left(\frac{-E}{kT}\right)} \tag{2.6}$$

where I_0 is the initial intensity, $I(T)$ is the intensity at a given temperature T, c is a constant, E is the activation energy for thermal quenching, and k is Boltzmann's constant.

Except thermal quenching, literature also found remarkable degradation of phosphor, when exposure to long-term stress tests at moderate/high temperature levels [121]. Degradation mainly consists in a decrease in conversion efficiency and in worsening of the chromatic properties of the light-emitting diode–phosphor system. Samples exposure to high temperature stress (T > 85 °C) can lead to a remarkable degradation of the efficiency of the phosphor plates, which maintain a linear response even after stress. As a consequence, the chromatic properties of the LED-phosphor systems can be significantly compromised: at the highest stress temperatures, the correlated color temperature can show a remarkable decrease. On the other hand, Tan *et al.* [125] detected phosphor degradation and dissolution, and diffusing of Zn activator for LED packages aged at high temperature–humidity conditions.

2.2.9. DELAMINATION

Delamination was reported as one of factors which cause light output degradation of LED packages [126]. Delamination may occur between chip surface and silicone encapsulant, between die and die attach, between lead frame and silicone encapsulant, between encapsulant and lead frame [127–129]. The light output degradation might be caused either by random scattering of phosphor [126] or by contamination of the LED package [117].

Thermal stress as well as moisture absorbed by the packages is considered to be the main cause for the delamination in electronic packages [130]. The mismatching coefficients of moisture expansion (CMEs) will induce hygro-mechanical stress in the package. The mismatching coefficients of thermal expansions (CTEs) in LED packages induce thermal stress when the package is heated in the reflow soldering process. And the presence of moisture in packages reduces interfacial adhesion strength and leads to delamination.

Luo *et al.* [131] reported that the moisture-induced stress was much lower than the thermal-induced stress in the same LED package, because the temperature of a LED module can reach steady after 1.5 minutes while its moisture field needs 46 days to reach balance. While E. H. Wong *et al.* [132] studied the mechanics and impact of hygroscopic swelling of polymeric materials in electronic packaging and found that the hygroscopic stress induced through moisture conditioning was significant compared to the thermal stress during solder reflow. It is because differential swelling occurs between the polymeric and non-polymeric materials, as well as among the polymeric materials consti-

tuting the electronic packages. This differential swelling induces hygroscopic stress in the package that adds to the thermal stress at high reflow temperature, raising the susceptibility of package to popcorn cracking.

The simulation results [126] show that voids and delaminations in the die attachment would enhance the thermal resistance greatly and decrease the LED's light extraction efficiency, depending on the defects' sizes and locations generated in packaging. The authors also stated that delamination between die and phosphor layer decreases the LED's relative light extraction efficiency when the ratio of the delamination length to the chip's length increases. However, the tendency of the decrease is small, and only 4% of light is lost at most even when the ratio of delamination length to chip size reaches 65%.

2.3. RELIABILITY TESTING METHODS

The reliability of LED packages has been studied by using a variety of accelerated testing methods, depending on the research objectives [13, 133–135]. It is known that the luminescence efficiency drops by about 15% and the lifetime shortens by half when the LED junction temperature increases by 10 °C. The increased LED temperature results in lower quantum efficiency, a shorter lifetime, and a color temperature shift due to a transition of the emission wavelength [136]. As a result, thermal performance has become a popular topic in the LED reliability [24, 27, 137, 138]. On the other hand, the humidity effect on the plastic LED packages has also attracted many concerns [139–142]. Fan *et al.* [143] demonstrated that WHTOL test could be used for prediction of LED lumen maintenance with rather short testing time, and life testing (HTOL) data for each mid-power LED under same testing condition show they follow the trend of WHTOL data as well. Recently, LED manufacturers are making efforts to improve the sulfur resistance, because silver-coating lead frames are widely used as the reflecting surface, which is very sensitive to sulfur and its compounds [117]. Sulfur test has been implemented by the LED industry, though few publications were found about the effects of sulfur on LED reliability [144–146]. However, as a new type of products, there are few test standards for the white-light LED packages [147]. Instead, LED manufacturers refer to the JEDEC standards, which are generally used in the reliability testing for IC products. Table 2.3 shows the reliability test plan for one type of mid-power white-light LED packages.

Table 2.3: Reliability test plan for the white-light LED packages

Test	Test standard	Stress condition
TPOL	Internal test	85 °C @ 120 mA, 10% duty cycle, 1 ms On/9 ms Off.
LTOL	JESD22-A108	-40 °C @ 100 mA.
HTOL	JESD22-A108	85 °C @ 100 mA.
WHTOL	JESD22-A101	85 °C/85%RH/1atm. @ 100 mA, 1 hour ON/OFF.
PTMCL	JESD22-A105	-40 °C to 85 °C @ 100 mA, 10 min dwell, 20 min transfer, with current 5 min ON, 5 min OFF.
TMCL	Internal test	no bias, -40 °C to 100 °C, 5 min dwell, 10 min transfer, 2 cycles/hour.
LTSL	JESD22-A119	no bias, @ Tb = -40 °C.
HTSL	JESD22-A103	no bias, @ Tb = 100 °C.
WHTSL	Internal test	no bias, @ Tb = 85 °C / 85%RH.
TMSK	Internal test	no bias, air-to-air, -40 °C to 100 °C, 30 min dwell, 10 seconds transfer, 1 cycle/1 hour.
MSL	JSTD-020D	Moisture sensitivity level 3: preconditioning at 30 °C and 60%RH for 192 hours, followed by 260 °C Pb-free reflow solder profiles. Reflow needs to be completed between 15 minutes and 4hrs after precondition.
ESD/HBM	JESD22-A114	HBM, 1 kV
Salt Spray	JESD22-A107	Tb = 35 °C, pH = 6.0-7.5, 30 gm/m^2/day.
H_2S	IEC60068-2-43	Concentration: 10±1 ppm H_2S, temperature: 25±2 °C, relative humidity: 75±3%; exposure time: 4, 7, 14, or 21 days.
VVF	JESD22-B103	12 sweeps = 4 sweeps per XYZ axis, 20-2000 Hz log sweep in 4 minutes (1 decade/minute), 80 Hz crossover, 1.5 mm displacement below & 20 G acceleration above crossover.

2.4. DEGRADATION MODELING

Traditionally, reliability assessment of devices has been based on accelerated life tests (ALT). However, for highly reliable products as LED packages, little information about reliability is provided by either the high temperature operating life tests (HTOL), or the wet-high temperature operating life tests (WHTOL), in which few or no failures are typically observed [143]. As the LEDs' lifetime has been claimed as high as 35,000 hours [148], for LED manufacturers, it is unacceptable to perform such an ALT to get enough failure data. Fortunately, there are some characteristics that degrade over time, which can be used as indicators of LED degradation. These characteristics includes lumen output [149], color shift [150], electrical parameters [151, 152] , and so forth.

One alternative instead of the ALT-based lifetime modeling, is to monitor the LEDs' lumen output for a period of time and assess its reliability from the changes in performance observed during that period. According to this methodology, a standard of the

lifetime prediction for LED packages/modules, was released and widely applied in the LED industry in the year of 2011 [153]. However, this standard uses average normalized lumen maintenance data and performs non-linear regression for lifetime modeling, so it cannot capture the failure distribution, although the failure distribution is much more relevant in reliability analysis. This may be not effective for maintenance decision making by either LED manufacturers or designers.

Many efforts have been made to develop lifetime models by using degradation data, and a few statistical methodologies were proposed [154–157]. Among them, the general path model (regression model) [155, 158, 159] and the stochastic model [160, 161] are two of the most popular models. Furthermore, Bayesian network was also introduced into the models to obtain more accurate lifetime prediction [162–164].

2.4.1. REGRESSION MODEL

In a degradation test, measurements of performance are obtained as it degrades over time for a random sample of test units. Thus, the general approach is to model the degradations of the individual units using the same functional form and differences between individual units using random effects. The model is [165]:

$$y_{ij} = D(t_{ij}; \boldsymbol{\alpha}, \boldsymbol{\beta}) + \epsilon_{ij} \tag{2.7}$$

where $D(t_{ij}; \boldsymbol{\alpha}, \boldsymbol{\beta})$ is the actual degradation path of unit i at a pre-specified time t_{ij}; $\alpha = (\alpha_1; \alpha_2; \ldots; \alpha_p)^T$ is a vector of fixed effects which remains constant for each unit; $\beta = (\beta_1; \beta_2; \ldots; \beta_p)^T$ is a vector of random effects which vary according to the diverse material properties of the different units and their production processes or handing conditions, and ϵ is the associated random error of the i_{th} unit at time t_{ij}. The $\epsilon_{ij} (i = 1, \ldots, n; j = 1, \ldots, m_i)$ are assumed to be independently and identically distributed (iid) with zero mean and unknown variance σ_ϵ^2.

Failure definition for the general degradation path models is that the performance measurement y_{ij} exceeds (or is lower than) the critical threshold D_f at time t , and pdf is the probability density failure distribution of samples. The cumulative probability of failure function $F(t)$ is given as follows:

$$F(t) = P(T \leq t) = P(D(t; \boldsymbol{\alpha}, \boldsymbol{\beta}) \geq D_f) \tag{2.8}$$

when the degradation measurements are increasing with time or

$$F(t) = P(T \leq t) = P(D(t; \boldsymbol{\alpha}, \boldsymbol{\beta}) \leq D_f) \tag{2.9}$$

when the degradation measurements are decreasing with time.

To estimate the time to failure distribution, $F(t)$, based on the degradation data, several statistical methods have been proposed by researchers, including the approximation method [164], the analytical method [166], the two-stage method and others [167]. These methods can be performed by involving two basic steps: (1) estimating the parameters for degradation path model by using nonlinear least square regression; (2) evaluating the time to failure distributions $F(t)$ [158].

By using the general degradation path model, more accurate reliability results were predicted through analyzing the lumen maintenance data collected from the IES LM-80-08 lumen maintenance test standard [158, 159]. More literatures on LED lifetime predictions by using regression methods can be referred to [168–171].

2.4.2. STOCHASTIC PROCESS MODEL

Most of the previous studies used regression-based methods to analyze the LED devices, which do not capture the dynamic and random characteristic during degradation process. The random nature of the degradation process reflects a close connection between the system state and system reliability, and thus allowing us to better understand the failure mechanisms of the product under study. Making use of the degradation information in conjunction with the degradation characteristic allows us to accurately evaluate device reliability and predict the remaining useful life [172]. The dynamic degradation can often be well described by some stochastic processes. Among the stochastic processes, the Wiener process with a positive drift has nice mathematical properties and physical interpretations, and thus received much attention. It has been applied to model the degradation of light-emitting diode [173–178]. The Wiener process degradation model is written as follows [172]:

$$X(t) = \beta t + \sigma B(t) \tag{2.10}$$

where β is the drift rate, t is the time, $B(t)$ is the standard Brownian motion, and σ is the diffusion coefficient. The mean and variance of $B(t)$ are βt and $\sigma^2 t$, respectively.

According to the property of the Wiener process, $\Delta X(t) = X(t+\Delta t) - X(t)$ is independent of $X(t)$, and $\Delta X \sim N(\beta(t+\Delta t-t), \sigma^2(t+\Delta t-t)$; and if $t = 0$, then $X(t) \sim N(\beta t, \sigma^2 t)$.

If a failure is defined to be the event that the Wiener process crosses a critical boundary/threshold C, then the failure time, also called the first passage time, follows an inverse Gaussian distribution (IG) with a probability distribution function (PDF) given by

[179]:

$$f_T(t) = \sqrt{\frac{\lambda}{2\pi t^3}} \exp\left[-\frac{\lambda}{2\mu^2}\frac{(t-\mu)^2}{t}\right], t > 0, \lambda > 0, \mu = C/\beta, \lambda = C^2/\sigma^2 \tag{2.11}$$

Given the degradation data, the unknown parameters β, σ can be obtained by the method of maximum likelihood estimation (MLE) [180].

The Wiener process degradation model can be used to describe the dynamic degradation process of devices easily. However, this model only applies to devices with linear degradation characteristic. In order to extend its application, researchers proposed a variety of modified Wiener process models. These models were developed by time scaling techniques [172, 181, 182], nonlinear drift coefficient [183–188], or an adaptive parameter which can be updated dynamically [189–191]. These models can be used to describe the nonlinear degradation behavior of the devices. For instance, it is widely considered that LED package degrades exponentially with time when they were aged at high temperature conditions [133].

In addition, some researchers also were interested in improving the parameter estimation accuracy. Park *et al.* [192] developed an estimator which includes both the degradation data and the failure data. This estimator has been proven to be more accurate than that uses only degradation data [175]. Huang *et al.* [193] proposed a new estimator by including more information into the likelihood function while neglecting the dependency between the degradation data. The mean time to failure (MTTF) has been obtained and shows comparable result with IES TM-21-11 predictions, indicating the feasibility of the proposed method. Some other researchers modeled the Wiener process degradation model by considering the inherent randomness of degradation itself as well as measurement errors [194–196]. In this way, the estimation accuracy can be improved.

Except for the Wiener process, Gamma process has been also widely applied to describe the degradation behavior of the devices [197–199]. Peng and Tseng [200] described the nonlinear degradation characteristics of LED packages by using the gamma process. An exact relationship between the lifetime distributions of the constant stress accelerated degradation test (CSADT) and the step stress accelerated degradation test (SSADT) was derived. It allows engineers to extrapolate the product's lifetime distribution under typical stress. Furthermore, Hao and Li [201] modeled the degradation of LED packages by assuming that the lumen maintenance and the color shift are governed by a random effects Gamma process, and the dependency of lumen maintenance and color shift is described by a Frank copula function.

2.4.3. BAYESIAN NETWORK MODEL

A Bayesian network (BN) is a probabilistic graphical model that represents a set of random variables and their conditional or probabilistic dependencies by using a directed acyclic graph (DAG). BN is often also referred to as a Bayesian belief network (BBN), belief network, or casual probabilistic network. BN is a probabilistic approach that is used to model and predict the behavior of a system based on observed stochastic events. A Bayesian network consists of a set of nodes and directional arcs. Each node represents a random variable that denotes an attribute, feature, or hypothesis on the system under study. Each directional arc represents the relationship between nodes. This relationship is usually a direct causal relationship, and its strengths can be quantified by conditional probabilities. Compared with traditional statistical models, the BN does not distinguish between independent and dependent variables. Alternatively, it approximates the entire joint probability distribution of the system under study. Recently, the Bayesian network has been used in the reliability evaluation of LEDs [202–204].

The drawback is that BN cannot deal with time-dependent situations because the directional arcs used are time-independent. In order to overcome this problem, Kalman filter and particle filter were developed. Both of these methods were the so-called dynamic Bayesian network, which are useful for modeling time series data, such as LED lumen degradation or color shift [205]. However, the applications of Kalman filter are limited to linear systems with Gaussian noise. Therefore, extended Kalman filter (EKF) [206] and unscented Kalman filter (UKF) [206] was introduced for degradation process with nonlinear behavior and/or non-Gaussian noises. Compared to the EKF, which uses a first order Taylor approximation to linearize both the state and measurement models, the UKF increases the estimation accuracy by considering at least the second order Taylor expansion. Furthermore, the UKF eliminates the calculation of Jacobian and Hessian matrices in EKF, while develops an optimal sampling approach (sigma point sampling), which makes the estimation procedure easier [89].

However, both EKF and UKF rely on the Gaussian approximation and use mean and covariance to represent a probabilistic distribution. Therefore, they have difficulties in dealing with non-Gaussian problems (i.e., multimodal distributions or probabilistic distributions with heavy tail). Compared to EKF and UKF, the particle filter (PF) often provides better results for highly nonlinear/non-Gaussian systems [207]. PF is a class of nonlinear filters which do not require any assumption to the probabilistic distribution. It is based on the Sequential Monte Carlo (SMC) simulation method and uses a set of particles to approximate the posterior distribution. And it is much more effective than both EKF and UKF in solving problems with multimodal uncertainty distributions [89].

Recently, it has been used in the lifetime prediction for LED devices [208–210].

REFERENCES

[1] X. Qu, S. C. Wong, and C. K. Tse, *Temperature measurement technique for stabilizing the light output of rgb led lamps,* IEEE Transactions on Instrumentation and Measurement **59**, 661 (2010).

[2] Y. Cheung and H. Choi, *Color-tunable and phosphor-free white-light multilayered light-emitting diodes,* IEEE Transactions on Electron Devices **60**, 333 (2013).

[3] R. Hu, S. Yu, Y. Zou, H. Zheng, F. Wang, S. Liu, and X. Luo, *Near-/mid-field effect of color mixing for single phosphor-converted light-emitting diode package,* IEEE Photonics Technology Letters **25**, 246 (2013).

[4] H. K. Park, J. H. Oh, and Y. R. Do, *Toward scatter-free phosphors in white phosphor-converted light-emitting diodes,* Optics express **20**, 10218 (2012).

[5] Y. Sato, N. Takahashi, and S. Sato, *Full-color fluorescent display devices using a near-uv light-emitting diode,* Japanese Journal of Applied Physics **35**, L838 (1996).

[6] R. Mueller-Mach, G. O. Mueller, M. R. Krames, and T. Trottier, *High-power phosphor-converted light-emitting diodes based on iii-nitrides,* IEEE Journal of Selected Topics in Quantum Electronics **8**, 339 (2002).

[7] J. Hecht, *Photonic frontiers: Rgb leds for illumination: Color-tunable rgb led lighting goes far beyond replacement bulbs,* http://www.laserfocusworld.com/articles/print/volume-49/issue-08/features/photonic-frontiers-rgb-leds-for-illumination-color-tunable-rgb-led-lighting-goes-far-beyond-replacement-bulbs.html (2013), [online].

[8] J. Huang, D. S. Golubovic, S. Koh, D. Yang, X. Li, X. Fan, and G. Zhang, *Optical degradation mechanisms of mid-power white-light leds in lm-80-08 tests,* Microelectronics Reliability **55**, 2654 (2015).

[9] X.-M. Long, R.-J. Liao, J. Zhou, and Z. Zeng, *Thermal uniformity of packaging multiple light-emitting diodes embedded in aluminum-core printed circuit boards,* Microelectronics Reliability **53**, 544 (2013).

[10] R.-H. Horng, K.-C. Shen, Y.-W. Kuo, and D.-S. Wuu, *Gan light emitting diodes with wing-type imbedded contacts,* Optics express **21**, A1 (2013).

[11] S. Baek, G. Kang, D. Shin, K. Bae, Y. H. Kim, and K. Kim, *Improvement of light extraction efficiency in flip-chip light emitting diodes on sic substrate via transparent haze films with morphology-controlled collapsed alumina nanorods,* ACS applied materials & interfaces (2015).

[12] P. Zhu, C.-K. Tan, W. Sun, and N. Tansu, *Aspect ratio engineering of microlens arrays in thin-film flip-chip light-emitting diodes,* Applied Optics **54**, 10299 (2015).

[13] L. Liu, M. Ling, J. Yang, W. Xiong, W. Jia, and G. Wang, *Efficiency degradation behaviors of current/thermal co-stressed gan-based blue light emitting diodes with vertical-structure,* Journal of Applied Physics **111**, 093110 (2012).

[14] J. H. Son, Y. H. Song, B. J. Kim, and J.-L. Lee, *Effect of reflective p-type ohmic contact on thermal reliability of vertical ingan/gan leds,* Electronic Materials Letters **10**, 1171 (2014).

[15] E. F. Schubert, T. Gessmann, and J. K. Kim, *Light emitting diodes* (Wiley Online Library, 2005).

[16] Wikipedia, *Light-emitting diode,* https://en.wikipedia.org/wiki/Light-emitting_diode (year: unknown), [online].

[17] S.-P. Ying and A.-Y. Shiu, *Investigation of remote-phosphor white light-emitting diodes with improved scattered photon extraction structure,* Applied optics **54**, E30 (2015).

[18] J. Kim and M. Shin, *Thermal behavior of remote phosphor in light-emitting diode packages,* IEEE Electron Device Letters **36**, 832 (2015).

[19] C.-H. Huang, K.-J. Chen, M.-T. Tsai, M.-H. Shih, C.-W. Sun, W.-I. Lee, C.-C. Lin, and H. C. Kuo, *High-efficiency and low assembly-dependent chip-scale package for white light-emitting diodes,* Journal of Photonics for Energy **5**, 057606 (2015), 10.1117/1.JPE.5.057606.

[20] K.-J. Chen, H.-C. Chen, C.-C. Lin, C.-H. Wang, C.-C. Yeh, H.-H. Tsai, S.-H. Chien, M.-H. Shih, and H.-C. Kuo, *An investigation of the optical analysis in white light-emitting diodes with conformal and remote phosphor structure,* Journal of Display Technology **9**, 915 (2013).

[21] T. Yanagisawa and T. Kojima, *Degradation of ingan blue light-emitting diodes under continuous and low-speed pulse operations,* Microelectronics Reliability **43**, 977 (2003).

[22] T. Yanagisawa, *The degradation of gaalas red light-emitting diodes under continuous and low-speed pulse operations,* Microelectronics Reliability **38**, 1627 (1998).

[23] T. Hoang, P. LeMinh, J. Holleman, and J. Schmitz, *The effect of dislocation loops on the light emission of silicon leds,* in *Proceedings of 35th European Solid-State Device Research Conference, 2005 (ESSDERC 2005)* (IEEE) pp. 359–362.

[24] S. C. Yang, P. Lin, H. K. Fu, A. T. Lee, T. Te Chen, C. P. Wang, S. B. Huang, and P. T. Chou, *Accelerated degradation of high power light-emitting diode resulted from inhomogeneous current distribution,* Japanese Journal of Applied Physics **50**, 034301 (2011).

[25] G. Zu-Qiang and Q. Ke-Yuan, *Accurate measurement and influence on device reliability of defect density of a light-emitting diode,* Chinese Physics B **22**, 106108 (2013).

[26] J. Tharian, *Degradation-and failure mode analysis of iii-v nitride devices,* in *14th International Symposium on the Physical and Failure Analysis of Integrated Circuits, 2007 (IPFA 2007)* (IEEE) pp. 284–287.

[27] M. La Grassa, M. Meneghini, C. De Santi, M. Mandurrino, M. Goano, F. Bertazzi, R. Zeisel, B. Galler, G. Meneghesso, and E. Zanoni, *Ageing of ingan-based leds: Effects on internal quantum efficiency and role of defects,* Microelectronics Reliability **55**, 1775 (2015).

[28] G. Ferenczi, *Reliability of led's; are the accelerated ageing tests reliable?* Acta Physica Academiae Scientiarum Hungaricae **51**, 437 (1981).

[29] C. Henry and D. Lang, *Nonradiative capture and recombination by multiphonon emission in gaas and gap,* Physical Review B **15**, 989 (1977).

[30] S.-L. Chuang, A. Ishibashi, S. Kijima, N. Nakayama, M. Ukita, and S. Taniguchi, *Kinetic model for degradation of light-emitting diodes,* IEEE Journal of Quantum Electronics **33**, 970 (1997).

[31] O. Ueda, *Reliability issues in iii–v compound semiconductor devices: optical devices and gaas-based hbts,* Microelectronics Reliability **39**, 1839 (1999).

[32] M. Pavesi, F. Rossi, and E. Zanoni, *Effects of extreme dc-ageing and electron-beam irradiation in ingan/algan/gan light-emitting diodes,* Semiconductor science and technology **21**, 138 (2006).

[33] L. Sugiura, *Comparison of degradation caused by dislocation motion in compound semiconductor light-emitting devices,* Applied Physics Letters **70**, 1317 (1997).

[34] G. Lu, S. Yang, and Y. Huang, *Analysis on failure modes and mechanisms of led,* in *8th International Conference on Reliability, Maintainability and Safety, 2009 (ICRMS 2009)* (IEEE) pp. 1237–1241.

[35] L. Sugiura, *Dislocation motion in gan light-emitting devices and its effect on device lifetime,* Journal of Applied Physics **81**, 1633 (1997).

[36] M. Fukuda, *Laser and led reliability update,* Journal of Lightwave Technology **6**, 1488 (1988).

[37] X. Cao, P. Sandvik, S. LeBoeuf, and S. Arthur, *Defect generation in ingan/gan light-emitting diodes under forward and reverse electrical stresses,* Microelectronics Reliability **43**, 1987 (2003).

[38] X. Cao, P. Sandvik, S. LeBoeuf, and S. Arthur, *Defect generation in ingan/gan light-emitting diodes under forward and reverse electrical stresses,* Microelectronics Reliability **43**, 1987 (2003).

[39] O. Pursiainen, N. Linder, A. Jaeger, R. Oberschmid, and K. Streubel, *Identification of aging mechanisms in the optical and electrical characteristics of light-emitting diodes,* Applied Physics Letters **79**, 2895 (2001).

[40] A. Uddin, A. C. Wei, and T. G. Andersson, *Study of degradation mechanism of blue light emitting diodes,* Thin Solid Films **483**, 378 (2005).

[41] D. S. Meyaard, Q. Shan, Q. Dai, J. Cho, E. F. Schubert, M.-H. Kim, and C. Sone, *On the temperature dependence of electron leakage from the active region of gainn/gan light-emitting diodes,* Applied Physics Letters **99**, 041112 (2011).

[42] M. Pavesi, M. Manfredi, F. Rossi, M. Meneghini, E. Zanoni, U. Zehnder, and U. Strauss, *Temperature dependence of the electrical activity of localized defects in ingan-based light emitting diodes,* Applied Physics Letters **89**, 041917 (2006).

[43] M. Miyachi, T. Tanaka, Y. Kimura, and H. Ota, *The activation of mg in gan by annealing with minority-carrier injection,* Applied Physics Letters **72**, 1101 (1998).

[44] K. Kohler, T. Stephan, A. Perona, J. Wiegert, M. Maier, M. Kunzer, and J. Wagner, *Control of the mg doping profile in iii-n light-emitting diodes and its effect on the electroluminescence efficiency,* Journal of applied physics **97**, 104914 (2005).

[45] E. Glaser, T. Kennedy, W. Carlos, P. Ruden, and S. Nakamura, *Recombination processes in ingan light-emitting diodes studied through optically detected magnetic resonance,* Applied physics letters **73**, 3123 (1998).

[46] M. S. Kumar, S. J. Chung, H. W. Shim, C. H. Hong, E. K. Suh, and H. J. Lee, *Anomalous current–voltage characteristics of ingan/gan light-emitting diodes depending on mg flow rate during p-gan growth,* Semiconductor Science and Technology **19**, 725 (2004).

[47] M.-K. Kwon, I.-K. Park, J.-Y. Kim, J.-O. Kim, B. Kim, and S.-J. Park, *Gradient doping of mg in p-type gan for high efficiency ingan–gan ultraviolet light-emitting diode,* IEEE Photonics Technology Letters **19**, 1880 (2007).

[48] M.-K. Kwon, I.-K. Park, J.-Y. Kim, J.-O. Kim, B. Kim, and S.-J. Park, *Gradient doping of mg in p-type gan for high efficiency ingan–gan ultraviolet light-emitting diode,* IEEE Photonics Technology Letters **19**, 1880 (2007).

[49] S. Nakamura, T. Mukai, M. Senoh, and N. Iwasa, *Thermal annealing effects on p-type mg-doped gan films,* Japanese Journal of Applied Physics **31**, L139 (1992).

[50] S. M. Myers, A. F. Wright, G. A. Petersen, W. R. Wampler, C. H. Seager, M. H. Crawford, and J. Han, *Diffusion, release, and uptake of hydrogen in magnesium-doped gallium nitride: Theory and experiment,* Journal of Applied Physics **89**, 3195 (2001).

[51] B. A. Hull, S. E. Mohney, H. S. Venugopalan, and J. C. Ramer, *Influence of oxygen on the activation of p-type gan,* Applied Physics Letters **76**, 2271 (2000).

[52] G. Meneghesso, S. Levada, E. Zanoni, G. Salviati, N. Armani, F. Rossi, M. Pavesi, M. Manfredi, A. Cavallini, and A. Castaldini, *Failure mechanisms of gan-based leds related with instabilities in doping profile and deep levels,* in *42nd IEEE Annual International Reliability Physics Symposium Proceedings, 2004* (IEEE) pp. 474–478.

[53] G. Meneghesso, S. Levada, E. Zanoni, S. Podda, G. Mura, M. Vanzi, A. Cavallini, A. Castaldini, S. Du, and I. Eliashevich, *Failure modes and mechanisms of dc-aged gan leds,* physica status solidi (a) **194**, 389 (2002).

[54] G. Meneghesso, S. Levada, R. Pierobon, F. Rampazzo, E. Zanoni, A. Cavallini, A. Castaldini, G. Scamarcio, S. Du, and I. Eliashevich, *Degradation mechanisms of gan-based leds after accelerated dc current aging,* in *International Electron Devices Meeting, 2002 (IEDM'02)* (IEEE) pp. 103–106.

[55] G. Meneghesso, F. Magistrali, D. Sala, M. Vanzi, C. Canali, and E. Zanoni, *Failure mechanisms due to metallurgical interactions in commercially available algaas/gaas and algaas/ingaas hemts,* Microelectronics Reliability **38**, 497 (1998).

[56] M. Meneghini, L. Trevisanello, S. Levada, G. Meneghesso, G. Tamiazzo, E. Zanoni, T. Zahner, U. Zehnder, V. Harle, and U. Straus, *Failure mechanisms of gallium nitride leds related with passivation,* in *IEEE International Electron Devices Meeting, 2005 (IEDM Technical Digest)* (IEEE) pp. 4 pp.–1012.

[57] M. Meneghini, L.-R. Trevisanello, G. Meneghesso, and E. Zanoni, *A review on the reliability of gan-based leds,* IEEE Transactions on Device and Materials Reliability **8**, 323 (2008).

[58] D. L. Barton, M. Osinski, P. Perlin, C. J. Helms, and N. H. Berg, *Life tests and failure mechanisms of gan/algan/ingan light-emitting diodes,* in *Optoelectronics and High-Power Lasers & Applications* (International Society for Optics and Photonics) pp. 17–27.

[59] J. Wu, C. Huang, and C. Liao, *Fracture strength characterization and failure analysis of silicon dies,* Microelectronics Reliability **43**, 269 (2003).

[60] C. Bohm, T. Hauck, A. Juritza, and W. Muller, *Weibull statistics of silicon die fracture,* in *Proceedings of 6th Electronics Packaging Technology Conference, 2004 (EPTC 2004)* (IEEE) pp. 782–786.

[61] M.-H. Chang, D. Das, P. Varde, and M. Pecht, *Light emitting diodes reliability review,* Microelectronics Reliability **52**, 762 (2012).

[62] D. L. Barton, M. Osinski, P. Perlin, P. G Eliseev, and J. Lee, *Single-quantum well ingan green light emitting diode degradation under high electrical stress,* Microelectronics Reliability **39**, 1219 (1999).

[63] M. Meneghini, A. Tazzoli, G. Mura, G. Meneghesso, and E. Zanoni, *A review on the physical mechanisms that limit the reliability of gan-based leds,* IEEE Transactions on Electron Devices **57**, 108 (2010).

[64] G. Meneghesso, S. Levada, E. Zanoni, G. Scamarcio, G. Mura, S. Podda, M. Vanzi, S. Du, and I. Eliashevich, *Reliability of visible gan leds in plastic package,* Microelectronics Reliability **43**, 1737 (2003).

[65] M. Meneghini, L.-R. Trevisanello, U. Zehnder, G. Meneghesso, and E. Zanoni, *Reversible degradation of ohmic contacts on p-gan for application in high-brightness leds,* IEEE Transactions on Electron Devices **54**, 3245 (2007).

[66] E. Jung and H. Kim, *Rapid optical degradation of gan-based light-emitting diodes by a current-crowding-induced self-accelerating thermal process,* IEEE Transactions on Electron Devices **61**, 825 (2014).

[67] B. Yan, J. P. You, N. T. Tran, Y. He, and F. G. Shi, *Influence of die attach layer on thermal performance of high power light emitting diodes,* IEEE Transactions on Components and Packaging Technologies **33**, 722 (2010).

[68] J. You, Y. He, and F. Shi, *Thermal management of high power leds: Impact of die attach materials,* in *International Microsystems, Packaging, Assembly and Circuits Technology, 2007 (IMPACT 2007)* (IEEE, 2007) pp. 239–242.

[69] N. Lobo Ploch, H. Rodriguez, C. Stolmacker, M. Hoppe, M. Lapeyrade, J. Stellmach, F. Mehnke, T. Wernicke, A. Knauer, V. Kueller, *et al.*, *Effective thermal management in ultraviolet light-emitting diodes with micro-led arrays,* IEEE Transactions on Electron Devices **60**, 782 (2013).

[70] M. Khizar, K. Acharya, and M. Y. A. Raja, *Improved local thermal management of algan-based deep-uv light emitting diodes,* Semiconductor Science and Technology **22**, 1081 (2007).

[71] F. Wu, Y. Wu, B. An, and F. Wu, *Analysis of dark stain on chip surface of high-power led,* in *7th International Conference on Electronic Packaging Technology, 2006 (ICEPT'06)* (IEEE) pp. 1–4.

[72] P. McCluskey, K. Mensah, C. O'Connor, F. Lilie, A. Gallo, and J. Fink, *Reliability of commercial plastic encapsulated microelectronics at temperatures from 125 °C to 300 °C,* in *The Third European Conference on High Temperature Electronics, 1999 (HITEN 9)* (IEEE) pp. 155–162.

[73] P. McCluskey, K. Mensah, C. O'Connor, and A. Gallo, *Reliable use of commercial technology in high temperature environments,* Microelectronics Reliability **40**, 1671 (2000).

[74] X. Luo, X. Fu, F. Chen, and H. Zheng, *Phosphor self-heating in phosphor converted light emitting diode packaging,* International Journal of Heat and Mass Transfer **58**, 276 (2013).

[75] M. Meneghini, M. Dal Lago, N. Trivellin, G. Meneghesso, and E. Zanoni, *Thermally activated degradation of remote phosphors for application in led lighting,* IEEE Transactions on Device and Materials Reliability **13**, 316 (2013).

[76] R.-J. Xie and N. Hirosaki, *Silicon-based oxynitride and nitride phosphors for white leds—a review,* Science and Technology of Advanced Materials **8**, 588 (2007).

[77] M. Arik, S. Weaver, C. Becker, M. Hsing, and A. Srivastava, *Effects of localized heat generations due to the color conversion in phosphor particles and layers of high brightness light emitting diodes,* in *ASME 2003 International Electronic Packaging Technical Conference and Exhibition* (American Society of Mechanical Engineers, 2003) pp. 611–619.

[78] R.-J. Xie, N. Hirosaki, N. Kimura, K. Sakuma, and M. Mitomo, *2-phosphor-converted white light-emitting diodes using oxynitride/nitride phosphors,* Applied Physics Letters **90**, 191101 (2007).

[79] R. Pązik, K. Zawisza, A. Watras, K. Maleszka-Bagińska, P. Boutinaud, R. Mahiou, and P. J. Dereń, *Thermal quenching mechanisms of the eu 3+ luminescence in ca 9 al (po 4) 7 obtained by citric route,* Materials Research Bulletin **48**, 337 (2013).

[80] P. F. Smet, J. Botterman, A. B. Parmentier, and D. Poelman, *Thermal quenching at the microscopic level in multi-phase thiosilicate phosphors,* Optical Materials **35**, 1970 (2013).

[81] J. Zhang, B. Chen, Z. Liang, X. Li, J. Sun, L. Cheng, and H. Zhong, *Optical transition and thermal quenching mechanism in casno 3: Eu 3+ phosphors,* Journal of Alloys and Compounds **612**, 204 (2014).

[82] H. Ye, S. Koh, C. Yuan, and G. Zhang, *Thermal analysis of phosphor in high brightness led,* in *13th International Conference on Electronic Packaging Technology and High Density Packaging (ICEPT-HDP), 2012* (IEEE, 2012) pp. 1535–1539.

[83] B. Yan, J.-P. You, N. T. Tran, and F. G. Shi, *Influence of phosphor configuration on thermal performance of high power white led array,* in *IEEE International Symposium on Advanced Packaging Materials (APM), 2013* (IEEE, 2013) pp. 274–289.

[84] E. Juntunen, O. Tapaninen, A. Sitomaniemi, and V. Heikkinen, *Effect of phosphor encapsulant on the thermal resistance of a high-power cob led module,* IEEE Transactions on Components, Packaging and Manufacturing Technology **3**, 1148 (2013).

[85] L. Zhou, B. An, Y. Wu, and S. Liu, *Analysis of delamination and darkening in high power led packaging,* in *16th IEEE International Symposium on the Physical and Failure Analysis of Integrated Circuits, 2009 (IPFA 2009)* (IEEE) pp. 656–660.

[86] M. Meneghini, L. Trevisanello, C. Sanna, G. Mura, M. Vanzi, G. Meneghesso, and E. Zanoni, *High temperature electro-optical degradation of ingan/gan hbleds,* Microelectronics Reliability **47**, 1625 (2007).

[87] B.-M. Song and B. Han, *Analytical/experimental hybrid approach based on spectral power distribution for quantitative degradation analysis of phosphor converted led,* IEEE Transactions on Device and Materials Reliability **14**, 365 (2014).

[88] M. Meneghini, M. Dal Lago, N. Trivellin, G. Meneghesso, and E. Zanoni, *Degradation mechanisms of high-power leds for lighting applications: an overview,* IEEE Transactions on Industry Applications **50**, 78 (2014).

[89] J. Fan, K.-C. Yung, and M. Pecht, *Prognostics of chromaticity state for phosphor-converted white light emitting diodes using an unscented kalman filter approach,* IEEE Transactions on Device and Materials Reliability **14**, 564 (2014).

[90] G. Lu, M. Y. Mehr, W. van Driel, X. Fan, J. Fan, K. Jansen, and G. Zhang, *Color shift investigations for led secondary optical designs: Comparison between bpa-pc and pmma,* Optical Materials **45**, 37 (2015).

[91] N. Narendran, Y. Gu, J. Freyssinier, H. Yu, and L. Deng, *Solid-state lighting: failure analysis of white leds,* Journal of Crystal Growth **268**, 449 (2004).

[92] R. Baillot, Y. Deshayes, L. Bechou, T. Buffeteau, I. Pianet, C. Armand, F. Voillot, S. Sorieul, and Y. Ousten, *Effects of silicone coating degradation on gan mqw leds performances using physical and chemical analyses,* Microelectronics Reliability **50**, 1568 (2010).

[93] M. Y. Mehr, W. D. van Driel, S. Koh, and G. Zhang, *Reliability and optical properties of led lens plates under high temperature stress,* Microelectronics Reliability **54**, 2440 (2014).

[94] A. Rivaton, B. Mailhot, J. Soulestin, H. Varghese, and J. L. Gardette, *Comparison of the photochemical and thermal degradation of bisphenol-a polycarbonate and trimethylcyclohexane–polycarbonate,* Polymer Degradation and Stability **75**, 17 (2002).

[95] F. Arnold, *Mechanisms of thermal and photodegradations of bisphenol a polycarbonate,* in *Polymer Durability*, Advances in Chemistry, Vol. 249 (American Chemical Society, 1996) Book section 5, pp. 59–76, doi:10.1021/ba-1996-0249.ch005.

[96] I. B. Rufus, H. Shah, and C. E. Hoyle, *Identification of fluorescent products produced by the thermal treatment of bisphenol-a-based polycarbonate,* Journal of Applied Polymer Science **51**, 1549 (1994).

[97] D. T. Clark and H. S. Munro, *Surface and bulk aspects of the natural and artificial photo-ageing of bisphenol a polycarbonate as revealed by esca and difference uv spectroscopy,* Polymer Degradation and Stability **8**, 195 (1984).

[98] A. Factor, J. C. Carnahan, S. B. Dorn, and P. C. Van Dort, *The chemistry of γ-irradiated bisphenol-a polycarbonate,* Polymer Degradation and Stability **45**, 127 (1994).

[99] A. Rivaton, *Recent advances in bisphenol-a polycarbonate photodegradation,* Polymer Degradation and Stability **49**, 163 (1995).

[100] A. Rivaton, D. Sallet, and J. Lemaire, *The photo-chemistry of bisphenol-a polycarbonate reconsidered: Part 2—ftir analysis of the solid-state photo-chemistry in 'dry'conditions,* Polymer degradation and stability **14**, 1 (1986).

[101] J. Lemaire, J.-L. Gardette, A. Rivaton, and A. Roger, *Dual photo-chemistries in aliphatic polyamides, bisphenol a polycarbonate and aromatic polyurethanes—a short review,* Polymer Degradation and Stability **15**, 1 (1986).

[102] A. Rivaton, D. Sallet, and J. Lemaire, *The photochemistry of bisphenol-a polycarbonate reconsidered,* Polymer Photochemistry **3**, 463 (1983).

[103] M. Diepens and P. Gijsman, *Photodegradation of bisphenol a polycarbonate,* Polymer Degradation and Stability **92**, 397 (2007).

[104] M. Y. Mehr, W. Van Driel, K. Jansen, P. Deeben, M. Boutelje, and G. Zhang, *Photodegradation of bisphenol a polycarbonate under blue light radiation and its effect on optical properties,* Optical Materials **35**, 504 (2013).

[105] Y.-H. Lin, J. P. You, Y.-C. Lin, N. T. Tran, and F. G. Shi, *Development of high-performance optical silicone for the packaging of high-power leds,* IEEE Transactions on Components and Packaging Technologies **33**, 761 (2010).

[106] C.-H. Lin, H.-T. Li, S.-C. Huang, C.-W. Hsu, K.-C. Chen, and W.-B. Chen, *Development of uv stable led encapsulants,* in *4th International Microsystems, Packaging, Assembly and Circuits Technology Conference, 2009 (IMPACT 2009)* (IEEE) pp. 565–567.

[107] C.-W. Hsu, C.-C. M. Ma, C.-S. Tan, H.-T. Li, S.-C. Huang, T.-M. Lee, and H. Tai, *Effect of thermal aging on the optical, dynamic mechanical, and morphological properties of phenylmethylsiloxane-modified epoxy for use as an led encapsulant,* Materials Chemistry and Physics **134**, 789 (2012).

[108] N. Grassie, M. I. Guy, and N. H. Tennent, *Degradation of epoxy polymers: 2—mechanism of thermal degradation of bisphenol-a diglycidyl ether,* Polymer Degradation and Stability **13**, 11 (1985).

[109] M. Bahadur, A. W. Norris, A. Zarisfi, J. S. Alger, and C. C. Windiate, *Silicone materials for led packaging,* in *SPIE Optics+ Photonics* (International Society for Optics and Photonics) pp. 63370F–63370F–7.

[110] W. Huang, Y. Zhang, Y. Yu, and Y. Yuan, *Studies on uv-stable silicone-epoxy resins,* Journal of applied polymer science **104**, 3954 (2007).

[111] G. R. Atkins, R. M. Krolikowska, and A. Samoc, *Optical properties of an ormosil system comprising methyl-and phenyl-substituted silica,* Journal of Non-Crystalline Solids **265**, 210 (2000).

[112] L. L. Hench and D. R. Ulrich, *Ultrastructure processing of ceramics, glasses, and composites* (Wiley, 1984).

[113] J.-y. Bae, Y. Kim, H.-Y. Kim, Y.-w. Lim, and B.-S. Bae, *Sol-gel synthesized linear oligosiloxane-based hybrid material for a thermally-resistant light emitting diode (led) encapsulant,* RSC Advances **3**, 8871 (2013).

[114] J.-y. Bae, Y. Kim, H.-Y. Kim, Y.-w. Lim, and B.-S. Bae, *Sol–gel synthesized linear oligosiloxane-based hybrid material for a thermally-resistant light emitting diode (led) encapsulant,* RSC Advances **3**, 8871 (2013).

[115] J.-S. Kim, S. Yang, and B.-S. Bae, *Thermal stability of sol–gel derived methacrylate oligosiloxane-based hybrids for led encapsulants,* Journal of sol-gel science and technology **53**, 434 (2010).

[116] E. Jung, M. S. Kim, and H. Kim, *Analysis of contributing factors for determining the reliability characteristics of gan-based white light-emitting diodes with dual degradation kinetics,* IEEE Transactions on Electron Devices **60**, 186 (2013).

[117] G. Mura, G. Cassanelli, F. Fantini, and M. Vanzi, *Sulfur-contamination of high power white led,* Microelectronics Reliability **48**, 1208 (2008).

[118] L. Zhang, Y. Zhu, H. Chen, K. Leung, Y. Wu, and J. Wu, *Failure analysis on reflector blackening between lead frame electrodes in leds under whtol test,* Microelectronics Reliability **55**, 799 (2015).

[119] L. Volpe and P. Peterson, *The atmospheric sulfidation of silver in a tubular corrosion reactor,* Corrosion Science **29**, 1179 (1989).

[120] L. Zhang, Y. Zhu, W. Wang, X. Bi, H. Chen, K.-S. Leung, Y. Wu, and J. Wu, *Study on ag-plated cu lead frame and its effect to led performance under thermal aging,* IEEE Transactions on Device and Materials Reliability **14**, 1022 (2014).

[121] M. Meneghini, M. Dal Lago, N. Trivellin, G. Meneghesso, and E. Zanoni, *Thermally activated degradation of remote phosphors for application in led lighting,* IEEE Transactions on Device and Materials Reliability **13**, 316 (2013).

[122] H. Yunsheng, W. ZHUANG, H. Huaqiang, L. Ronghui, C. Guantong, L. Yuanhong, and X. HUANG, *High temperature stability of eu 2+-activated nitride red phosphors,* Journal of Rare Earths **32**, 12 (2014).

[123] J. J. Joos, K. W. Meert, A. B. Parmentier, D. Poelman, and P. F. Smet, *Thermal quenching and luminescence lifetime of saturated green sr 1- xeuxga 2 s 4 phosphors,* Optical Materials **34**, 1902 (2012).

[124] J. S. Kim, Y. H. Park, J. C. Choi, and H. L. Park, *Temperature-dependent emission spectrum of ba3mgsi2o8: Eu2+, mn2+ phosphor for white-light-emitting diode,* Electrochemical and Solid-State Letters **8**, H65 (2005).

[125] C. M. Tan, B. K. E. Chen, G. Xu, and Y. Liu, *Analysis of humidity effects on the degradation of high-power white leds,* Microelectronics Reliability **49**, 1226 (2009).

[126] L. Tan, J. Li, K. Wang, and S. Liu, *Effects of defects on the thermal and optical performance of high-brightness light-emitting diodes,* IEEE Transactions on Electronics Packaging Manufacturing **32**, 233 (2009).

[127] X. Luo, B. Wu, and S. Liu, *Effects of moist environments on led module reliability,* IEEE Transactions on Device and Materials Reliability **10**, 182 (2010).

[128] H.-H. Kim, S.-H. Choi, S.-H. Shin, Y.-K. Lee, S.-M. Choi, and S. Yi, *Thermal transient characteristics of die attach in high power led pkg,* Microelectronics Reliability **48**, 445 (2008).

[129] A. Gladkov and A. Bar-Cohen, *Parametric dependence of fatigue of electronic adhesives,* IEEE Transactions on Components and Packaging Technologies **22**, 200 (1999).

[130] J. Hu, L. Yang, and M. Whan Shin, *Mechanism and thermal effect of delamination in light-emitting diode packages,* Microelectronics Journal **38**, 157 (2007).

[131] M. D. Ries, D. R. Banks, D. P. Watson, and K. G. Hoebener, *Attachment of solder ball connect (sbc) packages to circuit cards,* IBM Journal of Research and Development **37**, 597 (1993).

[132] E. H. Wong, R. Rajoo, S. W. Koh, and T. B. Lim, *The mechanics and impact of hygroscopic swelling of polymeric materials in electronic packaging,* Journal of Electronic Packaging **124**, 122 (2002).

[133] L. Trevisanello, M. Meneghini, G. Mura, M. Vanzi, M. Pavesi, G. Meneghesso, and E. Zanoni, *Accelerated life test of high brightness light emitting diodes,* IEEE Transactions on Device and Materials Reliability **8**, 304 (2008).

[134] S. Buso, G. Spiazzi, M. Meneghini, and G. Meneghesso, *Performance degradation of high-brightness light emitting diodes under dc and pulsed bias,* IEEE Transactions on Device and Materials Reliability **8**, 312 (2008).

[135] M.-Y. Tsai, C.-H. Chen, and W.-L. Tsai, *Thermal resistance and reliability of high-power led packages under whtol and thermal shock tests,* IEEE Transactions on Components and Packaging Technologies **33**, 738 (2010).

[136] A. Christensen and S. Graham, *Thermal effects in packaging high power light emitting diode arrays,* Applied Thermal Engineering **29**, 364 (2009).

[137] S.-C. Yang, P. Lin, C.-P. Wang, S. B. Huang, C.-L. Chen, P.-F. Chiang, A.-T. Lee, and M.-T. Chu, *Failure and degradation mechanisms of high-power white light emitting diodes,* Microelectronics Reliability **50**, 959 (2010).

[138] C.-P. Wang, T.-T. Chen, H.-K. Fu, T.-L. Chang, P.-T. Chou, and M.-T. Chu, *Analysis of thermal characteristics and mechanism of degradation of flip-chip high power leds,* Microelectronics Reliability **52**, 698 (2012).

[139] S. Chan, W. Hong, K. Kim, Y. Yoon, J. Han, and J. S. Jang, *Accelerated life test of high power white light emitting diodes based on package failure mechanisms,* Microelectronics Reliability **51**, 1806 (2011).

[140] E. Nogueira, M. Vázquez, and C. Algora, *Accelerated life testing in epoxy packaged high luminosity light emitting diodes,* Journal of Electronic Packaging **133**, 034501 (2011).

[141] C. M. Tan and P. Singh, *Time evolution degradation physics in high power white leds under high temperature-humidity conditions,* IEEE Transactions on Device and Materials Reliability **14**, 742 (2014).

[142] C. M. Tan, B. Chen, X. Li, and S. J. Chen, *Rapid light output degradation of gan-based packaged led in the early stage of humidity test,* IEEE Transactions on Device and Materials Reliability **12**, 44 (2012).

[143] H. Fan, X. Li, J. Shen, and M. Chen, *An effective prediction method for led lumen maintenance,* in *13th International Conference on Electronic Packaging Technology and High Density Packaging (ICEPT-HDP), 2012* (IEEE) pp. 1560–1563.

[144] S. Guoxi, D. Shasha, Y. Youxing, Z. Zhiping, and J. G. Liu, *Failure mode and test method of sulfur induced light decay in lead-frame led package,* in *12th China International Forum on Solid State Lighting (SSLCHINA), 2015*, pp. 79–84.

[145] T. Hirofumi and M. Yoshiteru, *A measure against the latest problem of led package,* in *International Conference on Electronics Packaging and iMAPS All Asia Conference (ICEP-IACC), 2015*, pp. 678–681.

[146] Y. S. Lee, K. H. Kim, W. H. Kim, M. H. Choi, C. H. Jung, J. H. Choi, and J. P. Kim, *Effect of cross-linking density of silicone encapsulant on sulfur compound gas permeability of light-emitting diode,* IEEE Transactions on Components, Packaging and Manufacturing Technology **5**, 163 (2015).

[147] I. LM, *Lm-80-08. approved method: Measuring lumen maintenance of led light sources,* Illuminating Engineering Society of North America (2008).

[148] B. Hamon, L. Mendizabal, G. Feuillet, A. Gasse, and B. Bataillou, *A new lifetime estimation model for a quicker led reliability prediction,* in *SPIE Optical Engineering+ Applications* (International Society for Optics and Photonics, 2014) pp. 919007–919007.

[149] C.-C. Tsai, W.-C. Cheng, J.-K. Chang, S.-Y. Huang, J.-S. Liou, G.-H. Chen, Y.-C. Huang, J.-S. Wang, and W.-H. Cheng, *Thermal-stability comparison of glass-and silicone-based high-power phosphor-converted white-light-emitting diodes under thermal aging,* IEEE Transactions on Device and Materials Reliability **14**, 4 (2014).

[150] E. K. Ji, Y. H. Song, M.-J. Lee, and D.-H. Yoon, *Thermally stable phosphor-in-glass for enhancement of characteristic in high power led applications,* Materials Letters **157**, 89 (2015).

[151] Y. Chiou, T. Chiang, D. Kuo, S. Chang, T. Ko, and S. Hon, *The reliability analysis of gan-based light-emitting diodes with different current-blocking layers,* Semiconductor Science and Technology **26**, 085005 (2011).

[152] Y. Deshayes, L. Béchou, and Y. Ousten, *Stark effects model used to highlight selective activation of failure mechanisms in mqw ingan/gan light-emitting diodes,* IEEE Transactions on Device and Materials Reliability **10**, 164 (2010).

[153] I. E. S. o. N. America, *Projecting long term lumen maintenance of led light sources,* (2011), [IESNA].

[154] S. Tang, C. Yu, X. Wang, X. Guo, and X. Si, *Remaining useful life prediction of lithium-ion batteries based on the wiener process with measurement error,* Energies **7**, 520 (2014).

[155] S. J. Bae and P. H. Kvam, *A nonlinear random-coefficients model for degradation testing,* Technometrics **46**, 460 (2004).

[156] G. Whitmore and F. Schenkelberg, *Modelling accelerated degradation data using wiener diffusion with a time scale transformation,* Lifetime Data Analysis **3**, 27 (1997).

[157] W. Nelson, *Analysis of performance-degradation data from accelerated tests,* IEEE Transactions on Reliability **30**, 149 (1981).

[158] J. Fan, K.-C. Yung, and M. Pecht, *Lifetime estimation of high-power white led using degradation-data-driven method,* IEEE Transactions on Device and Materials Reliability **12**, 470 (2012).

[159] F.-K. Wang and Y.-C. Lu, *Useful lifetime analysis for high-power white leds,* Microelectronics Reliability **54**, 1307 (2014).

[160] J. Tang and T. Su, *Estimating failure time distribution and its parameters based on intermediate data from a wiener degradation model,* Naval Research Logistics (NRL) **55**, 265 (2008).

[161] T.-R. Tsai, C.-W. Lin, Y.-L. Sung, P.-T. Chou, C.-L. Chen, and Y. Lio, *Inference from lumen degradation data under wiener diffusion process,* IEEE Transactions on Reliability **61**, 710 (2012).

[162] H. Hao and C. Su, *A bayesian framework for reliability assessment via wiener process and mcmc,* Mathematical Problems in Engineering **2014** (2014).

[163] N. C. Laurenciu and S. D. Cotofana, *A nonlinear degradation path dependent end-of-life estimation framework from noisy observations,* Microelectronics Reliability **53**, 1213 (2013).

[164] M. A. Freitas, E. A. Colosimo, T. R. d. Santos, and M. C. Pires, *Reliability assessment using degradation models: Bayesian and classical approaches,* Pesquisa Operacional **30**, 194 (2010).

[165] C. J. Lu and W. O. Meeker, *Using degradation measures to estimate a time-to-failure distribution,* Technometrics **35**, 161 (1993).

[166] W. Q. Meeker, L. A. Escobar, and C. J. Lu, *Accelerated degradation tests: Modeling and analysis,* Technometrics **40**, 89 (1998).

[167] C. J. Lu, W. Q. Meeker, and L. A. Escobar, *A comparison of degradation and failure-time analysis methods for estimating a time-to-failure distribution,* Statistica Sinica **6**, 531 (1996).

[168] J. I. Park and S. J. Bae, *Direct prediction methods on lifetime distribution of organic light-emitting diodes from accelerated degradation tests,* IEEE Transactions on Reliability **59**, 74 (2010).

[169] J. Xie and M. Pecht, *Reliability prediction modeling of semiconductor light emitting device,* IEEE Transactions on Device and Materials Reliability **3**, 218 (2003).

[170] M. Cai, D. Yang, K. Tian, P. Zhang, X. Chen, L. Liu, and G. Zhang, *Step-stress accelerated testing of high-power led lamps based on subsystem isolation method,* Microelectronics Reliability **55**, 1784 (2015).

[171] F.-K. Wang and T.-P. Chu, *Lifetime predictions of led-based light bars by accelerated degradation test,* Microelectronics Reliability **52**, 1332 (2012).

[172] Y. Wang, Z.-S. Ye, and K.-L. Tsui, *Stochastic evaluation of magnetic head wears in hard disk drives,* IEEE Transactions on Magnetics **50**, 1 (2014).

[173] H. Liao and E. A. Elsayed, *Reliability inference for field conditions from accelerated degradation testing,* Naval Research Logistics (NRL) **53**, 576 (2006).

[174] C.-Y. Peng and S.-T. Tseng, *Mis-specification analysis of linear degradation models,* IEEE Transactions onReliability **58**, 444 (2009).

[175] T.-R. Tsai, C.-W. Lin, Y.-L. Sung, P.-T. Chou, C.-L. Chen, and Y. Lio, *Inference from lumen degradation data under wiener diffusion process,* IEEE Transactions on Reliability **61**, 710 (2012).

[176] J. Chiang, Y. Lio, and T. Tsai, *Degradation tests using geometric brownian motion process for lumen degradation data,* Quality and Reliability Engineering International **31**, 1797 (2015).

[177] Z.-S. Ye, Y. Wang, K.-L. Tsui, and M. Pecht, *Degradation data analysis using wiener processes with measurement errors,* IEEE Transactions on Reliability **62**, 772 (2013).

[178] T.-R. Tsai, Y. Lio, and N. Jiang, *Optimal decisions on the accelerated degradation test plan under the wiener process,* Quality Technology & Quantitative Management **11**, 461 (2014).

[179] K. A. Doksum and A. Hbyland, *Models for variable-stress accelerated life testing experiments based on wiener processes and the inverse gaussian distribution,* Technometrics **34**, 74 (1992).

[180] C.-M. Liao and S.-T. Tseng, *Optimal design for step-stress accelerated degradation tests,* IEEE Transactions on Reliability **55**, 59 (2006).

[181] X. Wang, N. Balakrishnan, and B. Guo, *Residual life estimation based on a generalized wiener degradation process,* Reliability Engineering & System Safety **124**, 13 (2014).

[182] X. Wang, B. Guo, and Z. Cheng, *Residual life estimation based on bivariate wiener degradation process with time-scale transformations,* Journal of Statistical Computation and Simulation **84**, 545 (2014).

[183] A. Molini, P. Talkner, G. G. Katul, and A. Porporato, *First passage time statistics of brownian motion with purely time dependent drift and diffusion,* Physica a-Statistical Mechanics and Its Applications **390**, 1841 (2011).

[184] R. Harman and F. Stulajter, *Optimality of equidistant sampling designs for the brownian motion with a quadratic drift,* Journal of Statistical Planning and Inference **141**, 2750 (2011).

[185] E. Urdapilleta, *Series solution to the first-passage-time problem of a brownian motion with an exponential time-dependent drift,* Journal of Physics a-Mathematical and Theoretical **45** (2012), 10.1088/1751-8113/45/18/185001.

[186] J. Li, *Some limit results for probabilities estimates of brownian motion with polynomial drift,* Indian Journal of Pure & Applied Mathematics **41**, 425 (2010).

[187] E. Urdapilleta, *Survival probability and first-passage-time statistics of a wiener process driven by an exponential time-dependent drift,* Physical Review E **83** (2011), 10.1103/PhysRevE.83.021102.

[188] X.-S. Si, W. Wang, C.-H. Hu, D.-H. Zhou, and M. G. Pecht, *Remaining useful life estimation based on a nonlinear diffusion degradation process,* IEEE Transactions on Reliability **61**, 50 (2012).

[189] X.-S. Si, W. Wang, C.-H. Hu, M.-Y. Chen, and D.-H. Zhou, *A wiener-process-based degradation model with a recursive filter algorithm for remaining useful life estimation,* Mechanical Systems and Signal Processing **35**, 219 (2013).

[190] W. Zhao-Qiang, H. Chang-Hua, W. Wenbin, and S. Xiao-Sheng, *An additive wiener process-based prognostic model for hybrid deteriorating systems,* IEEE Transactions on Reliability **63**, 208 (2014).

[191] H. Zeyi, X. Zhengguo, W. Wenhai, and S. Youxian, *Remaining useful life prediction for a nonlinear heterogeneous wiener process model with an adaptive drift,* IEEE Transactions on Reliability **64**, 687 (2015).

[192] C. Park and W. Padgett, *Accelerated degradation models for failure based on geometric brownian motion and gamma processes,* Lifetime Data Analysis **11**, 511 (2005).

[193] J. Huang, D. S. Golubović, S. Koh, D. Yang, X. Li, X. Fan, and G. Zhang, *Degradation modeling of mid-power white-light leds by using wiener process,* Optics express **23**, A966 (2015).

[194] G. Whitmore, *Estimating degradation by a wiener diffusion process subject to measurement error,* Lifetime data analysis **1**, 307 (1995).

[195] S. Tang, X. Guo, C. Yu, H. Xue, and Z. Zhou, *Accelerated degradation tests modeling based on the nonlinear wiener process with random effects,* Mathematical Problems in Engineering **2014** (2014).

[196] X.-l. Wang, B. Guo, Z.-j. Cheng, and P. Jiang, *Residual life estimation based on bivariate wiener degradation process with measurement errors,* Journal of Central South University **20**, 1844 (2013).

[197] X. Wang, P. Jiang, B. Guo, and Z. Cheng, *Real-time reliability evaluation for an individual product based on change-point gamma and wiener process,* Quality and Reliability Engineering International **30**, 513 (2014).

[198] M. H. Ling, K. L. Tsui, and N. Balakrishnan, *Accelerated degradation analysis for the quality of a system based on the gamma process,* IEEE Transactions on Reliability **64**, 463 (2015).

[199] H. Wang, T. Xu, and Q. Mi, *Lifetime prediction based on gamma processes from accelerated degradation data,* Chinese Journal of Aeronautics **28**, 172 (2015).

[200] C.-Y. Peng and S.-T. Tseng, *Progressive-stress accelerated degradation test for highly-reliable products,* IEEE Transactions on Reliability **59**, 30 (2010).

[201] H. Hao, C. Su, and C. Li, *Led lighting system reliability modeling and inference via random effects gamma process and copula function,* International Journal of Photoenergy **2015** (2015).

[202] P. Lall, J. Wei, and P. Sakalaukus, *Bayesian probabilistic model for life prediction and fault mode classification of solid state luminaires,* in *IEEE Conference on Prognostics and Health Management (PHM), 2014* (IEEE) pp. 1–10.

[203] P. Lall, J. Wei, and P. Sakalaukus, *Life prediction and classification of failure modes in solid state luminaires using bayesian probabilistic models,* in *IEEE 64th Electronic Components and Technology Conference (ECTC), 2014* (IEEE) pp. 2053–2062.

[204] P. Lall, P. Sakalaukus, J. Wei, and L. Davis, *Ssl and led life prediction and assessment of cct shift,* in *IEEE Intersociety Conference on Thermal and Thermomechanical Phenomena in Electronic Systems (ITherm), 2014* (IEEE) pp. 1179–1185.

[205] T. Sutharssan, *Prognostics and health management of light emitting diodes*, Thesis (2012).

[206] P. Lall, J. Wei, and L. Davis, *Prediction of lumen output and chromaticity shift in leds using kalman filter and extended kalman filter based models,* in *IEEE Conference on Prognostics and Health Management (PHM), 2013* (IEEE) pp. 1–14.

[207] E. Zio and G. Peloni, *Particle filtering prognostic estimation of the remaining useful life of nonlinear components,* Reliability Engineering & System Safety **96**, 403 (2011).

[208] A. Padmasali and S. Kini, *Prognostic algorithms for l70 life prediction of solid state lighting,* Lighting Research and Technology , 1477153515579233 (2015).

[209] P. Lall and H. Zhang, *Assessment of lumen degradation and remaining life of light-emitting diodes using physics-based indicators and particle filter,* Journal of Electronic Packaging **137**, 021002 (2015), 10.1115/1.4028957.

[210] J. Fan, K.-C. Yung, and M. Pecht, *Predicting long-term lumen maintenance life of led light sources using a particle filter-based prognostic approach,* Expert Systems with Applications **42**, 2411 (2015).

3

ANALYSIS TECHNIQUES

3.1. SIMULATION TECHNOLOGIES

3.1.1. THERMAL SIMULATION

THERMAL simulations play an important role in the design of many engineering applications, including internal combustion engines, turbines, heat exchanger, piping systems, and electronic components.

A thermal simulation is performed based on the theories of heat transfer. That is, conduction, convection, and radiation [1]. Thermal simulation includes: steady-state thermal analysis and transient-state thermal analysis, whereas the first one in more popular in LED industry. A steady-state thermal analysis can be used to determine temperatures in an object that are caused by thermal loads that do not vary over time. Such loads include the following: convections, radiation, heat flow rates, heat fluxes, heat generation rates, constant temperature boundaries. In linear steady state analysis, material properties such as conductivity and convection coefficient are linear. Temperature and fluxes at the final thermal equilibrium state are of interest. The basic finite element equation is:

$$([K_c] + [H])\{T\} = \{p\} \tag{3.1}$$

where $[K_c]$ is the conductivity matrix, $[H]$ is the boundary convection matrix due to free convection, $\{T\}$ is an unknown nodal temperature, {p} is the thermal loading vector. The system of linear equation is solved to find nodal temperature $\{T\}$ [1].

Thermal simulation has been widely used in LED industry [2–4]. Thermal simulation helps engineers to improve the performance and to evaluate the reliability of LED packages. Available commercial softwares include: ANSYS, ICEPAK, FLOTHERM, and so forth.

3.1.2. OPTICAL SIMULATION

If we consider light as an electromagnetic wave or a particle traveling through space, a light ray can be defined as a line normal to the direction of wave propagation. A light ray, or ray, obeys the laws of geometrical optics. A light ray can be transmitted, reflected, and refracted through an optical system. The light paths can be determined by relatively simple formulae. Ray tracing for optical design is based on a calculation of how rays travel through the system, and can be broken into two major types, sequential and non-sequential.

Sequential Ray Tracing – Image-forming systems, such as cameras, binoculars, and the human eye, typically use sequential ray tracing. Systems are called sequential when the exact order in which rays strike each surface in the system is exactly known. Ray trac-

ing for sequential systems is relatively straightforward. Because the order of intersection is known for each surface, ray propagation can be calculated systematically. Also, because sequential systems are concerned with imaging they are constrained to point-to-point mapping. Any deviation from an object point mapping to an image point is termed an aberration. A large portion of an optical engineer's job in designing an imaging system is to reduce or eliminate the effects of aberrations. Because imaging system rays act in such a well-described manner, only a few of them need to be traced to accurately describe the properties of the entire system. Tracing only two well-chosen rays (the marginal and chief rays) can tell you much about an imaging system; tracing several hundred rays can almost completely define the optical characteristics of the system [5].

Non-sequential Ray Tracing – In a non-sequential system the order of ray surface intersection is not known, and these systems are typically not concerned with image formation. Non-imaging systems include fiber optics, light pipes, solar concentrators, luminaires, and headlamps. Since in non-imaging systems rays do not act in a well-prescribed manner, and there is no imaging constraint (points don't have to map to points), many rays need to be traced in order to analyze system performance. This can be on the order of millions or tens of millions of rays. In fact, before the advent of computerized ray tracing, non-imaging illumination system analysis was practical for only a limited number of special cases. Instead of tracing a few well-chosen rays, non-sequential analysis requires many rays to be started randomly from an extended source (such as an incandescent filament) and traced through the system. Typically the random location and direction of rays from a source are determined through Monte Carlo simulation [6]. A detector is placed at the area of interest and rays are collected, binned, and analyzed. From this analysis intensity, luminance, and illuminance can be determined. A major source of statistical error, due to finite sampling, arises when simulating incoherent extended sources. The amount of error based solely on finite sampling can be calculated. Using statistical analysis one can show that error, or signal-to-noise ratio, at the detector for a system where each ray carries equal energy is

$$\frac{Signal}{Noise} = \sqrt{N_{det}} \tag{3.2}$$

where N_{det} is the total number of rays that hits the detector. Since the signal-to-noise ratio increases only as the square root of the number of rays hitting the detector, a large number of rays must be traced to achieve acceptable error. Using the appropriate number of source rays ensures statistical accuracy while minimizing the computational time [5].

Popular programs include *Lighttools*, *TracePro*, and so forth.

In this thesis, *Lighttools* will be used to simulate the lumen degradation of an LED packages due to the degradation of package materials, including chip, phosphors, package housing, encapsulant, lead frames, and so forth.

3.2. FAILURE ANALYSIS TECHNIQUES

Failure analysis is the process of collecting and analyzing data to determine the cause of a failure, often with the goal of determining corrective actions or liability. It is an important discipline in many branches of manufacturing industry, such as the electronics industry, where it is a vital tool used in the development of new products and for the improvement of existing products. The failure analysis process relies on collecting failed components for subsequent examination of the cause or causes of failure using a wide array of methods, especially microscopy and spectroscopy [7]. The failure analysis techniques include nondestructive testing methods and destructive testing methods. The nondestructive testing methods are valuable because the failed products are unaffected by analysis, so inspection sometimes starts using these methods. The nondestructive testing methods include followings: electrical analysis, X-xay, and C-SAM, etc.. The destructive testing methods include SEM/EDX, XPS, and so forth.

3.2.1. ELECTRICAL ANALYSIS

In failure analysis, electrical analysis can be used to detect circuit shortening/opening and reverse current of the device. It is also used to measure electrical parameters shifting, and to confirm malfunction of failed devices.

Leakage current is measured to verify the deterioration of LED chips during reliability tests. It is because increase of non-radiative SRH recombination can be detected in term of increase of leakage current [8]. When operating an LED device, the injection current is assigned into several processes including radiative recombination with emitting photons, non-radiative Shockley–Read–Hall recombination (SRH), Auger recombination, and leakage current out of the active layer [9]. Then the rate equation can be expressed as [10, 11]:

$$dn/dt = J/ed - An - Bn^2 - Cn^3 - J_L/ed_1 \tag{3.3}$$

where n is the carrier density; J is the injection current density; e is the unit charge; d is the active layer thickness; A, B and C are the coefficients of SRH, radiative, and Auger recombination; J_L is the leakage current; d_1 is the minority carrier diffusion length in the p-type confining layer.

In Eq. 3.3, the term is given by the non-radiative SRH recombination rate as

$$A = \frac{1}{2} N_T \sigma v \tag{3.4}$$

where N_T is the defect density, σ is the capture cross section, and v is the thermal velocity. Increase of the defect density, causes the degradation of the lumen output, as well as electrical performance.

On the other hand, the $I-V$ characteristic is often used to detect series resistance increase and shift of ideality factor of the LED chip. For an LED which is operated at high injecting current, it follows following relationship [12]:

$$V_F = R_S I + \frac{(\ln I - \ln I_S) nKT}{q} \tag{3.5}$$

where I is the forward current, V_F is the forward voltage, R_S is the series resistance, n is the ideality factor, k is the Boltzmann constant (8.6173×10^{-5}eV/K), T is the measurement temperature, and q is electron charge.

Except for leakage current and $I-V$ characteristic, $C-V$ characteristic is also frequently used to monitor chip deterioration [13], because $C-V$ characteristic reflects the apparent charge concentration of the active layers.

3.2.2. X-RAY INSPECTION

X-rays are a form of wavelike electromagnetic energy carried by particles called photons. X-rays can be generated by using an X-ray machine. X-ray imaging provides direct visualization of devices' superficial and internal structures, typically with little need of sample preparation or modification. X-ray imaging systems play a critical role in failure analysis laboratories. The nondestructive nature of x-ray technique avoids sample destruction and helps users save time, reduce cost, and diminish the risk processing errors [14]. The heart of an X-ray machine is an electrode pair – a cathode and an anode – that sits inside a glass vacuum tube. The cathode is a heated filament. When passing current through the filament, it is heated up. Electrons are sputtered off of the filament surface due to heat generated in the filament. These electrons are then drawn by the positively-charged anode, a flat disc made of tungsten.

Basically, the voltage difference between the cathode and anode is extremely high, so the electrons fly through the tube with a great deal of force. As indicated in Fig. 3.1, when a speeding electron collides with a tungsten atom, an electron in one of the atom's lower orbitals is knocked loose. An electron in a higher orbital immediately falls to the

lower energy level, releasing its extra energy in the form of a photon. It's a big drop, so the photon has a high energy level – which is called as X-ray photon [15].

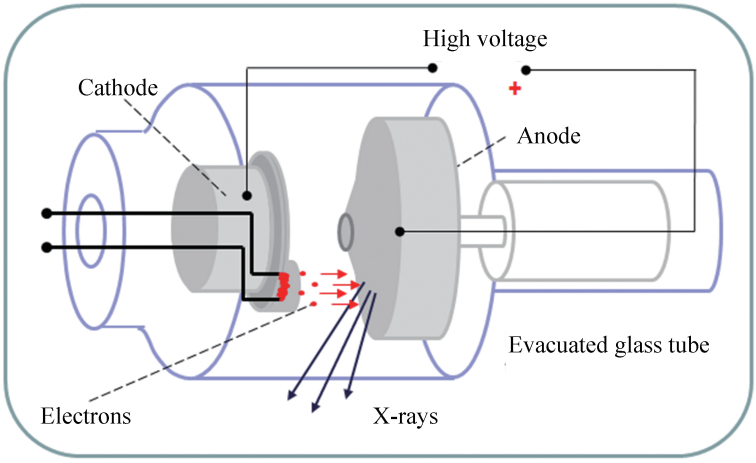

Figure 3.1: Working principle of an X-ray machine

Due to their ability to penetrate certain materials, X-rays are used for a number of nondestructive evaluation and testing (NDE/NDT) applications. When the sample location cannot be inspected using external appearance related metrology tools, X-Ray imaging can be used to detect the internal structure of the sample due to its intensity change as a function of material density. This contrast image can show the internal structure of the sample without any physical destruction to the diagnosed region. The major applications are [16]:

- Defect inspection in IC packaging layer delamination, burst crack, void, and bonding inspection.
- Potential defects in the PCB manufacturing process e.g.: mis-alignment, bridge or open circuit.
- SMT soldering void inspection and measurement.
- Defect inspection of open, short or abnormal connections in the interconnects.
- Solder ball array inspection in BGA packaging and flip chip packaging.
- Inspection of crack in high density plastic material or void in metal.
- Chip dimension measurement, wire arc measurement, solding percentage measurement.

3.2.3. SAM INSPECTION

Scanning acoustic microscopy (SAM) is a well-established and useful technique for imaging and investigating the properties of materials such as metals, ceramics and composites, as well as integrated circuits and biological samples [17]. The SAM is based on the interaction between ultrasonic waves and matter. The presence of inhomogeneities and discontinuities along their propagation paths inside the matter causes modifications in the amplitude and polarity of ultrasonic waves. As the pulses travel through the sample, reflections occur at defects or not bonded interface due to difference in acoustic impedance. Practically, an acoustic microscope is based on a source of pulsed ultrasonic waves of fixed frequency, produced by a piezoelectric crystal transducer equipped with an acoustic lens to focus the waves in a spot. The transducer mechanically scans over the selected portion of the object so as to cover an entire area of inspection. The transducer and sample are immersed in a fluid coupling medium. De-ionized water is typically used since it is a safe, non-hostile environment for most packages. The acoustic microscope transducer is capable of x, y, and z-direction movement. The z-axis is used to focus the ultrasonic pulse at particular depths within a sample while the x and y axes permit acquisition at various locations in the plane of focus, analogous to using a high powered optical microscope [18]. Fig. 3.2 shows a schematic diagram of a typical SAM.

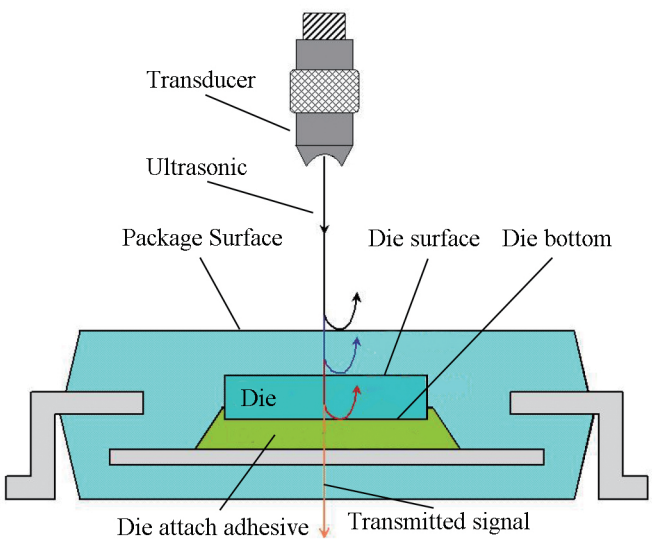

Figure 3.2: A schematic diagram of a typical SAM [18]

Depending on their scanning modes, SAM can be broken into 4 types: A-scan, B-scan, C-scan, and T-scan. C-scan, an image of the x-y plane, is the most common acoustic image. In the C-scan, images are formed by the sound waves reflected from the interfaces within the packages. They could be the sound waves reflected from the interface between the mold compound and die, the mold compound and lead frame, the mold compound and die attach pad or the die and die attach pad. The interface of interest can be selected by placing the data gate at the signal reflected from that interface in the A-scan. C-scans are capable of showing the condition of a bonded surface by analyze the reflected wave's phase and amplitude. C-scan is widely used in the detection of delamination and pop-corn effect. The major applications are [19]:

- Normally used to detect delaminations or cracks inside the package, SAT is capable of detecting micro gaps down to 0.13 μm.
- IC package level structure analysis.
- IC package quality on PCBA level.
- PCB/IC substrate structure analysis.
- Wafer level structure analysis.
- WLCSP structure analysis.
- CMOS structure analysis.

3.2.4. SEM/EDX

Scanning electron microscopy with energy dispersive X-ray spectroscopy (SEM/EDX) is one of the most widely-used surface analytical techniques. The analysis of the characteristic x radiation can yield both qualitative identification and quantitative compositional information from regions of a specimen as small as a micrometer in diameter [17]. High resolution images of surface topography, with excellent depth of field, are produced using a highly-focused, scanning (primary) electron beam. The primary electrons enter a surface with an energy of 0.5 – 30 kV and generate many low energy secondary electrons. The intensity of these secondary electrons is largely governed by the surface topography of the sample. An image of the sample surface can thus be constructed by measuring secondary electron intensity as a function of the position of the scanning primary electron beam. High spatial resolution is possible because the primary electron beam can be focused to a very small spot (< 10 nm) [20]. SEM/EDX has a typical analysis depth of 1–3 μm.

In addition to low energy secondary electrons, backscattered electrons and X-rays are generated by primary electron bombardment. The intensity of backscattered electrons can be correlated to the atomic number of the element within the sampling volume. Hence, some qualitative elemental information can be obtained. The analysis of characteristic X-rays (EDX or EDS analysis) emitted from the sample gives more quantitative elemental information. Such X-ray analysis can be confined to analytical volumes as small as 1 cubic micron [20].

SEM, accompanied by X-ray analysis, is considered a relatively rapid, inexpensive, and basically non-destructive approach to surface analysis. It is often used to survey surface analytical problems before proceeding to techniques that are more surface-sensitive and specialized. Fig. 3.3 shows a schematic of the SEM/EDX system.

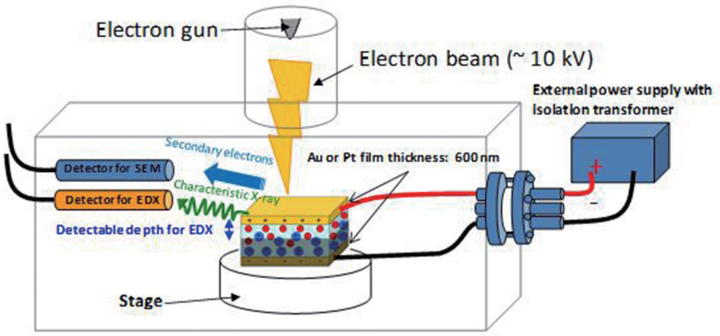

Figure 3.3: A typical schematic of the SEM/EDX system [21]

The major applications of the SEM/EDX are [22]:

- Imaging of a corroded copper surface.
- EDX analysis and mapping of dust from Beijing.
- Microstructure of a sputter-deposited silver film.
- Composition of a metallic brake pad.
- Pinhole in paint caused by cracks in the steel substrate.

3.2.5. XPS

X-ray photoelectron spectroscopy (XPS) is also known as electron spectroscopy for chemical analysis (ESCA) [23]. It is one of the most widely used surface analysis technique because it can be applied to a broad range of materials and provides valuable quantitative and chemical state information from the surface of the material being studied. The

average depth of analysis for an XPS measurement is approximately 5 nm. Spatial distribution information can be obtained by scanning the micro focused x-ray beam across the sample surface. Depth distribution information can be obtained by combining XPS measurements with ion milling (sputtering) to characterize thin film structures. The information XPS provides about surface layers or thin film structures is important for many industrial and research applications where surface or thin film composition plays a critical role in performance including: nanomaterials, photovoltaics, catalysis, corrosion, adhesion, electronic devices and packaging, magnetic media, display technology, surface treatments, and thin film coatings used for numerous applications [24].

XPS is typically accomplished by exciting a samples surface with mono-energetic Al $k\alpha$ x-rays causing photoelectrons to be emitted from the sample surface. An electron energy analyzer is used to measure the energy of the emitted photoelectrons. From the binding energy and intensity of a photoelectron peak, the elemental identity, chemical state, and quantity of a detected element can be determined [24]. XPS instruments func-

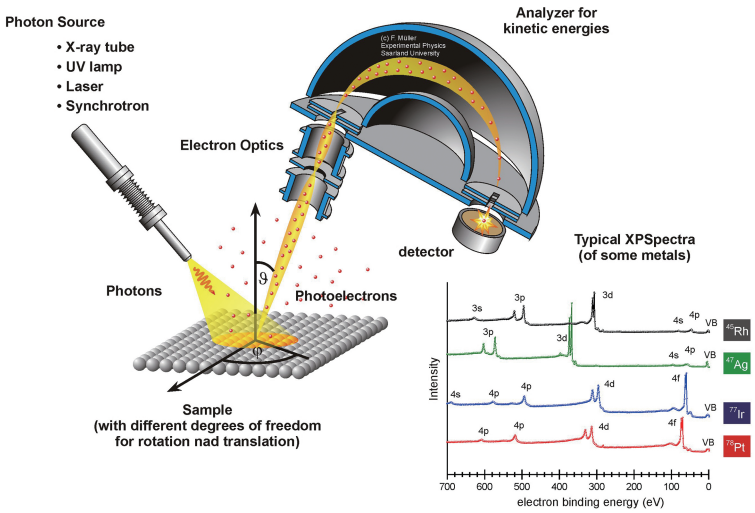

Figure 3.4: A typical schematic of XPS [25]

tion in a manner analogous to SEM/EDS instruments that use a finely focused electron beam to create SEM images for sample viewing and point spectra or images for compositional analysis. The size of the x-ray beam can be increased to support the efficient analysis of larger samples with homogeneous composition. In contrast to SEM/EDS which has a typical analysis depth of 1–3 μm, XPS is a surface analysis technique with a typical analysis depth of less than 5 nm and is therefore better suited for the compositional analysis of ultra-thin layers and thin microscale sample features [24]. A typical of

the XPS system is shown in Fig. 3.4.

XPS analysis applications include [26]:

- Oxidation analysis of specimen (oxidation depth and oxidation state).
- Depth profiling of multi-layer membrane.
- Surface composition analysis.
- Surface staining/coloration ingredients analysis.

REFERENCES

[1] A. Jamnia, *Practical guide to the packaging of electronics: thermal and mechanical design and analysis* (CRC Press, 2008).

[2] G.-y. Yu, X.-p. Zhu, S.-h. Hu, W.-w. Hao, and T.-t. Guo, *Thermal simulation and optimization design on a high-power led spot lamp,* Optoelectronics Letters **7**, 117 (2011).

[3] C.-J. Weng, *Advanced thermal enhancement and management of led packages,* International Communications in Heat and Mass Transfer **36**, 245 (2009).

[4] L. Yin, L. Yang, W. Yang, Y. Guo, K. Ma, S. Li, and J. Zhang, *Thermal design and analysis of multi-chip led module with ceramic substrate,* Solid-State Electronics **54**, 1520 (2010).

[5] A. E. F. Taylor, *Illumination fundamentals,* https://optics.synopsys.com/lighttools/pdfs/illuminationfund.pdf (year: unknown), [online].

[6] J. Hammersley, *Monte carlo methods* (Springer Science & Business Media, 2013).

[7] Wikipedia, *Failure analysis,* https://en.wikipedia.org/wiki/Failure_analysis (year: unknown), [online].

[8] M. Meneghini, A. Tazzoli, G. Mura, G. Meneghesso, and E. Zanoni, *A review on the physical mechanisms that limit the reliability of gan-based leds,* IEEE Transactions on Electron Devices **57**, 108 (2010).

[9] G. Zu-Qiang and Q. Ke-Yuan, *Accurate measurement and influence on device reliability of defect density of a light-emitting diode,* Chinese Physics B **22**, 106108 (2013).

[10] H.-Y. Ryu, H.-S. Kim, and J.-I. Shim, *Rate equation analysis of efficiency droop in ingan light-emitting diodes,* Applied Physics Letters **95**, 081114 (2009).

[11] Q. Dai, Q. Shan, J. Wang, S. Chhajed, J. Cho, E. F. Schubert, M. H. Crawford, D. D. Koleske, M.-H. Kim, and Y. Park, *Carrier recombination mechanisms and efficiency droop in gainn/gan light-emitting diodes,* Applied Physics Letter **97**, 133507 (2010).

[12] D.-g. LI, W.-l. WANG, F.-s. MIN, and H.-p. SHEN, *Relation between ideal factor and lifetime,* Chinese Journal of Liquid Crystals and Displays **6**, 019 (2008).

[13] C. G. Moe, M. L. Reed, G. A. Garrett, A. V. Sampath, T. Alexander, H. Shen, M. Wraback, Y. Bilenko, M. Shatalov, and J. Yang, *Current-induced degradation of high performance deep ultraviolet light emitting diodes,* Applied Physics Letters **96**, 213512 (2010).

[14] E. D. R. Committee *et al.*, *Microelectronics Failure Analysis: Desk Reference* (Asm International, 2011).

[15] T. HARRIS, *How x-rays work,* http://science.howstuffworks.com/x-ray2.htm (year: unknown), [online].

[16] iST Group, *X-ray inspection (2d x-ray),* http://www.istgroup.com/english/3_service/03_01_detail.php?MID=125&SID=127&ID=330 (year: unknown), [online].

[17] B. Khuri-Yakub, *Scanning acoustic microscopy,* Ultrasonics **31**, 361 (1993).

[18] L. Ma, S. Bao, D. Lv, Z. Du, and S. Li, *Application of c-mode scanning acoustic microscopy in packaging,* in *8th International Conference on Electronic Packaging Technology, 2007(ICEPT 2007)* (IEEE) pp. 1–6.

[19] iST Group, *Scanning acoustic tomography (sat),* http://www.istgroup.com/english/3_service/03_01_detail.php?MID=43&SID=89&ID=235 (year unknown), [online].

[20] Surface Science Western, *Scanning electron microscopy coupled with energy dispersive x-ray (sem/edx) spectroscopy,* http://www.surfacesciencewestern.com/analytical-services/scanning-electron-microscopy-coupled-with-energy-dispersive-x-ray-semedx-spectroscopy/ (year: unknown), [online].

[21] S. Kuwabata, A. Imanishi, T. Tsuda, and T. Torimoto, *Use of ionic liquid under vacuum conditions* (INTECH Open Access Publisher, 2013).

[22] Surface Science Western, *Scanning electron microscopy coupled with energy dispersive x-ray (sem/edx) spectroscopy,* http://www.surfacesciencewestern.com/analytical-services/scanning-electron-microscopy-coupled-with-energy-dispersive-x-ray-semedx-spectroscopy/ (year: unknown), [online].

[23] J. F. Watts, *X-ray photoelectron spectroscopy,* Surface science techniques , 5 (1994).

[24] Physical Electronics, *Xps/esca,* https://www.phi.com/surface-analysis-techniques/xps-esca.html (year: unknown), [online].

[25] Rob, *X-ray photoelectron spectroscopy,* http://www.rowbo.info/XPS.html (year: unknown), [online].

[26] iST Group, *Xps/esca,* http://www.istgroup.com/english/3_service/03_01_detail.php?MID=5&SID=90&ID=324 (year: unknown), [online].

4

OPTICAL DEGRADATION KINETICS CAUSED BY PACKAGE MATERIALS

A degradation mechanism analysis methodology is proposed for the mid-power white-light LED packages in this chapter. Based on the degradation data obtained from a series of ageing tests which are performed on the individual packaging material, the degradation kinetics of lumen output and spectral power distribution (SPD) of the LED packages are investigated by using optical simulation. As a result, although the reflectivity of the packaging materials decreased severely for the blue lights (i.e., 450 nm), simulation showed that lights at this wavelength were little absorbed in the LED package. More specifically, it is found that, (1) the degradation of the blue lights is mainly due to blue chip deterioration, while rarely affected by degradation of the silicone encapsulant and other packaging materials; (2) the degradation of the down-converted lights is significantly attributed to degradation of the blue chips, the phosphors, the lead frames and the package housing and; (3) the degradation of the silicone encapsulant, contributes about 1.35% to the total lumen degradation within 168 hours, while has no more contribution to the lumen degradation with further ageing duration. The simulation results have been validated by experiments and successfully applied to the degradation mechanism analysis of LED packages in LM-80-08 tests.

Parts of this chapter have been published in IEEE Transactions on Electron Devices **63**, 2807 (2016) [1].

4.1. INTRODUCTION

MID-POWER white-light LED package is a relatively new category of LED products which are typically driven within a range of 0.2 W to 1 W. Recently, due to their good performance, cost attractiveness and, low energy consumption as compared to conventional lighting solutions, the mid-power white-light LEDs have been widely utilized in many indoor lighting products, such as TLED, Bulb, and Par lamp.

Generally, the mid-power white-light LED package is composed of four components, i.e., blue dies, silicone/phosphor component, copper-based lead frames, and plastic package housing. For such type of LEDs, blue lights are pumped by the dies and then converted into white lights when passing through the silicone mixed with phosphors that are dispersed into the package housing. The target correlated color temperature (CCT), is achieved by carefully tuning the concentration of the phosphors during manufacturing. A schematic of the mid-power LEDs is illustrated in Fig. 4.1.

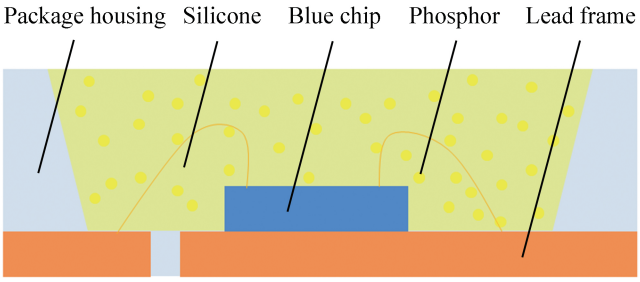

Figure 4.1: The structure of a mid-power white-light LED package

Recently, driven by demands of cost-down, manufacturers have successfully developed mid-power white-light LEDs which can be powered up to 1.5 W by means of integrating more chips inside one package and overdriving the package with higher forward currents. The trend in smaller package size and more compact integration imposes new challenges that are commonly found in LED packages. As a consequence, degradation of the LED package housing materials [2–4], as well as the yellowing of the encapsulant [5, 6], are frequently reported by researchers. Side chain and ring oxidation as well as the formation and subsequent oxidation of phenolic end groups were postulated to be the main reasons for discoloration and yellowing of the plastic materials [7, 8]. In addition to the yellowing, due to bad hermetic protection of the silicone encapsulant, contamination of silver-coating lead frames was also reported [9]. Actually, several studies demonstrate that even a very little percentage of H_2S in the atmosphere can produce silver sulphides on the parts being in contact with environment [10, 11]. On the other

hand, blue chip deterioration is also considered as one of the degradation mechanisms in LED packages [12–15]. Recently published literature has reported a decay of about 5% of the total lumen output is attributed to the chip deterioration even though no deterioration in the p-n junction is observed [16]. All these degradation could result in poor lumen maintenance, leading to shorter LED life and chromaticity shift. A summary is also referred as in [17] for the reliability issues involved in the mid-power LED packages.

In spite of many studies on the degradation mechanisms of the LED products, there are few researchers focusing on the lumen degradation kinetics induced by package material degradation. However, the degradation of different package materials may induce different lumen degradation kinetics. Understanding the degradation kinetics can help the researchers to decouple the degradation mechanisms, which are generally a combination of chip-level deterioration and package-level degradation. This is very important for failure analysis, because only knowing the major degradation mechanism can it help engineers and researchers to improve the reliability of the LED products. For this purpose, Tan *et al.* [18] proposed a statistical methodology in which the Akaike information criterion (AIC) is used to verify the number of failure mechanisms in the given set of data and the Bayes' posterior probability theory is utilized to determine the probability of each failure data belonging to different failure mechanisms. This method has been successfully used in decoupling the degradation mechanisms of a type of ultra-bright white LEDs [19]. On the other hand, by comparing temperature-dependent output degradation with the modification of chromatic properties or the evolution of leakage currents, different contributing factors that predominantly determine the reliability characteristics of an LED products was estimated by Jung *et al.* [20]. Recently, Song *et al.* [21] proposed an analytical/experimental hybrid procedure to quantify the effect of each mechanism on pc-LED degradation. The model decomposes the spectral power distribution (SPD) change into the contributions of individual package material, making it an attractive methodology in failure analysis. This methodology, however, confronts difficulties when involving in LED package with more complicated structures. For example, a mid-power LED which is packaged with phosphor-dispensing silicone encapsulant, as illustrated in Fig. 4.1. For this type of LED packages, the SPD changes were contributed to deterioration of chip and phosphor, yellowing of package housing and silicone encapsulant, as well as deterioration of the lead frames. It is not easy to study the optical degradation by using the analytical/experimental hybrid procedure to separate the contributions of all these package components. Instead, optical simulation is a much easier way to separately see the optical degradation kinetics induced by each individual packaging component.

In this chapter, a numerical model is presented to explore the lumen degradation kinetics of one type of mid-power white-light LEDs. At first, package material ageing tests are performed. At this step, the reflectivity of the package housing and the silver coating lead frames, and the transmissivity of the silicone bulk are obtained. Secondly, a simulation model is established by using the commercial light tracing software *Lighttools* [22]. After a series of simulations, the SPD of the LED package is collected corresponding to different degradation amount of the package materials. Finally, by comparing the degradation trends of the SPD, the contribution of chip-level degradation and package-level degradation to the total lumen degradation is decoupled.

4.2. PACKAGE MATERIAL DEGRADATION TESTS

Thermal ageing tests are respectively performed on the package housing, and the silicone encapsulant. The objective is to explore the degradation of surface reflectivity of the package housing, as well as the transmissivity of the encapsulant. For convenience, the package housing and the encapsulant are prepared as round plates with a diameter of 30 mm. However, due to lack of equipment, the lead frames are directly obtained from the production line. An illustration of the samples can be referred to Fig. 4.2. It should be noticed that there are a plenty of etching holes on the lead frames. These etching holes will affect the actual reflectivity of the silver-coating surface. In order to obtain the exact reflectivity, a black plate with very low reflectivity (5%) is utilized as the background of the etching holes during reflectivity measurement. With the assumption that the thickness of the lead frames is small enough such that the lights will not be reflected or absorbed by the side walls of the lead frames, how the actual reflectivity of the lead frames can be calculated is explained in the following paragraph.

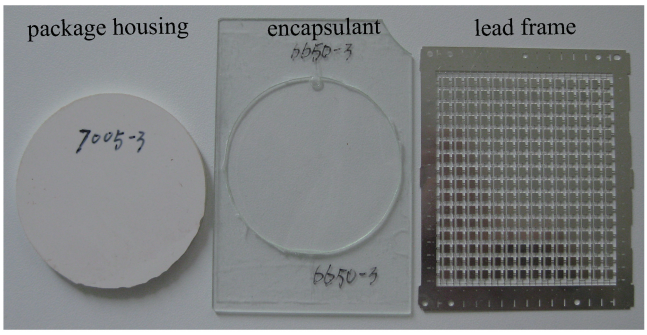

Figure 4.2: An illustration of the package housing, the encapsulant and the lead frames

At first, assume the total area of the etching holes and the surface of the lead frames are A_1 and A_2 , and the reflectivity of the background behind the etching holes and the silver coating surface of the lead frames are $R_1(\lambda)$ and $R_2(\lambda)$ respectively. It is also assumed that the intensity of the incident lights and reflected lights are $I_i(\lambda)$ and $I_o(\lambda)$ respectively. Then the total reflectivity of the measured sample is:

$$R(\lambda) = \frac{I_o(\lambda)}{I_i(\lambda)} = \frac{A_1}{A_1 + A_2} R_1(\lambda) + \frac{A_2}{A_1 + A_2} R_2(\lambda) \tag{4.1}$$

where λ is the wavelength of the lights. According to Eq. (4.1), the reflectivity of the lead frames can be calculated as:

$$R_2(\lambda) = \frac{(A_1 + A_2)R(\lambda) - A_1 R_1(\lambda)}{A_2} \tag{4.2}$$

In most applications, the highest temperature that the LED package may experience during operation is about 130 °C, which is also the maximum junction temperature that chip supplier guaranteed. However, to accelerate the degradation process, the package housing samples are placed into a climate chamber in which the ambient temperature is set as 170 °C. For comparison, several package housing samples are also aged at an ambient temperature 130 °C to show the actual degradation of the package housing.

Similar to the ageing tests for the package housing samples, the silicone encapsulant samples are also placed into a climate chamber for high temperature storage test. However, the ambient temperature is set as high as 200 °C. This temperature is much higher than that the silicone encapsulant may experience in the LED packages. However, the silicone-based encapsulant shows excellent thermal stability even though the ageing temperature has exceeded the junction temperature of the blue chips during operation. As the objective of this study is to understand the relationship between lumen degradation and packaging materials, it is reasonable to accelerate the material degradation process by ageing them at temperatures that higher than that in application conditions. These data are not available for lifetime prediction.

The lead frames are aged by hydrogen sulfide (H_2S) with an ambient temperature of 25 °C during ageing test. Actually, temperature is not the major stress factor for the degradation of the lead frames. However, harmful elements in the atmosphere, such sulfur and chloride, should be the main reason which induces deterioration of the lead frames.

All samples are taken out for optical measurement after a series of pre-defined periods. The reflectivity of the package housing samples, the reflectivity of the lead frames, and the transmissivity of the transparent encapsulant are collected. Due to incomplete

surface layout, the reflectivity of the lead frame was then calculated according to Eq. (4.2). Finally, the measurement data are presented in Fig. 4.3, Fig. 4.4, and Fig. 4.5 respectively.

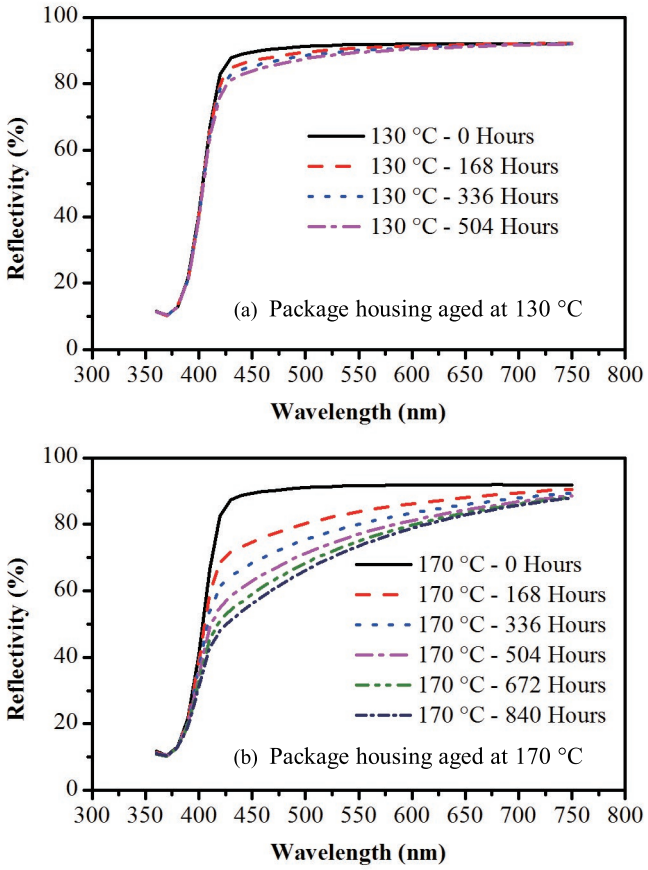

Figure 4.3: Reflectivity of package housing aged at 130 °Cand 170 °C

On the other hand, the emission spectra of the blue chip, is directly obtained from chip supplier, as indicated in Fig. 4.6(a). The emission spectra, the excitation spectra and the emission spectra of the phosphors also are provided by phosphor suppliers, as can be seen from Fig. 4.6(b). Ageing tests are not performed for the blue dies and the phosphor materials. Instead, a series of pre-assumed emission efficiency of the blue dies are used to indicate the chip-level degradation which may be triggered during electrical operation of the LED packages. The same strategies apply to degradation of the phosphors.

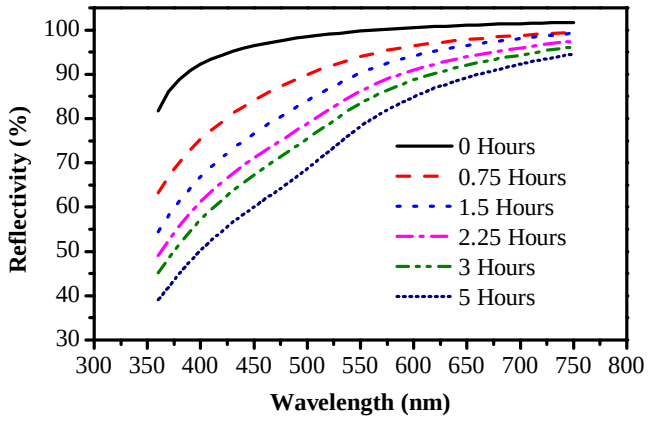

Figure 4.4: Reflectivity of lead frames exposure to H_2S atmosphere

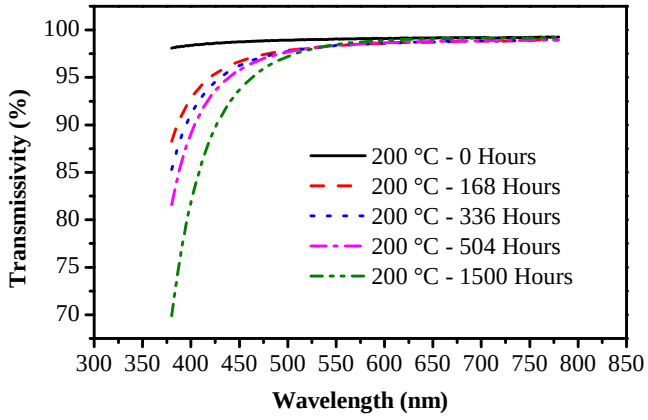

Figure 4.5: Transmissivity of encapsulant aged at 200 °C

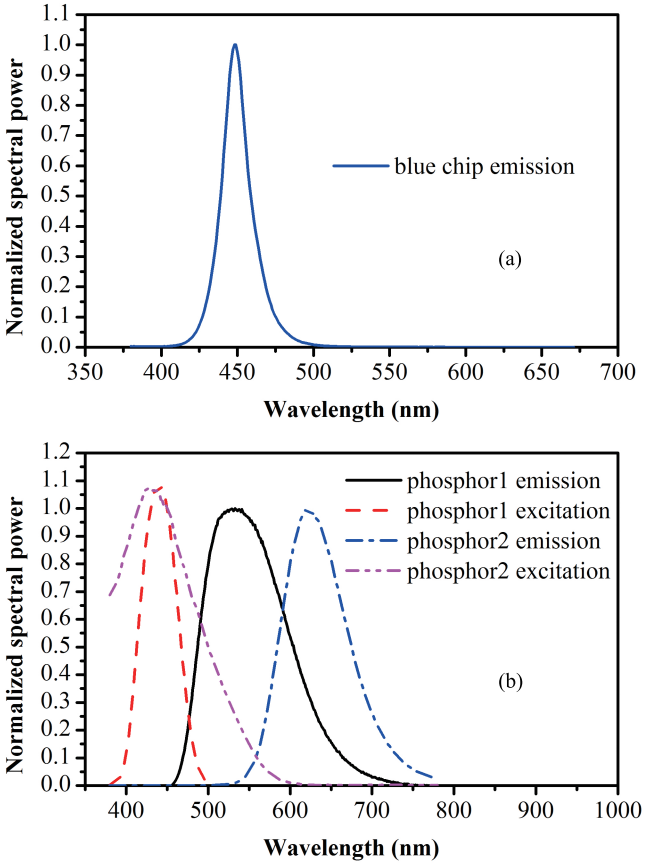

Figure 4.6: Emission spectra of the blue chip and phosphors

4.3. OPTICAL SIMULATION MODELING

4.3.1. SIMULATION MODEL SET-UP

As indicated in Fig. 4.7, a type of mid-power white-light LED package, with 3 mm×3 mm×0.52 mm in dimensions, is created by using the 3-D modeling software *Lighttools* [22]. The package cup is ϕ2.6 mm×0.32 mm in dimensions. For this type of LED package, two blue dies are attached at the center area of the package cup and connected in series with gold wires. However, the effects of the gold wires are considered to be negligible, so the gold wires are not created in the simulation model. Silicone is used as a encapsulant, which protects the LED dies from mechanical damage, while still offer excellent light extraction from the package at the same time. In mid-power white-light LED packages, the silicone encapsulant is generally mixed with phosphor powders and

dispensed into the package cup.

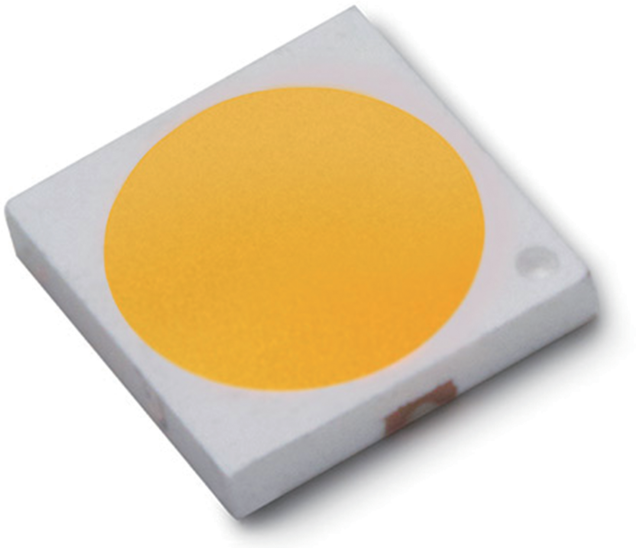

Figure 4.7: LED package model used for optical simulation

A commercial light tracing software *Lighttools* [22], is used for the optical simulations. The optical property of the lead frames, the package housing, and the silicone encapsulant are defined respectively. Smooth optical is used for optical property definition of the lead frames. Then the wavelength-dependent reflectivity, which is measured in previous section, is input into the simulation model. The settings of the package housing are similar to that of the lead frames. The surface optical property of the silicone is also set in terms of smooth optical mode. For simplicity, lights transmitting through the silicone surface are assumed to be 100%, implying that Fresnel loss is not considered in the simulation model. This is reasonable because interface deterioration between different materials is not accounted for in this study.

The material property of the phosphor-mixed silicone encapsulant is defined by using the user material definition tab in *Lighttools*. The input parameters include the excitation spectra, the emission spectra, the absorption efficiency, the emission efficiency, and the Mie particle size distribution of the green and red phosphors, and bulk transmissivity of the silicone encapsulant. Then the SPD of the LED package is calculated by carefully adjusting the mean free paths of both the green and red phosphors, until the desired color coordinate is obtained, as shown in Fig. 4.8. In this figure, the SPD of an LED package with a correlated color temperature (CCT) of 2700 K is presented. The SPD

is with a peak wavelength of 450 nm for the pumped blue lights, and a peak wavelength of 610 nm for the down-converted lights.

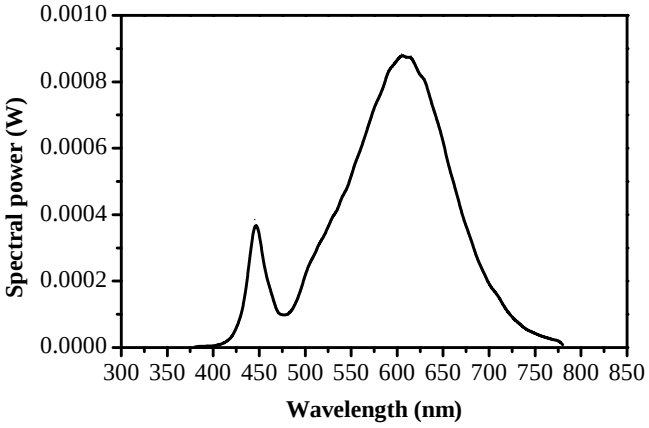

Figure 4.8: Spectral power distribution of an LED package

In order to understand the lumen degradation kinetics of the LED package, optical parameters are adjusted successively according to data measured in the previous section. These parameters are listed as follows:

(1) Emission efficiency of the blue dies;

(2) Emission efficiency of the phosphors;

(3) Bulk transmissivity of the silicone encapsulant;

(4) Reflectivity of package housing;

(5) Reflectivity of the lead frames.

4.3.2. SIMULATION RESULTS

Uniform degradation of the SPD was observed at wavelength range from 380 nm to 780 nm when the emission efficiency of the blue dies is reduced from 100% to 85% of their initial values, as presented in Fig. 4.9. Without loss of generality, the spectral power at wavelength range from 440 nm to 460 nm and wavelength range from 600 nm to 620 nm are averaged respectively. Then the averaged values are employed to represent the degradation of the blue lights and the down-converted light. As a consequence, the degradation of the blue chip efficiency induces exactly the same amount of degradation

of the blue lights and the down-converted lights, as indicated in Fig. 4.10. The result is exactly in line with that reported in [21].

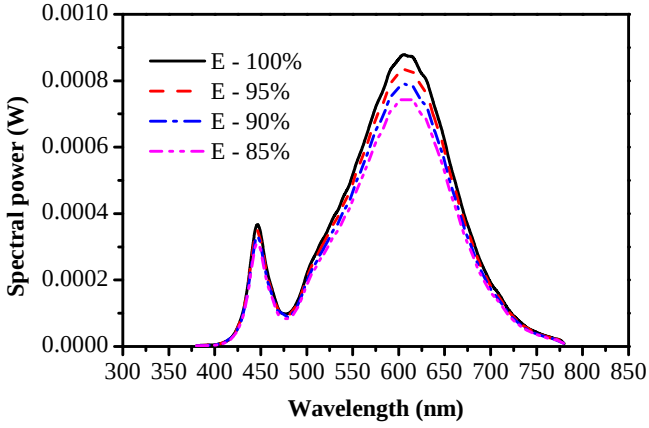

Figure 4.9: Spectral power distribution of the LED package at different chip emission efficiency

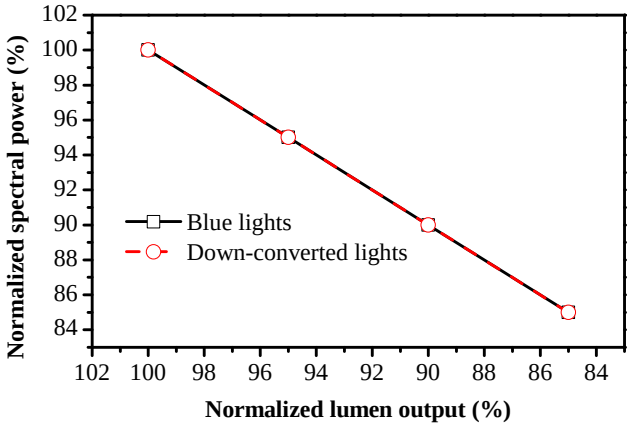

Figure 4.10: Chip degradation: Degradation of spectral power versus chip efficiency

Contrast to that in blue chip degradation, the degradation of the phosphors shows only SPD degradation at the wavelengths of the down-converted lights, as presented in Fig. 4.11. The simulation result showed no decrease for the pumped blue lights, even though a large decrease has been found for the down-converted lights and the lumen output. In this case, the down-converted lights decreased from 100% to 80.4%, and the lumen output decreased from 100% to 82.5%, as indicated in Fig. 4.12.

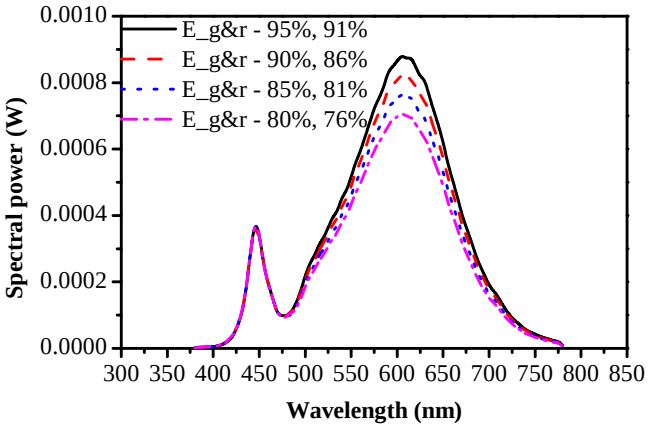

Figure 4.11: Spectral power distribution of the LED package at different phosphor conversion efficiency

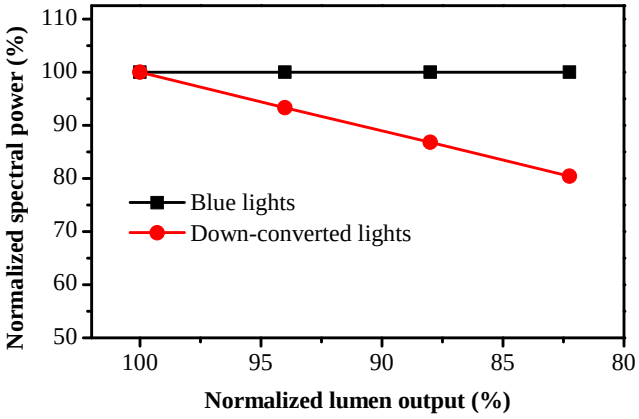

Figure 4.12: Phosphor degradation: Averaged spectral power versus lumen degradation

It is found that silicone degradation contributes to about 1.35% of lumen degradation within 168 hours, as shown in Fig. 4.13. However, further ageing the silicone plate induces very little lumen degradation, although gradual degradation of the blue lights is observed. After ageing for 1500 hours, the normalized spectra power of the blue lights degrades to 98.82% of its initial value. The result indicates excellent thermal stability of the silicone material in our LED products. It is worth noticing that the silicone plate is aged at an ambient temperature of 200 °C. It is expected that, for LED products with lower ambient temperature, the degradation of the blue lights should be much less than the simulation result. In fact, after an initial degradation, the degradation of the

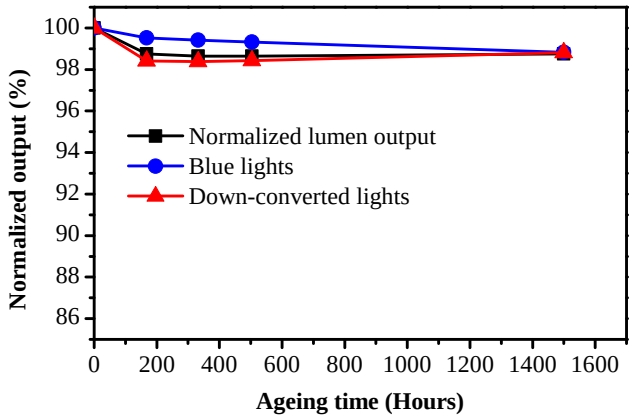

Figure 4.13: Silicone degradation: Normalized spectral power versus ageing time

blue lights should be neglected if the ambient temperature is as low as 120 °C [23]. On the other hand, it is found that the down-converted lights are not sensitive to silicone degradation after a sharp decrease at the initial ageing duration, even though the silicone samples are aged at the ambient temperature which is as high as 200 °C. The early degradation is also found in [23]. The reason is probably due to shrinkage or continuous cross-link reaction of the silicone during ageing test, which is still unclear until now.

It is interesting that, though 5.2% of the lumen output has been triggered in the simulation model by using degradation data of the housing material, which were aged at 170 °C for 840 hours (see Fig. 4.3(b)), the blue lights of the LED package have little degradation, as compared to about 6.8% degradation of the down-converted lights, as indicated in Fig. 4.14. It indicates that the degradation of the package housing affects only the down-converted lights, even though blue lights are much more sensitive to the package housing degradation, as can be seen from Fig. 4.3(b). The same degradation kinetics is also observed in lead frames, as shown in Fig. 4.15. This phenomenon can be explained by the theory of transmission path of light rays in LED packages and the theory of the Bouger-Lambert-Beer law [24].

As described in our previous publication [24], because of high absorption coefficient of the phosphors, most of blue light was down-converted to longer wavelength when propagating through the silicone. Based on this fact, blue lights which were finally extracted out of the package were mainly composed of lights which never hit the phosphor particles. On the other hand, the down-converting light were not absorbed by phosphors, because this light was not in the range of the absorption spectra of the phosphors.

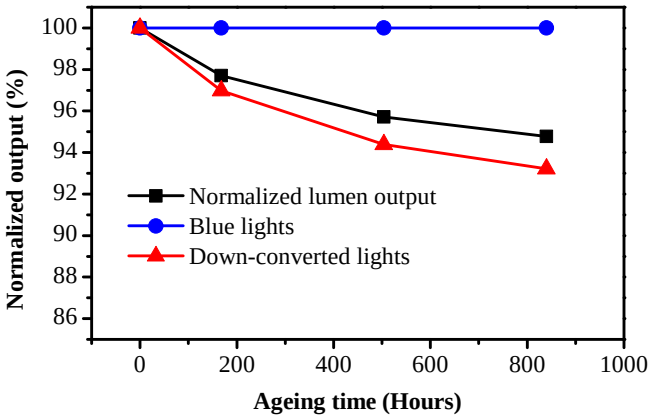

Figure 4.14: Package housing degradation: Normalized spectral power versus ageing time

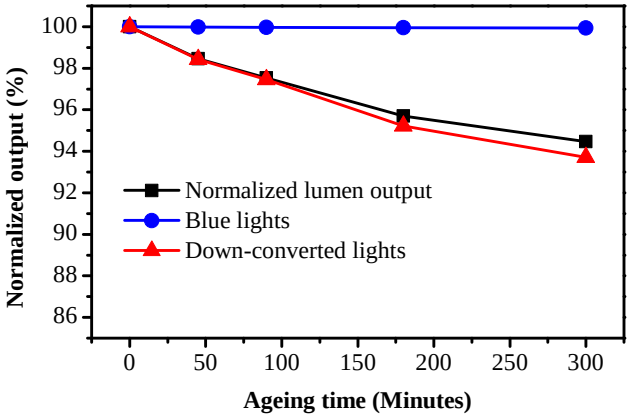

Figure 4.15: Lead frame degradation: Normalized spectral power versus ageing time

As a consequence, the down-converting light would be scattered by phosphor particles and reflected by the package housing/lead frames and propagated through the silicone plate randomly. The scattering and reflection might occur many times before lights finally leave the package. It is, therefore, obvious that converted light went through a much longer path than the blue light before exiting the package.

On the other hand, it is well-known that lights propagating through medium follow

Bouguer–Lambert–Beer law, which is stated as

$$\frac{I}{I_0} = e^{-\alpha L} \tag{4.3}$$

where I_0 and I are the intensity of the incident light and emergent light, L is the distance of transmission path, α is an exponential constant, which is related to material properties, such as transmittance of silicone plate, reflectivity of package inner surface, absorption efficiency of phosphor particles and so forth. Suppose the light output degrades from I to I' after a certain period of ageing, the degradation rate can be calculated as

$$\frac{I'}{I} = e^{(\alpha-\alpha')L} \tag{4.4}$$

Based on equation above, it is clear that longer transmission path L of the down-converting light, than that of the blue light, leading to higher degradation rate before outgoing the package.

In summary, several conclusions are obtained as follows:

(1) Blue chip deterioration induces the same degradation trend of the blue light and down-converted light output;

(2) Silicone degradation only induces initial lumen degradation within a few hundred hours during thermal ageing test;

(3) Silicone degradation may affect the blue light output of an LED package, while the degradation amount should be very limited;

(4) Degradation of phosphor emission efficiency, package housing and lead frame reflectivity has very few effects on the blue light output of an LED package, while has significant effects on the down-converted lights, as well as the lumen output.

4.3.3. VALIDATION AND APPLICATION

The simulation model can be validated by performing two experiments. The first one is to stimulate chip deterioration by applying instantaneous electrostatic human body model (HBM) discharge (ESD) to one LED package [25]. After discharge stimulating, the LED package's lumen output is measured and then sent back for further discharge stimulation. These steps may be repeated several times until comparable lumen degradation is observed. The discharge stimulation destroys the LED chips only while does not induce degradation of the package materials. As a result, the lumen degradation is only attributed to the degradation of emission efficiency of the chip. As presented in

Fig. 4.16, the degradation of the blue lights and down-converted lights are much close to each other. A gap of 0.4% between them should be due to the measurement accuracy of the optical measurement system, as the spectrometer is much less sensitive to degradation of shorter wavelengths (blue lights in this experiment). The other experiment

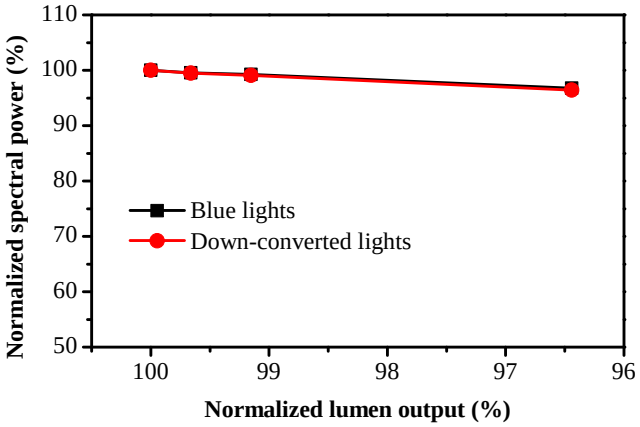

Figure 4.16: Spectral power degradation due to chip deterioration

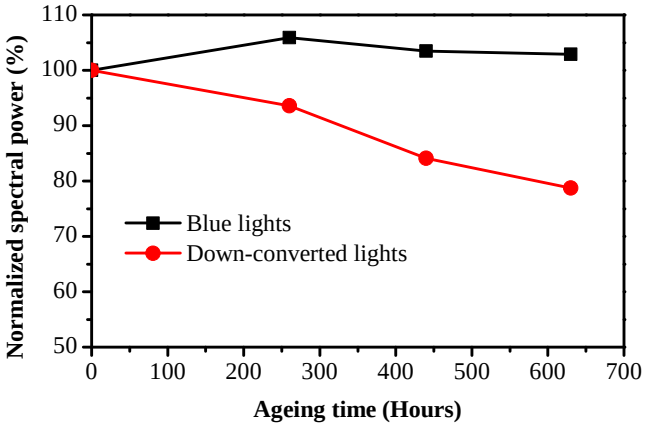

Figure 4.17: Spectral power degradation due to lead frame degradation

is H_2S gas ageing test. This test reduces the reflectivity of the silver-coating lead frames rapidly. In this test, ambient temperature is 40 °C, relative humidity is 80% RH, and concentration of the H_2S gas is kept constantly at 15 ppm. As a result, the down-converted light output decreases to 80% of its initial value, while the blue light output is not de-

graded after ageing for 630 hours, as indicated in Fig. 4.17. The slightly increase of the blue lights is probably due to the silicone curing effect at the initial stage of the ageing test.

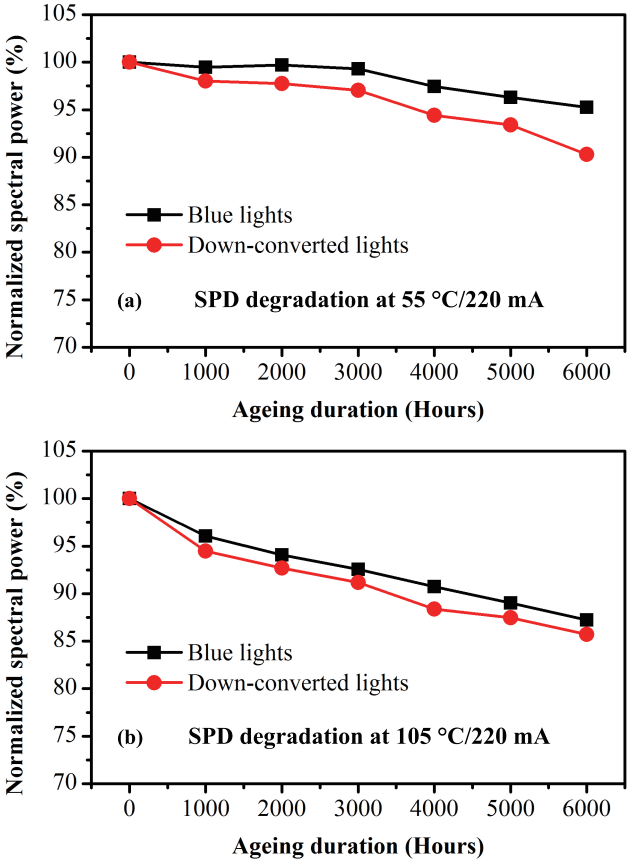

Figure 4.18: Spectral power degradation in LM-80-08 tests

It is difficult to validate the simulation results of package housing degradation, silicone degradation and phosphor degradation due to lack of equipments. However, the validation experiments for chip deterioration and lead frame degradation have provided promising results, indicating the usefulness of the simulation.

Attempts are also successfully made to analyze the lumen degradation mechanisms of the mid-power white-light LED packages, which are stressed for 6000 hours by LM-80-08 tests [26]. Fig. 4.18 shows the normalized spectra power distribution of the LEDs at the stress condition of 55 °C/220 mA and 105 °C/220 mA respectively. In Fig. 4.18(a),

it is found that both the degradation of the blue lights and the down-converted lights show parallel trends with the ageing time, though a gap of 1.6% has already observed after 1000 hours. The gap is considered as early degradation of the LED packages, as it is almost consistent from 1000 hours to 6000 hours. Based on the simulation result, the early degradation is speculated to be induced by silicone degradation, as a gap of 1.35% is also observed in the simulation model. Though in the simulation model, the ageing temperature of the silicone is much higher than that in the LM-80-08 ageing chamber, the lumen degradation in both simulation model and LM-80-08 test is comparable, because the initial degradation of silicone encapsulant is not sensitive to temperature. It is worth noticing that a gap of 1.5% of the blue lights and down-converted lights is also observed for LED samples aged for 1000 hours at 55 °C/220 mA. The gap in this stress condition is much close to that observed at 105 °C/220 mA, so the early degradation is non-temperature sensitive. This is well in agreement with the simulation result, as indicated in Fig. 4.13.

On the other hand, parallel degradation of the blue lights and down-converted lights in LED samples aged at 105 °C/220 mA, indicates the lumen degradation is mainly due to chip deterioration. As a consequence, the major degradation mechanisms for LED samples aged at 105 °C/220 mA should be chip deterioration, as well as the early degradation of the silicone encapsulant.

For LED samples aged at 55 °C/220 mA, the degradation mechanisms are much more complicated than LED samples aged at 105 °C/220 mA. It seems that silicone encapsulant degradation contributes to the first 1.5% lumen degradation after 1000 hours. From 1000 hours to 3000 hours, the lumen degradation is mainly induced by packaging materials, such lead frames, and package housing. It was also reported that phosphor degradation might occur for LED packages aged at high temperature and humidity combined stress conditions [27]. However, the phosphors has been reported to be very stable during thermal ageing, thus eliminating any significant nonradioactive quenching processes that existed in the aged samples [28]. On the other hand, Hu *et al.* [29] reported highly thermal-stability of the Nitride phosphors after ageing for 30 minutes at 1000 °C. Moreover, Cheng *et al.* [30] reported the highly thermal-stability of a broadband glass phosphors which were fabricated by sintering the mixture of multiple phosphors (including YAG, LuAG, and Nitride) and SiO_2-based glass. The samples showed only around 1% lumen degradation after ageing for 1008 hours at 150 °C. All these evidences indicate low possibility of the phosphor degradation in high ambient temperature conditions.

From 3000 hours to 6000 hours, it is found that chip-level degradation has been trig-

gered. This degradation mechanism has been verified by comparing the output power of the blue lights of several non-stressed samples and stressed samples [31]. In order to gain reliable comparison, the silicone encapsulant was removed prior to optical measurement. A gap of 4.5% between the non-stressed and stressed blue chips, well agrees with that observed in Fig. 4.18(a). Noticing that in Fig. 4.18(a) the spectra power was measured without removing silicone encapsulant. This degradation mechanism, combining with the package-level degradation mechanisms which are induced by either degradation of the lead frames or of the package housing, contributes to the lumen degradation of the LED packages. A detailed degradation mechanisms analysis has been performed in our previous study [31].

4.4. SUMMARY

The effects of degradation of blue chips, decrease of conversion efficiency of the phosphors, yellowing of silicone encapsulant, reflectivity decrease of the silver-coating lead frames and the package housing, are investigated thoroughly by using optical simulation. The simulation results have been validated by experiments. As a consequence, the simulation can be used to decouple the chip-level degradation mechanisms and package-level degradation mechanisms of the mid-power white-light LED packages. Furthermore, the silicone-induced degradation mechanisms are also decoupled with the fact that silicone degradation induces only initial lumen degradation of the LED packages. Finally, the simulation results are successfully applied to the degradation mechanism analysis of the LEDs stressed in LM-80-08 tests.

REFERENCES

[1] J. Huang, D. S. Golubović, S. Koh, D. Yang, X. Li, X. Fan, and G. Zhang, *Degradation mechanism decoupling of mid-power white-light leds by spd simulation,* IEEE Transactions on Electron Device **63**, 2807 (2016).

[2] A. Torikai and H. Hasegawa, *Accelerated photodegradation of poly (vinyl chloride),* Polymer Degradation and Stability **63**, 441 (1999).

[3] N. Narendran, Y. Gu, J. Freyssinier, H. Yu, and L. Deng, *Solid-state lighting: failure analysis of white leds,* Journal of Crystal Growth **268**, 449 (2004).

[4] J. W. Jang, S. Y. Choi, and J. K. Son, *Degradation model of led based on accelerated life test,* in *18th IEEE International Symposium on the Physical and Failure Analysis of Integrated Circuits (IPFA), 2011* (IEEE) pp. 1–4.

[5] J.-S. Liou, C.-C. Tsai, W.-C. Cheng, S.-Y. Huang, G.-H. Cheng, J.-K. Chang, J. Wang, and W.-H. Cheng, *Mttf evaluations of encapsulation materials for led package in accelerated thermal tests,* in *16th Opto-Electronics and Communications Conference*.

[6] M. Bahadur, A. W. Norris, A. Zarisfi, J. S. Alger, and C. C. Windiate, *Silicone materials for led packaging,* in *SPIE Optics+ Photonics* (International Society for Optics and Photonics) pp. 63370F–63370F–7.

[7] M. Y. Mehr, W. Van Driel, K. Jansen, P. Deeben, M. Boutelje, and G. Zhang, *Photodegradation of bisphenol a polycarbonate under blue light radiation and its effect on optical properties,* Optical Materials **35**, 504 (2013).

[8] M. Y. Mehr, W. van Driel, H. Udono, and G. Zhang, *Surface aspects of discolouration in bisphenol a polycarbonate (bpa-pc), used as lens in led-based products,* Optical Materials **37**, 155 (2014).

[9] G. Mura, G. Cassanelli, F. Fantini, and M. Vanzi, *Sulfur-contamination of high power white led,* Microelectronics Reliability **48**, 1208 (2008).

[10] T. Graedel, *Corrosion mechanisms for silver exposed to the atmosphere,* Journal of the Electrochemical Society **139**, 1963 (1992).

[11] B. H. Chudnovsky, *Degradation of power contacts in industrial atmosphere: silver corrosion and whiskers,* in *Proceedings of the Forty-Eighth IEEE Holm Conference on Electrical Contacts, 2002.* (IEEE, 2002) pp. 140–150.

[12] E. Jung and H. Kim, *Rapid optical degradation of gan-based light-emitting diodes by a current-crowding-induced self-accelerating thermal process,* IEEE Transactions on Electron Devices **61**, 825 (2014).

[13] M. Meneghini, L.-R. Trevisanello, G. Meneghesso, and E. Zanoni, *A review on the reliability of gan-based leds,* IEEE Transactions on Device and Materials Reliability **8**, 323 (2008).

[14] T. Yanagisawa and T. Kojima, *Degradation of ingan blue light-emitting diodes under continuous and low-speed pulse operations,* Microelectronics Reliability **43**, 977 (2003).

[15] K. Kohler, T. Stephan, A. Perona, J. Wiegert, M. Maier, M. Kunzer, and J. Wagner, *Control of the mg doping profile in iii-n light-emitting diodes and its effect on the electroluminescence efficiency,* Journal of applied physics **97**, 104914 (2005).

[16] C. M. Tan and P. Singh, *Time evolution degradation physics in high power white leds under high temperature-humidity conditions,* IEEE Transactions on Device and Materials Reliability **14**, 742 (2014).

[17] H. Fan, X. Li, J. Shen, and M. Chen, *An effective prediction method for led lumen maintenance,* in *13th International Conference on Electronic Packaging Technology and High Density Packaging (ICEPT-HDP), 2012* (IEEE) pp. 1560–1563.

[18] C. M. Tan and N. Raghavan, *An approach to statistical analysis of gate oxide breakdown mechanisms,* Microelectronics Reliability **47**, 1336 (2007).

[19] C. M. Tan, B. E. Chen, Y. Foo, R. Chan, G. Xu, and Y. Liu, *Humidity effect on the degradation of packaged ultra-bright white leds,* in *10th Electronics Packaging Technology Conference, 2008(EPTC 2008)* (IEEE, 2008) pp. 923–928.

[20] E. Jung, M. S. Kim, and H. Kim, *Analysis of contributing factors for determining the reliability characteristics of gan-based white light-emitting diodes with dual degradation kinetics,* IEEE Transactions on Electron Devices **60**, 186 (2013).

[21] B.-M. Song and B. Han, *Analytical/experimental hybrid approach based on spectral power distribution for quantitative degradation analysis of phosphor converted led,* IEEE Transactions on Device and Materials Reliability **14**, 365 (2014).

[22] Anonymous, *Lighttools illumination design software,* https://optics.synopsys.com/lighttools/ (year: unknown), [online].

[23] Y.-H. Lin, J. P. You, Y.-C. Lin, N. T. Tran, and F. G. Shi, *Development of high-performance optical silicone for the packaging of high-power leds,* IEEE Transactions on Components and Packaging Technologies **33**, 761 (2010).

[24] J. Huang, D. S. Golubovic, S. Koh, D. Yang, X. Li, X. Fan, and G. Zhang, *Degradation mechanisms of mid-power white-light leds under high-temperature–humidity conditions,* IEEE Transactions on Device and Materials Reliability **15**, 220 (2015).

[25] C.-M. Liao and S.-T. Tseng, *Optimal design for step-stress accelerated degradation tests,* IEEE Transactions on Reliability **55**, 59 (2006).

[26] I. LM, *Lm-80-08. approved method: Measuring lumen maintenance of led light sources,* Illuminating Engineering Society of North America (2008).

[27] C. M. Tan, B. K. E. Chen, G. Xu, and Y. Liu, *Analysis of humidity effects on the degradation of high-power white leds,* Microelectronics Reliability **49**, 1226 (2009).

[28] B. Ma and J. Kim, *Complex-stress accelerated lifetime test for high-power light-emitting diodes,* Electronics letters **48**, 449 (2012).

[29] H. Yunsheng, W. ZHUANG, H. Huaqiang, L. Ronghui, C. Guantong, L. Yuanhong, and X. HUANG, *High temperature stability of eu 2+-activated nitride red phosphors,* Journal of Rare Earths **32**, 12 (2014).

[30] W.-H. Cheng, L.-Y. Chen, and W.-C. Cheng, *High-thermal-stability white light-emitting-diodes employing broadband glass phosphor,* in *SPIE Optical Engineering+ Applications* (International Society for Optics and Photonics, 2014) pp. 91900N–91900N.

[31] J. Huang, D. S. Golubović, S. Koh, D. Yang, X. Li, X. Fan, and G. Zhang, *Optical degradation mechanisms of mid-power white-light leds in lm-80-08 tests,* Microelectronics Reliability **55**, 2654 (2015).

5

DEGRADATION MECHANISMS OF MID-POWER WHITE-LIGHT LEDS

In this chapter, the optical degradation mechanisms of mid-power white-light LED packages has been studied by using high temperature operation life test (HTOL), wet-high temperature operation life test (WHTOL) and highly-accelerated temperature-humidity test (HAST). As a result, it was found that, (1) for LED packages aged under HTOL, the major degradation mechanism is different for samples aged at 55 °C and ambient temperature higher than 85 °C, with which lead frames deterioration is the major degradation mechanism at 55 °C while Ohmic contact deterioration is the major degradation mechanism at 105 °C for the aged LED packages; (2) for LED packages aged under WHTOL, both deterioration of the Ohmic contacts of the blue chip and yellowing of the package encapsulant are considered as the major degradation mechanisms; (3) for LED packages aged under HAST, the failure mechanism is considered as the result of blue light over-absorption, which generates very high temperature inside the silicone bulk, resulting in serious carbonization.

Parts of this chapter have been published in Microelectronics Reliability **55**, 2654 (2015) [1], IEEE Transactions on Device and Materials Reliability **15**, 220 (2015) [2], and IEEE Transactions on Device and Materials Reliability **15**, 478 (2015) [3].

5.1. INTRODUCTION

MID-POWER white-light LED is a relatively new category of LED products that are typically driven within a range of 0.2 W to 1 W. Fig. 5.1 shows two kinds of typical mid-power LEDs in the market. Generally, the mid-power LED packages are composed of four components: blue die, lead-frames, silicone/phosphor component and package housing. More specifically, for samples used in our experiments, two pieces of 0.6-mm^2 area blue dies were mounted onto the lead-frame by die attach, and gold wires were bonded to connect both blue dies in series and then connect them to lead-frames. After wire bonding, silicone mixed with phosphors was dispersed into the package housing and was cured as the encapsulant of the package. Blue lights are converted into white lights after passing through the silicone mixed with phosphors that are dispersed into the package housing. The specified correlated color temperature (CCT) is achieved by carefully tuning the concentration of the phosphors during manufacturing.

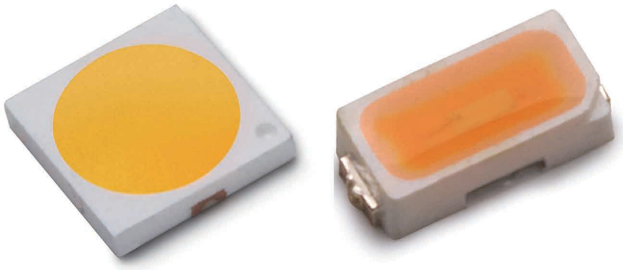

Figure 5.1: Typical mid-power white-light LEDs

Unlike high-power LED packages, mid-power LED packages use plastic package and copper lead frames instead of the traditional ceramic material due to the lower requirement in heat dissipation [4]. Under high temperatures typically experienced by LEDs used for lighting, the plastic packaging that reduces the cost of the device is also a source of reliability issues, such as color shift and lumen degradation[5, 6]. Recently, driven by demands of cost-down, manufacturers have successfully developed mid-power white-light LEDs which can be powered up to 1.5 W by means of integrating more chips inside one package and overdriving the package with higher forward currents. The trend in smaller package size and more compact integration imposes new challenges in rising LED temperatures in packages. Under high ambient temperature and Joule-heating, it has been found that LED packages might suffer from degradation of the Ohmic contacts and active layer [7], deterioration of the lead-frame's silver-coating [8–10], yellowing of encapsulant [11, 12], silicone carbonization [13, 14], as well as phosphor thermal

quenching [15].

Besides, LED packages may also suffer from serious reliability issues when operated under environment with a high humidity and high temperature. This is often the case in tropical countries. For instance, LED can be exposed to an average humidity of 83.4%RH and temperature of 125 °C if it is a LED headlight in Singapore's automotive [16]. In order to understand the effects of moistures on the LED products, the industry conducts qualification experiments, such as wet-high temperature operation life test (WHTOL) [17, 18], highly-accelerated temperature and humidity stress test (HAST) [19, 20]. Results showed that the optical degradation of LED packages was mainly due to delamination of packages [21], lights scattering of water particles inside the silicone volume [22], bubble generation in the encapsulant [19], and dissolution of phosphors [23].

These factors could lead to optical degradation of LED packages [24, 25] and finally the shortening of their service lifetime. Reliability issues involved in the mid-power LED packages have been summarized as in Table 5.1 [4, 26]. However, due to complex interactions among multiple failure modes and limited data at the moment, the failure mechanisms are still an opaque issue.

Table 5.1: Optical degradation mechanisms of mid-power LEDs

Failure mode	**Failure mechanism**	**Triggered stress**
Chip deterioration	Crystal defects, dopant diffusion, Ohmic contact deterioration	Thermal-mechanical stress, electrical overstress, thermal stress
Encapulsant carbonization/yellowing	Decrease in transparency	Thermal stress, photo-degradation, electrical overstress
Package housing yellowing	Decrease in reflectivity	Thermal stress, photo-degradation
Lead frame deterioration	Copper diffusion, metal recrystallization, contamination	Thermal-mechanical stress, hygro-mechanical stress, corrosive elements (S, Cl, etc.)
Phosphor degradation	Quantum efficiency by thermal quenching of phosphor	Thermal stress

Based on the understanding that optical degradation of LED packages can be accelerated if stressed under the combined effect of humidity and temperature, some

studies have been conducted to develop new methodologies to replace the traditionally temperature-only-based test, such as IES LM-80-08 [27]. Fan *et al.* [4] demonstrated that wet-high temperature operation life test (WHTOL) could be used for the prediction of LED lumen maintenance with shorter testing time (one third of LM-80-08 test time). More aggressively, Liu *et al.* [28, 29] presented their results by highly-accelerated temperature and humidity stress test (HAST). The authors claimed that this type of accelerated tests could be applied for lifetime extrapolation from HAST to WHTOL. However, our previous study [30] indicated that the degradation mechanisms in these two different conditions were much different. It was found that the rapid lumen degradation during HAST was mainly due to serious silicone carbonization [30], while for WHTOL, the degradation was due to chip deterioration and package housing yellowing [31]. Up to now the failure mechanisms of silicone carbonization have not yet fully been understood.

The objective of this chapter is to investigate the degradation mechanisms of the the mid-power LED packages under various stress conditions. These stress conditions involve current, temperature, moisture, and pressure. Specifically, the remaining parts of this chapter are organized as follows.

In section 5.2, the reliability of mid-power white-light LEDs was investigated by high temperature operation life test (HTOL). According to the test standard (IES standard LM-80-08) [27], the ageing duration lasted as long as 6000 hours. After finishing the tests, optical and electrical characteristics of the aged samples were analyzed subsequently. Furthermore, failure analysis of the LED packages was also performed to further study the failure modes and failure mechanisms.

In section 5.3, the optical degradation of mid-power LED packages was studied by wet-high temperature operation life test (WHTOL). Optical characteristics, spectral power degradation, and electrical deterioration were studied. Failure analysis of the degraded samples was also performed to further investigate the degradation mechanisms.

In section 5.4, the failure mechanisms of silicone carbonization occurred during highly-accelerated temperature and humidity stress test (HAST), were investigated through the combined experiments, failure analysis and simulation. A series of experiments as well as failure analysis were performed to separate or eliminate some possible root causes. Blue chip Joule-heating, phosphor's self-heating, and blue light over-absorption in silicone were carefully analyzed.

5.2. OPTICAL DEGRADATION MECHANISMS UNDER HTOL

5.2.1. EXPERIMENT SETUP

In order to reduce effects of sample deviation during testing, 28 pieces of MP-3030-EMC LED packages (with 2 blue chips connected in series) were prepared for each stressing condition. The sample size is enough for statistical analysis according to the standard LM-80-08 [27]. The LED packages were soldered onto Metal-core Printed Circuit Boards (MCPCBs). The MCPCBs have a thermal conductivity of 2.2 W/m·K, which guaranteed the reliable heat-dissipation during testing.

After the initial measurement, samples were aged by using 3 climate-ageing chambers, which were specially designed for IES LM-80-08 test. The samples were first mounted onto an integrated thermal control system, which regulated the ageing temperature during testing. Two thermal couples were used to monitor the test temperature. One was mounted onto the center area of the MCPCB for case temperature monitoring, while the other one was placed several centimeters away from the surface of the MCPCB for ambient temperature monitoring. Based on the feedback of both thermal couples, the case temperature was automatically adjusted by the integrated thermal control system when the monitored temperature ran out of the specified limit. According to our test condition, the case temperature was maintained within an error of ±2 °C. In addition, the driving current was also monitored. SpikeSafe Test System was used to provide and record the driving current. The variation of the driving current is controlled within ±3% of its setting value. In addition to this, power protection was also pre-defined. When the driving current is 60% higher/lower than the setting output, the DC supply would be disconnected from the samples and test suspended. This assures no thermal runaway, power outage, surge in current due to unstable power lines if any, and so on. According to the IES standard LM-80-08 [27], the samples were aged at temperatures of 55 °C, 85 °C and 105 °C, combining with two driving currents (i.e., 160 mA and 220 mA) respectively.

On the other hand, thermal resistance was also measured on 3 pieces of LED packages by using T3ster system. As there is no auxiliary equipment for radiant power measurement, the input electrical power was considered instead of total Joule power by default in the T3ster system. The thermal resistance from LED junction to the solder joints was obtained, i.e., Rth_{j-s} = 17 °C/W. As a result, the highest junction temperature for LED packages aged at 105 °C/160 mA was calculated as in Eq. (5.1):

$$T_j = 105 + 6.4 \times 0.16 \times 17 = 122.4 \tag{5.1}$$

Similarly, the highest junction temperature is calculated as 129 °C for LED packages

aged at 105 °C/220 mA. For LEDs aged at other stress conditions, the junction temperatures were confirmed to be less than 125 °C, implying all samples were aged at normal conditions.

After a series of predefined ageing period, the samples were taken out of the ageing chambers for optical and electrical measurement. The measurement system is composed of: (1) a constant current power supply, which not only provides constant driving currents, but also measure the voltage drop of each LED package at the same time; (2) a half-meter integrated sphere, which is used to obtain uniform light distribution; (3) a spectrometer with 1040 charge coupled devices (CCDs), which is responsible for light spectra collection. In order to obtain accurate optical parameters, the system was re-calibrated and discoloration of the MCPCB was compensated prior to each measurement. In addition, 3 non-stressed samples were measured to monitor the stability of the measurement system. These samples are used as reference. The measurement was executed by driving the LEDs with a mono pulse current, which is finished within 35 milliseconds in order to avoid LED packages self-heating. The measurement current is the same as the stressing current for the LED packages. An acquisition time of 20 milliseconds was provided to ensure enough light exposure. Parameters including forward voltage, and spectral power, were collected. Fig. 5.2 provides pictures of the tested samples, the test equipment and the measurement system. By using this measurement system, optical and electrical measurement of the samples was performed at a series of predefined time, i.e., 0 hours, 48 hours, 168 hours, 500 hours, 1000 hours, 2000 hours, 3000 hours, 4000 hours, 5000 hours, and 6000 hours.

After the end of the ageing tests, the data were fitted in terms of least square method, based on the hypothesis that the optical output was exponentially degraded along with ageing time. Only LED packages with gradual degradation was considered, and those suffered sudden optical degradation were excluded as their degradation mechanisms were different. As a result, the sample size used for data fitting is 26 pieces (the other 2 samples failed due to ESD attack) for the condition of 105 °C/220 mA, and 28 pieces for other stress conditions. According to the IES standard TM-21-11 [32], the collected data were first normalized at 0 hour for each individual sample tested; then performed an exponential least squares curve-fit through the individual values for Eq. (5.2), all fitted data were left-censored by eliminating measurement data obtained before 1000 hours.

$$\Phi(t) = \Phi_0 \exp(-\alpha t) \tag{5.2}$$

where $\Phi(t)$ is the normalized optical output at time t, Φ_0 is the projected initial constant derived by the least squares curve-fit, and α is the decay rate constant which is related

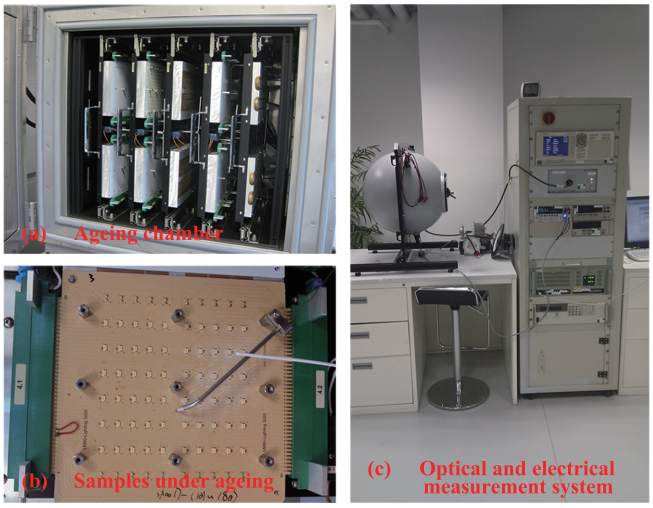

Figure 5.2: LED samples, reliability testing and measurement systems

to ageing stress level.

5.2.2. RESULTS AND DISCUSSION

OPTICAL DEGRADATION CHARACTERISTICS

The individual lumen values of all samples at different measurement point were normalized to their initial values, according to the IES standard TM-21-11 [32]. As a result, the normalized optical output was found to follow exponential degradation kinetics, as shown in Fig. 5.3. Sharp optical degradation was observed after ageing for 1000 hours. The phenomenon was more prominent at stress condition of 105 °C. At this stress condition, 5% of optical degradation has been observed, which is much higher than the normalized optical degradation for LEDs stressed at 55 °C and 85 °C.

The optical degradation does not seem to be temperature sensitive when the case temperature was lower than 85 °C. For LED packages aged at 55 °C and 85 °C, almost the same trend was sustained after ageing for 6000 hours, as plotted in Fig. 5.3. In addition, as can be seen from Fig. 5.4, the optical degradation was not current-sensitive neither by comparing optical output of LED packages aged at 85 °C/160 mA and 85 °C/220 mA. The difference of lumen maintenance is due to the initial degradation. However, after ageing for 2000 hours, the lumen maintenance shows parallel trends. Similar optical degradation kinetics indicated that the degradation mechanisms were not neither temperature-activating dominant [2], nor current-activating dominant at 55 °C and 85

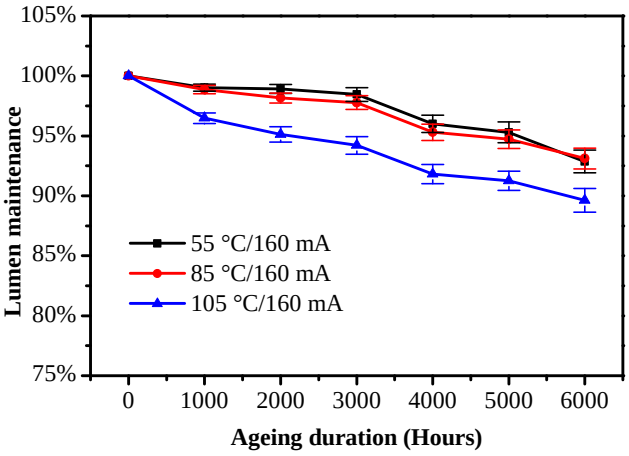

Figure 5.3: Optical degradation of sample aged at different case temperatures

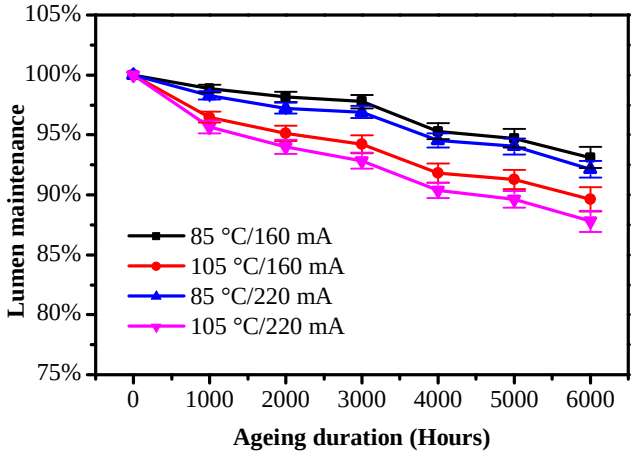

Figure 5.4: Optical degradation of sample aged at different case temperatures

°C. For LED packages aged at 105 °C, as can be observed in Fig. 5.4, significant difference was observed between 160 mA and 220 mA, as the standard error bars of the lumen maintenance at each readout point for these stressing conditions did not overlap each other. Due to Joule-heating effect, the junction temperatures for LED packages stressed by 105 °C/160 mA and 105 °C/220 mA is close to the maximum junction temperature (125 °C) guaranteed by manufacturer. It can be easily concluded that the LED package were much more sensitive to current stress when junction temperatures were around

the upper limit of the blue chip's capacity.

In order to further understand the optical degradation kinetics, activation energy was calculated in terms of Arrhenius equation. The decay rate constant was calculated by the least squares curve-fit outlined in IES TM-21-11. The correlation to Arrhenius equation is in Eq. (5.3):

$$\alpha = A \cdot \exp\left(-\frac{E_a}{kT}\right) \tag{5.3}$$

where A is the pre-exponential factor which is related to effects of uncertain stress, k is the Boltzmann constant (8.6173x10^{-5} eV/K), T is the case temperature of the stress condition, and E_a is the activation energy. According to the IES standard TM-21-11, the current effect was considered in terms of thermal effect, as the current effect was mainly transferred to Joule heating. The calculation was performed respectively for LED packages with different driving current. Table 5.2 listed the activation energy E_a calculated from different stress conditions.

Table 5.2: Optical degradation mechanisms of mid-power LEDs

Temperature		**55 °C-85 °C**	**85 °C-105 °C**
Current	160 mA	0.0005	0.214
	220 mA	0.056	0.254

As presented in Table 5.2, the activation energy was close to 0 eV for LED packages stressed in temperatures ranging from 55 °C to 85 °C. An activation energy of 0 eV indicates that only temperature effect cannot appropriately describe the degradation kinetics of the LED devices. Except for temperature effect, the effects of other stress, such as humidity, should be carefully accounted for. However, the calculated activation energy has been reached 0.254 eV when LED packages were aged in the range of 85 °C to 105 °C (driving current was held at 220 mA). Additional thermal ageing tests for the LED packages from the same batch also showed consistent E_a , which was 0.273 eV (samples were aged at 85 °C and 105 °C respectively, while driving currents were held at 240 mA). This activation energy is similar to that reported value in [33, 34]. However, this activation energy is much lower than that reported in [5], in which the activation energy was calculated as high as 1.5 eV for samples aged at 180 °C and 230 °C, indicating that an accelerating degradation test at such a high temperature (180 °C to 230 °C) is not feasible for reliability evaluation of LED packages which are operated at application conditions (solder temperature ranges from 85 °C to 105 °C).

SPECTRA ANALYSIS

To investigate and separate the effects of degradation due to chip and package related, first, the silicone encapsulant was carefully removed from the stressed and non-stressed LEDs, and then optical measurement was performed by using an integration sphere system to obtain the LED source degradation directly. The spectra were collected by a spectrometer as described in previous section. 4 pieces of non-stressed LED packages and 4 pieces of stressed LED packages (randomly selected from samples aged at 55 °C/220 mA) were measured respectively.

The total spectral power of the emission wavelengths ranging from 440 nm to 460 nm (peak wavelength is 451 nm for the blue lights.) was averaged for both the non-stressed and stressed LED packages respectively. After that, the average value of the non-stressed LED packages was normalized to 100%, and the percentage of the averaged spectral power of the stressed LED packages to that of the averaged non-stressed LED packages was plotted in Fig. 5.5. As presented in Fig. 5.5, a decrease of the spectral power was observed for those stressed LED packages, as compared to that of the non-stressed LED packages, indicating the chip deterioration of the stressed LED packages. The degradation linearly increases with the measurement current. As a consequence, a measurement current of 220 mA, induces a degradation value of 4.5%.

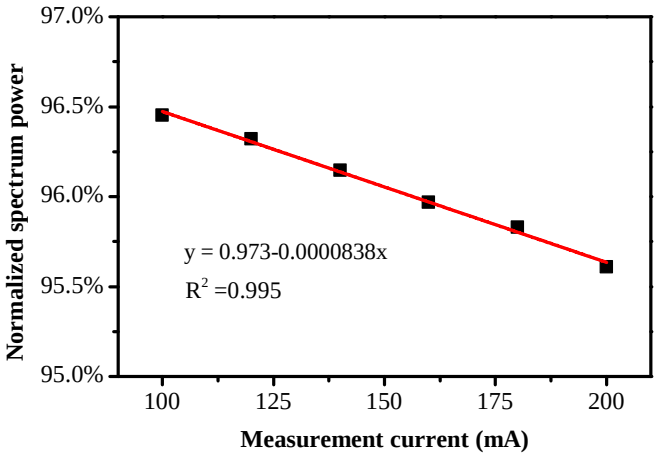

Figure 5.5: Degradation of blue light intensity vs. measurement current

Secondly, the spectra of the stressed LED packages collected at readouts from 0 hour to 6000 hours, were also averaged and normalized. Similar to previous paragraph, the total spectral power of the emission wavelengths from 440 nm to 460 nm (peak wave-

length is 451 nm for the blue lights.), and down-converted wavelengths from 600 nm to 620 nm (peak wavelength is 610 nm for the down-converted lights.) obtained at each individual readout, was averaged respectively for the individual stress condition. Then, the average values obtained at 0 hour was normalized to 100%, and the percentage of the averaged spectral power obtained at other readouts to that obtained at 0 hour was plotted in Fig. 5.6.

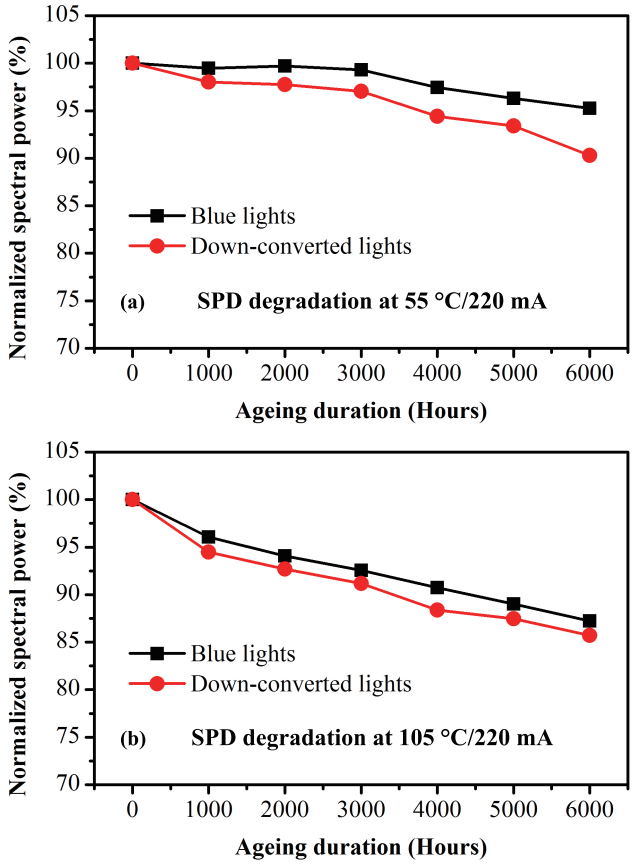

Figure 5.6: Degradation of light intensity at peak wavelengths

As indicated in Fig. 5.6(a), for samples aged at 55 °C, it was found that degradation of the blue lights' normalized spectral power was about 4.7% at 6000 hours, which is quite close to that measured by first removing the silicone of the LED samples. This finding demonstrates that spectra directly collected from the aged LED packages can be used to separate the effects of degradation due to chip and package related.

Based on this conclusion, it is found that the rapid optical degradation for LED packages aged at 105 °C, was mainly attributed to the degradation of intensity of the blue lights, as shown in Fig. 5.6(b). In details, blue chip deterioration attributes about 12% and package-related degradation attributes 1.8% to the total lumen degradation. In addition, it is interesting that the package-related degradation has been triggered after 1000 hours, while no more contributions after that, as the difference between the normalized spectral powers of the blue lights and down-converted lights is almost the same from 1000 hours to 6000 hours.

While for LED packages aged at 55 °C, the spectral degradation showed much more complicated degradation kinetics than that of LED packages aged at 105 °C. It was found that the initial optical degradation was only attributed to the reduction of down-converted light degradation because very little degradation was observed on the blue lights until 2000 hours. A difference of 1.5% was observed between the spectral power of the blue lights and down-converted lights after aged for 1000 hours, indicating package-related degradation has been triggered. As the percentage amount is quite similar to that of LED packages aged at 105 °C, it is considered that this initial degradation is triggered by stresses rather than temperature. An elevated temperature from 55 °C to 105 °C did not induce higher package-related degradation at this readout. By ageing the samples from 1000 hours to 6000 hours, the degradation of the blue lights and down-converted lights increased from 0.3% to 4.7% and from 2% to 9.7% respectively, indicating chip deterioration attributes about 4.7% and package-related degradation attributes 5% to the lumen degradation after 6000 hours.

CHIP DETERIORATION BY I-V CHARACTERISTICS ANALYSIS

Fig. 5.7 shows the $I-V$ characteristics of the non-stressed and stressed LED packages. In our previous analysis, we have found chip-related deterioration at 55 °C and 105 °C. It has been found that the chip-related degradation of the LED packages is due to either junction deterioration or Ohmic contact deterioration [7, 35]. In order to understand the effects of blue chip degradation to optical performance, the $I-V$ characteristics was studied in terms of series resistance and ideality factors at high current region (forward current > 1mA) by following equation [36]:

$$I\frac{dV_F}{dI} = R_S I + \frac{nkT}{q} \tag{5.4}$$

where I is the forward current, V_F is the forward voltage, R_S is the series resistance, n is the ideality factor, k is the Boltzmann constant (8.6173x10^{-5} eV/K), T is the measurement temperature, and q is electron charge. The currents vary from 1×10^{-3} A to 2×10^{-1}

A and corresponding forward voltages were collected for least square fitting.

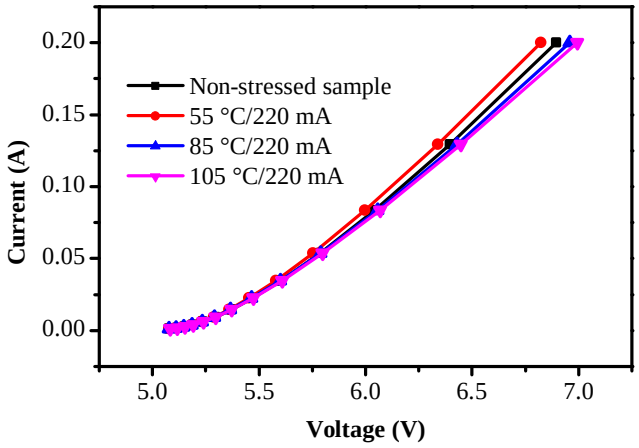

Figure 5.7: $I-V$ characteristics of LED packages

Notice that the LED packages used in our experiments uses 2 pieces of blue chips that were connected in series. As the equation above can only apply in one single chip, the forward voltage V_F in the equation is only half of the voltage measured from the LED package. This is reasonable because the blue chips are produced by not only using the same materials and processes. They are also classified in the same bin. Furthermore, the blue chips undergo similar stress condition, such as electrical and thermal stress. As a result, the performance and degradation kinetics of the blue chips in one LED package should be similar to each other. The calculated ideality factor and series resistance are shown in Table 5.3.

Table 5.3: Ideality factors and series resistance for samples stressed by 220 mA

Parameter	**n**	**R_S**
Non-stressed	2.16	3.40
55 °C	2.01	3.38
85 °C	2.01	3.54
105 °C	1.95	3.71

For the non-stressed LED packages, it is found that the ideality factor n is calculated as 2.16, which is in line with that reported in [37], in which an ideality of 1.5 to 2.5 was found in GaN-based p-n structures grown on SiC substrates. For the LED with an ideality factor higher than 2.0, Shah *et al.* [38] proposed a model in which the GaN-

based p-n junction diode was modeled by a series of diodes, i.e., the actual GaN p-n junction diode, unipolar heterojunction diodes, and a reverse-biased Schottky diode at the metal/p-type GaN junction. According to Shah's model, the LED in our samples can be modeled by an actual GaN p-n junction diode, which is connected in series with an unipolar heterojunction diodes which are assumed to be very leaky, so that Ohmic rather than rectifying characteristics are exhibited [38].

For samples aged at 55 °C, significant reduction of the ideality factor n was observed as compared with that of the non-stressed samples. At this case temperature, a value of ideality factor around 2.0 was calculated, implying perfect space-charge recombination and p-n junction improvements of the blue chip after ageing test [39]. An ideality factor of 2.0 also indicates that Ohmic rather than rectifying characteristics are exhibited in the unipolar heterojunction diodes after ageing test. The p-n junction improvement of blue chip was due to annealing effect of the thermal stress, which had been proposed by many researchers [40–42]. In addition, the series resistance of samples aged at these case temperatures was similar with that of the non-stressed samples, indicating no obvious deterioration of the Ohmic contacts of the blue chip. However, as already verified in the spectra analysis, the degradation of the spectral power of the blue chip was found as around 4.5% for LED packages aged at 55 °C after 6000 hours. As no junction deterioration or Ohmic contact deterioration was observed at this condition, the degradation was considered as being induced by either transmittance decrease of the indium tin oxide (ITO), or refractivity deterioration of the multi-layer structure of the chip surface, as reported in [43]. However, this needs to be further verified in the future.

On the other hand, for samples aged at 85 °C and 105 °C, significant changes were found on the series resistance R_S , indicating Ohmic contacts deterioration was triggered [41]. The increase of the series resistance, would affect the emission efficiency of the blue chips, thus rendering the lumen degradation of the LED packages [7]. However, an ideality factor of 1.95 to 2.01 shows that the LED is in perfect carriers recombination in the space charge region, mediated by recombination centers located near the intrinsic Fermi level [39]. The increase in series resistance is ascribed to the thermally activated metal-metal and metal-semiconductor inter-diffusion [43, 44]. A reduction of the active acceptor concentration, due to the interaction between hydrogen and magnesium, can worsen the properties of the anode contact, and vary the resistivity and injection properties of the p-layer, thus leading to the measured $I-V$ modifications [45] and optical degradation.

PACKAGE DEGRADATION INVESTIGATION BY PHYSICS ANALYSIS

Fig. 5.8 shows the appearances of a non-stressed sample and a stressed sample aged at 55 °C and 105 °C. No obvious difference was found between epoxy material compound (EMC) appearance of the non-stressed samples and of samples aged at 55 °C, while slight yellowing was observed on the outer surface of samples aged at 105 °C.

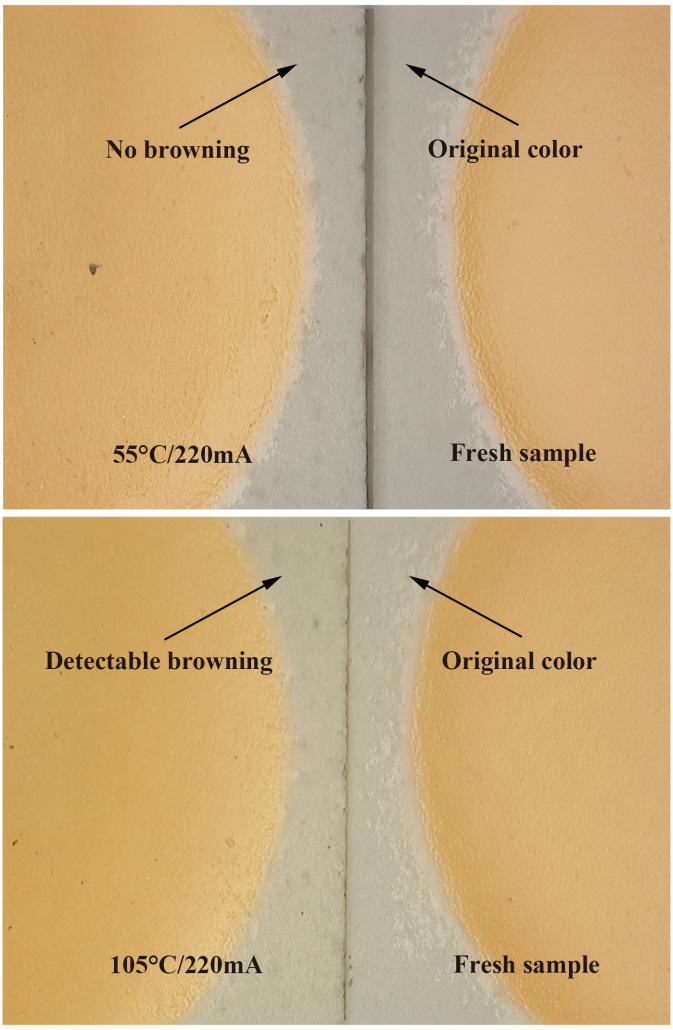

Figure 5.8: Appearance of samples before aging and after ageing for 6000 hours

Silicone carbonization was eliminated from the aged samples by observing the silicone surface that attaches to the chip, as indicated in Fig. 5.9. However, silicone yel-

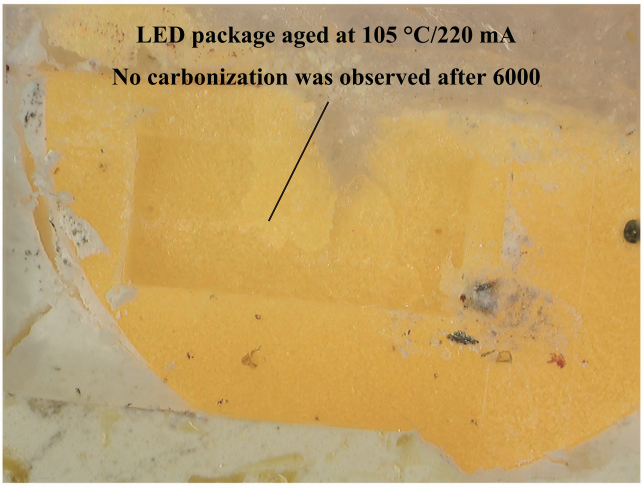

Figure 5.9: Silicone of LED pakcages aged at 105 °C/220 mA

Table 5.4: Element content of silicone gel in Non-stressed LED packages

Element	Weight%	Atomic%
C K	53.25	67.29
O K	18.24	17.30
Si K	28.51	15.40
Totals	100.00	

Table 5.5: Element content of silicone gel in LED packages aged at 55 °C

Element	Weight%	Atomic%
C K	55.68	66.90
O K	26.58	23.98
Si K	17.74	9.12
Totals	100.00	

Table 5.6: Element content of silicone gel in LED packages aged at 105 °C

Element	Weight%	Atomic%
C K	49.50	63.01
O K	23.11	22.08
Si K	27.39	14.91
Totals	100.00	

lowing was found by analyzing the element content of the silicone gel near the upper surface of the chip using by means of Energy Dispersive X-Ray Spectroscopy (EDX). As presented in Table 5.4 to Table 5.6, the atomic% of the element C and O of the silicone residuals, of the LED samples aged at 55 °C and 105 °C, is similar to each other, while is about 5% higher than that detected from the non-stressed LED samples. Similar atomic% indicates the change of the element C and O is not due to temperature. The change of the element C and O also implies silicone degradation [46], which was considered as a contributor of the initial lumen degradation of the LED packages, as the silicone degradation was only observed at the initial ageing duration, as shown in Fig. 5.10.

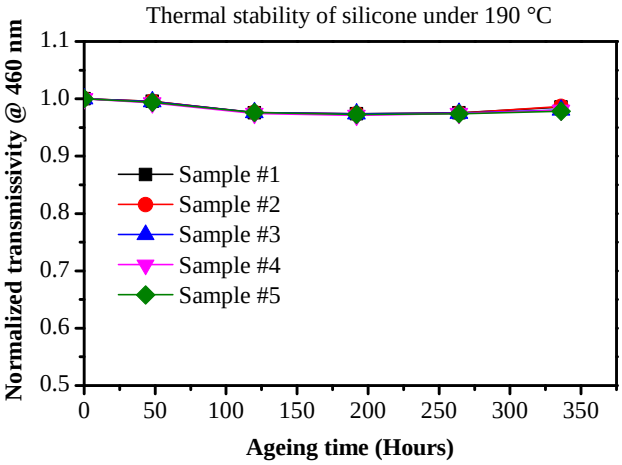

Figure 5.10: Silicone transmittance vs. ageing time in high temperature storage test

As presented in Fig. 5.11 are the C-SAM results of LED packages aged at 55 °C. Delamination was not observed neither at the chip/silicone interface nor the silicone/lead frames interface. Delamination was not observed at the interface of die/die attach gel neither. Similar results were also observed on LED packages aged at 105 °C. However, the picture was not shown here due to content limitation.

Energy Dispersive X-Ray Spectroscopy (EDX) analysis shows that there are no S, Cl, Br, and I were found on the silver-coating lead frames, thus eliminating chemical contamination as the root cause of the lead frame degradation [9], as indicated in Fig. 5.12 . However, shallow pits were observed at the lead frames of samples aged at 55 °C, as shown in Fig. 5.13. It was speculated that, for samples aged at 55 °C, higher relative humidity as compared that at 105 °C, leads to an osteoporosis structure of the silver coating

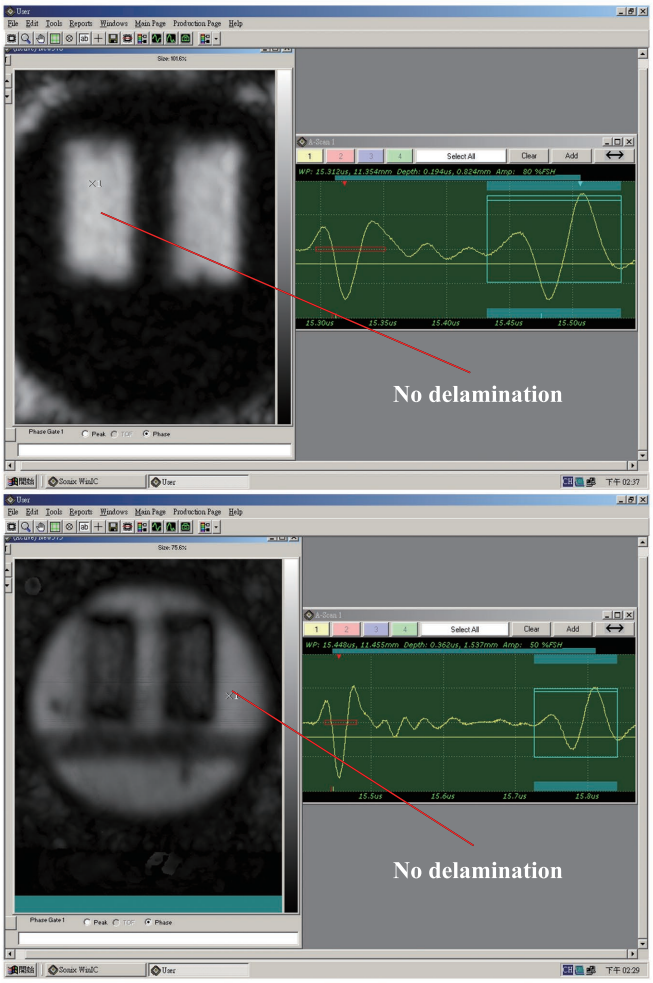

Figure 5.11: No delamination was found in the aged packages by using C-SAM

due to internal stress induced by moisture penetration, resulting in the deterioration of the reflectivity of the lead frames.

Actually, it is found that the relative humidity is still around 13% when case temperature is 55 °C, as shown in Fig. 5.14. Same observation had also been observed by Fan et al. [47]. The effect of moisture ingress into the electronic packages, though not LED packages, had been reported as considerable even at a low relative humidity of 10%, as in the case of the ageing chamber [48]. For LED packages aged at temperatures at 55 °C, influence of moistures should be carefully taken into account.

The quantum efficiency of the phosphors was not detected due to lack of equip-

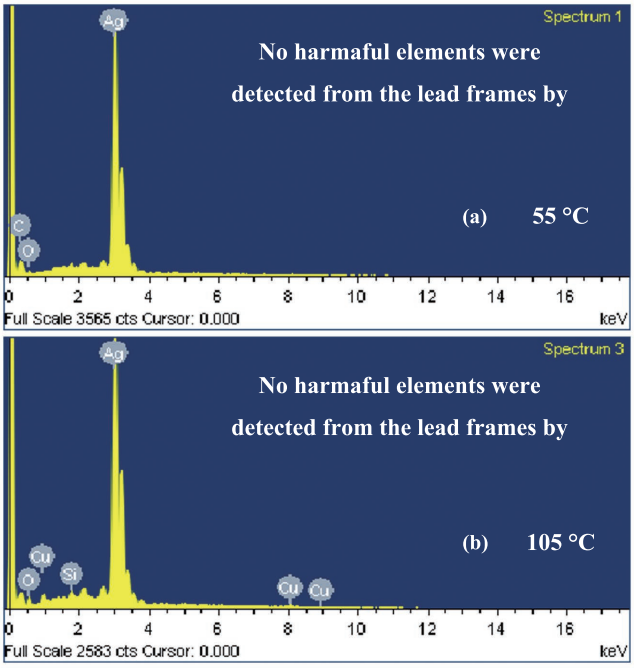

Figure 5.12: No harmful elements were found by using EDX analysis

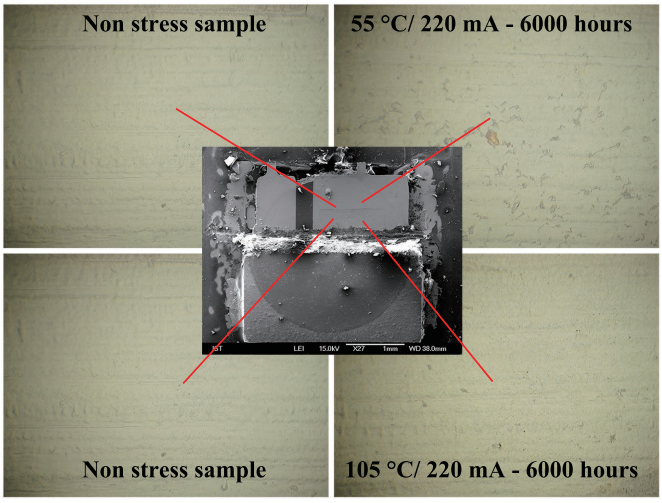

Figure 5.13: Morphology of the surface of the silver-coating lead-frame

ment. However, YAG-(Ce^{3+}) phosphors had been reported to be very stable during ther-

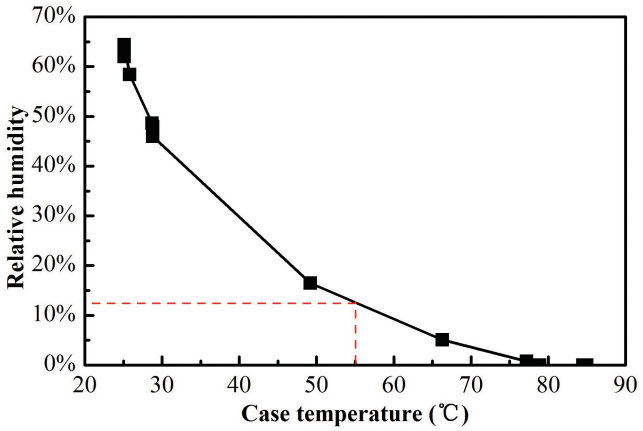

Figure 5.14: Measured relative humidity versus increase of case temperature

mal ageing, thus eliminating any significant nonradioactive quenching processes that existed in the aged samples [49]. On the other hand, Hu *et al.* [50] reported highly thermal-stability of the Nitride phosphors after ageing for 30 minutes at 1000 °C. Moreover, Cheng *et al.* [51] reported the highly thermal-stability of a broadband phosphors which were fabricated by sintering the mixture of multiple phosphors (including YAG, LuAG, and Nitride) on SiO_2-based glass. All these evidences indicate low possibility of the phosphor degradation in LM-80-08 tests as the highest temperature is only around130 °C in our experiments.

5.3. OPTICAL DEGRADATION MECHANISMS UNDER WHTOL TEST

5.3.1. EXPERIMENT SETUP

20 pieces of MP-3030-EMC LED packages (with 2 blue chips connected in series) were assembled onto an Aluminum-based metal core printed circuit board (MCPCB) by using SAC305 lead-free solder paste. All LED packages were distributed uniformly and connected in series on the MCPCB. At the same time, thermal pad was attached onto a heat sink carefully, on which the MCPCB was then mounted with 5 screws. This ensures good heat dissipation from LED packages to the heat sink. Total 4 pieces of MCPCBs were prepared and only one MCPCB was aged per test condition.

The samples were placed into a climate chamber after finishing the initial optical measurement. During ageing test, the ambient temperature and relative humidity of the chambers were maintained at a constant value of 85 °C and 90%RH, 95 °C and 45%RH

and, 95 °C and 95%RH respectively. For convenience, the test was named as WHTOL 85 °C/90%RH for the first test condition and the same strategy was applied to the rest. Furthermore, the LED packages were also stressed by a constant driving current (160 mA per unit). Under these stressing conditions, the highest solder temperature of the LED packages was measured to be 107 °C, and the corresponding junction temperature was calculated as about 130 °C. Hence, over-stressing would be performed in our tests since the nominal driving current is 120 mA according to the product specification. The specification defines the maximum driving current as 240 mA at 25 °C (ambient temperature) and 120 mA at 85 °C (ambient temperature) respectively. Furthermore, the maximum junction temperature guaranteed is limited to 125 °C in the specification.

In order to analyze the differences of degradation mechanisms between environments with and without moistures, another group of samples was aged by means of high temperature operation life test (HTOL). In this ageing test, the stressed current was the same as that in the WHTOL test and the solder temperature was controlled at 105 °C until the end of the test. Both the solder temperature and driving current are almost the same as that in WHTOL 95 °C/95%RH, so any difference of the degradation kinetics between HTOL 105 °C and WHTOL 95 °C/95%RH could be attributed to the effects of moistures.

The samples were taken out of the climate chambers for optical and electrical measurement at a series of predefined readout points. In order to obtain accurate optical parameters, the system was re-calibrated prior to measurement. After that, a Keithley Digital Multimeter was used to light up the LED packages with a constant current and integrated sphere was used to measure the light spectra. The acquisition time was 25 ms to ensure complete exposure and integration. The complete measurement was finished within 35 ms to avoid LED packages self-heating.

After finishing all ageing tests, the data were fitted in terms of least square method, based on the hypothesis that the optical output degrades exponentially during ageing. According to the IES standard TM-21-11 [32], collected data were normalized to a value of 100% at 0 hour for each individual sample under test; then exponential least squares curve-fit was performed through the individual values for the following equation:

$$\Phi(t) = \Phi_0 \exp(-\alpha t) \tag{5.5}$$

where $\Phi(t)$ is the normalized optical output at time t, Φ_0 is the projected initial constant derived by the least squares curve-fit, and α is the decay rate constant which is related to ageing stress level.

Except for analysis of the optical degradation, several degraded samples were also

analyzed by means of non-destructive and destructive analysis. $I-V$ characteristics, package materials discoloration, interface delamination, and contamination were carefully detected.

5.3.2. RESULTS

LUMEN DEGRADATION

According to the IES standard TM-21-11, the individual lumen values of all samples at different measurement points were normalized to their initial values, and then averaged, as mentioned in previous section. The average normalized data were plotted in Fig. 5.15. As a result, the lumen degradation showed very good exponential degradation kinetics in all test conditions, regardless of conditions with or without humidity. The degradation rate became faster as the relative humidity increased. As observed from Fig. 5.15, when the relative humidity rose from 0%RH (assume no humidity in HTOL 105 °C), to 45%RH (WHTOL 95 °C/45%RH), and to 95%RH (WHTOL 95 °C/95%RH), the lumen maintenance decreased to 97.7%, 96.3%, and 91.9% respectively after 1000 hours. As both the driving current and the solder temperature were similar to each other among all test conditions, the difference of the degradation rate was apparently induced by different relative humidity in the climate chambers.

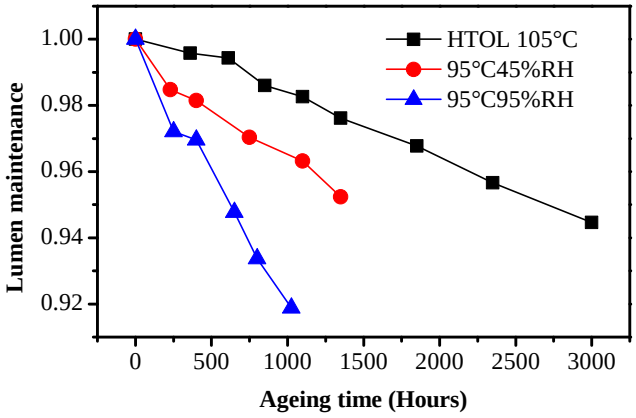

Figure 5.15: Average lumen degradation of LED packages in different stress conditions

On the other hand, the lumen degradation mechanisms were explored by using statistics methodology. First of all, the degradation trend was fitted and extrapolated to the time that the LED package's lumen output reached 90% of its initial value (MTTF90%). The MTTF90% of each individual sample was then collected for probability distribution

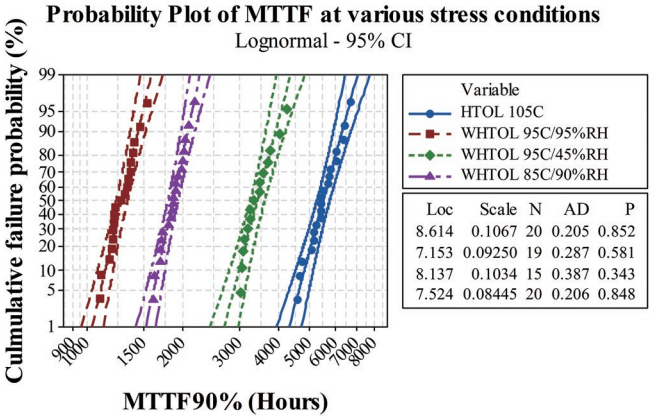

Figure 5.16: Statistics distribution of the MTTF90% in all the stress conditions

analysis. The reason that MTTF90% but not MTTF70% (as defined in IES TM-21-11) was used is because the projected MTTF90% was much closer to the testing duration as the lumen maintenance was in the range of 90%~95% in our ageing tests. The analysis results were plotted in Fig. 5.16. Statistics analysis shows similar degradation mechanisms among all stress conditions as the shape parameters of the lognormal distributions are very closed to each other [52], indicating that WHTOL test could be applied as an efficient accelerated life test method instead of the IES test standard LM-80-08 [27], which only accounts for effects of temperatures and is very time-consuming for lifetime prediction.

Based on the result of the statistics analysis, the Hallberg-Peck's model was used to describe the effect of temperature and humidity combined on LEDs' life as follows:

$$AF = \left[\frac{RH_a}{RH_u}\right]^n \exp\left[\left(\frac{E_a}{k}\right)\left(\frac{1}{T_u} - \frac{1}{T_a}\right)\right] \tag{5.6}$$

where RH_a is the humidity at testing condition, RH_u is the humidity at usage conditions, n is the humidity factor, E_a is the activation energy, and k is the Boltzmann constant.

The activation energy was obtained as 0.47 eV, which was very similar to that reported in [19]. The humidity factor n was also obtained and the value was calculated as 1.21. The humidity factor was smaller than results reported previously by other researchers. For instance, n was calculated as 1.6 in [4], 2.02 in [17], and 2.29 in [20] respectively. The reason is probably because our LED packages were stressed by much

higher current than that in [17, 20]. Higher current implies higher temperature inside the packages than temperature outside the packages. Finally, the relative humidity inside the package decreases due to higher saturated vapor pressure inside the LED packages. In addition, higher temperature may drive part of the moistures outside the package due to effects of moisture expansion. All these reasons could reduce the effects of the moisture, and, thus, yield a smaller humidity factor. The other reason is that the moisture resistance may differ among different types of LED package.

COLOR SHIFT

Fig. 5.17 shows the average color shift of LED packages in each test condition. The color shift was characterized in terms of $u'v'$, which is the distance deviating from the color points measured before ageing test. As could be observed from the plot, the color shift increased as a parabola along with ageing time. All samples showed slight color shift ($u'v' < 0.002$), with the exception of the samples in WHTOL 95 °C/95%RH. The color shift was similar for samples aged in HTOL 105 °C and WHTOL 95 °C/45%RH, indicating that the package-related degradation mechanisms triggered by moistures was identical when the relative humidity was lower than 45%RH. This conjecture was made under the assumption that only package-related degradation mechanisms induced color shift, which will be discussed in a latter section. On the other hand, a rapid color shift was observed for those samples aged in WHTOL 95 °C/95%RH after 250 hours. The color shift went up to 0.005 after 1000 hours, indicating that the LED packages were much more sensitive in environment with high humidity and high temperatures than in environment without moisture.

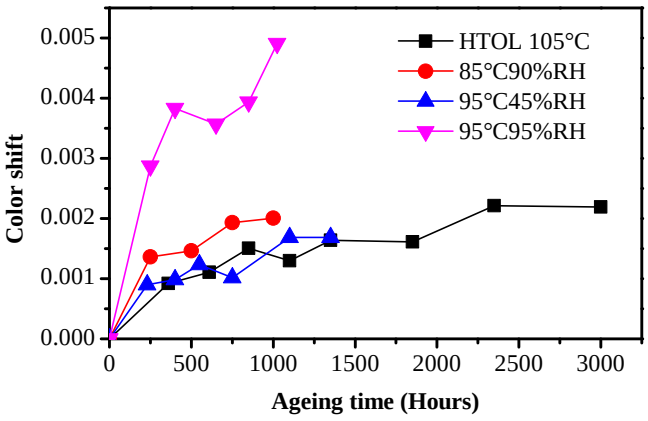

Figure 5.17: Color shift of LED packages in different stress conditions

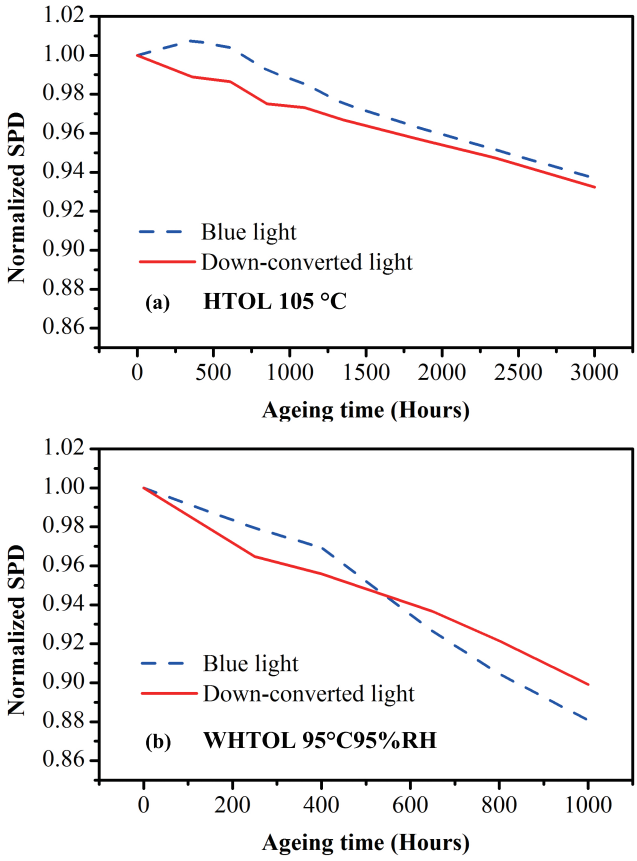

Figure 5.18: Normalized spectral power degradation of LED packages in WHTOL 95 °C/95%RH and HTOL 105 °C

The color shift was further analyzed in terms of light spectral power degradation. Only samples aged in HTOL 105 °C and WHTOL 95 °C/95%RH were analyzed due to similar color shift kinetics in other stress conditions. As shown in Fig. 5.18(a), for LED packages aged in HTOL 105 °C, the normalized spectral power of blue lights increased at the beginning, and then gradually decreased after 500 hours. The increase a of spectral power was probably due to transmittance improvements of the silicone plate as silicone was cured continuously until the crosslinking was completed during ageing test. The spectral power of both blue lights and down-converted lights degraded proportionally after 1500 hours (that is, the same percentage of degradation for the blue lights and red lights), indicating that the chip-related deterioration was dominating in HTOL 105 °C. On the other hand, for LED packages aged in WHTOL 95 °C/95%RH, as presented in Fig.

5.18(b), the spectral power of blue and red lights showed different degradation kinetics. The spectral power of blue lights decreased rapidly after 400 hours. The amount of spectral power degradation had exceeded that of red lights after 600 hours, indicating the blue lights were absorbed significantly during the ageing test, probably due to a decrease of reflectivity of the package encapsulant. The rapid degradation of blue lights explained the sharp increase of color shift in WHTOL 95 °C/95%RH.

ELECTRICAL CHARACTERISTICS

Fig. 5.19 shows the $I-V$ curve of the non-stressed and stressed LED packages. A right-shift of the curves was observed for LED packages aged in HTOL 105 °C and WHTOL 95 °C/95%RH.

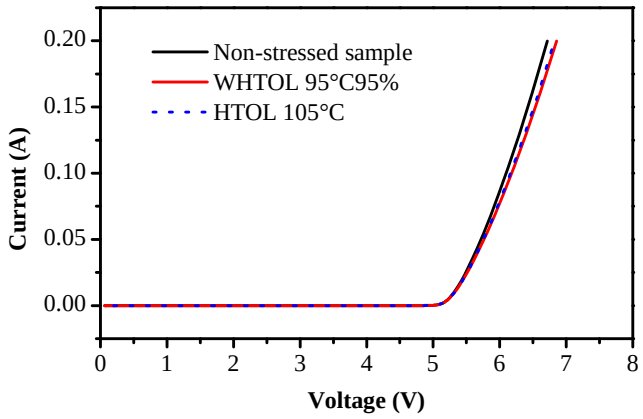

Figure 5.19: $I-V$ Curve of LED packages in HTOL 105 °C and WTHOL 95 °C/95%RH

The reverse current measured at -10 V, and forward voltage measured at 10 μA were also collected and presented in Table 5.7.

Table 5.7: Electrical parameters of $I-V$ characteristics

Stress Condition	**I_r @ 10 V (A)**	**V_f @ 10 μA (V)**
Non stressed	2.0×10^{-08}	4.8
WHTOL 95 °C/95%RH	4.0×10^{-08}	4.8
HTOL 105 °C	6.0×10^{-08}	4.79

It was found that the reverse current I_R, and forward voltage at small driving current, was very similar to that of the non-stressed LED packages. All these parameters

demonstrated that no obvious deterioration of the active layer. However, significant changes of the forward voltage were observed in the stressed LED packages, especially for samples aged in WHTOL 95 °C/95%RH, even though the ageing duration was much shorter than that in HTOL 105 °C. Similar phenomenon was also reported in recently published papers [52, 53]. It was reported that an increase of the forward voltage (in terms of increase of series resistance) attributed to the first 5% lumen degradation in temperature-humidity conditions even though no deterioration in the p-n junction is observed [52].

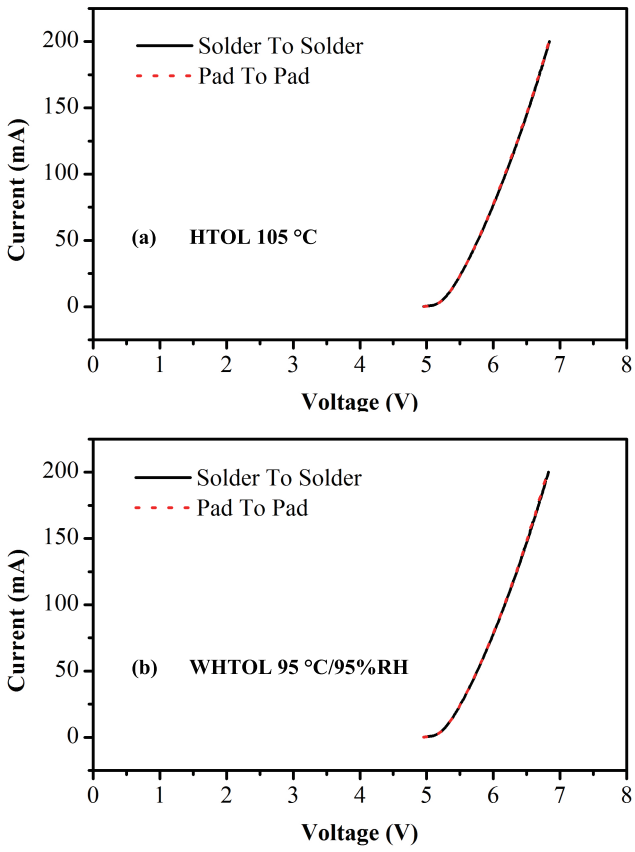

Figure 5.20: $I-V$ curve measured at different positions

The increase of the forward voltage was mainly attributed to the deterioration of the Ohmic contacts. This has been confirmed by measuring the I-V curves at different positions. More specifically, the degraded sample's $I-V$ curves in WHTOL 95 °C/95%RH and

HTOL 105 °C were measured at the two ends of the solder joints of the package and the gold pads of the blue chips, respectively. As presented in Fig. 5.20, similar trend of the $I-V$ curves measured at different positions eliminates the possibility of deterioration of the solder joints and wire bonding on the lead frames, thus verifying the deterioration of the Ohmic contacts indirectly. An explanation for deterioration of the Ohmic contact was the thermally activated metal-metal and metal-semiconductor inter-diffusion [43, 44]. A reduction of the active acceptor concentration, due to the interaction between hydrogen and magnesium, can worsen the properties of the anode contact, and vary the resistivity and injection properties of the p-layer, thus leading to the measured $I-V$ modifications [45]. However, the reason is not yet clear for the phenomenon that the forward voltage increased more rapidly in WHTOL than in HTOL.

FAILURE ANALYSIS

At first, several degraded LED packages were inspected by optical microscope. In order to clearly emphasize discoloration, a non-stressed sample was used for comparison. Significant yellowing of the EMC encapsulant was found for LED packages aged in WHTOL 95 °C/95%RH. For those samples aged in HTOL 105 °C, only very slight yellowing of the EMC encapsulant was observed, even though a much longer ageing duration than samples aged in WHTOL 95 °C/95%RH, as presented in Fig. 5.21. In contrast to LED packages in HTOL 105 °C, it was obvious that moisture significantly affected the stability of the package encapsulant in WHTOL 95 °C/95%RH. Furthermore, small and dense cavities were observed in the inner surface of the package encapsulant, probably due to the dissolution of EMC under combined humidity, temperature, and blue light exposure.

Serious delamination was also observed at the interface of EMC encapsulant and lead frames. Actually, delamination had been frequently reported and considered as the main failure mode by researchers [18, 21, 52, 54, 55]. Due to delamination, foreign materials ingress was found at the interface, as seen in Fig. 5.22. However, no foreign material ingress was observed at the interface of silicone and lead frames, indicating excellent adhesion of the silicone. For LED packages aged in HTOL 105 °C, neither delamination, nor foreign material ingress was observed.

On the other hand, the surface of the lead frame was also inspected by optical microscope. No significant blackening was found on the silver-coating, as seen in Fig. 5.23. It was further confirmed by X-ray photoelectron spectroscopy (XPS) that the element S could not be found and the amount of Cl was negligible for the stressed samples in WHTOL 95 °C/95%RH, thus eliminating the contamination of the silver surface as the root cause, as indicated in Table 5.8.

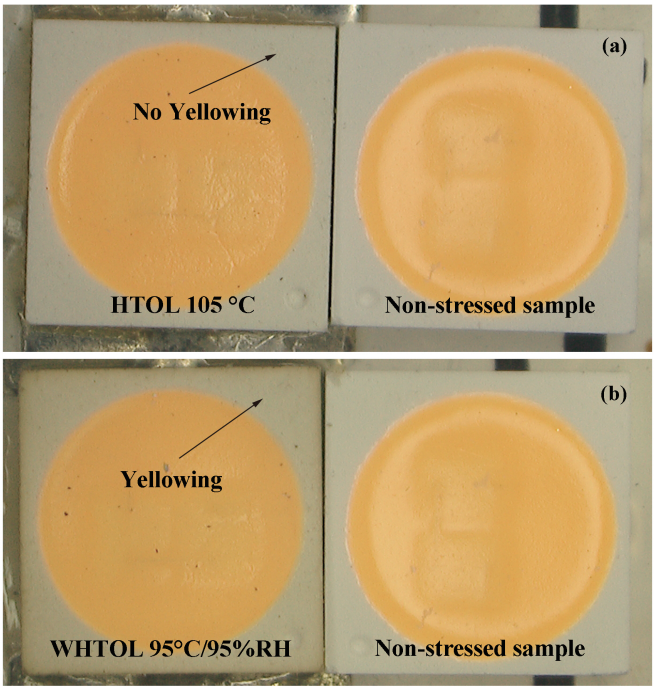

Figure 5.21: Discoloration of the package encapsulant (EMC)

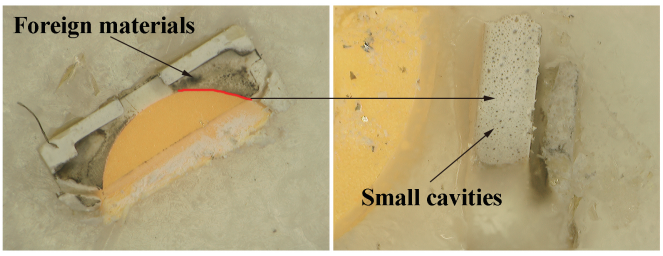

Figure 5.22: Small cavities was observed at the inner surface of LED encapsulant

Table 5.8: Lead frame XPS results for WHTOL 95 °C/95%RH

Peak	Position BE (eV)	Atomic Mass	Atomic Conc (%)	Mass Conc (%)
Cu 2p^{-}	933.9	63.549	1.71	5.46
O 1s	531.2	15.999	20.51	16.5
Sn 3d	485.1	118.744	0.37	2.24
Ag 3d	368.4	107.878	4.53	24.59
C 1s	283.6	12.011	63.99	38.65
Cl 2p	203.2	35.46	0	0
Si 2s	152.7	28.086	8.89	12.55

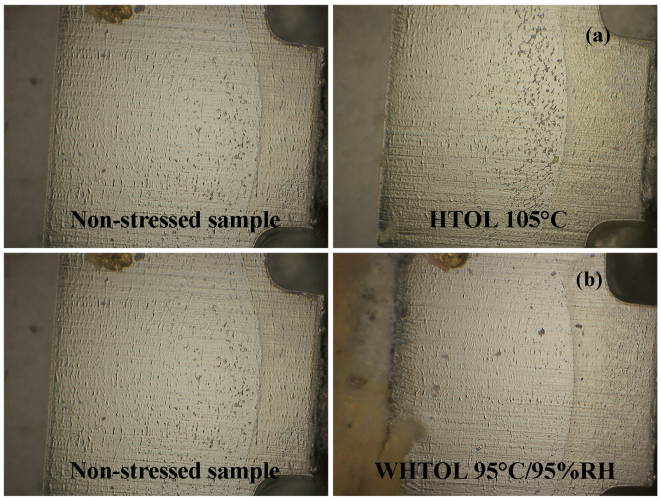

Figure 5.23: No obvious discoloration on the surface of silver-coating lead frame

5.3.3. DISCUSSION

OPTICAL DEGRADATION MECHANISMS – EFFECTS OF CHIP DETERIORATION

The chip deterioration had been widely reported since LED was invented in 1960s. The degradation mechanisms of chip are very complex. Generation of crystal defects in the multi-quantum wells (MQWs) [56], dopant diffusion from p-GaN layer to active layer [57], electro-migration inducing thermal runaway [58], as well as electrical contact metallurgical inter-diffusion [59], were the main mechanisms which result in optical degradation during operation. Generally, the chip deterioration could be characterized in terms of leakage current, parasitic resistance and ideality factor [5].

In order to understand the lumen degradation kinetics due to chip deterioration, one single LED package was driven at a series of temperatures which started from 70 °C to 100 °C to simulate the efficiency degradation of blue chip during ageing test. This is because the efficiency of LED chip reduces as the junction temperature increases. The spectral power of the blue and down-converted light was then normalized to the value measured at room temperature. As a result, the spectral power of down-converted light decreased proportionally as well as that of blue lights, as presented in Fig. 5.24. In other words, chip deterioration results in the same degradation trend for blue and red lights. The results demonstrated that the lumen degradation was mainly due to chip deterioration in HTOL 105 °C, as proportional decrease of blue and red light was observed, as shown indicated in Fig. 5.18. As no significant leakage current was detected, the chip deterioration was only attributed to the p-contact deterioration, which induced

the increase of the series resistance of the LED packages. The increase of series resistance then resulted in the increase of the junction temperature when LEDs were driven at constant currents. Finally, higher junction temperature rendered optical degradation of the white-light LED packages due to the effect of "efficiency droop" of LED packages [60]. An example of the "efficiency droop" characteristic was illustrated as in Fig. 5.25, which shows linear optical degradation as junction temperature increased.

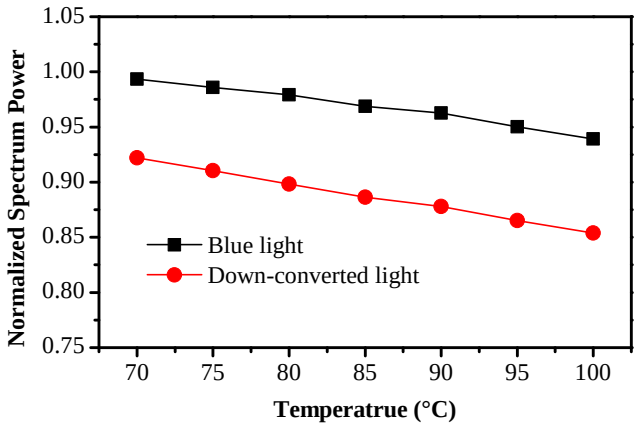

Figure 5.24: Blue chip degradation kinetics

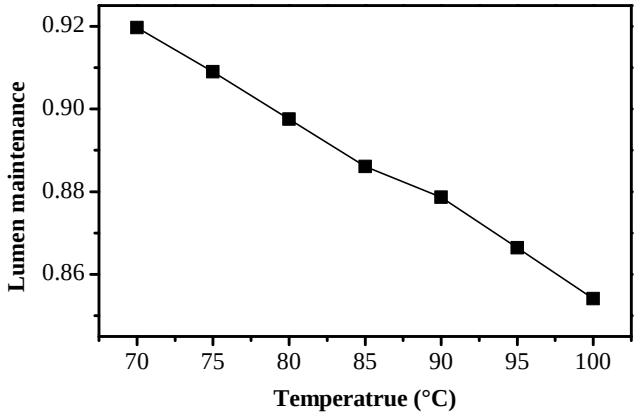

Figure 5.25: "Efficiency droop" of LED packages due to increase of junction temperature

On the other hand, though many researchers reported that increase of leakage currents in LED packages may result in optical degradation during ageing test, the effects

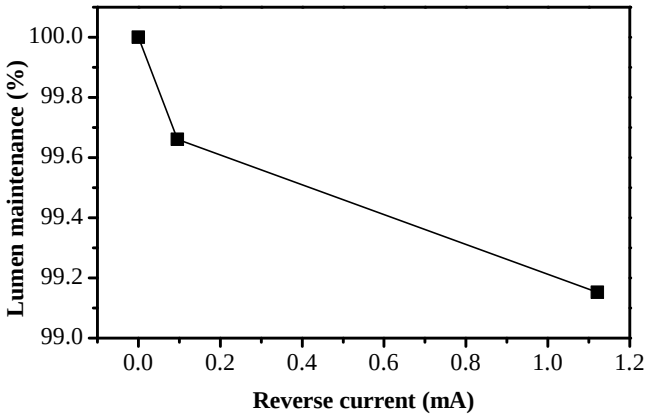

Figure 5.26: Lumen maintenance vs. reverse current

were limited only in lower driving current region. For mid-power LED packages driven by high forward currents, only 1% of lumen decay (in ohter word, the lumen maintenance is 99%) was found even though the leakage current had reached 1 mA, as shown in Fig. 5.26, thus eliminating the effects of leakage current on the light output, as the measured reverse currents were much lower than 1 mA for LED packages aged in HTOL 105 °C and WHTOL 95 °C/95%RH. In Fig. 5.26, the leakage current was obtained by continuously stimulating the LED packages with instantaneous discharge generated through an electrostatic discharge generator.

OPTICAL DEGRADATION MECHANISMS – EFFECTS OF PACKAGE MATERIAL DEGRADATION

Package material degradation was the other degradation mode which not only influences the lumen maintenance, but also color shift. Silicone carbonization, package encapsulant yellowing, and blackening of silver-coating lead frames were considered as the root causes of package-related degradation by researchers. In addition, phosphor dissolution was also reported [23]. However, YAG(Ce^{3+}) phosphors have been reported to be very stable, thus eliminating any significant nonradioactive quenching processes that existed in the aged samples [49]. Water resistance was also determined by measuring the electrical conductivity. The phosphor powders showed no hydrolysis after 30 minutes. Furthermore, damp heat test showed little $\Delta u'v'$ after 1000 hours, demonstrating the stability of the phosphors used in our LED packages.

In order to understand the optical degradation kinetics due to package materials degradation, a series of optical simulation was performed to investigate spectral power distribution output of the LED package. The materials include lead frames, package

housing, silicone and phosphors. The degradation test of the phosphors was not performed due to lack of experiment equipments. Except for the phosphors, the degradation data of the rest materials were obtained by performing ageing tests on the prepared samples. For reference, effects of the chip degradation were also simulated by assuming the emitting efficiency degrades from 100% to 85%. The simulation results have been partly verified by a sulfur-corrosion test which stimulated the degradation of the lead frames in the LED packages. A detailed description of the experiments and simulations can be referred to Chapter 4. The results showed that degradation of package materials mainly affected the spectral output of the down-converted light, while less impacted the blue light, even though the blue light was more sensitive to the degradation of package materials, as indicated in Fig. 5.27 to 5.31. The degradation of the silicone encapsulant, however, triggered gradual degradation of the blue light spectral output, while rarely affected the down-converted light spectral output after an initial degradation within 168 hours. The chip efficiency decrease induced the same degrading amount for the blue light and down-converted light spectral outputs, which is in accordance with the experiment result shown in previous section. The simulation results can be explained by theory of transmission path of light rays in LED packages and the theory of the Bouger-Lambert-Beer law. A detailed description of the model can be referred to Chapter 4.

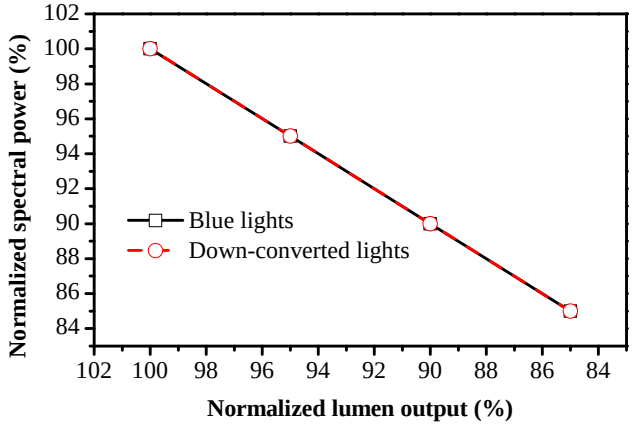

Figure 5.27: Chip degradation: Degradation of spectral power versus chip efficiency

As presented in Fig. 5.18(b), it was found that the blue lights degraded faster than the down-converted lights in WHTOL 95 °C/95% RH, which was contributed to the silicone encapsulant. Chip deterioration mechanism also induces decrease of the blue light spectral output, but at the same time it induces the same degrading amount of the

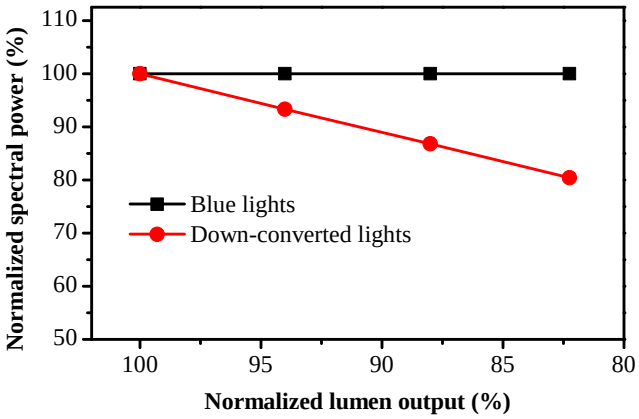

Figure 5.28: Phosphor degradation: Averaged spectral power versus lumen degradation

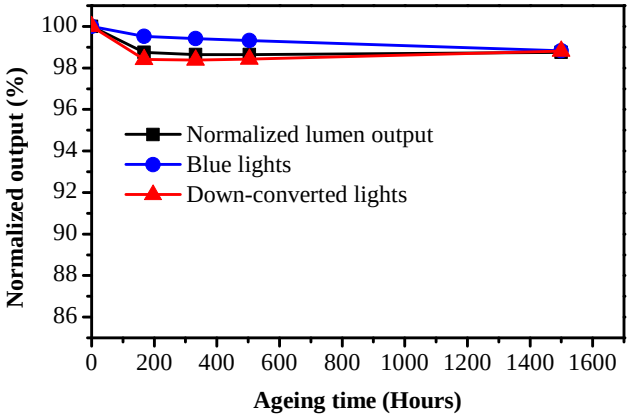

Figure 5.29: Silicone degradation: Normalized spectral power versus ageing time

down-converted light spectral output. If we consider the degradation effects of the lead frames and package housing, a faster degradation of the down-converted light spectral output than that of the blue light spectral output would be expected, which is in the opposite of the result observed in 5.18(b). In other words, both silicone encapsulant and chip degradation contribute to the degradation of the blue light spectral output in WHTOL 95 °C/95% RH, and the degradation of the silicone encapsulant is the root cause of the phenomenon that the blue lights degraded faster than the down-converted lights in WHTOL 95 °C/95% RH. Due to phosphor self-heating effect, the degradation of silicone encapsulant has been reported by some researchers. The temperature inside the sili-

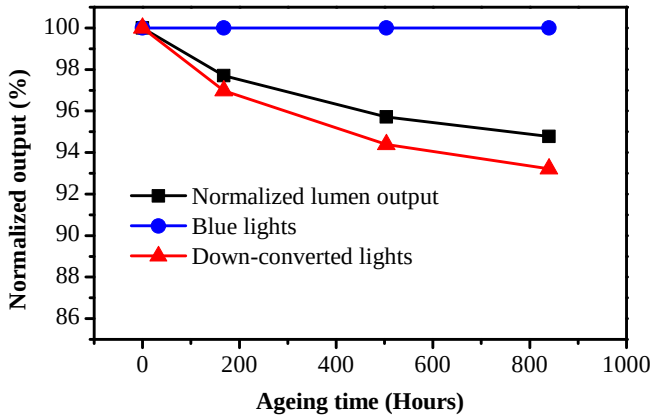

Figure 5.30: Package housing degradation: Normalized spectral power versus ageing time

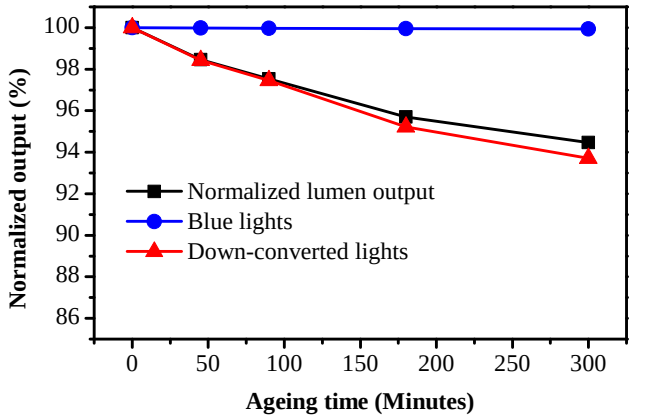

Figure 5.31: Lead frame degradation: Normalized spectral power versus ageing time

cone encapsulant varied from 195 °C to 316 °C [61–64], depending on the LED products.

However, the rapid degradation of the blue lights was mainly contributed to the large color shift, while performed few effects on the lumen output. In a word, the lumen output was mainly attributed to the degradation of down-converted lights, as well as to chip deterioration in WHTOL, as shown in Fig. 5.32.

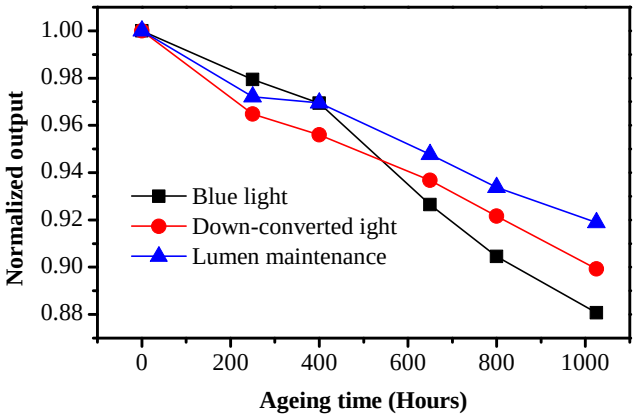

Figure 5.32: Degradation kinetics of light output and spectral power density

5.4. OPTICAL DEGRADATION MECHANISMS UNDER HAST

5.4.1. MOTIVATION EXAMPLE

As reported in our previous study [30], a rapid lumen degradation was observed in LED packages that were stressed by a constant current in HAST within 96 hours, even though the ambient temperature was limited to 105 °C. Microscopy observation showed severe carbonization in the bulk silicone, especially at the interface of the upper surface of blue chip. Fig. 5.33 shows the cross-section of both the LED packages which were stressed with and without driving current, respectively. It was found that silicone carbonization appeared only when the current was applied. It was speculated that the silicone carbonization was due to either the self-heating of phosphors, or over-absorption of blue lights, which may induce extremely high temperature in silicone volume. To fully understand the failure mechanisms, following studies have been conducted.

5.4.2. HIGH TEMPERATURE STORAGE

First, high temperature storage tests were performed in order to explore the thermal characteristics of the silicone. Five pieces of silicone plate, with 30 mm in diameter and 1 mm in thickness, were prepared on quartz glasses. Before ageing, the transmissivity of the silicone plates was measured for each sample. Then the silicone plates were placed into a storage chamber and then aged successively according to a stressing sequence until silicone carbonization was found. The stressing sequence is presented in Table 5.9: initially 336 hours at 190 °C, followed by 24 hours at 250 °C, and finally 24 hours at

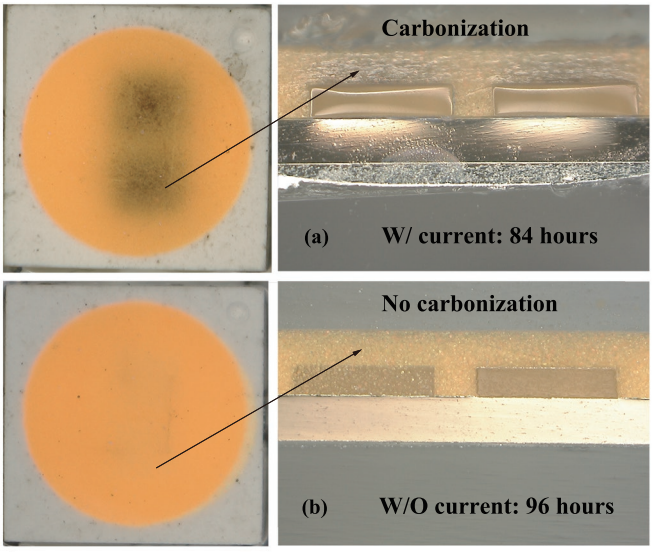

Figure 5.33: Cross-section of the LED packages after ageing test

300 °C, respectively.

Table 5.9: High temperature storage of the silicone plates

Temperature (°C)	190	250	300
Duration (Hours)	336	24	24

It was found that the thermal characteristics of silicone plates were quite stable when ageing at 190 °C. No discoloration was observed after 336 hours. Furthermore, the normalized transmissivity remained as high as 98% of its initial value, as shown in Fig. 5.34.

However, significant silicone yellowing has been found at the stress sequence of 250 °C, even though the test duration was much shorter than that in 190 °C. The yellowing indicates molecular structure decomposition in silicone plates due to high storage temperature. However, it is far less than carbonization. Fig. 5.35 shows the appearance of the silicone plates at end of the stressing sequence of 190 °C and 300 °C, respectively. It is obvious that the silicone plates aged with higher chamber temperature (300 °C) were blacken rapidly, demonstrating that the silicone carbonization would be triggered only if the temperature inside the silicone volume is higher than 300 °C.

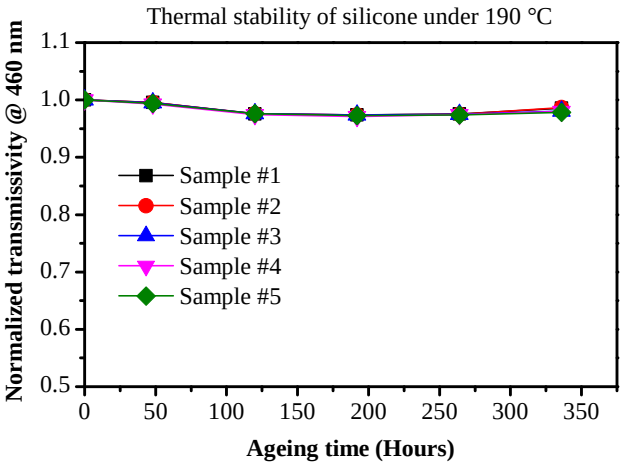

Figure 5.34: Silicone transmittance vs. ageing time in high temperature storage test

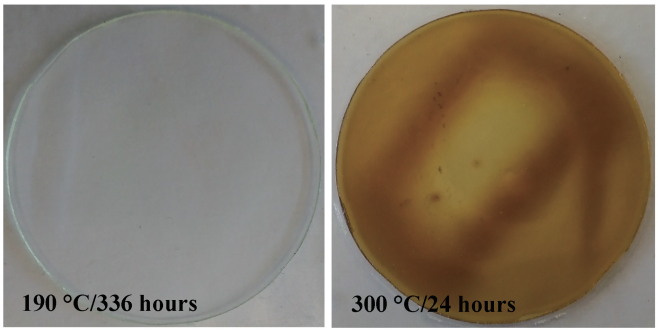

Figure 5.35: Appearance of silicone plates after storage ageing test

5.4.3. DISCUSSION OF THE ROOT CAUSE OF SILICONE CARBONIZATION

Some researchers reported that the carbonization of silicone plates was mainly due to a combination of Joule heating and the elevated ambient temperatures [25], which was often found in high-power white-light LED packages during high temperature bias test. The most apparent evidence is the blackening of silicone, near the top surface of the blue chip, or near the lead frame [44]. A significant Joule heating due to the high resistances of the Ohmic contacts [65], the n-type and p-type cladding layers [41, 53], and the degradation of heat conduction materials [66, 67] were reported during operation applications [68, 69]. Self-heating induces serious carbonization if the junction temperature is higher than the critical temperature of silicone carbonization.

Another potential carbonization mechanism is the phosphor self-heating [64, 70]. For white-light LEDs, down-converted phosphors are applied to down-convert the blue light spectra to a longer wavelength, i.e., down-converted lights. Unfortunately, not all absorbed blue lights are transferred to down-converted lights. Due to non-radiative transfer and Stokes shift, part of the absorbed blue lights is released in terms of heat [71]. The heat accumulation increases rapidly at higher operating ambient temperature [15], because of the thermal quenching characteristic of phosphors [72, 73]. This results from the enhancement of cascade multi-phonon relaxation, a temperature dependent energy transfer or crossover process [74]. Based on this analysis, some researchers reported a much higher temperature inside silicone than the junction temperature of blue chip. The temperature inside the silicone volume varied from 195 °C to 316 °C [61–64], depending on the LED products.

In addition to the effects of Joule heating and phosphor self-heating, shorter wavelength irradiation damage is considered as another possible root cause of silicone carbonization. For a practical LED package under the blue light radiation, high temperature and a small amount of oxygen, epoxy resin will be gradually discolored. This is due to the opening of C-O and C=O bonds, and the dissociative C and O atoms occurring on the die surface. Finally a large amount of carbon or carbon oxide could accumulate on the interface between die and silicone, resulting in a black zone and darkening of the die surface [75].

JOULE HEATING EFFECTS OF THE LED PACKAGES

A schematic diagram depicting the heat dissipation of the LED packages is shown in Fig. 5.36. Due to low thermal conductivity and large length scale from lateral side, heat dissipation to the ambient through the silicone encapsulant is neglected. Similarly, heat dissipation through the silicone and epoxy material compound (EMC) can also be neglected [66]. As a result, a 1-D schematic of the thermal resistance network from junction to heat sink is shown in Fig. 5.37. Deterioration of any component in the 1-D model can increase thermal accumulation. First, the deterioration of the LED chips were detected. For this purpose, $I-V$ characteristics of the stressed LED packages were measured by using a Keithley Digital Multimeter. The $I-V$ curve of the stressed LED package showed the similar characteristics as compared to the non-stressed sample, demonstrating the excellent electrical performance of the stressed LED chip, as shown in Fig. 5.38. Next, C-Mode Scanning Acoustic Microscopy (CSAM) was applied to the stressed/non-stressed samples, as shown in Fig. 5.39. The delamination has been found in the die/silicone interface and lead frame/silicone. This delamination may lead to the increase in the junction temperature of the LEDs. Hence, it is necessary to know the

junction temperature of the degraded LEDs. Because all LED packages showed consistent lumen degradation, only one degraded LED was measured. Fig. 5.40 shows the differential structure function of thermal resistance measured by using T3ster. The thermal resistance from the junction of the blue chips to MCPCB is about 17 °C/W.

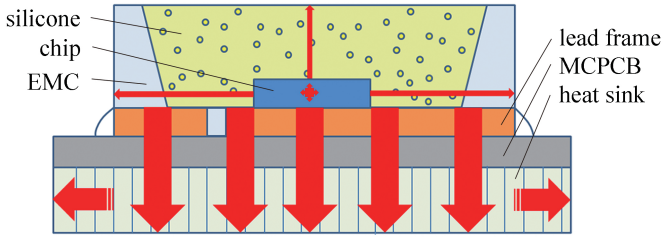

Figure 5.36: Heat dissipation path of the LED packages

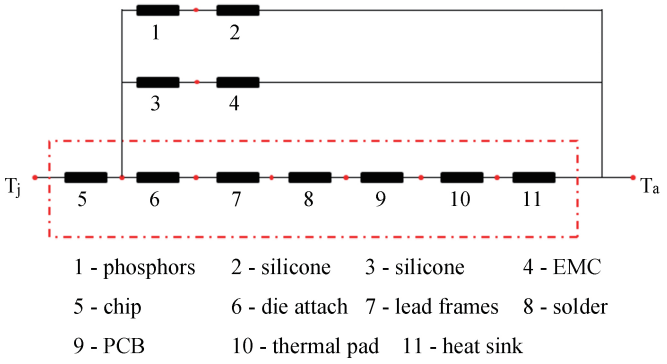

Figure 5.37: Thermal resistance from junction to heat sink

On the other hand, the solder temperature of the aged LED package is monitored during HAST test. An average value of 110 °C was recorded after monitoring for 2 hours. Then the junction temperature of the blue chip can calculated as below:

$$T_j = T_s + R_{th} \cdot P \tag{5.7}$$

where T_j is the junction temperature, T_s is the solder temperature, R_{th} is the thermal resistance of aged samples, and is the electrical power. According to the thermal resistance of the tested LED package, the junction temperature was obtained as $T_j = 127$ °C. The junction temperature is much lower than 300 °C, so it can be concluded that the carbonization of silicone is not resulted from high junction temperature.

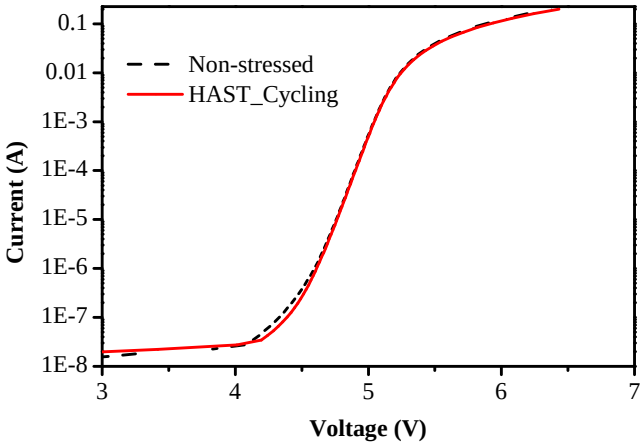

Figure 5.38: $I-V$ characteristics of the LED packages

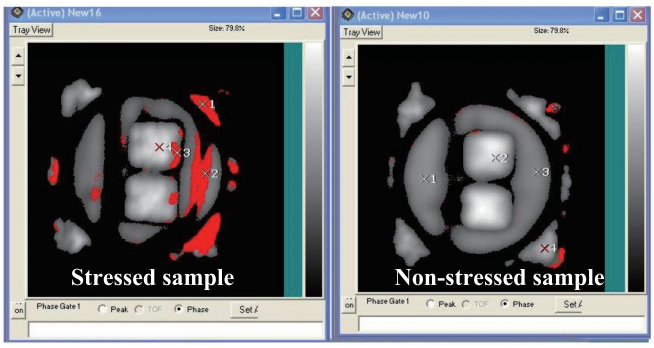

Figure 5.39: Delamination detection by using CSAM

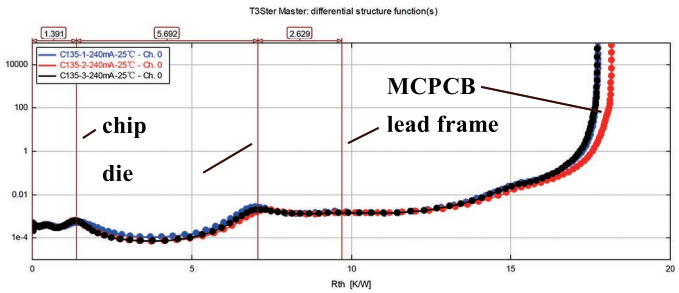

Figure 5.40: Thermal resistance of the LED packages

SELF-HEATING EFFECTS OF THE PHOSPHORS

To investigate the effect of phosphor self-heating due to thermal quenching, high temperature operation life test (HTOL) was performed. In this test, the solder temperature of the LED packages was maintained at 105 °C with a variation of ±2 °C. The solder temperature in HTOL was similar to that of LED packaged aged in HAST. Then the LED packages were stressed with a constant driving current of 220 mA for 6000 hours. The images of silicone appearance before and after 6000 hours in HTOL 105 °C are shown in Fig. 5.41. It is obvious that the self-heating effects of the phosphors cannot result in silicone carbonization. The test also showed good thermal stability of the phosphors in our LED packages.

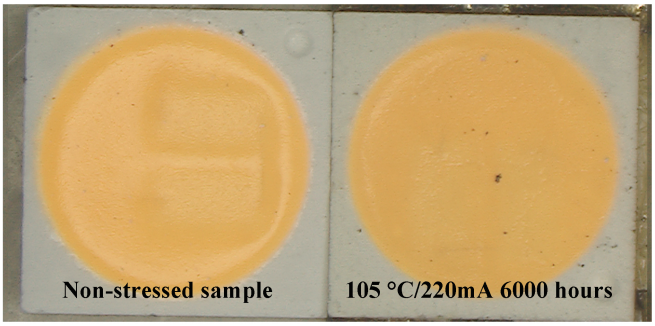

Figure 5.41: Silicone appearance before and after 6000 hours in HTOL 105 °C

There has been a concern that hydrolysis may occur in phosphors due to their exposure to high humidity environment. The hydrolysis lowers the quantum efficiency of the phosphors, and finally accelerates the self-heating of the phosphors [71]. To study this effect, we performed the following test. The phosphor powders were first dissolved in de-ionized waters, and then the electrical conductivity of this solution was measured. The test duration was about 30 minutes. The results are presented in Table 5.10. The solution showed very stable electrical conductivity after 30 minutes, indicating there is no hydrolysis in the phosphors.

Table 5.10: Solution conductivity for phosphors dissolved in water

Time (minutes)	0	1	4	7	15	30
Electrical conductivity (μS)	6.4	6.7	6.6	6.6	6.7	6.6

Table 5.11: Solution conductivity for phosphors dissolved in water

Time (hours)	**500**		**1000**	
Sample number	Δ x	Δ y	Δ x	Δ y
1	0.001	-0.002	0.001	-0.001
2	0.001	0	0.001	0
3	0.001	0	0.001	-0.001
4	0.001	0	0.001	-0.001
5	0.001	0	0.001	0

Furthermore, a long term WHTOL test was also performed to study the hydrolysis stability of phosphors. The phosphor samples were placed into a climate chamber, in which the ambient temperature is 85 °C and the relative humidity is 93% respectively. The color shift was measured intermediately according to the CIE 1931 color space. The results showed very little color shift appeared after 1000 hours, as indicated in Table 5.11. These data were consistent with what were observed in the HAST test. In fact, for LED packages aged without bias in HAST, a color shift of -0.001 in Δx , and 0 in Δy were observed after 96 hours. In addition, only 3% lumen decay was found. Both package-level and phosphor material experiments demonstrated that the phosphors did not degrade significantly in high humidity environment.

The last concern is that the phosphor self-heating may increase significantly due to blue light over-absorption. As the LED packages are placed in a high humidity environment, the blue lights emitted from the chip are trapped by water particles inside the silicone volume, thus increase the absorption possibility by the phosphors. As a result, the self-heating of the phosphors may increase with the absorption possibility. It is difficult to verify this hypothesis directly. However, a comparison experiment can be performed to investigate this hypothesis. For this purpose, two groups of LEDs were prepared. One group of LEDs was packaged by silicone dispensed with phosphors and the other group of LEDs was packaged by silicone without phosphors. Both groups of LEDs were stressed with a constant current in the HAST chamber. The results show that the self-heating of the phosphors is not the major mechanism of the silicone carbonization, because the lumen degradation of the LED packages encapsulated without phosphors is much worse than that with phosphors, as presented in Fig. 5.42 and Fig. 5.43.

The phenomenon can be explained as follows. For the LEDs packaged with phosphors, because most of the blue lights are absorbed by the phosphors, the blue lights are down-converted to a series of down-converted lights which have longer wavelengths. These down-converted lights, however, are not easily absorbed by the bulk silicone, as

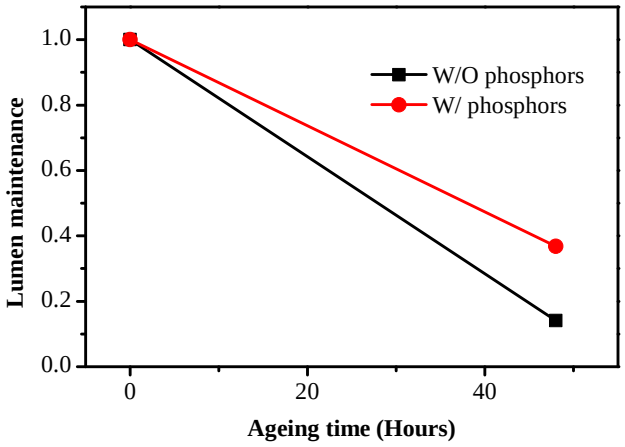

Figure 5.42: Lumen degradation of LED packages with and without phosphors

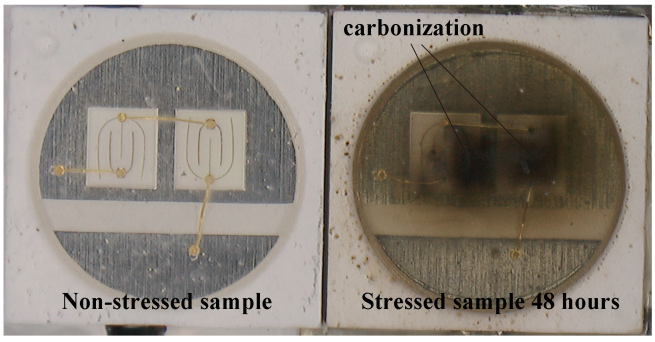

Figure 5.43: Silicone carbonization was also observed in LED packages without phosphors

indicated in Fig. 5.44. As a result, the silicone carbonization is expected to be less severe than that in the LEDs packaged without phosphors.

On the contrary, for the LEDs packaged without phosphors, the blue lights emitting from the blue chips, are either directly absorbed or scattered when propagating through the package. The scattering of the blue lights, increases the absorption probability. Higher blue light intensity and higher absorption probability of the blue lights, induces more severe silicone carbonization during the ageing test, thus resulting in lower lumen maintenance of the LED packages. A detailed description of the degradation mechanism will be provided in following sections.

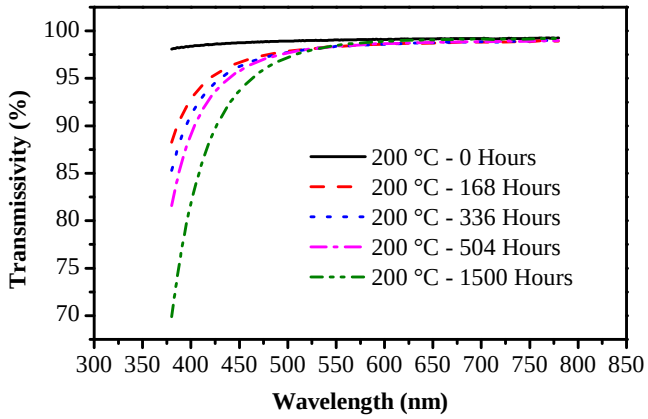

Figure 5.44: Silicone transmissivity versus lights wavelengths

BLUE LIGHT OVER-ABSORPTION BY SILICONE

Finally the root cause is limited to the over-absorption of blue lights by silicone bulk. This degradation mechanism can be explained as follows. Due to the permeability of silicone, water vapor ingress occurs when LED packages are exposed to high temperature-humidity environment. When the water vapors reach to the saturated concentration, they are condensed at the pore walls of the silicone bulk due to the adsorption effects. As a result, blue lights emitting from the LED dies are scattered and randomly propagate through the silicone bulk. The scattering may happen many times, until the blue lights are absorbed by the silicone bulk. The absorption of the blue lights, increases the temperature inside the silicone volume, finally leads to the carbonization.

It has been found that the light scattering and absorption behavior is very complicated in the phosphor-converted LED packages. Based on the revised Kubelka-Munk and Mie-Lorenz theories, Hu *et al.* [76] found that the output intensity of both the blue light and down-converted light was significantly affected by the size of the particles mixing in the silicone bulk. This is mainly due to the interaction mechanisms of light scattering and absorption when lights propagate through the silicone encapsulant [77]. On the other hand, a light scattering model was developed to qualitatively describe this phenomenon by Tan *et al.* [22]. In this model, the entrapped moisture in the silicone volume is modeled as embedded particles which will scatter the emission light from the LED die. The attenuated irradiance by the slab of water particles was obtained as follows:

$$I_t = I_0 \exp(-\rho \sigma_{scat} t) \tag{5.8}$$

where I_0 is the irradiance of the non-polarized incident light, ρ is the number of particles per unit volume, t is the thickness of the water slab entrapped in the silicone volume, and σ_{scat} is the cross section of light scattering. The cross section of light scattering can be expressed as [78]:

$$\sigma_{scat} = \frac{8\pi}{3}\left(2\pi\frac{n_{med}}{\lambda_0}\right)^4 r^6\left(\frac{(n_{wat}/n_{med})^2-1}{(n_{wat}/n_{med})^2+2}\right)^2 \tag{5.9}$$

where λ_0 is the vacuum wavelength of the emitting lights, n_{med} is the refractive index of the silicone, n_{wat} is the refractive index of the water particles, and r is the particle radius.

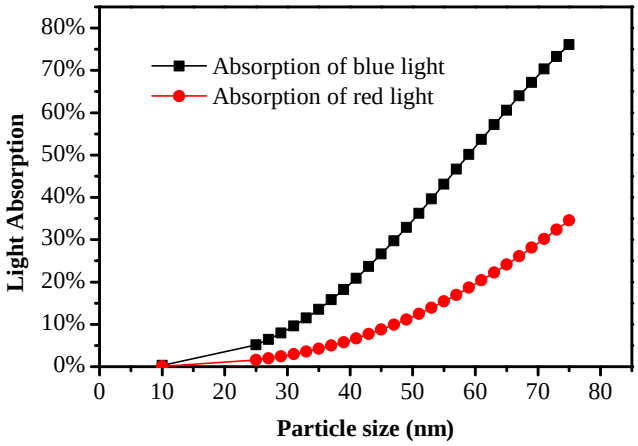

Figure 5.45: Absorption of emitting lights by silicone volume

Tan *et al.* [22] found that the lumen output decreased immediately as the size of the water particles inside the silicone bulk increased. According to [22, 79], the saturated concentration of water particles in polymer materials is only dependent on the relative humidity, while independent of temperature. Hence, the volume fraction of water in silicone is about 0.0753% in saturated water vapors. According to the attenuated irradiance model, the blue light absorption ratio with the pore size of the water particles can be calculated using Eq. (5.8) and (5.9). Fig. 5.45 shows the calculated absorption ratio of emitting lights by silicone volume with the particle size. It indicates that the absorption of the blue lights has been found as high as 40.7%, when the size of the water particles increases to 75 nm. This is reasonable because the pore size of the silicone volume is large enough to accommodate such water particles, as indicated in Fig. 5.46. The pore

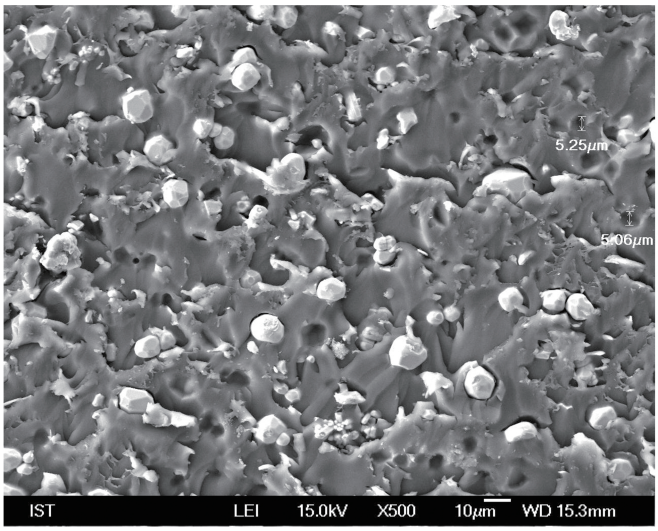

Figure 5.46: Measured pore sizes in the silicone volume

size measurement was performed by using a scanning electron microscope (SEM), from the silicone bulk of one aged LED package.

SIMULATION & VALIDATION

A finite element model is created to simulate the temperature distribution of the LED packages due to blue lights absorption by silicone bulks. For simplicity, the simulation model includes only one LED package, which is mounted onto a metal-core printed circuit board (MCPCB). The simulation model is shown in Fig. 5.47. The detailed dimensions of all components and the thermal conductivity of the materials are listed in Table 5.12.

In this model, the electrical power of the LED package is 1 W, and the radiation efficiency is set as 50% according to the optical measurement data. Two heat sources are created. One is the blue chip, and the other one is the silicone bulk. Only the silicone bulks above the blue chip are considered as heat source, which is in accordance with the area of carbonization observed on the degraded LED packages. The internal heat generation of the chip is calculated as 133 W/mm^3, which corresponds to 0.5 W of the total heat dissipation. The internal heat generation of bulk silicone is 1.1 W/mm^3 when the absorption ratio is 40%. This means that there is about additional 0.2 W heat generated in silicone. In our thermal model, natural convection heat transfer is assumed. The ambient temperature is set as 105 °C, which is in line with the ambient temperature

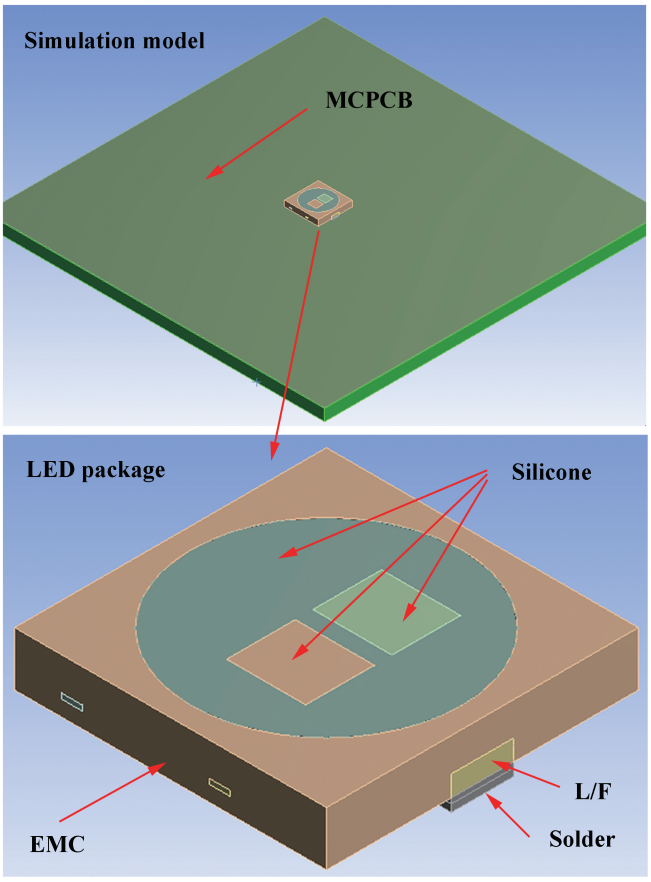

Figure 5.47: Thermal transferring simulation model

Table 5.12: Component dimension and material thermal conductivity

Component	Material	Dimension (mm×mm×mm)	Thermal Conductivity (W/m·K)
Encapsulant	Silicon	ϕ2.6×0.32	0.2
Housing	EMC	3.0×3.0×0.52	0.36
Chip active layer	GaN	0.76×0.66×0.01	140
Chip substrate	Sapphire	0.76×0.66×0.13	46
Die attach	Silicone	0.76×0.66×0.002	0.2
Lead frames	Copper	2.2×2.6×0.2	400
Solder	SAC305	2.2×2.6×0.05	63.2
Solder pad	Copper	2.2×2.6×0.07	400
Insulation	Insulation	30×30×0.08	1.5
MCPCB	Aluminum	30×30×1.0	237.5

of the HAST chamber.

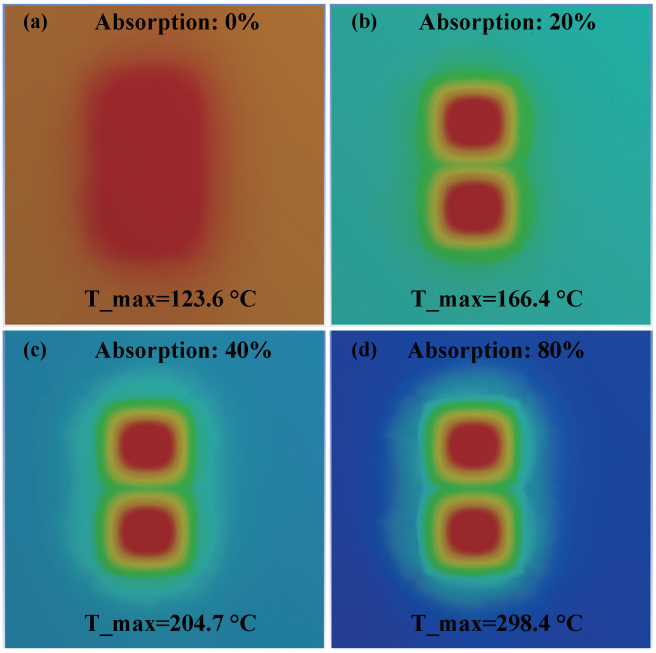

Figure 5.48: Temperature distribution inside the silicone volume

Fig. 5.48 shows the temperature distribution of the silicone volume. It is found that the maximum temperature of the silicone volume is around 125 °C when no blue lights are absorbed, which is in line with the junction temperature measured by T3ster, indicating the validity of our simulation model. However, the maximum temperature increases rapidly with the absorption ratio of the blue lights. In the worst case the temperature is up to 300 °C with the absorption ratio of 80%. It is worth noticing that the internal heat generation in silicone bulk is assumed uniformly distributed. However, the uniform distribution assumption can underestimate the maximum temperature. For silicone materials that are close to the upper surface of the blue chips, the heat generation can be much higher. As a result, the carbonization may occur first in these areas and then spread to other areas. For instance, when internal heat generation is 3 W/mm^3, the maximum temperature will be 366.8 °C. Such high temperature will result in serious carbonization of the silicone. On the other hand, the simulation model did not account for the effect of delamination. The internal temperature of the silicone is expected to be higher than the simulation result if this effect is included.

5.5. SUMMARY

The optical degradation mechanisms of mid-power white-light LED packages were comprehensively investigated by using HTOL, WHTOL and HAST. It was found that the LM-80-08 test methods triggered different degradation mechanisms, implying that lifetime prediction based on this standard may be misused. In the other hand, the degradation mechanism was found as silicone carbonization in the HAST test, which was considered to be a results of over-stressing on the LED packages. This mechanism was rarely observed in the usage applications. Compared to the former test method, the WHOTL was consider as an efficient accelerated life test method for the mid-power LED packages, as it triggered both the chip and package-related degradation mechanisms, which are frequently observed in the usage applications. In addition, it enables much larger optical degradation while uses only one third of the testing time in LM-80-08. A detailed summary is presented as follows:

In Section 5.2, the degradation mechanisms are different at different stress conditions for LED packages aged by the LM-80-08 test method. A series of data analysis and failure analysis revealed that the optical degradation was triggered by degradation of both the chips and lead frames due to humidity effect for LED packages aged at 55 °C. However, for LED packages aged at 105 °C, the degradation mechanism was mainly related to chip deterioration due to the deterioration of the Ohmic contact. As the degradation mechanisms are different in the LM-80-08 tests, the corresponding lifetime prediction method in the TM-21-11 standard may have been misused.

In Section 5.3, we found that the yellowing of the LED package housing was mainly triggered by the moisture rather than the temperature for mid-power LED packages aged by WHTOL; and WHTOL is an higher accelerated test method instead of the LM-80-08 method for the lifetime prediction of the mid-power LEDs. The optical degradation of the mid-power LED packages was found being contributed to both the serious yellowing of the package housing and deterioration of the chips. By comparing to yellowing of the LED packages aged by both HTOL and WHTOL, we concluded that the degradation mechanisms of yellowing are triggered by moisture rather than temperature, as the yellowing of the packages aged by HTOL was negligible. The deterioration of the chip, was contributed to the temperature and humidity effect, both of which induced the Ohmic contact degradation. The WHTOL triggered both chip-related and package-related degradation mechanisms, which is in accordance with what was found in the applications. In addition, statistics analysis found that the failure distributions are similar to each other for the LED packages aged by different WHTOL stress conditions. Compared to the LM-80-08 method, the WHTOL used one third of the testing

time, while triggered much larger optical degradation. In a word, WHTOL is a much more efficient test method instead of the LM-80-08 method for the lifetime prediction of the mid-power LEDs.

In Section 5.4, blue light over-absorption was found to be the degradation mechanisms of silicone carbonization for LED packages aged by HAST test, which can be explained by the scattering effect of the water particles. Due to the permeability of silicone, water vapor ingress occurs when LED packages are exposed to high temperature-humidity environment. When the water vapors reach to the saturated concentration, they are condensed at the pore walls of the silicone bulk due to the adsorption effects. As a result, blue lights emitting from the LED dies are scattered and randomly propagate through the silicone bulk. The scattering may happen many times, until the blue lights are absorbed by the silicone bulk. Simulation showed that the temperature of the silicone can be up to 300 °C due to the absorption of the blue lights, which leads to the silicone carbonization. Analysis also showed that the blue light over-absorption is strongly dependent on the water particle size.

REFERENCES

[1] J. Huang, D. S. Golubović, S. Koh, D. Yang, X. Li, X. Fan, and G. Zhang, *Optical degradation mechanisms of mid-power white-light leds in lm-80-08 tests,* Microelectronics Reliability **55**, 2654 (2015).

[2] J. Huang, D. Golubović, S. Koh, D. Yang, X. Li, X. Fan, and G. Zhang, *Degradation mechanisms of mid-power white-light leds under high-temperature–humidity conditions,* IEEE Transactions on Device and Materials Reliability **15**, 220 (2015).

[3] J. Huang, D. Golubović, S. Koh, D. Yang, X. Li, X. Fan, and G. Zhang, *Rapid degradation of mid-power white-light leds in saturated moisture conditions,* IEEE Transactions on Device and Materials Reliability **15**, 478 (2015).

[4] H. Fan, X. Li, J. Shen, and M. Chen, *An effective prediction method for led lumen maintenance,* in *13th International Conference on Electronic Packaging Technology and High Density Packaging (ICEPT-HDP), 2012* (IEEE) pp. 1560–1563.

[5] L. Trevisanello, M. Meneghini, G. Mura, M. Vanzi, M. Pavesi, G. Meneghesso, and E. Zanoni, *Accelerated life test of high brightness light emitting diodes,* IEEE Transactions on Device and Materials Reliability **8**, 304 (2008).

[6] W. D. van Driel and X. Fan, *Solid state lighting reliability: components to systems*, Vol. 1 (Springer Science & Business Media, 2012).

[7] M. Meneghini, L.-R. Trevisanello, G. Meneghesso, and E. Zanoni, *A review on the reliability of gan-based leds,* IEEE Transactions on Device and Materials Reliability **8**, 323 (2008).

[8] L. Zhang, Y. Zhu, W. Wang, X. Bi, H. Chen, K.-S. Leung, Y. Wu, and J. Wu, *Study on ag-plated cu lead frame and its effect to led performance under thermal aging,* IEEE Transactions on Device and Materials Reliability **14**, 1022 (2014).

[9] G. Mura, G. Cassanelli, F. Fantini, and M. Vanzi, *Sulfur-contamination of high power white led,* Microelectronics Reliability **48**, 1208 (2008).

[10] E. Jung, M. S. Kim, and H. Kim, *Analysis of contributing factors for determining the reliability characteristics of gan-based white light-emitting diodes with dual degradation kinetics,* IEEE Transactions on Electron Devices **60**, 186 (2013).

[11] M. Y. Mehr, W. van Driel, H. Udono, and G. Zhang, *Surface aspects of discolouration in bisphenol a polycarbonate (bpa-pc), used as lens in led-based products,* Optical Materials **37**, 155 (2014).

[12] M. Y. Mehr, W. D. van Driel, and G. Zhang, *Accelerated life time testing and optical degradation of remote phosphor plates,* Microelectronics Reliability **54**, 1544 (2014).

[13] P. McCluskey, K. Mensah, C. O. Connor, F. Lilie, A. Gallo, and J. Fink, *Reliability of commercial plastic encapsulated microelectronics at temperatures from 125 °C to 300 °C,* in *The Third European Conference on High Temperature Electronics, 1999 (HITEN 99)* (IEEE, 1999) pp. 155–162.

[14] P. McCluskey, K. Mensah, C. O'Connor, and A. Gallo, *Reliable use of commercial technology in high temperature environments,* Microelectronics Reliability **40**, 1671 (2000).

[15] R.-J. Xie, N. Hirosaki, N. Kimura, K. Sakuma, and M. Mitomo, *2-phosphor-converted white light-emitting diodes using oxynitride/nitride phosphors,* Applied Physics Letters **90**, 191101 (2007).

[16] S. Koh, W. V. Driel, and G. Zhang, *Thermal and moisture degradation in ssl system,* in *13th International Conference on Thermal, Mechanical and Multi-Physics Simulation and Experiments in Microelectronics and Microsystems (EuroSimE), 2012* (IEEE, 2012) pp. 1–6.

[17] E. Nogueira, M. Vázquez, and N. Núñez, *Evaluation of algainp leds reliability based on accelerated tests,* Microelectronics Reliability **49**, 1240 (2009).

[18] S. Zhou, Q. Zhang, B. Cao, and S. Liu, *Evaluation of gan-based blue light emitting diodes based on temperature/humidity accelerated tests,* in *Electronic Packaging Technology & High Density Packaging (ICEPT-HDP), 2010 11th International Conference on* (IEEE, 2010) pp. 930–934.

[19] S. Chan, W. Hong, K. Kim, Y. Yoon, J. Han, and J. S. Jang, *Accelerated life test of high power white light emitting diodes based on package failure mechanisms,* Microelectronics Reliability **51**, 1806 (2011).

[20] E. Nogueira, M. Vázquez, and C. Algora, *Accelerated life testing in epoxy packaged high luminosity light emitting diodes,* Journal of Electronic Packaging **133**, 034501 (2011).

[21] J. Hu, L. Yang, and M. Whan Shin, *Mechanism and thermal effect of delamination in light-emitting diode packages,* Microelectronics Journal **38**, 157 (2007).

[22] C. M. Tan, B. Chen, X. Li, and S. J. Chen, *Rapid light output degradation of gan-based packaged led in the early stage of humidity test,* IEEE Transactions on Device and Materials Reliability **12**, 44 (2012).

[23] C. M. Tan, B. K. E. Chen, G. Xu, and Y. Liu, *Analysis of humidity effects on the degradation of high-power white leds,* Microelectronics Reliability **49**, 1226 (2009).

[24] D. L. Barton, M. Osinski, P. Perlin, C. J. Helms, and N. H. Berg, *Life tests and failure mechanisms of gan/algan/ingan light-emitting diodes,* in *Optoelectronics and High-Power Lasers & Applications* (International Society for Optics and Photonics) pp. 17–27.

[25] D. L. Barton, M. Osinski, P. Perlin, P. G Eliseev, and J. Lee, *Single-quantum well ingan green light emitting diode degradation under high electrical stress,* Microelectronics Reliability **39**, 1219 (1999).

[26] M.-H. Chang, D. Das, P. Varde, and M. Pecht, *Light emitting diodes reliability review,* Microelectronics Reliability **52**, 762 (2012).

[27] I. T. P. Committee, *Approved Method: Measuring Lumen Maintenance of LED Light Sources*, Report (IESNA LM-80-08. Illuminating Engineering Society of North America. New York, 2008).

[28] L. Liu, J. Yang, and G. Wang, *The investigation of led's reliability through highly accelerated stress testing methods,* in *14th International Conference on Electronic Materials and Packaging (EMAP), 2012* (IEEE) pp. 1–3.

[29] L. Liu, J. Yang, and G. Wang, *The investigation of led's reliability through highly accelerated stress testing methods,* in *14th International Conference on Electronic Materials and Packaging (EMAP), 2012* (IEEE) pp. 1–3.

[30] J. Huang, S. Koh, X. Li, and G. Zhang, *Investigation of lumen degradation mechanisms of mid-power led by hast,* in *15th International Conference on Electronic Packaging Technology (ICEPT), 2014* (IEEE, 2014) pp. 1437–1441.

[31] J. Huang, S. Koh, D. Yang, X. Li, X. Fan, and G. Zhang, *Degradation mechanisms of mid-power white-light leds under high temperature-humidity conditions,* IEEE Transactions on Device and Materials Reliability **15**, 220 (2015).

[32] I. E. S. o. N. America, *Projecting long term lumen maintenance of led light sources,* (2011), [IESNA].

[33] T. Yanagisawa and T. Kojima, *Long-term accelerated current operation of white light-emitting diodes,* Journal of Luminescence **114**, 39 (2005).

[34] S. Koh, C. Yuan, B. Sun, B. Li, X. Fan, and G. Zhang, *Product level accelerated lifetime test for indoor led luminaires,* in *14th International Conference on Thermal, Mechanical and Multi-Physics Simulation and Experiments in Microelectronics and Microsystems (EuroSimE), 2013*, pp. 1–6.

[35] L. Liu, M. Ling, J. Yang, W. Xiong, W. Jia, and G. Wang, *Efficiency degradation behaviors of current/thermal co-stressed gan-based blue light emitting diodes with vertical-structure,* Journal of Applied Physics **111**, 093110 (2012).

[36] D.-g. LI, W.-l. WANG, F.-s. MIN, and H.-p. SHEN, *Relation between ideal factor and lifetime,* Chinese Journal of Liquid Crystals and Displays **6**, 019 (2008).

[37] V. Dmitriev, *Gan based pn structures grown on sic substrates,* MRS Internet Journal of Nitride Semiconductor Research **1**, e29 (1996).

[38] C.-X. Wang, G.-W. Yang, H.-W. Liu, Y.-H. Han, J.-F. Luo, C.-X. Gao, and G.-T. Zou, *Experimental analysis and theoretical model for anomalously high ideality factors in zno/diamond pn junction diode,* Applied physics letters **84**, 2427 (2004).

[39] W. Shockley and W. Read Jr, *Statistics of the recombinations of holes and electrons,* Physical review **87**, 835 (1952).

[40] J. Hu, L. Yang, and M. W. Shin, *Electrical, optical and thermal degradation of high power gan/ingan light-emitting diodes,* Journal of Physics D: Applied Physics **41**, 035107 (2008).

[41] M. Meneghini, L.-R. Trevisanello, U. Zehnder, G. Meneghesso, and E. Zanoni, *Reversible degradation of ohmic contacts on p-gan for application in high-brightness leds,* IEEE Transactions on Electron Devices **54**, 3245 (2007).

[42] M. Miyachi, T. Tanaka, Y. Kimura, and H. Ota, *The activation of mg in gan by annealing with minority-carrier injection,* Applied Physics Letters **72**, 1101 (1998).

[43] M. Meneghini, L. Trevisanello, C. Sanna, G. Mura, M. Vanzi, G. Meneghesso, and E. Zanoni, *High temperature electro-optical degradation of ingan/gan hbleds,* Microelectronics Reliability **47**, 1625 (2007).

[44] M. Meneghini, A. Tazzoli, G. Mura, G. Meneghesso, and E. Zanoni, *A review on the physical mechanisms that limit the reliability of gan-based leds,* IEEE Transactions on Electron Devices **57**, 108 (2010).

[45] M. Meneghini, L. Trevisanello, S. Levada, G. Meneghesso, G. Tamiazzo, E. Zanoni, T. Zahner, U. Zehnder, V. Harle, and U. Straus, *Failure mechanisms of gallium nitride leds related with passivation,* in *IEEE International Electron Devices Meeting (IEDM Technical Digest), 2005* (IEEE) pp. pp.1–4.

[46] M. Y. Mehr, W. Van Driel, K. Jansen, P. Deeben, M. Boutelje, and G. Zhang, *Photodegradation of bisphenol a polycarbonate under blue light radiation and its effect on optical properties,* Optical Materials **35**, 504 (2013).

[47] X. Fan and C. Yuan, *Effect of temperature gradient on moisture diffusion in high power devices and the applications in led packages,* in *IEEE 63rd Electronic Components and Technology Conference (ECTC), 2013* (IEEE, 2013) pp. 1466–1470.

[48] D. S. Peck, *Comprehensive model for humidity testing correlation,* in *24th Annual Reliability Physics Symposium, 1986.* (IEEE, 1986) pp. 44–50.

[49] B. Ma and J. Kim, *Complex-stress accelerated lifetime test for high-power light-emitting diodes,* Electronics letters **48**, 449 (2012).

[50] H. Yunsheng, W. ZHUANG, H. Huaqiang, L. Ronghui, C. Guantong, L. Yuanhong, and X. HUANG, *High temperature stability of eu 2+-activated nitride red phosphors,* Journal of Rare Earths **32**, 12 (2014).

[51] W.-H. Cheng, L.-Y. Chen, and W.-C. Cheng, *High-thermal-stability white light-emitting-diodes employing broadband glass phosphor,* in *SPIE Optical Engineering+ Applications* (International Society for Optics and Photonics, 2014) pp. 91900N–91900N.

[52] C. M. Tan and P. Singh, *Time evolution degradation physics in high power white leds under high temperature-humidity conditions,* IEEE Transactions on Device and Materials Reliability **14**, 742 (2014).

[53] E. Jung and H. Kim, *Rapid optical degradation of gan-based light-emitting diodes by a current-crowding-induced self-accelerating thermal process,* IEEE Transactions on Electron Devices **61**, 825 (2014).

[54] B. Wu, X. Luo, Z. Zha, and S. Liu, *Effect investigation of delamination on optical output of high power leds,* in *12th International Conference on Electronic Packaging Technology and High Density Packaging (ICEPT-HDP), 2011* (IEEE, 2011) pp. 1–5.

[55] J. Hu, L. Yang, and M. W. Shin, *Thermal effects of moisture inducing delamination in light-emitting diode packages,* in *Asia-Pacific Optical Communications* (International Society for Optics and Photonics, 2006) pp. 635516–635516.

[56] T. Yanagisawa and T. Kojima, *Degradation of ingan blue light-emitting diodes under continuous and low-speed pulse operations,* Microelectronics Reliability **43**, 977 (2003).

[57] M. Pavesi, F. Rossi, and E. Zanoni, *Effects of extreme dc-ageing and electron-beam irradiation in ingan/algan/gan light-emitting diodes,* Semiconductor science and technology **21**, 138 (2006).

[58] O. Ueda, *Reliability issues in iii–v compound semiconductor devices: optical devices and gaas-based hbts,* Microelectronics Reliability **39**, 1839 (1999).

[59] S.-L. Chuang, A. Ishibashi, S. Kijima, N. Nakayama, M. Ukita, and S. Taniguchi, *Kinetic model for degradation of light-emitting diodes,* IEEE Journal of Quantum Electronics **33**, 970 (1997).

[60] L. Liu, M. Ling, J. Yang, W. Xiong, W. Jia, and G. Wang, *Efficiency degradation behaviors of current/thermal co-stressed gan-based blue light emitting diodes with vertical-structure,* Journal of Applied Physics **111**, 093110 (2012).

[61] H. Ye, S. Koh, C. Yuan, and G. Zhang, *Thermal analysis of phosphor in high brightness led,* in *13th International Conference on Electronic Packaging Technology and High Density Packaging (ICEPT-HDP), 2012* (IEEE, 2012) pp. 1535–1539.

[62] B. Yan, J.-P. You, N. T. Tran, and F. G. Shi, *Influence of phosphor configuration on thermal performance of high power white led array,* in *IEEE International Symposium on Advanced Packaging Materials (APM), 2013* (IEEE, 2013) pp. 274–289.

[63] E. Juntunen, O. Tapaninen, A. Sitomaniemi, and V. Heikkinen, *Effect of phosphor encapsulant on the thermal resistance of a high-power cob led module,* IEEE Transactions on Components, Packaging and Manufacturing Technology **3**, 1148 (2013).

[64] X. Luo, X. Fu, F. Chen, and H. Zheng, *Phosphor self-heating in phosphor converted light emitting diode packaging,* International Journal of Heat and Mass Transfer **58**, 276 (2013).

[65] G. Meneghesso, S. Levada, E. Zanoni, G. Scamarcio, G. Mura, S. Podda, M. Vanzi, S. Du, and I. Eliashevich, *Reliability of visible gan leds in plastic package,* Microelectronics Reliability **43**, 1737 (2003).

[66] B. Yan, J. P. You, N. T. Tran, Y. He, and F. G. Shi, *Influence of die attach layer on thermal performance of high power light emitting diodes,* IEEE Transactions on Components and Packaging Technologies **33**, 722 (2010).

[67] J. You, Y. He, and F. Shi, *Thermal management of high power leds: Impact of die attach materials,* in *International Microsystems, Packaging, Assembly and Circuits Technology, 2007 (IMPACT 2007)* (IEEE, 2007) pp. 239–242.

[68] N. Lobo Ploch, H. Rodriguez, C. Stolmacker, M. Hoppe, M. Lapeyrade, J. Stellmach, F. Mehnke, T. Wernicke, A. Knauer, V. Kueller, *et al.*, *Effective thermal management in ultraviolet light-emitting diodes with micro-led arrays,* IEEE Transactions on Electron Devices **60**, 782 (2013).

[69] M. Khizar, K. Acharya, and M. Y. A. Raja, *Improved local thermal management of algan-based deep-uv light emitting diodes,* Semiconductor Science and Technology **22**, 1081 (2007).

[70] M. Meneghini, M. Dal Lago, N. Trivellin, G. Meneghesso, and E. Zanoni, *Thermally activated degradation of remote phosphors for application in led lighting,* IEEE Transactions on Device and Materials Reliability **13**, 316 (2013).

[71] R.-J. Xie and N. Hirosaki, *Silicon-based oxynitride and nitride phosphors for white leds—a review,* Science and Technology of Advanced Materials **8**, 588 (2007).

[72] R. Pązik, K. Zawisza, A. Watras, K. Maleszka-Bagińska, P. Boutinaud, R. Mahiou, and P. J. Dereń, *Thermal quenching mechanisms of the eu 3+ luminescence in ca 9 al (po 4) 7 obtained by citric route,* Materials Research Bulletin **48**, 337 (2013).

[73] P. F. Smet, J. Botterman, A. B. Parmentier, and D. Poelman, *Thermal quenching at the microscopic level in multi-phase thiosilicate phosphors,* Optical Materials **35**, 1970 (2013).

[74] J. Zhang, B. Chen, Z. Liang, X. Li, J. Sun, L. Cheng, and H. Zhong, *Optical transition and thermal quenching mechanism in casno 3: Eu 3+ phosphors,* Journal of Alloys and Compounds **612**, 204 (2014).

[75] L. Zhou, B. An, Y. Wu, and S. Liu, *Analysis of delamination and darkening in high power led packaging,* in *16th IEEE International Symposium on the Physical and Failure Analysis of Integrated Circuits, 2009 (IPFA 2009)* (IEEE) pp. 656–660.

[76] R. Hu, H. Zheng, J. Hu, and X. Luo, *Comprehensive study on the transmitted and reflected light through the phosphor layer in light-emitting diode packages,* Journal of Display Technology **9**, 447 (2013).

[77] R. Hu, B. Cao, Y. Zou, Y. Zhu, S. Liu, and X. Luo, *Modeling the light extraction efficiency of bi-layer phosphors in white leds,* IEEE Photonics Technology Letters **25**, 1141 (2013).

[78] A. Cox, A. J. DeWeerd, and J. Linden, *An experiment to measure mie and rayleigh total scattering cross sections,* American Journal of Physics **70**, 620 (2002).

[79] E.-H. Wong and R. Rajoo, *Moisture absorption and diffusion characterisation of packaging materials—-advanced treatment,* Microelectronics Reliability **43**, 2087 (2003).

6

DEGRADATION MODELING OF MID-POWER WHITE-LIGHT LEDS

In this chapter, a modified Wiener process has been employed for the modeling of the degradation of LED devices. By using this method, dynamic and random variations, as well as the non-linear degradation behavior of LED devices, can be easily accounted for. The parameter estimation accuracy has been improved by including more information into the likelihood function while neglecting the dependency between the random variables. Degradation model has been established for LED packages which are aged under constant stress accelerated degradation test (CSADT). As a consequence, the mean time to failure (MTTF) has been obtained and shows comparable result with IES TM-21-11 predictions, indicating the feasibility of the proposed method. The cumulative failure distribution was also presented corresponding to different combinations of lumen maintenance and color shift. The results demonstrate that a joint failure distribution of LED devices could be modeled by simply considering their lumen maintenance and color shift as two independent variables. Finally, we also made efforts to extend the modeling method to the range of step stress accelerated degradation test (SSADT).

Parts of this chapter have been published in Optics express **23**, A966 (2015) [1], in Reliability Engineering & System Safety **154**, 152 (2015) [2].

6.1. INTRODUCTION

A rapid growth of the LED-based lighting applications has revolutionized the lighting market from backlight, flash, and automotive lamps, to general lighting including indoor and outdoor illuminations. Due to the fast evolution of the LED technologies, LED packages were frequently claimed a lifetime as high as 36,000 hours [3–5]. Nowadays, it is normal for the LED products with a lifetime more than 100,000 hours in the outdoor applications and 70,000 hours in the indoor applications. As highly reliable products, LED devices may not suffer from mortal deterioration even if accelerated life tests were applied. This implies that catastrophic failures of LED devices seldom occurred in the usage period. Therefore, the reliability test has become an annoying difficulty by using the traditional time-to-failure accelerated life test (ALT) and corresponding statistics method.

Though failures were seldom observed during life tests, previous studies revealed that LED devices could suffer from gradual performance degradation, such as lumen decay, and color shift [6–8]. The gradual degradation mechanisms could be attributed to deterioration of the Ohmic contacts and semiconductor chips [9], silver-coating lead frame damage, encapsulant yellowing [10, 11], silicone carbonization [12, 13], as well as phosphor thermal quenching [14]. Multiple failure modes and failure mechanisms render the difficulties of describing the LED degradation by using a physic model. As a consequence, the way in which a full set of the degradation data is used becomes important for accurate lifetime prediction of LED devices.

In fact, using degradation data for lifetime prediction was studied by statisticians a few decades ago. As one of the pioneers, Nelson discussed a special situation in which the degradation measurement was destructive [15]. After that, Lu and Meeker [16] developed a statistical method which was so-called “general degradation path model”, in which degradation measures were used to estimate the time-to-failure distribution for a broad class of degradation models. As one special case of the general degradation path model, the IES standard TM-21-11 [17] proposed a detailed methodology to use lumen degradation data for the lifetime prediction of LED devices. According to the standard, an LED light source would be considered as failure as long as the lumen output drops to 70% of its initial value. However, the color shift, as another essential performance characteristic of the optical degradation of LED devices, was not included in the standard.

The drawback of the IES standard TM-21-11 is that, it uses regression-based methods to analyze the average lumen degradation data, thus cannot capture the dynamic and random characteristic of the optical degradation process [18]. The random nature of the degradation process reflects a close connection between the LED device’s perfor-

mances and its lifetime. So taking the random effects into consideration allows engineers to better understand the optical degradation distribution and perform more accurate lifetime prediction. Motivated by these advantages, a few researchers proposed to use the Wiener process to deal with the LED device's optical degradation [19–21]. The proposed Wiener process model could be easily used to describe the dynamic and random characteristics of the degradation process. The drawback of these stochastic models is that, they are only available for linear degradation behaviors, thus limiting the applications in a more broad class of degradation processes. Over the past years, researchers were making efforts to develop more flexible models for directly describing the nonlinear degradation through a stochastic process [22–26]. More recent works can be referred to the publications of Si *et al.* [27, 28], Wang *et al.* [29], Wang *et al.* [30, 31], Wang *et al.* [32], and Huang *et al.* [33]. In these papers, researchers have modeled nonlinear degradation by using time-scaling techniques [30–32], nonlinear drift coefficient [22–27], or an adaptive parameter which can be updated dynamically [28–30]. While these models have only been developed for the degradation process in CSADT, there are few studies for the SSADT modeling, which use stochastic models to describe nonlinear degradation processes [21, 34].

In fact, compared to CSADT, SSADT enables comparable lifetime prediction accuracy while using smaller sample size and less test resources [35, 36]. Therefore, the SSADT has been widely applied in reliability tests for LEDs [37, 38], transistors [39], and missile tanks [40]. Based on Nelson's equivalent accumulative damage theory, Tseng [35] and Yao [41], respectively, presented a segmented nonlinear accelerated degradation model (SNADM), which tackles the problem that the degradation rate of the products varies with time during SSADT. However, these models are regression-based and, thus, cannot capture the dynamics or random variations of the degradation process. In order to solve this problem, Kjell *et al.* [42], Liao *et al.* [34], and Tsai *et al.* [43] proposed a stochastic-based SSADT model using Brownian motion and Gamma process. The stationary and independent incremental property of the stochastic processes renders simplicity of the modeling of SSADT.

In this chapter, we first discuss the degradation modeling of mid-power white-light LEDs (MP LEDs), which are stressed under CSADT. Firstly, the modified Wiener process with a time-dependent drift parameter was presented and an improved likelihood function was proposed. Secondly, the Frank copula function was employed to characterize both the lumen maintenance and color shift. The joint distribution of lumen maintenance and color shift was obtained through this function. Finally, the LEDs' cumulative failure distribution at a specified usage condition was predicted by performing acceler-

ated degradation tests (ADT).

After obtaining the degradation model for LED packages aged under CSADT, we also made efforts to extend the modified Wiener process to the range of SSADT. At the first step, a SSADT model was established by using the modified Brownian motion theory. Secondly, a likelihood function was presented for the parameter estimation. At the end, a set of experiments, including CSADT and SSADT, were conducted on one type of mid-power white-light LED packages. After the experiments, parameter estimation was performed on data obtained from both SSADT and CSADT in order to verify that.

6.2. DEGRADATION MODELING FOR CSADT TEST

6.2.1. THEORY OF WIENER PROCESS

The modified Wiener process $\{X(t), t \geq 0\}$ was defined as following expression [30, 44]:

$$M_1 : X(t) = X(0) + \int_0^t \eta(t;\theta)dt + \sigma_B B(t) \tag{6.1}$$

where $\eta(t)$ is the drift rate, σ_B is the diffusion coefficient, and $B(t)$ is the standard Brownian motion. Generally, the Wiener process is characterized by three basic properties as below:

(P1) The increment $\Delta X(t) = X(t+\Delta t) - X(t)$ is independent of $X(t)$, which means that if $0 \leq s_1 \leq t_1 \leq s_2 \leq t_2$, then $X(t_1) - X(s_1)$ and $X(t_2) - X(s_2)$ are independent random variables, and the similar condition holds for n increments.

(P2) $\Delta X(t) \sim N(\int_s^{s+t} \eta(t;\theta)dt, \sigma_B^2 t)$. Where $N(\int_s^{s+t} \eta(t;\theta)dt, \sigma_B^2 t)$ denotes the normal distribution with expected value $\int_s^{s+t} \eta(\tau;\theta)d\tau$, and variance $\sigma_B^2 t$.

(P3) According to (P2), if $s = 0$, $X(t) \sim N(\int_0^t \eta(t;\theta)dt, \sigma_B^2 t)$.

For this model, Si *et al.* [27] obtained the closed form of the analytical approximation to the distribution of the first hitting time of a threshold level C_0 by a time-space transformation. Under a mild assumption, the authors gave a probability distribution function (PDF) as follows:

$$f_T(t) = \frac{1}{\sqrt{2\pi t}}\left(\frac{S_B(t)}{t} + \frac{1}{\sigma_B}\eta(t;\theta)\right)\exp\left(-\frac{S_B^2(t)}{2t}\right) \tag{6.2}$$

where $S_B(t) = \frac{1}{\sigma_B}(C_0 - \int_0^t \eta(\tau;\theta)d\tau)$. As a special case, if $\int_0^t \eta(t;0)dt = \eta t$, $X(t)$ becomes the Wiener process with a constant drift, which is denoted as M_0, i.e.,

$$M_0 : X(t) = X(0) + \eta t + \sigma_B B(t) \tag{6.3}$$

In this case, the first hitting time to a critical threshold C_0, follows an inverse Gaussian distribution $IG(t|\mu,\lambda)$ with a PDF given by [45]:

$$f_T(t) = \sqrt{\frac{\lambda}{2\pi t^3}} \exp\left\{-\frac{\lambda}{2\mu^2}\frac{(t-\mu)^2}{t}\right\} \tag{6.4}$$

where $t>0$, $\mu = C_0/\eta > 0, \lambda = C_0^2/\sigma_B^2$.

6.2.2. MODELING FOR CSADT TEST

The parameter estimation of both the models M_0 and M_1 was performed according to the aforementioned properties of the Wiener process. Assume that X_{ijk} was the j^{th} degradation readout of the i^{th} unit of the samples under the k^{th} stress level. For any $0 \le t_j < t_{j+1}, j = 1,\ldots,m_k-1$, we have independent but not identical random variables:

$$\Delta X_{ijk} = X_{i(j+1)k} - X_{ijk} \sim N\left(\int_{t_j}^{t_{j+1}} \eta_k(t;\theta)dt, \sigma_B^2(t_{j+1}-t_j)\right) \tag{6.5}$$

$$k = 1,\ldots,n; j = 1,\ldots,m_k-1; i = 1,\ldots,l_k.$$

According to Eq. (6.5), the likelihood function was given by Liao *et al.* [20]:

$$\begin{aligned} L(\theta) = &\prod_{k=1}^{n}\prod_{i=1}^{l_k}\prod_{j=1}^{m_k-1} \frac{1}{\sqrt{2\pi\sigma_B^2(t_{j+1}-t_j)}} \\ &\cdot\exp\left(-\frac{\left(\left(x_{i(j+1)k}-x_{ijk}\right)-\int_{t_j}^{t_{j+1}}\eta_k(t;\theta)dt\right)^2}{2\sigma_B^2\left(t_{j+1}-t_j\right)}\right) \end{aligned} \tag{6.6}$$

The likelihood function in Eq. (6.6) considers only the independent increment properties of the Wiener process. This method does not make full use of the information, thus resulting in inaccurate estimation. In order to obtain sufficient estimation accuracy, we proposed an estimation method which combines both the property (P2) and (P3) into the likelihood function. By using this method, our likelihood function indicated a much faster convergence and higher estimation accuracy compared to Eq. (6.6). First, for any $0 < t_p < \ldots < t_q < \ldots < t_{m_k}, p = 2,\ldots,m_k-1, q = 3,\ldots,m_k; p < q$,we have

dependent random variables:

$$\begin{aligned} X_{ipk}(t_p) &\sim N\left(\int_0^{t_p} \eta_k(t;\theta)dt, \sigma_B^2 t_p\right) \\ X_{iqk}(t_q) &\sim N\left(\int_0^{t_q} \eta_k(t;\theta)dt, \sigma_B^2 t_q\right) \end{aligned} \tag{6.7}$$

For simplicity, we assumed the dependency between t_p and t_q was negligible. With this assumption, the likelihood function was presented as

$$\begin{aligned} L(\theta) = \prod_{k=1}^{n}\prod_{i=1}^{l_k}\prod_{p=1}^{m_k-1} & \frac{1}{\sqrt{2\pi\sigma_B^2 t_{p+1}(t_{p+1}-t_p)}} \\ & \cdot \exp\left(-\frac{\left(\left(x_{i(p+1)k}\right) - \int_0^{t_{p+1}} \eta_k(t;\theta)dt\right)^2}{2\sigma_B^2\left(t_{p+1}\right)}\right) \\ & \cdot \exp\left(-\frac{\left(\left(x_{i(p+1)k} - x_{ipk}\right) - \int_{t_p}^{t_{p+1}} \eta_k(t;\theta)dt\right)^2}{2\sigma_B^2\left(t_{p+1}-t_p\right)}\right) \end{aligned} \tag{6.8}$$

We would not try to provide a mathematical proof on the feasibility of this likelihood function, but only give a comparison of the results estimated by Eq. (6.6) and Eq. (6.8), which will be presented in section 6.2.5.

6.2.3. MODELING OF BIVARIATE DEGRADATION PROCESS

According to Sklar's theorem [46], if $H(x_1, x_2)$ is a joint distribution with margins $G_1(x_1)$ and $G_2(x_2)$, then there exists a copula C, such that for all (x_1, x_2)in the defined range,

$$H(x_1, x_2) = C\left(G_1(x_1), G(x_2)\right). \tag{6.9}$$

To solve Eq. (6.9), the most widely used copula is the Frank copula, which is a symmetric copula (for bivariate data) given by

$$C_\alpha(u,v) = \frac{1}{\alpha}\ln\left\{1 + \frac{[\exp(-\alpha u)-1]\cdot[\exp(-\alpha v)-1]}{\exp(-\alpha)-1}\right\}$$

with the corresponding density as

$$c_\alpha(u,v) = \frac{\alpha[1-\exp(-\alpha)]\cdot\exp[-\alpha(u+v)]}{\left\{1-\exp(-\alpha)-[1-\exp(-\alpha u)]\cdot[1-\exp(-\alpha v)]\right\}^2} \tag{6.10}$$

Assume that there exist two performance characteristics (PCs) governed by the Wiener

process at each stress level and, X_{ijk} and Y_{ijk} were the j^{th} degradation readouts of the two PCs (lumen degradation and color shift in this paper) of the i^{th} unit of the samples under the k^{th} stress level, then according to expression Eq. (6.5), we have

$$\begin{aligned}\Delta X_{ijk} = X_{i(j+1)k} - X_{ijk} \sim N\left(\int_{t_j}^{t_{j+1}} \eta_k(t;\theta)dt, \sigma_X^2(t_{j+1}-t_j)\right)\\ \Delta Y_{ijk} = Y_{i(j+1)k} - Y_{ijk} \sim N\left(\int_{t_j}^{t_{j+1}} \eta_k(t;\theta)dt, \sigma_Y^2(t_{j+1}-t_j)\right)\end{aligned} \tag{6.11}$$

Consider the joint distribution of ΔX_{ijk} and ΔY_{ijk} as

$$\begin{aligned}&H(\Delta X_{ijk}, \Delta Y_{ijk})\\ &= C\left[\Phi\left(\frac{\Delta x_{ijk} - \int_{t_j}^{t_{j+1}} \eta_k(t;\theta)dt}{\sigma_X\sqrt{t_{j+1}-t_j}}\right), \Phi\left(\frac{\Delta y_{ijk} - \int_{t_j}^{t_{j+1}} \beta_k(t;\theta)dt}{\sigma_Y\sqrt{t_{j+1}-t_j}}\right)\right]\end{aligned} \tag{6.12}$$

Similar to Eq. (6.8), the likelihood function is then given by:

$$\begin{aligned}L(\theta) = &\prod_{k=1}^{n}\prod_{i=1}^{l_k}\prod_{j=1}^{m_k-1}\\ &c\left[\Phi\left(\frac{\Delta x_{ijk} - \int_{t_j}^{t_{j+1}} \eta_k(t;\theta)dt}{\sigma_X\sqrt{t_{j+1}-t_j}}\right), \Phi\left(\frac{\Delta y_{ijk} - \int_{t_j}^{t_{j+1}} \beta_k(t;\theta)dt}{\sigma_Y\sqrt{t_{j+1}-t_j}}\right)\right]\\ &\cdot\phi\left(\frac{\Delta x_{ijk} - \int_{t_j}^{t_{j+1}} \eta_k(t;\theta)dt}{\sigma_X\sqrt{t_{j+1}-t_j}}\right)\cdot\phi\left(\frac{\Delta y_{ijk} - \int_{t_j}^{t_{j+1}} \beta_k(t;\theta)dt}{\sigma_Y\sqrt{t_{j+1}-t_j}}\right)\\ &\cdot\phi\left(\frac{x_{ijk} - \int_{0}^{t_{j+1}} \eta_k(t;\theta)dt}{\sigma_X\sqrt{t_{j+1}}}\right)\cdot\phi\left(\frac{y_{ijk} - \int_{0}^{t_{j+1}} \beta_k(t;\theta)dt}{\sigma_Y\sqrt{t_{j+1}}}\right)\end{aligned} \tag{6.13}$$

Let C_1 and C_2 be the threshold values of the two PCs, the reliability function under the use stress S_u is

$$R(t) = P\left\{\sup_{s<t} X(s|S_u) \le C_1, \sup_{s<t} Y(s|S_u) \le C_2\right\} \tag{6.14}$$

When σ_X and σ_Y is small, Eq. (6.14) can be approximated by [47]:

$$\begin{aligned}R(t|S_u) &= P\{X(t|S_u) \le C_1, Y(t|S_u) \le C_2\}\\ &= C(R_X(t|S_u), R_Y(t|S_u)\end{aligned} \tag{6.15}$$

where $R_X(t|S_u) = P\{X(t|S_u) \le C_1\}$ and $R_Y(t|S_u) = P\{Y(t|S_u) \le C_1\}$.

Finally, the culmulative distribution function (CDF) of the first hitting time of the threshold levels C_1 and C_2 is obtained as

$$F_T(t|S_u) = 1 - R(t|S_u) \tag{6.16}$$

6.2.4. EXPERIMENTS

The LED device used for the ageing tests was one kind of commercially available mid-power white-light LED packages – MP-3030-EMC LED packages (with 2 blue chips connected in series) with a correlated color temperature (CCT) of 2700 K. As indicated in Fig. 6.1, the mid-power LED packages are composed of four components: blue die, lead-frames, phosphor-dispensing silicone and package house. More specifically, 1 piece of 0.6 mm^2 area blue die was mounted onto the lead-frame by die attach, and gold wires were bonded to connect the blue die to lead-frames. After wire bonding, silicone mixed with phosphors was dispersed into the package house to convert the blue lights (with the emission wavelength in the range of 450 nm – 470 nm) to green and red lights. Finally, the specified CCT was achieved by carefully tuning the amount of blue, green and red lights.

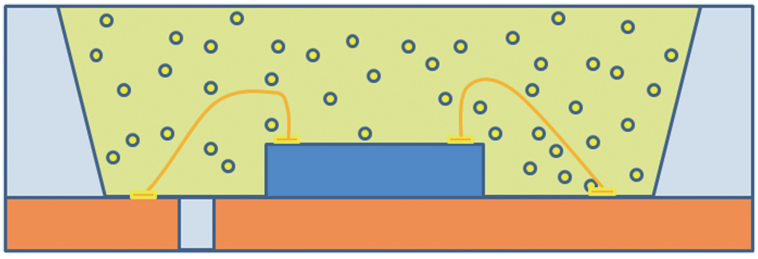

Figure 6.1: The structure of the aged LED packages

At first, the LED packages were assembled onto a metal-core printed circuit (MCPCB) with the dimension of 13 cm×13 cm. Then the MCPCB was attached on a heat sink by using thermal glues and fastened by 5 screws. After that, the test samples were placed into 3 climate chambers respectively depending on the test conditions. In details, the stress conditions were listed as in Table 6.1.

The samples were taken out of the climate chambers for optical measurement at a series of predefined time points and then back to the chamber for further ageing. After finishing all ageing tests, all collected lumen data were normalized to a value of 100% at 0 hour for each individual sample tested, and the color shift was calculated according to the CIE 1976 color space. These data were then used for lifetime estimation based on

Table 6.1: Stress conditions for LED packages

Chmaber	Temperature (°C)	Relative Humidity	Current (mA)	Sample Size (pieces)
WHTOL 85 °C/90%RH	85	90%	160	20
WHTOL 95 °C/45%RH	95	45%	160	20
WHTOL 95 °C/95%RH	95	95%	160	20

the aforementioned Wiener process models.

6.2.5. RESULTS AND DISCUSSION

DATA ANALYSIS

The lumen maintenance and color shift were presented in Fig. 6.2 and Fig. 6.3. Apparently it was found that the lumen maintenance decreases exponentially, and the color shift increases linearly after a sharp jump. In this paper, we employed the exponential degradation model to describe the lumen maintenance as it was widely used and verified by researchers [17, 48–50]. The model was written as follows:

$$\Phi(t;S_k) = \Phi \cdot \exp(-\alpha_k t) \tag{6.17}$$

where $\Phi(t;S_k)$ is the normalized optical outputs of LED devices aged by the k^{th} stress condition at time t, Φ_k is the projected initial constant, and α_k is the decay rate constant which is related to ageing stress levels.

Though many results were reported on the modeling of color shift, there is no specific physic model for color shift of LED devices [51–53]. From the viewpoint of statistics, Fan *et al.* [54] proposed a nonlinear dual-exponential model to describe the chromaticity state shift process. The dual-exponential model, however, was too complex to extrapolate the relationship between degradation data and stress level. On the other hand, Koh *et al.* [55] demonstrated that a linear model could be feasible for the color shift of LED devices by analyzing both the experiment and simulation data. As shown in Fig. 6.3, the color shift expressed by $\Delta u'v'$, is nonlinear if we include the color shift calculated from the first readout, because there is a sharp jump at this point. This phenomenon is probably due to early degradation during ageing tests. The early degradation been extensively observed in mid-power LED packages. However, the rest readouts show very good linear trend. From this point of view, it is reasonable to describe color shift as linear degradation. Therefore, by excluding the early degradation from the measured color

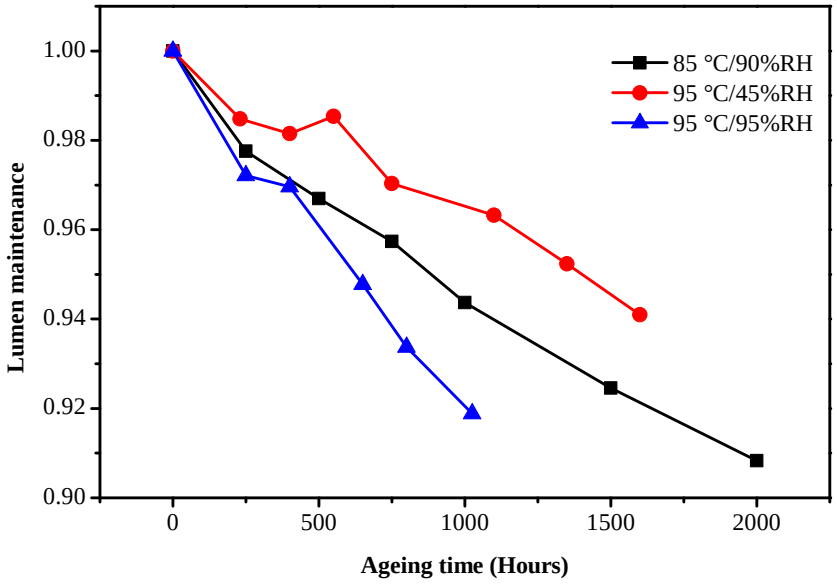

Figure 6.2: Lumen maintenance of the stressed LEDs

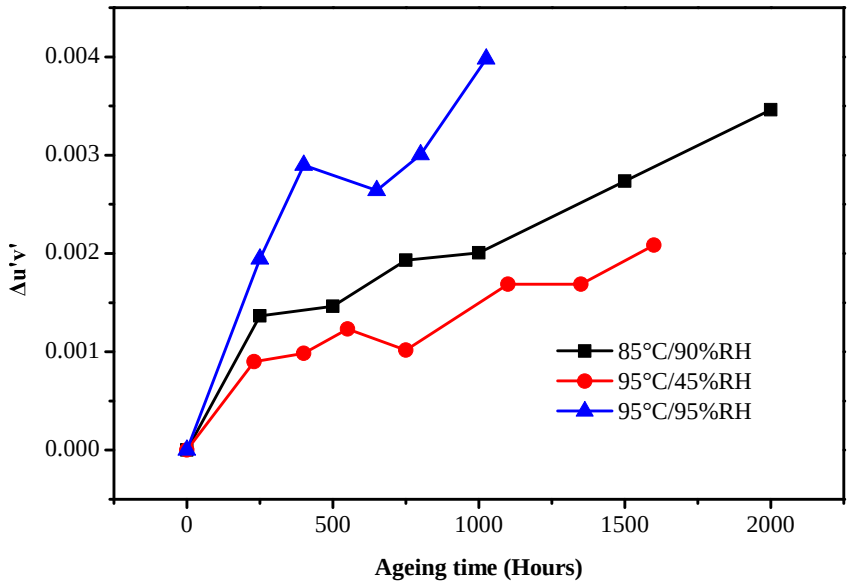

Figure 6.3: Color shift of the stressed LEDs

shift, the model was presented as follows:

$$\Delta u'v'(t;T_k) = A_k + B_k t \tag{6.18}$$

where $\Delta u'v'(t;T_k)$ is the color shift of LED devices aged at the k^{th} stress condition at time t, A_k is the projected initial, and B_k is the decay rate constant which is related to ageing stress levels.

After determining the degradation models, the unknown parameters were estimated by means of the modified Wiener process, as will be presented in coming paragraphs.

PARAMETER ESTIMATION

According to the analysis above, M_1 and M_0 was applied to describe the degradation behavior of lumen degradation and color shift respectively.

Let $Y(0) = \Phi_k$, and $\int_0^t \eta(t;\theta)dt = \Phi_k \exp(-\alpha t)$, then substituting them into Eq. (6.1), the Wiener process of lumen degradation was expressed as:

$$\Phi(t;S_k) = \Phi_k \exp(-\alpha_k t) + \sigma_Y B_Y(t) \tag{6.19}$$

Similar to the lumen maintenance, let $x(0) = A_k$, and $\int_0^t \eta(t;\theta)dt = B_k t$, then substituting them into Eq. (6.1), the Wiener process of color shift degradation was expressed as:

$$\Delta u'v'(t;T_k) = A_k + B_k t + \sigma_X B_X(t) \tag{6.20}$$

The parameter α_k and B_k are assumed to be dependent of the stress levels, such as temperature and humidity. Here, the Hallberg-Peck's model is used to describe the effect of temperature and humidity combined on LED degradation as follows [56]:

$$\begin{aligned} \alpha_k &= \alpha_0 \exp\left[\left(\frac{-E_{a\_lumen}}{k_b}\right)\left(\frac{1}{T_k} - \frac{1}{T_0}\right)\right]\left(\frac{RH_k}{RH_0}\right)^{n\_lumen} \\ B_k &= B_0 \exp\left[\left(\frac{-E_{a\_color}}{k_b}\right)\left(\frac{1}{T_k} - \frac{1}{T_0}\right)\right]\left(\frac{RH_k}{RH_0}\right)^{n\_color} \end{aligned} \tag{6.21}$$

where RH_k and T_k are the relative humidity and temperature at testing condition respectively, and RH_0 and T_0 is the relative humidity and temperature at usage condition, E_{a_lumen} and E_{a_color} n_lumen are the activation energies, and n_color are the humidity factors, k_b is the Boltzmann constant. In this chapter, $k = 1,2,3$, corresponding to WHTOL 85 °C/90%RH, WHTOL 95 °C/45%RH and WHTOL 95 °C/95%RH.

For simplicity, we assumed the diffusion coefficient σ_X and σ_Y are independent of the stress levels. Then the unknown parameters Φ_k, A_k, E_{a_lumen}, E_{a_color}, n_lumen,

$n_{\_color}$, σ_X and σ_Y were estimated according to the likelihood function Eq. (6.8). The parameters including the copula constant α were also estimated according to the likelihood function Eq. (6.13). Bayesian Markov chain Monte Carlo simulation (MCMC) was performed because the model in such a situation is very complicated and analytically intractable and becomes cumbersome. More details about the algorithm can be referred to [57]. After 150,000 iterations, all parameters became convergent, as the Monte Carlo error (MC error) for each parameter of interest is less than about 5% of the sample standard deviation (Std) [57]. Similar results were obtained from both methods, as could be seen in Table 6.2 and Table 6.3.

Table 6.2: Parameter estimation results without copula

Parameter	Mean	Std	MC error	2.5%	Median	97.5%
Φ_1	0.9898	0.001116	7.4E-06	0.9876	0.9898	0.9919
Φ_2	0.9959	0.001013	8.61E-06	0.9939	0.9959	0.9979
Φ_3	0.9957	0.00124	9.05E-06	0.9932	0.9957	0.9981
E_{a_lumen}	0.5469	0.04147	0.000443	0.4658	0.5469	0.6289
$n_{\_lumen}$	1.107	0.06169	0.000814	0.9877	1.106	1.229
α_0	2.15E-05	1.09E-06	1.57E-08	1.94E-05	2.15E-05	2.37E-05
σ_Y	0.000345	9.16E-06	2.32E-08	0.000328	0.000345	0.000364
A_1	0.000839	8.32E-05	5.38E-07	0.000676	0.000839	0.001002
A_2	0.000576	7.63E-05	7.87E-07	0.000426	0.000576	0.000726
A_3	0.001055	9.31E-05	7.87E-07	0.000873	0.001055	0.001238
E_{a_color}	0.8235	0.08751	0.000987	0.6544	0.8226	0.9976
$n_{\_color}$	1.519	0.1448	0.002329	1.247	1.515	1.817
B_0	4.99E-07	5.93E-08	9.74E-10	3.9E-07	4.97E-07	6.22E-07
σ_X	2.63E-05	7.01E-07	1.77E-09	2.5E-05	2.63E-05	2.77E-05

Fig. 6.4 and Fig. 6.5 show the fitted models of LEDs stressed under WHTOL 85 °C/90%RH. For comparison, the scatter plot of the measured data, as well as the degradation models fitted by both the likelihood function Eq. (6.6) and Eq. (6.8), were plotted together. Obviously the model fitted by Eq. (6.6) seriously deviates from the measured data while the one fitted by Eq. (6.8) matches the data very well. The results demonstrate that significant improvements of the estimation accuracy have been obtained by using the likelihood function in Eq. (6.8). The same results were also obtained in WHTOL 95 °C/45%RH and WHTOL 95 °C/95%RH. The results are not presented here due to content limitation.

Fig. 6.6 shows the lifetime plots which are fitted by both the modified Wiener process and the Wiener process (logarithm transformation was performed to linearize the raw data prior to MCMC simulation) for LEDs stressed under WHTOL 85 °C/90%RH. It is found that both models show very similar results, indicating the feasibility of the

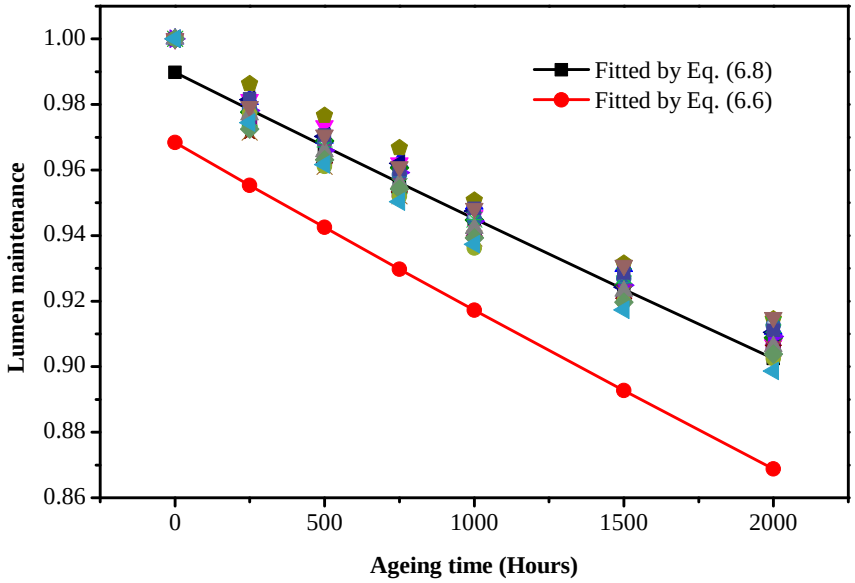

Figure 6.4: Fitted lumen degradation model by likelihood function Eq. (6.6) and Eq. (6.8)

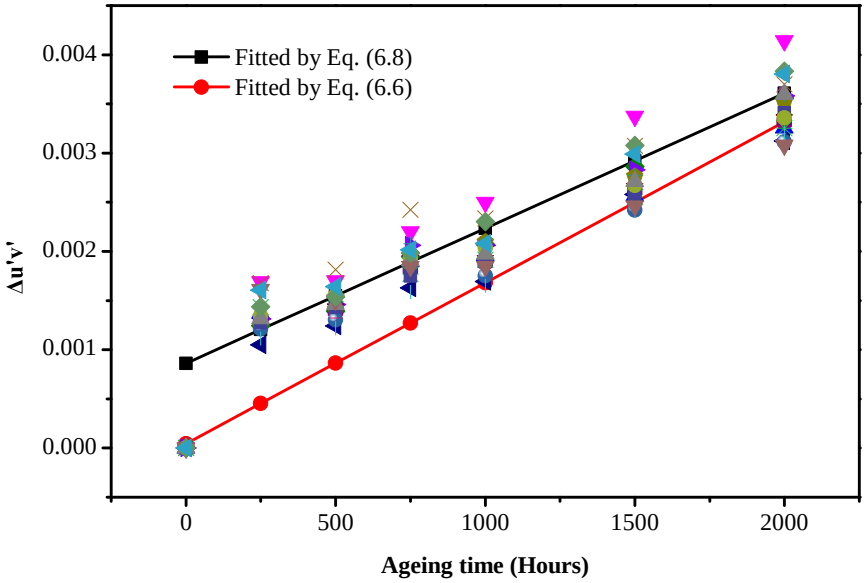

Figure 6.5: Fitted color shift model by likelihood function Eq. (6.6) and Eq. (6.8)

Table 6.3: Parameter estimation results with copula

Parameter	Mean	Std	MC error	2.50%	Median	97.50%
Φ_1	0.9898	0.001116	7.68E-06	0.9876	0.9898	0.9919
Φ_2	0.9959	0.001018	9.83E-06	0.9939	0.9959	0.9979
Φ_3	0.9956	0.001246	9.79E-06	0.9932	0.9956	0.9981
E_{a_lumen}	0.5467	0.04143	0.000461	0.4663	0.5465	0.6286
$n_{\_lumen}$	1.105	0.06263	0.000921	0.9844	1.104	1.229
α_0	2.15E-05	1.10E-06	1.72E-08	1.94E-05	2.15E-05	2.37E-05
σ_Y	0.000345	9.24E-06	2.53E-08	0.000327	0.000345	0.000364
A_1	0.000844	8.33E-05	6.22E-07	0.000681	0.000844	0.001008
A_2	0.000579	7.68E-05	8.79E-07	0.000428	0.000579	0.00073
A_3	0.001052	9.25E-05	6.54E-07	0.00087	0.001052	0.001234
E_{a_color}	0.8321	0.08831	0.000973	0.6635	0.8305	1.01
$n_{\_color}$	1.528	0.1465	0.002395	1.257	1.523	1.834
B_0	4.93E-07	5.94E-08	1.01E-09	3.82E-07	4.91E-07	6.15E-07
σ_X	2.63E-05	7.03E-07	1.85E-09	2.49E-05	2.62E-05	2.77E-05
α	-0.1442	0.3203	0.000908	-0.7737	-0.1435	0.4806

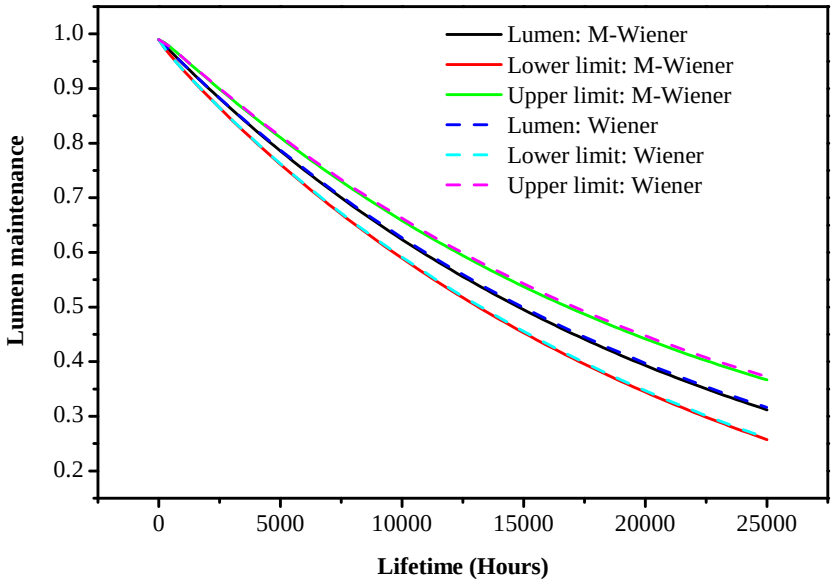

Figure 6.6: Lumen degradation models fitted by using both the modified Wiener process and the Wiener process

modified Wiener process. It should be noticed that, although both the Wiener process and the modified Wiener process show very closed results in describing the exponential lumen degradation of the LED packages, the Wiener process needs dada linearization

prior to parameter estimation, while the modified Wiener process does not need this type of data transformation. This advantage extends the applications of the modified Wiener process to the non-linear degradation behaviors for which the raw data cannot be linearized by any type of data transformation.

LIFETIME PREDICTION AT USAGE CONDITION

The usage condition was assumed to be as $RH_0 = 45\%$, and $T_0 = 85$ °C. Referring to the IES standard TM-21-11, the projected initial Φ_0 and A_0 in Eq. (6.19) and Eq. (6.20) were calculated as

$$\Phi_0 = \sqrt{\Phi_1 \Phi_2}, A_0 = (A_1 + A_2)/2 \tag{6.22}$$

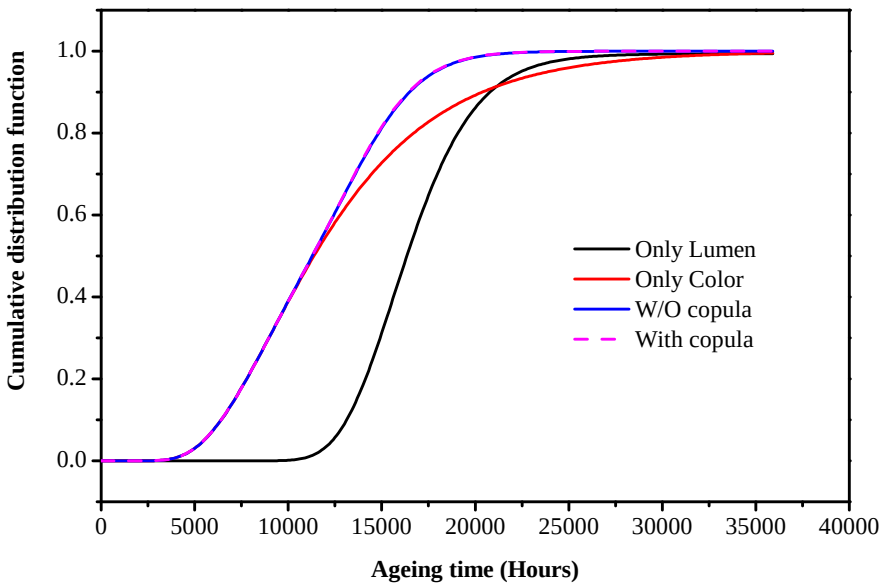

Figure 6.7: The cumulative failure function of LED devices by different methods

The rest unknown parameters in Eq. (6.19) and Eq. (6.20) could be found in Table 6.2 and Table 6.3. Given the critical thresholds of the lumen maintenance and color shift as $C_1 = 0.7$, $C_2 = 0.007$ [17, 58], the lifetime of the LED devices was then predicted according to Eq. (6.2) and Eq. (6.4). When only lumen maintenance was considered, the mean time to failure (MTTF) was calculated as 16,569 hours, which was much closed to that calculated by the IES standard TM-21-11, as the lifetime predicted was 17,031 hours according to this standard. Fig. 6.7 shows lifetime predicted corresponding to different combinations of both the lumen decay and color shift. Apparently the color shift first

reaches the critical threshold C_1 before the lumen maintenance decreases to 70% of its initial value. It is also interesting to note that the dependency of lumen maintenance and color shift is not strong, because the cumulative failure functions with and without copula α are almost the same, indicating that the reliability of LED devices can be modeled by simply considering the lumen maintenance and color shift as two independent variables.

6.3. DEGRADATION MODELING FOR SSADT TEST

6.3.1. MODELING FOR SSADT TEST

SSADT is a special type of ADT in which stress levels are increased during the test period in a specified discrete sequence. A typical stress pattern is shown in Fig. 6.8.

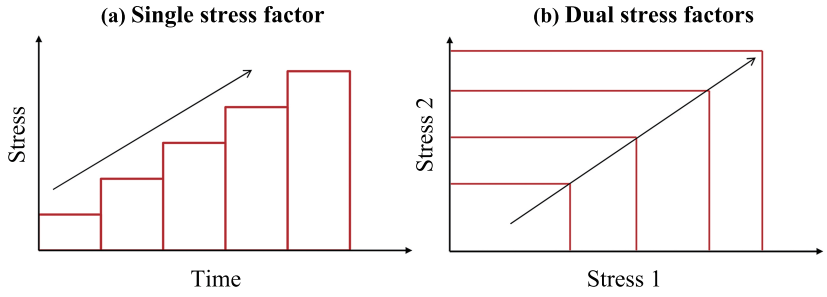

Figure 6.8: Step stress pattern with different stress factors

In this paper, the SSADT has been performed based on following assumptions:

(A1) In all accelerated stress levels, the failure modes and failure mechanisms are the same;

(A2) Testing data measured at each readout point in each stress level follow normal distribution;

(A3) The remaining life of the samples only depend on the currently failed cumulative fraction and current stress, and

(A4) The total degradation $\Delta D_T(t)$ induced by any combination of stress levels is equivalent to the degradation induced by a single stress level S_k, so $\Delta D_T(t_i) = \int_0^{\tau_k} \mu_k(\tau;\theta)d\tau$, where $i = 1,2,\ldots,k$, and τ_k is the equivalent test time under stress S_k.

When designing an SSADT plan, it is important to ensure that the degradation mechanisms are consistent in all stress sequences. In fact, this is one of the radical rules for all accelerated tests, including CASDT and SSADT. In general, this is guaranteed empirically, based on the products' properties and their practical operating conditions. For

instance, an LED package may be recommended to be operated with its junction temperature is lower than 125 °C. On the other hand, a few techniques were also proposed for the judgment of mechanism consistency in accelerated tests. They are - statistic distribution analysis [59], activation energy calculation [60, 61], and independent parameters in degradation models [35, 36].

For assumption (A2), it can be easily verified after all test data are obtained. For assumptions (A3) and (A4), it is actually based on Nelson's equivalent accumulative damage theory [62], which has widely been used in step stress accelerated tests.

Assume N units of samples are tested under a K-step stress accelerated test, and each sample is measured M_k times at the k^{th} stress level. Under each stress level, the measurement point M_k is allowed to be different. Without loss of generality, we assume that the stress series are $S_1, S_2, \ldots, S_k$, t_{k+1} is the time point at which the stress changes from the k^{th} stress level to the $(k+1)^{th}$ stress level. Thus, $t_1 = 0$ and t_{K+1} is the end time of the test.

For a K-step stress accelerated test, define $\Delta D(t; S_k)$ as the lumen degradation of LED package induced by stress S_k after time t. Based on assumption (A4), we have

$$\int_{t_1}^{t} \mu_1(t;\theta)\,dt = \Delta D(t - t_1; S_1), \qquad t_1 = 0 \tag{6.23}$$

$$\int_{\tau_k}^{\tau_k+(t-t_k)} \mu_k(t;\theta)\,dt = \Delta D(t - t_k; S_k), \qquad k = 2,3,\ldots,K. \tag{6.24}$$

From Eq. (6.23) and Eq. (6.24), the total degradation $\Delta D_T(t)$ of an LED package after a K-step stress accelerated test can be obtained as:

$$\Delta D_T(t) = \int_{t_1}^{t_2} \mu_1(t;\theta)\,dt + \int_{\tau_2}^{\tau_2+t_3-t_2} \mu_2(t;\theta)\,dt + \ldots + \int_{\tau_k}^{\tau_k+t-t_K} \mu_k(t;\theta)\,dt \tag{6.25}$$

More specifically, Eq. (6.25) is rewritten as:

$$\Delta D_T(t) = \begin{cases} \int_{t_1}^{t} \mu_1(t;\theta)\,dt, & 0 = t_1 \le t < t_2 \\ \int_0^{\tau_2} \mu_2(t;\theta)\,dt + \int_{\tau_2}^{\tau_2+(t-t_2)} \mu_2(t;\theta)\,dt, & t_2 \le t < t_3 \\ \ldots, & \ldots \\ \int_0^{\tau_k} \mu_k(t;\theta)\,dt + \int_{\tau_k}^{\tau_k+(t-t_k)} \mu_k(t;\theta)\,dt, & t_k \le t < t_{k+1} \\ \ldots, & \ldots \\ \int_0^{\tau_K} \mu_K(t;\theta)\,dt + \int_{\tau_K}^{\tau_K+(t-t_K)} \mu_K(t;\theta)\,dt, & t_K \le t < t_{K+1} \end{cases} \tag{6.26}$$

where

$$\int_0^{\tau_k} \mu_k(t;\theta)dt = \int_{t_1}^{t_2} \mu_1(t;\theta)dt + \ldots + \int_{\tau_2}^{\tau_2+t_3-t_2} \mu_2(t;\theta)dt + \int_{\tau_{k-1}}^{\tau_{k-1}+t_k-t_{k-1}} \mu_{k-1}(t;\theta)dt.$$

Then according to Eq. (6.1), the stochastic process of lumen degradation can be written as:

$$X(t) = \begin{cases} \int_0^t \mu_1(t;\theta)dt + \sigma_1 B(t) & 0 = t_1 \le t < t_2 \\ \int_0^{\tau_2+(t-t_2)} \mu_2(t;\theta)dt + \sigma_2 B(t) & t_2 \le t < t_3 \\ \ldots & \ldots \\ \int_0^{\tau_k+(t-t_k)} \mu_k(t;\theta)dt + \sigma_k B(t) & t_k \le t < t_{k+1} \\ \ldots & \ldots \\ \int_0^{\tau_K+(t-t_K)} \mu_K(t;\theta)dt + \sigma_K B(t) & t_K \le t < t_{K+1} \end{cases} \tag{6.27}$$

6.3.2. PARAMETER ESTIMATION

Assume that X_{ijk} is the j^{th} degradation readout of the i^{th} unit of the samples under the k^{th} stress level. For any $t_k = t_{k,1} < \ldots < t_{k,j} < \ldots \le t_{k+1}, j = 1,\ldots,M_k - 1$, we have independent but not identical random variables:

$$\Delta X_{ijk} = X_{i(j+1)k} - X_{ijk} \sim N\left(\int_{t_j}^{t_{j+1}} \mu_k(t;\theta)dt, \sigma_k^2(t_{j+1}-t_j)\right) \tag{6.28}$$
$$k = 1,\ldots,n; j = 1,\ldots,m_k - 1; i = 1,\ldots,l_k.$$

According to Eq. (6.28), the likelihood function was given by Liao *et al.* [20]:

$$L(\theta) = \prod_{k=1}^{n}\prod_{i=1}^{l_k}\prod_{j=1}^{m_k-1} \frac{1}{\sqrt{2\pi\sigma_k^2(t_{j+1}-t_j)}} \cdot \exp\left(-\frac{\left[\left(x_{i(j+1)k}-x_{ijk}\right) - \int_{t_j}^{t_{j+1}} \mu_k(t;\theta)dt\right]^2}{2\sigma_k^2\left(t_{j+1}-t_j\right)}\right) \tag{6.29}$$

The likelihood function in Eq. (6.29) considers only the independent increment properties of the Wiener process. This method does not make full use of the information, thus resulting in inaccurate estimation. In order to obtain sufficient estimation accuracy, we proposed an estimation method which combines both the property (P2) and (P3) into the likelihood function. This method has been used for parameter estimation for mid-power white-light LED packages which were aged by means of constant

stress accelerated degradation test (CSADT) [63]. Similarly, the method can be also utilized for parameter estimation in step stress accelerated degradation test (SSADT) with a few modifications.

Firstly, for any $t_k = t_{k,1} < t_{k,j} < \ldots < t_{k,q} \leq t_{k+1}, j = 2,\ldots,M_k - 1, q = 2,\ldots,M_k$ and $j < q$, we have dependent random variables:

$$\begin{aligned} X_{ijk}(t_j) &\sim N\left(\int_0^{t_j} \mu_k(t;\theta)dt, \sigma_k^2 t_j\right) \\ X_{iqk}(t_q) &\sim N\left(\int_0^{t_q} \mu_k(t;\theta)dt, \sigma_k^2 t_q\right) \end{aligned} \tag{6.30}$$

For simplicity, we assume the interdependency between $X_{ijk}(t_{k,j})$ and $X_{iqk}(t_{k,q})$ is negligible. With this assumption, the likelihood function is presented as:

$$\begin{aligned} L(\theta) = \prod_{k=1}^{K}\prod_{i=1}^{n_k}\prod_{j=1}^{M_k-1} & \frac{1}{\sqrt{2\pi\sigma_k^2(\tau_k + t_{k,j+1})(t_{k,j+1} - t_{k,j})}} \\ & \cdot \exp\left(-\frac{\left(\left(x_{i(j+1)k}\right) - \int_0^{(\tau_k + t_{j+1})} \mu_k(t;\theta)dt\right)^2}{2\sigma_k^2(\tau_k + t_{j+1})}\right) \\ & \cdot \exp\left(-\frac{\left(\left(x_{i(j+1)k} - x_{ijk}\right) - \int_{t_{k,j}}^{t_{k,j+1}} \mu_k(t;\theta)dt\right)^2}{2\sigma_k^2(t_{k,j+1} - t_{k,j})}\right) \end{aligned} \tag{6.31}$$

The explicit form of $\mu_k(t;\theta)$ is determined by the degradation models specified. For LED devices, it is well known that the lumen degradation can be described as $\Phi(t) = \Phi_0 e^{-\beta t^m}$ [48]. Then, the lumen degradation rate, namely the drift coefficient $\mu_k(t;\theta)$, can be obtained from the derivative of $\Phi(t)$. As a result, the time-dependent drift parameter of the Brownian motion is obtained as follows:

$$\mu_k(t;\theta) = -\beta t^{m-1}\Phi_0 e^{-\beta_k t^m} \tag{6.32}$$

where m is considered to be independent of stress levels, according to the theory of Tseng *et al.* [35]. This parameter is assumed to be 1 according to Ref. [64]. In this chapter, the parameter will not be set as 1, but will be fitted based on the degradation data. The parameter is dependent on the acceleration functions. The most widely used accelerated functions include Arrhenius model, Hallberg-Peck's model, and inverse power law model. These models can be employed for describing the effects of temperature, humidity-temperature, and electrical stress, respectively.

6.3.3. EXPERIMENTS

A 2-step SSADT experiment has been performed to illustrate the feasibility of the SSADT model. The LED packages used for experiments are shown in Fig. 6.9. The LED package was composed of five components: copper-based lead frames, molding compound package house, GaN-based LED chip, silicone/phosphor encapsulant, and gold wires which are used as electrical connections. These LED packages were first mounted onto metal-core printed circuit boards (MCPCBs). Each board contains 20 pieces of LED packages. After initial optical measurement, the samples were stored into a high temperature storage chamber for SSADT. At the first step, the ambient temperature was 130 °C. After ageing for 500 hours, the ambient temperature was switched to 140 °C and held until the end of the experiment. For comparison, 2 groups of LED samples were also separately placed into the high temperature storage chamber for CASDT. No electrical bias was applied during the ageing test. The detailed test conditions are shown in Table 6.4. During the ageing tests, the LED samples were taken out at every 100 hours interval for optical measurement.

Table 6.4: Stress conditions for SSADT and CSADT

Test type	Sample	Sample size (units)	Ambient temperature (°C)	Bias	Ageing duration (Hours)
SSADT	Group 1	20	130	No bias	500
SSADT	Group 1	20	140	No bias	500
CSADT	Group 2	20	130	No bias	500
CSADT	Group 3	20	140	No bias	500

It should be noticed that, in order to shorten the test duration, the ambient temperature is not selected according to maximum junction temperature that the LED manufacturer recommends (recommended maximum junction temperature is less than 125 °C). This implies that the data obtained in our experiments is not feasible for lifetime extrapolation for temperatures lower than 125 °C, because the degradation mechanisms may be different from that obtained from LED packages aged at junction temperatures less than 125 °C. However, our analysis showed that the degradation mechanism is similar between 130 °C and 140 °C, based on the theory proposed by Tseng *et al.* [35, 36]. According to the theory, in the degradation model there exist some constants which indicate consistent degradation mechanisms for LED samples aged at different stress levels. In our model, the constant is parameter as mentioned in the previous paragraph. As a consequence, the data in our experiments can be used for SSADT modeling, as will be discussed in the following paragraph. Furthermore, the data can be also used for

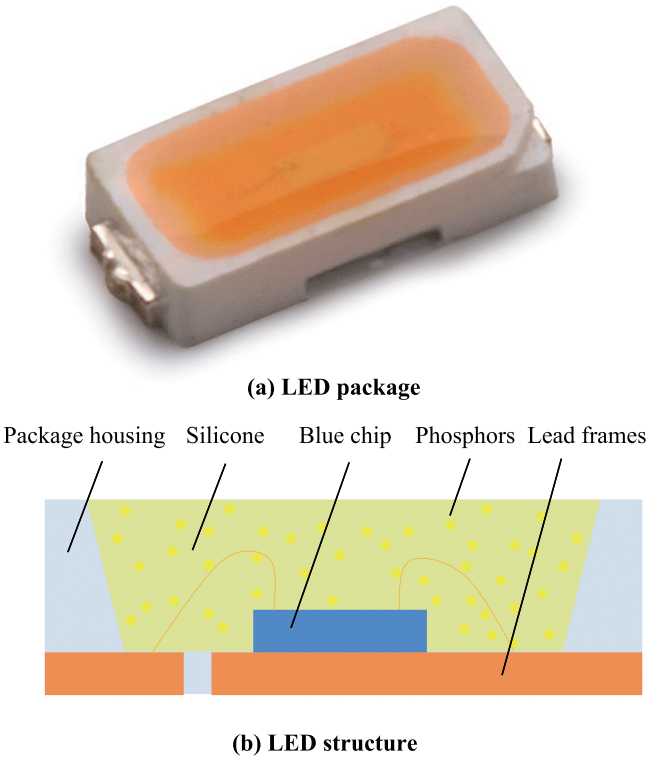

Figure 6.9: A type of white-light LED package and its structure

lifetime extrapolation if the operating temperature is between 130 °C and 140 °C.

6.3.4. RESULTS AND DISCUSSION

After finishing all the tests, the lumen outputs were normalized at 0 hour for each individual sample, as shown in Fig. 6.10(a) and Fig. 6.10(b). It has been found that the lumen degradation could be approximated by the exponential model. For the data obtained from SSADT, according to the analysis method provided in the IES standard [64], the activation energy is calculated as 0.59 eV, which is higher than that reported in [61], where the maximum junctions temperature is lower than 130 °C. However, when we calculate the independent parameter according to model presented in [35, 36]:

$$\Phi(t) = \Phi_0 e^{-\beta t^m} \tag{6.33}$$

It has been found that the values of the independent parameter is calculated as 0.808

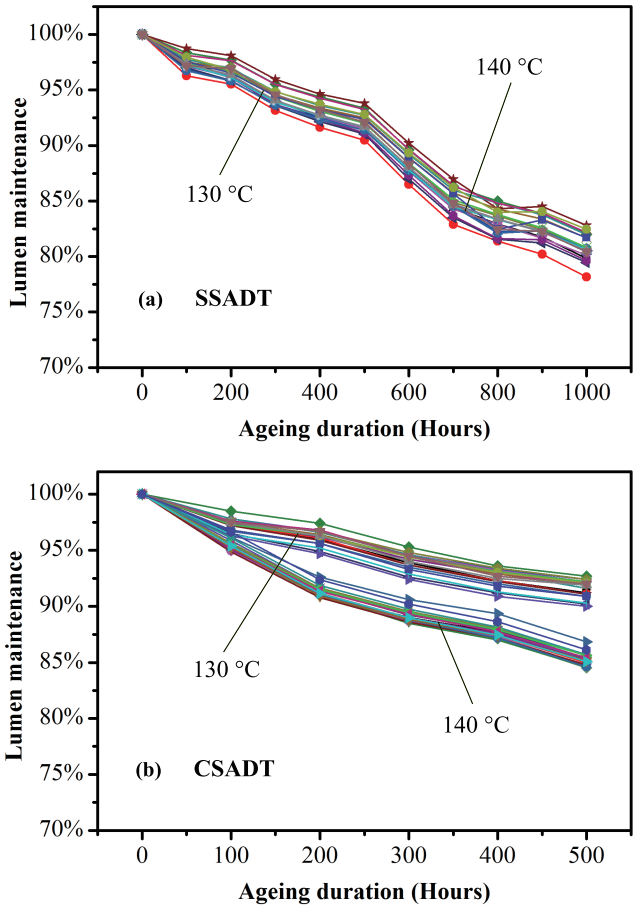

Figure 6.10: Normalized lumen output of LED packages aged by SSADT and CSADT

and 0.619 for both the SSADT data set collected from 0 hour to 500 hours, and data set collected from 500 hours and 1000 hours. The difference is 0.189 between the two independent parameters. According to Ref. [36], the degradation mechanisms can be regarded as consistent during the SSADT test.

The degradation mechanisms were further confirmed by using failure analysis. As can be seen in Fig. 6.11, I-V characteristics show no obvious difference between the fresh samples and aged samples, indicating that the blue dies did not deteriorate during the high temperature storage tests. However, yellowing of the package housing was found on the aged samples, which are stressed under either CSADT or SSADT. Due to longer ageing duration, the samples aged under SSADT show more significant yellow-

ing than those aged under CSADT, as presented in Fig. 6.12. Due to lack of equipments, we could not analyze the degradation of the silicone encapsulant lead frames, and phosphors. However, our previous research already showed very good performance for these two materials [65]. As a result, it was concluded that the major degradation was the yellowing of the package housing.

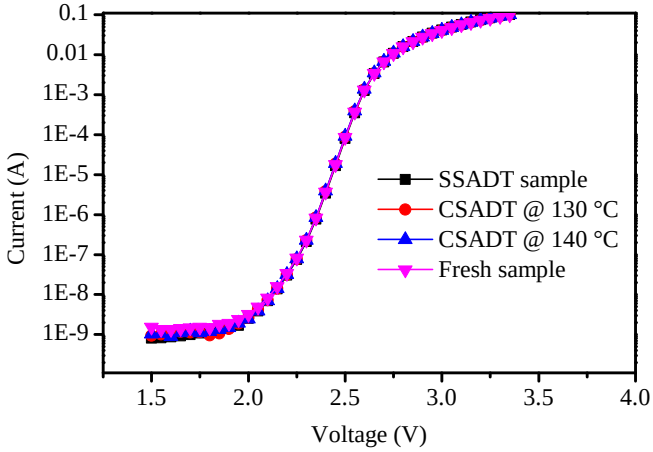

Figure 6.11: $I-V$ characteristics of fresh and aged samples

Normality test was also performed for the degradation data obtained from SSADT test. The analysis was completed by using the commercial statistical analysis code Minitab. A p-value larger than 0.1 will indicate that a data set passes the normality test. As shown in Table 6.5 and Table 6.6, most of the data sets follow normal distributions, indicating that Brownian motion process can be used for the degradation modeling.

Table 6.5: Normality test for normalized lumen output at each readout

Readouts (Hours)	**0**	**100**	**200**	**300**	**400**	**500**
P-value	1	0.523	0.381	0.296	0.402	0.551
Readouts (Hours)	**500**	**600**	**700**	**800**	**900**	**1000**
P-value	0.551	0.678	0.496	0.783	0.231	0.38

As a consequence, the lumen degradation model for the SSADT data can be written

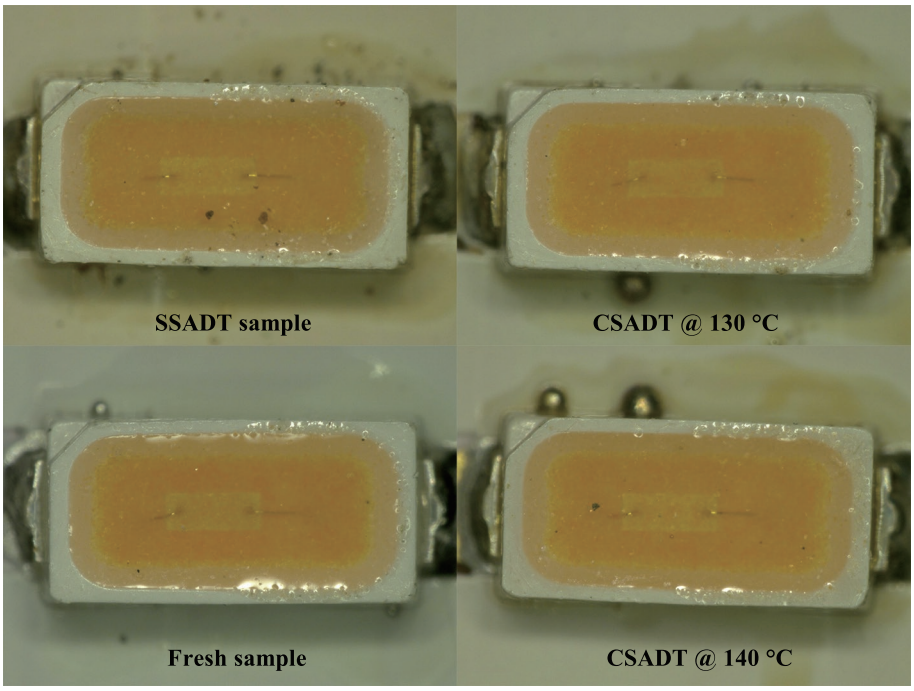

Figure 6.12: Yellowing of the package housing

as in Eq. (6.34):

$$X(t) = \begin{cases} \Phi_{10} \exp\left(-\alpha_1 t^m\right) + \sigma_1 B(t) & T_a = 130\ ^\circ\text{C} \\ \Phi_{20} \exp\left[-500^m \alpha_1 - \alpha_2 (t-500)^m\right] + \sigma_2 B\left(\frac{\alpha_1^{1/m}}{\alpha_2^{1/m}} \cdot 500 + t - 500\right) & T_a = 140\ ^\circ\text{C} \end{cases} \tag{6.34}$$

On the other hand, the lumen degradation model for the CSADT data is written as in Eq. (6.35):

Table 6.6: Normality test for normalized lumen degradation between two adjacent readouts

Readouts (Hours)	**0**	**0-100**	**100-200**	**200-300**	**300-400**	**400-500**
P-value	1	0.523	0.402	0.888	0.461	0.532
Readouts (Hours)	**400-500**	**500-600**	**600-700**	**700-800**	**800-900**	**900-1000**
P-value	0.532	0.38	0.113	0.01	0.005	0.839

$$X(t)=\begin{cases}\Phi_{10}\exp\left(-\alpha_1 t^m\right)+\sigma_1 B(t) & T_a=130\,^{\circ}\mathrm{C}\\ \\ \Phi_{20}\exp\left(-\alpha_2 t^m\right)+\sigma_2 B(t) & T_a=140\,^{\circ}\mathrm{C}\end{cases} \tag{6.35}$$

The unknown parameters in Eq. (6.34) and Eq. (6.35) include Φ_{10}, Φ_{20}, α_1, α_2, σ_1, σ_2, m. Based on Eq. (6.34) and Eq. (6.35), the unknown parameters can be estimated according to the likelihood function in Eq. (6.31). It is found that the likelihood function in Eq. (6.31) is very complicated and analytically intractable. Therefore, Bayesian Markov chain Monte Carlo simulation (MCMC) was performed. More details about the algorithm are referred to Ref. [66]. After 200,000 iterations, all parameters became convergent. The results are shown in Table 6.7 and Table 6.8.

Table 6.7: Parameter estimation results of SSADT

Parameter	mean	standard deviation	MC error	2.50%	median	97.50%
α_1	9.81E-04	1.01E-04	3.84E-06	8.01E-04	9.77E-04	1.20E-03
α_2	1.60E-03	1.60E-04	6.12E-06	1.31E-03	1.59E-03	0.001937
m	0.7128	1.62E-02	6.35E-04	0.6804	0.7126	0.744
Φ_{10}	1.001	0.001469	2.01E-05	0.9983	1.001	1.004
Φ_{20}	0.9967	0.003351	2.33E-05	0.9901	0.9967	1.003
σ_1	5.45E-04	2.78E-05	1.36E-07	4.94E-04	5.44E-04	6.03E-04
σ_2	6.73E-04	3.43E-05	1.35E-07	6.09E-04	6.71E-04	7.44E-04

Table 6.8: Parameter estimation results of CSADT

Parameter	mean	standard deviation	MC error	2.50%	median	97.50%
α_1	8.75E-04	6.21E-05	2.37E-06	7.59E-04	8.73E-04	1.00E-03
α_2	1.59E-03	1.09E-04	4.25E-06	1.39E-03	1.59E-03	1.81E-03
m	7.43E-01	1.09E-02	4.28E-04	7.23E-01	7.43E-01	7.65E-01
Φ_{10}	1.00E+00	1.29E-03	1.88E-05	9.98E-01	1.00E+00	1.00E+00
Φ_{20}	9.99E-01	1.60E-03	2.88E-05	9.96E-01	9.99E-01	1.00E+00
σ_1	4.89E-04	2.49E-05	6.26E-08	4.44E-04	4.88E-04	5.41E-04
σ_2	5.77E-04	2.93E-05	8.73E-08	5.23E-04	5.76E-04	6.38E-04

For comparison, the mean of parameters in Table 6.7 and Table 6.8 were re-arranged as shown in Table 6.9. The error between SSADT and CSADT has been calculated by dividing the parameter difference for each parameter obtained by CSADT. For instance, in Table 6.9, the error of the parameter σ_1 is calculated as $(0.000981-0.000875)\div 0.000875 = 12.11\%$. As shown in Table 6.9, except for parameter the estimated parameters obtained

Table 6.9: Parameter comparison between SSADT and CSADT

Temperature	130 °C				140 °C		
Parameter	α_1	Φ_{10}	σ_1	m	α_2	Φ_{20}	σ_2
SSADT	9.81E-04	1.00E+00	5.45E-04	7.13E-01	1.60E-03	9.97E-01	6.73E-04
CSADT	8.75E-04	1.00E+00	4.89E-04	7.43E-01	1.59E-03	9.99E-01	5.77E-04
Error	12.11%	0.00%	11.40%	-4.12%	0.38%	-0.25%	16.49%

from SSADT data are very close to that obtained from CSADT data, demonstrating the feasibility of our SSADT model. Fig. 6.13 shows the lumen degradation fitted by our SSADT model. The variations given by the SSADT model also match the variations of the experiment data very well. According to Eq. (6.2), the cumulative distribution functions (CDF) were plotted based on the parameters in Table 6.9, which is shown in Fig. 6.14. The mean time to failure (MTTF) calculated by using the data obtained from SSADT and CSADT was also given, as presented in Table 6.10. Both testing methods show similar MTTF at the same storage temperature. The slight difference of the MTTF between both testing methods may be due to the unbalance test duration between CSADT and SSADT. Prolonging the CSADT ageing time to 1000 hours (testing duration is 1000 hours in SSADT) should be performed to minimize the difference.

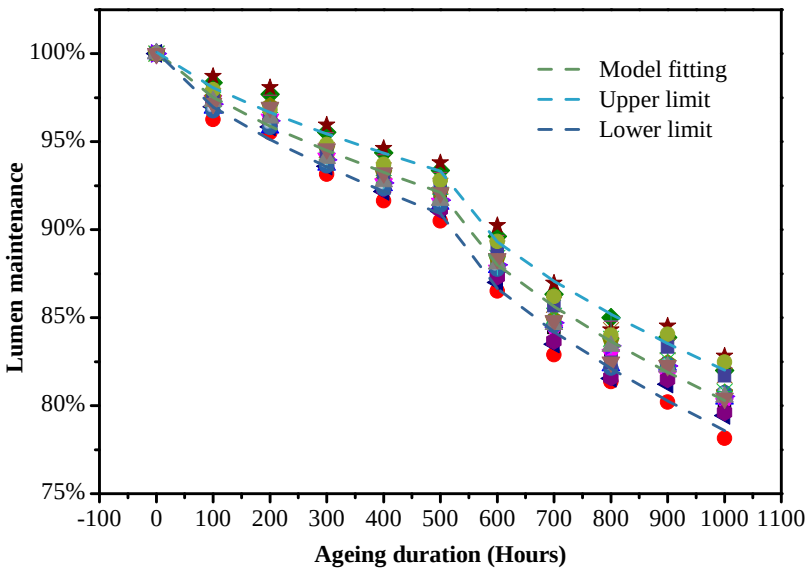

Figure 6.13: Lumen degradation fitted by SSADT model

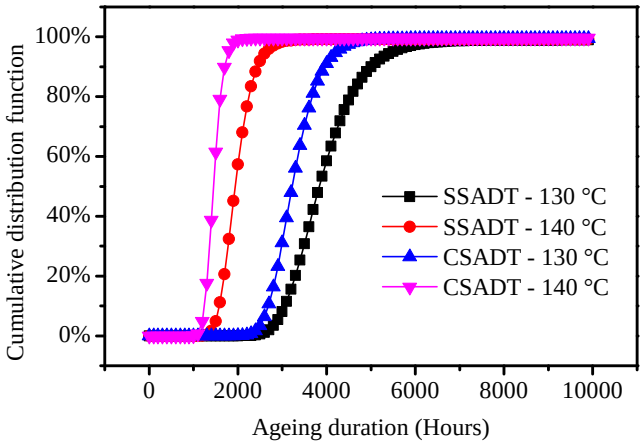

Figure 6.14: The cumulative failure function of LED devices at different stress conditions

Table 6.10: Stress conditions for SSADT and CSADT

Stress condition	**SSADT – 130 °C**	**SSADT – 140 °C**	**CSADT – 130 °C**	**CSADT – 140 °C**
MTTF (Hours)	3893	1962	3257	1458.5

It is worth noticing that, in this section, we utilized LED packages as an example to verify the feasibility of the model. However, this model is not limited to the application of LEDs, it can be also applied to more broad applications, including electronic products, automobiles, aerospace prototypes, etc, as long as the explicit form of $\mu_k(t;\theta)$ is given. The SSADT is especially suitable for reliability tests in which samples are very expensive and rare, or resources are limited.

6.4. SUMMARY

In this chapter, the lifetime prediction was performed by using a modified Wiener process which could be applied to describe the dynamic, random and non-linear degradation of LED devices. Degradation models of both the CSADT and SSADT were established based on the same stochastic process. With the assumption that the dependency between random variables was negligible, a simple but efficient likelihood function was proposed and the accuracy of parameter estimation was improved for both CSADT and SSADT. On the other hand, for degradation data obtained from CSADT, the Frank copula function was applied to describe the dependency between the lumen maintenance

and color shift. However, the cumulative failure function demonstrated that the dependency between them was very weak. Therefore, these two performance characteristics could be simply considered as independent variables, thus simplifying the degradation modeling of the LED devices. Due to complexity of the failure distribution, we could not obtain the interval estimation in this study. However, the Wiener process had provided favorable results, making it an attractive and promising method in degradation modeling of LED devices.

REFERENCES

[1] J. Huang, D. S. Golubović, S. Koh, D. Yang, X. Li, X. Fan, and G. Zhang, *Degradation modeling of mid-power white-light leds by using wiener process,* Optics express **23**, A966 (2015).

[2] J. Huang, D. S. Golubović, S. Koh, D. Yang, X. Li, X. Fan, and G. Zhang, *Lumen degradation modeling of white-light leds in step stress accelerated degradation test,* Reliability Engineering & System Safety **154**, 152 (2016).

[3] L. Liu, J. Yang, and G. Wang, *The investigation of led's reliability through highly accelerated stress testing methods,* in *14th International Conference on Electronic Materials and Packaging (EMAP), 2012* (IEEE) pp. 1–3.

[4] L. Liu, J. Yang, and G. Wang, *The investigation of led's reliability through highly accelerated stress testing methods,* in *14th International Conference on Electronic Materials and Packaging (EMAP), 2012* (IEEE) pp. 1–3.

[5] F.-K. Wang and Y.-C. Lu, *Useful lifetime analysis for high-power white leds,* Microelectronics Reliability **54**, 1307 (2014).

[6] C. M. Tan and P. Singh, *Time evolution degradation physics in high power white leds under high temperature-humidity conditions,* IEEE Transactions on Device and Materials Reliability **14**, 742 (2014).

[7] B.-M. Song and B. Han, *Analytical/experimental hybrid approach based on spectral power distribution for quantitative degradation analysis of phosphor converted led,* IEEE Transactions on Device and Materials Reliability **14**, 365 (2014).

[8] S. Chan, W. Hong, K. Kim, Y. Yoon, J. Han, and J. S. Jang, *Accelerated life test of high power white light emitting diodes based on package failure mechanisms,* Microelectronics Reliability **51**, 1806 (2011).

[9] M. Meneghini, L.-R. Trevisanello, G. Meneghesso, and E. Zanoni, *A review on the reliability of gan-based leds,* IEEE Transactions on Device and Materials Reliability **8**, 323 (2008).

[10] A. Torikai and H. Hasegawa, *Accelerated photodegradation of poly (vinyl chloride),* Polymer Degradation and Stability **63**, 441 (1999).

[11] H.-T. Li, C.-W. Hsu, and K.-C. Chen, *The study of thermal properties and thermal resistant behaviors of siloxane-modified led transparent encapsulant,* in *International Microsystems, Packaging, Assembly and Circuits Technology, 2007 (IMPACT 2007)* (IEEE) pp. 246–249.

[12] P. McCluskey, K. Mensah, C. O. Connor, F. Lilie, A. Gallo, and J. Fink, *Reliability of commercial plastic encapsulated microelectronics at temperatures from 125 °C to 300 °C,* in *The Third European Conference on High Temperature Electronics, 1999 (HITEN 99)* (IEEE, 1999) pp. 155–162.

[13] P. McCluskey, K. Mensah, C. O'Connor, and A. Gallo, *Reliable use of commercial technology in high temperature environments,* Microelectronics Reliability **40**, 1671 (2000).

[14] R.-J. Xie, N. Hirosaki, N. Kimura, K. Sakuma, and M. Mitomo, *2-phosphor-converted white light-emitting diodes using oxynitride/nitride phosphors,* Applied Physics Letters **90**, 191101 (2007).

[15] W. Nelson, *Analysis of performance-degradation data from accelerated tests,* IEEE Transactions on Reliability **30**, 149 (1981).

[16] C. J. Lu and W. O. Meeker, *Using degradation measures to estimate a time-to-failure distribution,* Technometrics **35**, 161 (1993).

[17] I. E. S. o. N. America, *Projection long term lumen maintenance of led light sources,* (2011).

[18] Y. Wang, Z.-S. Ye, and K.-L. Tsui, *Stochastic evaluation of magnetic head wears in hard disk drives,* IEEE Transactions on Magnetics **50**, 1 (2014).

[19] T.-R. Tsai, C.-W. Lin, Y.-L. Sung, P.-T. Chou, C.-L. Chen, and Y. Lio, *Inference from lumen degradation data under wiener diffusion process,* IEEE Transactions on Reliability **61**, 710 (2012).

[20] C.-M. Liao and S.-T. Tseng, *Optimal design for step-stress accelerated degradation tests,* IEEE Transactions on Reliability **55**, 59 (2006).

[21] C.-Y. Peng and S.-T. Tseng, *Progressive-stress accelerated degradation test for highly-reliable products,* IEEE Transactions on Reliability **59**, 30 (2010).

[22] A. Molini, P. Talkner, G. G. Katul, and A. Porporato, *First passage time statistics of brownian motion with purely time dependent drift and diffusion,* Physica a-Statistical Mechanics and Its Applications **390**, 1841 (2011), times Cited: 5 Katul, Gabriel/A-7210-2008 5.

[23] R. Harman and F. Stulajter, *Optimality of equidistant sampling designs for the brownian motion with a quadratic drift,* Journal of Statistical Planning and Inference **141**, 2750 (2011), times Cited: 1 1.

[24] E. Urdapilleta, *Series solution to the first-passage-time problem of a brownian motion with an exponential time-dependent drift,* Journal of Physics a-Mathematical and Theoretical **45** (2012), 10.1088/1751-8113/45/18/185001, times Cited: 0 0.

[25] J. Li, *Some limit results for probabilities estimates of brownian motion with polynomial drift,* Indian Journal of Pure & Applied Mathematics **41**, 425 (2010), times Cited: 0 0.

[26] E. Urdapilleta, *Survival probability and first-passage-time statistics of a wiener process driven by an exponential time-dependent drift,* Physical Review E **83** (2011), 10.1103/PhysRevE.83.021102, times Cited: 2 1 2.

[27] X.-S. Si, W. Wang, C.-H. Hu, D.-H. Zhou, and M. G. Pecht, *Remaining useful life estimation based on a nonlinear diffusion degradation process,* IEEE Transactions on Reliability **61**, 50 (2012).

[28] X.-S. Si, W. Wang, C.-H. Hu, M.-Y. Chen, and D.-H. Zhou, *A wiener-process-based degradation model with a recursive filter algorithm for remaining useful life estimation,* Mechanical Systems and Signal Processing **35**, 219 (2013).

[29] W. Zhao-Qiang, H. Chang-Hua, W. Wenbin, and S. Xiao-Sheng, *An additive wiener process-based prognostic model for hybrid deteriorating systems,* IEEE Transactions on Reliability **63**, 208 (2014).

[30] X. Wang, N. Balakrishnan, and B. Guo, *Residual life estimation based on a generalized wiener degradation process,* Reliability Engineering & System Safety **124**, 13 (2014).

[31] X. Wang, B. Guo, and Z. Cheng, *Residual life estimation based on bivariate wiener degradation process with time-scale transformations,* Journal of Statistical Computation and Simulation **84**, 545 (2014).

[32] Y. Wang, Z.-S. Ye, and K.-L. Tsui, *Stochastic evaluation of magnetic head wears in hard disk drives,* IEEE Transactions on Magnetics **50**, 1 (2014).

[33] H. Zeyi, X. Zhengguo, W. Wenhai, and S. Youxian, *Remaining useful life prediction for a nonlinear heterogeneous wiener process model with an adaptive drift,* IEEE Transactions on Reliability **64**, 687 (2015).

[34] C.-M. Liao and S.-T. Tseng, *Optimal design for step-stress accelerated degradation tests,* IEEE Transactions on Reliability **55**, 59 (2006).

[35] S.-T. Tseng and Z.-C. Wen, *Step-stress accelerated degradation analysis for highly reliable products,* Journal of Quality Technology **32**, 209 (2000).

[36] M. Cai, D. Yang, K. Tian, P. Zhang, X. Chen, L. Liu, and G. Zhang, *Step-stress accelerated testing of high-power led lamps based on subsystem isolation method,* Microelectronics Reliability **55**, 1784 (2015).

[37] M. Cai, D. Yang, S. Koh, C. Yuan, W. Chen, B. Wu, and G. Zhang, *Accelerated testing method of led luminaries,* in *13th International Conference on Thermal, Mechanical and Multi-Physics Simulation and Experiments in Microelectronics and Microsystems (EuroSimE), 2012* (IEEE) pp. 1/6–6/6.

[38] F. Haghighi and S. J. Bae, *Reliability estimation from linear degradation and failure time data with competing risks under a step-stress accelerated degradation test,* IEEE Transactions on Reliability **64**, 960 (2015).

[39] C. Wei-Wei, M. Xiao-Hua, H. Bin, Z. Jie-Jie, Z. Jin-Cheng, and H. Yue, *The degradation mechanism of an algan/gan high electron mobility transistor under step-stress,* Chinese Physics B **22**, 107303 (2013).

[40] Y. Jun, X. Mingge, and W. ZHONG, *Research of step-down stress accelerated degradation data assessment method of a certain type of missile tank,* Chinese Journal of Aeronautics **25**, 917 (2012).

[41] Y. J. Z. Weiqiang, *Assessing step-down stress accelerated degradation data via nonlinear accelerated model,* Journal of Beijing University of Aeronautics and Astronautics **12**, 1475 (2011).

[42] K. A. Doksum and A. Hbyland, *Models for variable-stress accelerated life testing experiments based on wiener processes and the inverse gaussian distribution,* Technometrics **34**, 74 (1992).

[43] C.-C. Tsai, S.-T. Tseng, and N. Balakrishnan, *Optimal design for degradation tests based on gamma processes with random effects,* IEEE Transactions on Reliability **61**, 604 (2012).

[44] X. Wang, P. Jiang, B. Guo, and Z. Cheng, *Real-time reliability evaluation with a general wiener process-based degradation model,* Quality and reliability engineering international **30**, 205 (2014).

[45] K. Doksum and A. Hoyland, *Models for variable-stress accelerated life testing experiments based on wiener processes and the inverse gaussian distribution,* Theory of Probability & Its Applications **37**, 137 (1993).

[46] F. Lindskog *et al.*, *Modelling dependence with copulas and applications to risk management*, Ph.D. thesis, Master Thesis, ETH Zürich (2000).

[47] Z. Pan, N. Balakrishnan, Q. Sun, and J. Zhou, *Bivariate degradation analysis of products based on wiener processes and copulas,* Journal of Statistical Computation and Simulation **83**, 1316 (2013).

[48] S. Yamakoshi, O. Hasegawa, H. Hamaguchi, M. Abe, and T. Yamaoka, *Degradation of high-radiance ga 1-x al x as led's,* Applied Physics Letters **31**, 627 (1977).

[49] J. Xie and M. Pecht, *Reliability prediction modeling of semiconductor light emitting device,* IEEE Transactions on Device and Materials Reliability **3**, 218 (2003).

[50] J.-M. Kang, J.-W. Kim, J.-H. Choi, D.-H. Kim, and H.-K. Kwon, *Life-time estimation of high-power blue light-emitting diode chips,* Microelectronics Reliability **49**, 1231 (2009).

[51] H.-K. Fu, C.-W. Lin, T.-T. Chen, C.-L. Chen, P.-T. Chou, and C.-J. Sun, *Investigation of dynamic color deviation mechanisms of high power light-emitting diode,* Microelectronics Reliability **52**, 866 (2012).

[52] Y. Lin, Z. Deng, Z. Guo, Z. Liu, H. Lan, Y. Lu, and Y. Cao, *Study on the correlations between color rendering indices and the spectral power distribution,* Optics express **22**, A1029 (2014).

[53] H.-T. Chen, S.-C. Tan, and S. Hui, *Color variation reduction of gan-based white light-emitting diodes via peak-wavelength stabilization,* IEEE Transactions on Power Electronics **29**, 3709 (2014).

[54] J. Fan, K.-C. Yung, and M. Pecht, *Prognostics of chromaticity state for phosphor-converted white light emitting diodes using an unscented kalman filter approach,* IEEE Transactions on Device and Materials Reliability **14**, 564 (2014).

[55] S. Koh, H. Ye, M. Yazdan Mehr, J. Wei, W. van Driel, L. Zhao, and G. Zhang, *Investigation of color shift of leds-based lighting products,* in *15th international conference on Thermal, mechanical and multi-physics simulation and experiments in microelectronics and microsystems (eurosime), 2014* (IEEE, 2014) pp. 1–5.

[56] H. Fan, X. Li, J. Shen, and M. Chen, *An effective prediction method for led lumen maintenance,* in *13th International Conference on Electronic Packaging Technology and High Density Packaging (ICEPT-HDP), 2012* (IEEE) pp. 1560–1563.

[57] D. J. Lunn, A. Thomas, N. Best, and D. Spiegelhalter, *Winbugs-a bayesian modelling framework: concepts, structure, and extensibility,* Statistics and computing **10**, 325 (2000).

[58] Standard, *Energy star program requirements for lamps (light bulbs),* (2013).

[59] C. M. Tan and P. Singh, *Time evolution degradation physics in high power white leds under high temperature-humidity conditions,* IEEE Transactions on Device and Materials Reliability **14**, 742 (2014).

[60] C. Guo, X. Xie, W. Ma, Y. Cheng, and Z. Li, *Failure-mechanism identification method in acceleratedtesting,* Chinese Journal of Semiconductors **27**, 560 (2006).

[61] S. Koh, C. Yuan, B. Sun, B. Li, X. Fan, and G. Zhang, *Product level accelerated lifetime test for indoor led luminaires,* in *14th International Conference on Thermal, Mechanical and Multi-Physics Simulation and Experiments in Microelectronics and Microsystems (EuroSimE), 2013*, pp. 1–6.

[62] W. Nelson, *Accelerated life testing-step-stress models and data analyses,* IEEE Transactions on Reliability **29**, 103 (1980).

[63] J. Huang, D. S. Golubović, S. Koh, D. Yang, X. Li, X. Fan, and G. Zhang, *Degradation modeling of mid-power white-light leds by using wiener process,* Optics express **23**, A966 (2015).

[64] I. E. S. o. N. America, *Projecting long term lumen maintenance of led light sources,* (2011), [IESNA].

[65] J. Huang, D. Golubović, S. Koh, D. Yang, X. Li, X. Fan, and G. Zhang, *Rapid degradation of mid-power white-light leds in saturated moisture conditions,* IEEE Transactions on Device and Materials Reliability **15**, 478 (2015).

[66] D. J. Lunn, A. Thomas, N. Best, and D. Spiegelhalter, *Winbugs-a bayesian modelling framework: concepts, structure, and extensibility,* Statistics and computing **10**, 325 (2000).

7

CONCLUSION & RECOMMENDATION

7.1. CONCLUSION

IN this thesis, a comprehensive research was performed on the reliability of mid-power white-light LED packages. The purpose of this research is to investigate the major degradation mechanisms of the mid-power white-light LED packages, which have been widely used in the indoor and/or outdoor illumination applications. By comparing the degradation mechanisms, a lifetime testing method have been proposed to replace the test standard, – LM-80-08, which is widely used in the LED industry while it needs 6,000 hours to perform the lifetime prediction. Furthermore, based on the new testing method, a new model for the lifetime was also proposed. Compared to the widely used standard TM-21-11, this model provides more accurate lifetime prediction for the LEDs. Specifically, the research was then broken into 3 parts. That is, (i) packaging material degradation kinetics analysis; (ii) LED package degradation mechanism analysis; and (iii) Lifetime prediction modeling. As a consequence, several conclusions were presented as follows:

– The chip-related and package-related can easily separated by the spectral power distribution analysis. The conclusion was made based on the simulation results. It was found that the LED package materials – lead frames, package housing, and phosphors, rarely affects blue light spectral output of the LED package. Different from the degradation of the LED package materials, the degradation of the chips, induces the same degradation trend of both the blue light and down-converted light spectral outputs. The degradation of the silicone encapsulant, however, rarely affects the down-converted light spectral output except for a sudden degradation at the initial degradation stage, even it was aged at 200 °C. The degradation of the silicone encapsulant triggered very slight degradation of the blue light spectral output, which can be negligible compared to that induced by the chips. Therefore, the degradation of the blue light spectral output was considered as the result of the chip-related degradation mechanisms; and the degradation of the down-converted light spectral output, was attributed to the degradation of both the chips and the package materials, but the contribution of the chips can be calculated because the induces the same degradation trend of both the blue light and down-converted light spectral outputs. The SPD analysis has been successfully used in the failure analysis of LED packages in HTOL and WHTOL tests.

– The TM-21-11 method may have been misused in lifetime prediction for LED packages, as the degradation mechanisms are different at different stress conditions for LED packages aged by the LM-80-08 test method. A series of data analysis and failure analysis revealed that the optical degradation was triggered by degradation of both the chips and lead frames due to humidity effect for LED packages aged at 55 °C. However, for LED

packages aged at 105 °C, the degradation mechanism was mainly related to chip deterioration due to the deterioration of the Ohmic contact. As the degradation mechanisms are different in the LM-80-08 tests, the corresponding lifetime prediction method in the TM-21-11 standard may have been misused.

– The yellowing of the LED package housing was mainly triggered by the moisture rather than the temperature for mid-power LED packages aged by WHTOL. The optical degradation of the mid-power LED packages was found being contributed to both the serious yellowing of the package housing and deterioration of the chips. By comparing to yellowing of the LED packages aged by both HTOL and WHTOL, we concluded that the degradation mechanisms of yellowing are triggered by moisture rather than temperature, as the yellowing of the packages aged by HTOL was negligible. The deterioration of the chip, was contributed to the temperature and humidity effect, both of which induced the Ohmic contact degradation.

– The WHTOL is an higher accelerated test method instead of the LM-80-08 method for the lifetime prediction of the mid-power LEDs. The WHTOL triggered both chip-related and package-related degradation mechanisms, which is in accordance with what was found in the applications. In addition, statistics analysis found that the failure distributions are similar to each other for the LED packages aged by different WHTOL stress conditions. Compared to the LM-80-08 method, the WHTOL used one third of the testing time, while triggered much larger optical degradation. In a word, the WHTOL is a much more efficient test method instead of the LM-80-08 method for the lifetime prediction of the mid-power LEDs.

– Blue light over-absorption was found to be the degradation mechanisms of silicone carbonization for LED packages aged by HAST test, which can be explained by the scattering effect of the water particles. Due to the permeability of silicone, water vapor ingress occurs when LED packages are exposed to high temperature-humidity environment. When the water vapors reach to the saturated concentration, they are condensed at the pore walls of the silicone bulk due to the adsorption effects. As a result, blue lights emitting from the LED dies are scattered and randomly propagate through the silicone bulk. The scattering may happen many times, until the blue lights are absorbed by the silicone bulk. Simulation showed that the temperature of the silicone can be up to 300 °C due to the absorption of the blue lights, which leads to the silicone carbonization. Analysis also showed that the blue light over-absorption is strongly dependent on the water particle size.

– Compared to the TM-21-11 method, the Wiener process-based lifetime model improves the prediction accuracy by considering both MTTF and variance. The model

is capable of describing the interdependency between lumen decay and color shift. The Frank copula function was applied to describe the dependency between the lumen maintenance and color shift. However, the cumulative failure function demonstrated that the dependency between them was very weak. Therefore, these two performance characteristics could be simply considered as independent variables, thus simplifying the degradation modeling of the LED devices. In addition, compared to the maximum likelihood estimator (MLE) proposed by former researchers, the MLE proposed in this thesis greatly improves the estimation accuracy.

7.2. RECOMMENDATIONS

(1) Separating package material effects

By analyzing the spectra of the simulation models, the chip-related and package-related degradation mechanisms were separated. However, as the spectra degradation kinetics related to the packaging materials (including package housing, lead frames, silicone encapsulant, phosphors) are very similar to each other, the lumen degradation mechanisms induced by these materials are not yet separated based on the current methodology. New methodologies should be developed to further study the degradation mechanisms in the future.

(2) Lack of material degradation data at operating conditions

More material degradation data should be collected. In the simulation model, we collected the degradation data of the packaging materials by various ageing tests. For instance, high temperature storage tests were performed for the package housing and the silicone encapsulant, while sulfur ageing tests were performed to stimulate the degradation of the lead frames. However, due to lack of test equipments, ageing tests were not designed for the blue chips and phosphors, and the emitting efficiency of the blue chips and phosphors was assumed to uniformly degrade to a specific efficiency in our simulation models. This assumption may not be true according to the actual operating conditions. On the other hand, the ageing stresses for the aged materials were different from that of an LED package may experience during operation. Therefore, experiments which simulate the usage operating conditions are necessary to reproduce the LED package's degradation. An ageing chamber with multi-functions should be designed. This type of chamber controls the amount of blue light radiation, the level of relative humidity, and as well as the temperature.

(3) Develop a lifetime model based on material degradation

Due to market demands, a variety of LED packages have been designed to meet the requirements of different applications. These LED packages were designed by using different structures, and different materials. Though it is well known that the lifetime of an LED package is closely related to its packaging structure and materials, a lifetime model has not yet been developed based on the degradation data of the packaging materials, which are already available prior to the design of the LED package. Basically, this type of model is important for R&D. With the model, the designer can easily adjust the structure of the package, and select the appropriate materials.

(4) Develop new failure analysis techniques

Current failure analysis uses the optical microscope, SEM/EDX, XPS and so forth, to determine the degradation mechanisms of the failed IC products. These failure analysis techniques are very efficient, because failure analysis is usually performed after the IC products failed, i.e., run out of functions. This is different from LED packages. Because the LED package is highly reliable, it degrades very slowly in electrical performance, lumen output, or color shift, while still works after tens of thousands of hours. An LED package is brought to perform failure analysis after a percentage of 10% to 15% in lumen degradation, depending on the reliability requirements. The degradation of the materials may be very subtle, so it is not easily to determine the root cause of degradation. An alternative is to directly measure the optical performance of the materials of the aged LED packages, such as reflectivity of the lead frames and package housing, transmissivity of the silicone encapsulant, etc.. However, the LED package is so small, that the requirements have been out of the capacity of current equipments. In the future, a simple and efficient methodology/equipment should be developed to meet this requirement.

(5) Effects of moisture are still unknown

In our study, we have found the moistures have a significant effect on the lumen output of LEDs. The moistures not only induce yellowing of package housing, but also decrease the light output of the blue chip. However, electrical analysis showed that neither the epi-layer of the chip itself, nor the Ohmic contact deteriorated. It is considered that moistures induced a decrease in the transparency of the Ohmic contact layer. However, the degradation mechanisms are not clear. We also found that moistures might also change the surface structure of the lead frame during LM80-08 test, where the ambient temperature was 55 °C. The mechanisms, however, also needs to be further studied in the future. On the other hand, we found serious silicone carbonization during HAST. It is considered that blue light over-absorption is

the root cause of the carbonization. A model showed that it is the water particles stop the blue light propagating through the silicone. The blue lights are scattered and reflected when emitting out of the chip, and finally absorbed by the silicone. It was found that the absorption ratio increases with the water particles. However, it is difficult to measure the particle size of these water particles. The size of the water particles should be measured in order to confirm the degradation mechanism in future work.

(6) Lifetime modeling by using Bysian filtering

A modified Wiener process was applied to describe the nonlinear degradation of the LED packages in our research. However, the developed method is only conditional on the current degradation data and does not consider the evolving path to date. In order to make the lifetime model depending on the history of the observations, a state space model should be developed to updating one parameter in the drifting function through Bayesian filtering. Bayesian filtering techniques including Kalman filter, particle filter, etc., combining with the non-linear Wiener process model, can provide more accurate lifetime prediction in the future.

SUMMARY

The rapid growth of light-emitting diodes (LED)-based lighting applications has revolutionized the lighting industry over the past few years. According to a report made by the U.S. Department of Energy (DOE), LED lighting is projected to gain significant market penetration. It is expected to represent 48% of lumen-hour sales of the general-illumination market by 2020, and 84% by 2030. Though these energy savings are impressive, there is a huge opportunity for even further savings by accelerating investment in cost and efficacy improvements. However, many problems have to be resolved when using LEDs. There are seven challenges that lighting designers face when using LEDs, these are: LED glare and shadowing, LED dimming not as smooth as claimed, lack of color and measurement standardization, thermal management, interchangeability, and need for lower costs. These challenges also relate to reliability and lifetime. For example, bad thermal management will seriously decrease the lumen output of an LED package. It has been indicated that the reliability of a white-light LED package can be attributed to a combination of chip-related and package-related mechanisms. Until now, it is still unclear which one is the major degradation for mid-power white-light LED packages during operating conditions. A significant amount of studies have been performed on reliability of high-power white-light LEDs, while few manuscripts were dedicated to the reliability of mid-power white-light LEDs. This is probably because mid-power white-light LED is a relatively new type of LED packages. Mid-power white-light LEDs are basically good for low- to medium-cost general lighting applications because mid-power white-light LEDs match the output, in terms of both luminosity and light quality of this target market. As the strong demands increase continuously for mid-power white-light LED products which have lower cost while higher luminosity, the reliability is becoming a critical issue. In this thesis, comprehensive research was performed on the reliability of mid-power white-light LED packages. In chapter 1, we described the research motivation, the reliability problems which are related to mid-power white-light LEDs, the objective of this thesis, and finally the research structure of the research project. In chapter 2, we first introduced the basics of white-light LEDs. The types, structures, and working principles of white-light LED packages were presented. Then, the optical degradation mechanisms of LED packages were summarized as (i) crystal defect and dislocation

generation and movement; (ii) dopant diffusion from p-layer to epi-layer; (iii) electrical contact metallurgical inter-diffusion; (iv) die cracking; (v) encapsulant carbonization; (vi) polymer materials yellowing; (vii) lead-frame deterioration; (viii) phosphor thermal quenching and long-term degradation; (ix) delamination. Chapter 2 also reviewed the reliability test methods, which are used in the LED industry. It revealed that as a new type of products, there are few test standards for the white-light LED packages. Instead, LED manufacturers refer to the JEDEC standards, which are generally used in the reliability testing for IC products. On the other hand, chapter 2 also reviewed the state-of-the-art of lifetime modeling technologies for the LEDs. These technologies include: (i) regression model; (ii) stochastic process model; (iii) Bayesian network model. In chapter 3, several failure analysis techniques are introduced. These techniques will be utilized in our research project. They are – (i) thermal simulation; (ii) optical simulation; (iii) electrical analysis; (iv) X-ray inspection; (v) SAM inspection; (vi) SEM/EDX; (vii) XPS. Due to content limitation, only the work principles and applications were presented briefly. In chapter 4, a degradation mechanism analysis methodology is proposed for the mid-power white-light LED packages in this chapter. Based on the degradation data obtained from a series of ageing tests which are performed on the individual packaging material, the degradation kinetics of lumen output and spectral power distribution (SPD) of the LED packages are investigated by using optical simulation. As a result, although the reflectivity of the packaging materials decreased severely for the blue lights (i.e., 450 nm), simulation showed that lights at this wavelength were little absorbed in the LED package. More specifically, it is found that, (1) the degradation of the blue lights is mainly due to blue chip deterioration, while rarely affected by degradation of the silicone encapsulant and other packaging materials; (2) the degradation of the down-converted lights is significantly attributed to degradation of the blue chips, the phosphors, the lead frames and the package housing and; (3) the degradation of the silicone encapsulant, contributes about 1.35% to the total lumen degradation within 168 hours, while it has no more contribution to the lumen degradation with further ageing duration. The simulation results have been validated by experiments and successfully applied to the degradation mechanism analysis of LED packages in LM-80-08 tests. In chapter 5, the optical degradation mechanisms of mid-power white-light LED packages has been studied by using high temperature operation life test (HTOL), wet-high temperature operation life test (WHTOL) and highly-accelerated temperature-humidity test (HAST). As a result, it was found that, (1) for LED packages aged under HTOL, the major degradation mechanism is different for samples aged at 55 °C and ambient temperature higher than 85 °C, with which lead frames deterioration is the major degradation mechanism at 55 °C

while Ohmic contact deterioration is the major degradation mechanism at 105 °C for the aged LED packages; (2) for LED packages aged under WHTOL, both deterioration of the Ohmic contacts of the blue chip and yellowing of the package encapsulant are considered as the major degradation mechanisms; (3) for LED packages aged under HAST, the failure mechanism is considered as the result of blue light over-absorption, which generates very high temperature inside the silicone bulk, resulting in serious carbonization. In chapter 6, a modified Wiener process has been employed for the modeling of the degradation of LED devices. By using this method, dynamic and random variations, as well as the non-linear degradation behavior of LED devices, can be easily accounted for. With a mild assumption, the parameter estimation accuracy has been improved by including more information into the likelihood function while neglecting the dependency between the random variables. The degradation model has been established for LED packages which are aged under constant stress accelerated degradation test (CSADT). As a consequence, the mean time to failure (MTTF) has been obtained and shows comparable result with IES TM-21-11 predictions, indicating the feasibility of the proposed method. The cumulative failure distribution was also presented corresponding to different combinations of lumen maintenance and color shift. The results demonstrate that a joint failure distribution of LED devices could be modeled by simply considering their lumen maintenance and color shift as two independent variables. Finally, we also made efforts to extend the modeling method to the range of step stress accelerated degradation test (SSADT). In chapter 7, the conclusions of the thesis are given. On the one hand, the author also pointed out several problems which should be further studied in the future. These problems are: (i) more efforts should be developed to completely separate the effects of packaging materials degradation; (ii) lack of material degradation data at operating conditions; (iii) new failure analysis techniques should be developed; (iv) effects of moistures are still unknown; (v) Bayesian filtering techniques for lifetime modeling should be developed.

SAMENVATTING

De snelle groei van de light-emitting diodes (LED)-gebaseerde verlichtingstoepassingen heeft een revolutie in de verlichting industrie in de afgelopen jaren teweeggebracht. Volgens een rapport van het Amerikaanse Department of Energy (DOE), zal de LED-verlichting naar verwachting een aanzienlijke marktpenetratie te krijgen. Verwacht wordt dat LED de verkoop van 48% van de lumen (of licht) uren in de algemene verlichting markt in 2020, en 84% in 2030 zal vertegenwoordigen De energiebesparingen zijn indrukwekkend en er is een enorme kans voor nog meer besparingen door het versnellen van investeringen en effectiviteit verbeteringen. Veel problemen worden opgelost door LEDs. Maar er zijn zeven uitdagingen die lichtontwerpers zien bij het gebruik van LED's, deze zijn: LED-glare en shadowing, LED dimmen niet zo glad als beweerd, gebrek aan kleur en meting standaardisatie, thermisch beheer, uitwisselbaarheid en de noodzaak van lagere kosten. Deze uitdagingen hebben ook betrekking op de betrouwbaarheid en levensduur. Zo zal een slechte warmtehuishouding de lichtopbrengst van een LED-package verlagen. De betrouwbaarheid van een wit licht LEDs kan worden toegeschreven aan een combinatie van chip-gerelateerde en package gerelateerde mechanismen. Tot nu toe is het nog onduidelijk welke de belangrijkste degradatie is voor mid-power wit licht LEDs tijdens bedrijfsomstandigheden. Een aanzienlijk deel van de studies zijn uitgevoerd op de betrouwbaarheid van de high-power wit licht LEDs, terwijl enkele manuscripten werden gewijd aan de betrouwbaarheid van de mid-power wit licht LEDs. Dit komt waarschijnlijk omdat mid-power LEDs een relatief nieuwe vorm is. Mid-power wit licht LED's zijn in principe goed voor lage tot gemiddelde-cost algemene verlichtingstoepassingen omdat mid-power wit licht LED overeenkomen met de output, zowel in termen van helderheid en licht kwaliteit van deze doelgroep. Er is een sterke vraag voor mid-power wit licht LED-producten met lagere kosten en een hogere helderheid. Als zodanig wordt de betrouwbaarheid dan een cruciaal punt. In dit proefschrift is uitgebreid onderzoek uitgevoerd naar de betrouwbaarheid van de mid-power wit licht LEDs. In hoofdstuk 1 beschreven we het onderzoek, de motivatie, de betrouwbaarheid problemen die gerelateerd zijn aan mid-power wit licht LEDs, de doelstelling van dit proefschrift en tenslotte de onderzoek structuur van het onderzoeksproject. In hoofdstuk 2, introduceerden we eerst de basis van wit licht LEDs. De types, structuren en wer-

kingsprincipes van wit licht LED-packages werden gepresenteerd. Vervolgens wordt de optische mechanismen van LED packages degradatie samengevat als (i) kristalgebreken en dislocatie opwekking en beweging; (ii) doterende diffusie van p-laag op epi-laag; (iii) elektrisch contact metallurgische inter-diffusie; (iv) scheurvorming; (v) verkolen van het inkapselingsmiddel; (vi) polymeermaterialen vergeling; (vii) lead-frame bederf; (viii) fosfor thermisch verharden en lange termijn degradatie; (ix) delaminatie. Hoofdstuk 2 beschrijft de betrouwbaarheid testmethoden, die worden gebruikt in de LED-industrie. Het bleek dat voor nieuw type van producten er weinig testnormen bestaan. In plaats daarvan, volgen LED-fabrikanten de JEDEC standaarden die algemeen worden gebruikt in de betrouwbaarheidstesten voor semiconductor producten. Anderzijds, hoofdstuk 2 beschrijft ook de state-of-the-art van lifetime modellering technologieën voor de LEDs. Deze technieken omvatten: (i) regressiemodel; (ii) stochastisch procesmodel; (iii) Bayesian netwerkmodel. In hoofdstuk 3 worden verschillende faal analyse technieken geïntroduceerd. Deze technieken zullen worden gebruikt in ons onderzoek. Ze zijn - (i) thermische simulatie; (ii) optische simulatie; (iii) elektrische analyse; (iv) X-ray inspectie; (v) SAM inspectie; (vi) SEM / EDX; (vii) XPS. Alleen de werk principes en toepassingen zijn kort gepresenteerd. In hoofdstuk 4 wordt een degradatie mechanisme analyse methodiek voorgesteld voor de mid-power wit licht LED-packages in dit hoofdstuk. Gebaseerd op de degradatie gegevens van een reeks verouderingstests die worden uitgevoerd op de individuele verpakkingsmateriaal wordt de afbraakkinetiek van lichtopbrengst en spectrale energieverdeling (SPD) van de LED-packages onderzocht door middel van optische simulatie. Dientengevolge, hoewel het reflectievermogen van het verpakkingsmateriaal ernstig verminder door de blauwe golflengtes (d.w.z. 450 nm), simulatie toonde dat licht bij deze golflengte weinig wordt geabsorbeerd in de LED-package. Meer in het bijzonder, wordt geconstateerd dat (1) de afbraak van de blauwe golflengtes is voornamelijk te wijten aan blue chip verslechtering, terwijl zelden beïnvloed door de afbraak van de siliconen inkapselingsmiddel en andere verpakkingsmaterialen; (2) de afbraak van fosfor conversie materialen aanzienlijk toegeschreven is aan de afbraak van blue chips, de fosfor, de lead frames en het behuizingsmateriaal en; (3) de afbraak van de siliconen inkapseling draagt ongeveer 1.35% bij aan het totale lumen degradatie binnen 168 uur, terwijl het geen bijdrage meer levert aan de lumen degradatie op de langere duur. De simulatieresultaten zijn gevalideerd door experimenten en met succes toegepast op de degradatiemechanisme analyse van LED-packages in LM-80-08 testen. In hoofdstuk 5 zijn de optische mechanismen van mid-power wit licht LED degradatie bestudeerd met behulp van hoge temperatuur operatie life test (HTOL), nat-hoge temperatuur operatie life test (WHTOL) en zeer versnelde temperatuur-vochtigheid-test (

HAST). Als resultaat werd gevonden dat (1) voor LEDs onder HTOL, het degradatiemechanisme verschilt voor monsters bij 55 °C versus omgevingstemperatuur hoger dan °C, waar lead frames de verslechtering domineert bij 55 °C, is dit door Ohmic degradatie bij 105 °C; (2) voor LEDs onder WHTOL, zowel achteruitgang van de Ohmse contacten van de blue chip en vergeling van het inkapselingsmiddel zijn de belangrijkste degradatiemechanismen; (3) voor LEDs onder HAST is het faalmechanisme het resultaat van blauw licht absorptie, die een zeer hoge temperatuur genereert in de bulk siliconen, met ernstig carbonisatie als gevolg. In hoofdstuk 6 is het zogenaamde Wiener proces gebruikt voor het modelleren van de degradatie van LEDs. Met deze methode kan eenvoudig de dynamische en willekeurige variaties, alsook het niet-lineaire gedrag van LED degradatie worden verklaard. Het degradatie model is vastgesteld voor LEDs die onder constante spanning zijn getest in versnelde afbraak-testen (CSADT). Als gevolg hiervan is de gemiddelde tijd tot falen (MTTF) verkregen met een vergelijkbaar resultaat als IES TM-21-11 voorspellingen. De cumulatieve faal verdeling werd ook vastgesteld die overeenkomt met verschillende combinaties van lumen decay en kleurverschuiving. De resultaten tonen aan dat een gezamenlijk faal distributie van LEDs kan worden gemodelleerd door simpelweg gezien hun lumen decay en kleurverschuiving als twee onafhankelijke variabelen te beschouwen. Tot slot hebben we ook de modelleer methode uitgebreiden naar versnelde stap spanning afbraak-testen (SSADT). In hoofdstuk 7 worden de conclusies en aanbeveling van het proefschrift gegeven. De aanbevelingen zijn: (i) uitgebreid onderzoek naar de degradatie effecten van de verschillende verpakkingsmaterialen; (ii) het ontbreken van materiaal degradatie bij bedrijfsomstandigheden; (iii) nieuwe faal analyse technieken moeten worden ontwikkeld; (iv) de exacte gevolgen van vocht zijn nog niet bekend; (v) Bayesiaanse filtering technieken voor lifetime modellering moet worden ontwikkeld.

ACKNOWLEDGEMENTS

First of all, I would like to give the great thanks to my promotor Prof. Kouchi Zhang for giving me the opportunity to pursue a PhD degree in TU Delft Beijing Research Centre. I am also very grateful for his encouragement, and valuable suggestions during the past four years. You brought me to a new world of illumination technologies. You gave me the opportunity not only to learn how to do scientific research, but also to develop personal skills rather than technologies. I appreciate it very much for your faith and support on me when I was stuck in the difficulties during the research.

I also like to thank my boss Dr. Dušan S Golubović, the development director of Mid-power platform - R&D, Lumileds. You are always very supportive and helpful. I greatly appreciate the support and freedom I was given to carry my PhD in the company. You gave me the opportunity to learn the advanced lighting technologies from the most talented people in the industry area. You were also very helpful persuading the human resource to allow me to continue the research in the company. I am also very grateful for the discussions about LED technologies and the instructions on scientific writing.

I would like to thank Mr. Xiupeng Li, the head of reliability team of Philips Lighting (Shanghai) for providing reliability test resources, including climate ageing chambers, microscopy, and so forth. You are also very helpful for me to figure out the reliability test plan and to make the test schedule. Thanks a lot for that.

I would like to thank my daily supervisors Prof. Xuejun Fan, Dr. Sau Koh, and Prof. Daoguo Yang. They have spent a lot of time on coaching me of the scientific research. I would like to give my appreciations to Prof. Xuejun Fan first. Thanks for all instructions and inspirations during the scientific research and thesis writing, which help a lot leading me to the truth. You also gave many suggestions on writing journal publications. I also like to thank Dr. Sau Koh for his discussions about the technical questions during the research. You still gave a lot of suggestions on the scientific writing after you had left BRC. I would like also to thank Prof. Daoguo Yang. Your advice is very critical on the research structure. You also spent a lot of time helping me on the writing. Finally, I also like to thank Dr. Willem Van Driel, an expert of the LED reliability. You spent a lot of time discussing with me about the thesis writing. Your suggestions are very important.

My thanks also go to my colleagues:

– Yuhua Lee, an expert in LED chip manufacturing. You are humorous and friendly. Thanks for the experience sharing about life and work. You have a wide range of knowledge in the LED chip area. Thanks for all the discussions about the chip manufacturing, testing and failure analysis, which are very useful for analyzing the degradation mechanisms of LED packages.

– Lisa Liu, a Sr. material engineer who is very talented in the degradation mechanisms of the polymers. You are nice and patient. I am very happy for the collaboration with you in the past years. Thanks for all the discussions about the LED failure analysis. I also appreciate it very much for providing LED packaging materials and ageing data. In addition, thank you very much for introducing me to material suppliers, with this I can communicate with the material experts to solve the problems I had during the research.

– Lufei Zhang, an optical engineer who is very good at optical simulation. Thank you very much for coaching me on how to do an optical simulation, even when you are very busy on your own projects.

– Min Cui, a thermal engineer who is very good at thermal analysis. Thank you very much for coaching me on how to do a thermal simulation for the LED package. I appreciate it very much that you worked overtime with me to establish the simulation model before the Chinese new year. Many thanks also to you for helping me measure the thermal resistance of the LED samples.

I would like to thank Dr. Haibin Chen from Hongkong Univerity of Technology for his great support for failure analysis of LED packages. I am very grateful for the discussion on the results of X-ray, C-SAM, SEM/EDS, and XPS analysis.

Thanks also go to Dr. Xiufang Yen from Epistar for her great helps on measuring the electrical parameters of the LED chips.

I also appreciate very much for the work of Candy Tsai, and Bobby Hsieh. Both of them are from Integrated Service Technology Inc. Thank you very much for performing the reliability test. You are always patient and supportive. It is pleasure to cooperate with you.

I would like to give my thanks to my BRC colleagues: Mingzhi Dong, Bo Sun and Guangjun Lu for the great discussions and brainstorms, which are important for the research. I also like to thank all other BRC colleagues. It's pleasure working with all of you.

Many thanks also were given to the ECTM colleagues Xandra Tober and Marian Roozenburg for helping me get starting in TU Delft. My appreciations also go to all other ECTM colleagues. Thanks a lot for helping me study in a multi-cultural environment.

My thanks also extend to my colleagues and partners whose contributions are not

explicitly evident in this thesis, but I can assure you that they have been helpful. They are: Arnout Reints Bok, Cheuk Yan Chan, Elton Xu, Anthony Zhang, Leo Zhang, Mengming Zhu, Jun Yuan, Warren Tian, Zhaoxin Wang, Xiaosong Yan, Chensheng KU, Wei Chye Lim, Christopher Zhang, John Peng, Penny Wu, Sean Ho, Chong Qiao, Ray Lin, Marc Donker, Haibo Fan, Jinfeng Li, Longgang Ding, Jun Zhao, Lisa Sun, Wei Wu, Baiming Zhang, Taiyong Yang, Alan Lu, Chenfeng Shi, Guoqiao Tao, Junxing Shen, Wentao Guan, Huahui Kuang, Yenxue Lai.

My acknowledgements also go to all the people I might have forgotten to add. It's due to the pressure of finalizing a thesis which is also the cause for the lack of a personal thank you.

Finally, I would like to give the greatest thanks to my family. Without their understandings and encouragements, I will not be able to finish the PhD research.

LIST OF PUBLICATIONS

JOURNAL PAPERS

1. **J. Huang**, D.S.Golubović, Sau Koh, Daoguo Yang, Xiupeng Li, Xuejun Fan, and G.Q. Zhang, *Optical degradation mechanisms of mid-power white-light LEDs in LM-80-08 tests*, Microelectronics Reliability **55**, 2654 (2015).

2. **J. Huang**, D.S.Golubović, Sau Koh, Daoguo Yang, Xiupeng Li, Xuejun Fan, and G.Q. Zhang, *Degradation mechanisms of mid-power white-light LEDs under high temperature-humidity conditions*, IEEE Transactions on Device and Materials Reliability **15**, 220 (2015).

3. **J. Huang**, D.S.Golubović, Sau Koh, Daoguo Yang, Xiupeng Li, Xuejun Fan, and G.Q. Zhang, *Rapid degradation of mid-power white-light LEDs in saturated moisture conditions*, IEEE Transactions on Device and Materials Reliability **15**, 438 (2015).

4. **J. Huang**, D.S.Golubović, Sau Koh, Daoguo Yang, Xiupeng Li, Xuejun Fan, and G.Q. Zhang, *Degradation modeling of mid-power white-light LEDs by using Wiener process*, Optics Express **23**, A966 (2015).

5. **J. Huang**, D.S.Golubović, Sau Koh, Daoguo Yang, Xiupeng Li, Xuejun Fan, and G.Q. Zhang, *Degradation mechanism decoupling of mid-power white-light LEDs by SPD simulation*, IEEE Transactions on Electron Devices **63**, 2807 (2016).

6. **J. Huang**, D.S.Golubović, Sau Koh, Daoguo Yang, Xiupeng Li, Xuejun Fan, and G.Q. Zhang, *Lumen degradation modeling of white-light LEDs in step stress accelerated degradation test*, Reliability Engineering and System Safety **154**, 152 (2016).

7. Miao Cai, Daoguo Yang, Yuezhu Mo, **J. Huang**, Luqiao Yin, Lianqiao Yang, Xianping Chen,Wenbin Chen, and Guoqi Zhang, *Determining the thermal stress limit of LED lamps using highly accelerated decay testing*, Applied Thermal Engineering **102**, 1451 (2016).

CONFERENCE PAPERS

1. **J. Huang**, Sau Koh, Daoguo Yang, Xiupeng Li, and G.Q. Zhang, *Investigation of lumen degradation mechanisms of mid-power LED by HAST*, 2014 15th International Conference on Electronic Packaging Technology (ICEPT) *2014* (IEEE) pp. 1437–1441. (JCAP Outstanding Paper Award)

CURRICULUM VITÆ

Jianlin HUANG

20-08-1984 Born in Guangxi, China.

EDUCATION

2003–2007 Undergraduate in Mechanical Engineering
Guilin University of Electronics Technology

2007–2010 Postgraduate in Mechatronics
Guilin University of Electronics Technology
Thesis: Mechanical performance of FBGA module mounted on a flexible printed circuit (FPC)
Promotor: Prof. dr. Daoguo Yang

2012–2016 PhD. in Microelectronics
Delft University of Technology
Thesis: Optical degradation mechanisms and accelerated reliability evaluation for LEDs
Promotor: Prof. dr. G.Q. Zhang